

6th European Young Engineers Conference

www.eyec.ichip.pw.edu.pl

Copyright © 2017, Faculty of Chemical and Process Engineering,
Warsaw University of Technology

Edited by:

Bartosz Nowak, MSc Eng.

Łukasz Werner, MSc Eng.

Patrycja Wierzba, MSc Eng.

ISBN 978-83-936575-4-4

Printed in 100 copies

The authors are responsible for the content of the papers.

All papers reviewed by Scientific Committee.

Published by:

Faculty of Chemical and Process Engineering

Warsaw University of Technology

Printed in Poland by:

Institute for Sustainable Technologies – National Research Institute

26-600 Radom, 6/10 Pułaskiego Street,

phone (+48) 48 36-442-41, fax (+48) 48 36-447-65

<http://www.itee.radom.pl>

Contents

Introduction	12
Scientific Committee.....	13
Scientific Commission	14
Łukasz Makowski, PhD DSc	14
Anna Jackiewicz-Zagórska, PhD	14
Oleksandr Ivashchuk, PhD.....	15
Aldona Zalewska, PhD.....	15
Alessandro Benedetti, PhD	16
Jakub Bujalski, PhD	17
Organizing Committee	18
Special Guests	19
Prof. Jörg Vienken, PhD	19
<i>David vs Goliath – Bacteria, endotoxins and biofilms.....</i>	<i>20</i>
<i>Artificial Membranes for Life Sciences: Lessons learnt from dialysis applications.....</i>	<i>21</i>
Prof. Tomasz Sosnowski, PhD.....	23
<i>Aerosol and health – the engineer’s perspective.....</i>	<i>24</i>
Prof. Shinji Sakai, PhD	25
<i>Tissue engineering using enzymes.....</i>	<i>26</i>
Prof. Ilya Vorotyntsev, PhD.....	27
<i>Perspective of membrane gas separation applications.....</i>	<i>28</i>
Assist. Prof. Masaki Nakahata, PhD	29
<i>Engineering functional polymeric materials cross-linked by intermolecular interactions.....</i>	<i>29</i>
Marta Mazurkiewicz-Pawlicka, PhD	30
<i>Carbon nanomaterials for energy storage and conversion applications.....</i>	<i>30</i>
Articles.....	31
Sorption of heavy metal cations using natural zeolites	
<i>Kamila Brylewska</i>	<i>31</i>
Preparation, characterization and antitubercular activity of polymeric nanoformulation of isoniazid	
<i>Monika Budnicka.....</i>	<i>40</i>
The parameters of helicoidal structure of liquid crystals	
<i>Anna Drzewicz</i>	<i>52</i>
A new method to compare micromixedness results obtained in iodide-iodate method using different reactant concentrations	
<i>Michał Fedoryk.....</i>	<i>63</i>
New, simple method of determining necessary conditions of dead zone formation in catalyst pellet	

<i>Grzegorz Król</i>	79
The influence of the classic pore precursors on the morphology of polyesters membranes for tissue engineering	
<i>Aleksandra Kruk</i>	87
Investigation of high-temperature resistant optical fiber elements for sensor construction	
<i>Anna Kurzych</i>	100
Experimental results of the vertical-cavity surface-emitting laser for optical fiber sensors application	
<i>Anna Kurzych</i>	108
The four-channel polarimeter to examining the selected optical elements	
<i>Marlena Kwiatkowska</i>	118
Hydrodynamic studies of magnetically assisted external loop airlift	
<i>Joanna Lechowska</i>	125
The influence of materials phase changes on spectral characteristic in optical fiber taper	
<i>Joanna E. Moś</i>	135
Optical properties of Photonic Crystal Fiber filled by ZnO nanoparticles fluid	
<i>Natalia Przybysz</i>	142
Synthetic pathways of 4-(alkyl-1-yn-1-yl)-bromo/chlorobenzenes as useful intermediates for highly birefringent Liquid Crystals	
<i>Marta Pytlarczyk</i>	149
Cracking of precipitation hardened alloys induced by Nd-YAG laser beam	
<i>Łukasz Rakoczy</i>	158
Stability of water silica suspension with polymer addition	
<i>Diana Rymuszka</i>	164
Preparation of methyl ester of L-serine	
<i>Agnieszka Sebai</i>	176
Determination of CMC values of the surfactant solutions	
<i>Magdalena Szaniawska</i>	186
Polyphenols – description and preliminary study of alcohol extraction	
<i>Anna Taraba</i>	194
Carbon-based nanomaterials in chemistry	
<i>Tomasz Wawer</i>	202
Recovery of zinc(II) from chloride solutions using hollow fibre contactor with pyridine derivatives extractant	
<i>Aleksandra Wojciechowska</i>	211
Recovery of iron(III) from chloride solutions	
<i>Aleksandra Wojciechowska</i>	221
Tapered long- period fiber gratings made by filament heating	
<i>Renata Wonko</i>	230

Abstracts.....	236
Building a Mobile Liquid Nitrogen Generator	
<i>Paweł Antkowiak.....</i>	<i>236</i>
Sorption properties of mesoporous ZSM-5 and BEA zeolites	
<i>Kamila Brylewska.....</i>	<i>237</i>
Polymer nanospheres with isoniazid preparation and antituberculosis activity studies	
<i>Monika Budnicka.....</i>	<i>238</i>
Synthesis of nanohydroxyapatite using microwave energy	
<i>Agnieszka Chodara.....</i>	<i>239</i>
The effect of substrate temperature on the properties of tungsten boride layers deposited by radio frequency magnetron sputtering and pulsed laser deposition	
<i>Justyna Chrzanowska.....</i>	<i>240</i>
The influence of irydoids content on effectiveness of cosmetic formulations	
<i>Marta Dąbrowska.....</i>	<i>241</i>
Stability testing of cosmetic bases for skin care products using multiple light scattering method	
<i>Marta Dąbrowska.....</i>	<i>242</i>
The degradation tests of ceramic-polymer composites with hydroxyapatite for orthopedic implants	
<i>Sylvia Dąbrowska.....</i>	<i>243</i>
Synthesis and characterization of palladium catalysts supported on SBA-16 materials	
<i>Paulina Dębek.....</i>	<i>244</i>
Hydrodeoxygenation of anisole as bio-oil model compound over Ru/MCM-41 catalysts	
<i>Paulina Dębek.....</i>	<i>245</i>
Heterogeneous degradation of xenobiotics by sunlight radiation	
<i>Emilia Drozdek.....</i>	<i>246</i>
Analysis of IR spectra of three ring liquid crystalline chiral esters	
<i>Anna Drzewicz.....</i>	<i>247</i>
Helical pitch of bicomponent systems of 3FnXPhY series	
<i>Anna Drzewicz.....</i>	<i>248</i>
Investigations of Fe thin films deposited on Si substrates by XRR, RBS, AFM and HSEM	
<i>Aneta Duda.....</i>	<i>249</i>
A new method to compare micromixedness results obtained in iodide-iodate method using different reactant concentrations	
<i>Michał Fedoryk.....</i>	<i>250</i>
Membrane assisted continuous-flow reactions	
<i>Tamás Földi.....</i>	<i>251</i>

1-alkyl-4-(dimethylamino) pyridinium bis(trifluomethylsulfonyl)imides as electrolytes for supercapacitors	
<i>Agnieszka Gabryelczyk</i>	252
The influence of ionic liquids structure on corrosion parameters in lead-acid battery	
<i>Agnieszka Gabryelczyk</i>	253
Study of series of antiferroelectric smectic mixtures composed with smectogens exhibiting synclinic and anticlinic phases	
<i>Katarzyna Gaładyk</i>	254
Surface properties of the layers based on cerium doped black glass on austenitic stainless steel substrate	
<i>Magdalena Gawęda</i>	255
Cerium doped amorphous materials based on silicon oxycarbide and their possible applications	
<i>Magdalena Gawęda</i>	256
The determination of benzophenanthridine and protopine derivatives in biological fluids	
<i>Aleksandra Główka</i>	257
Antioxidant activity of <i>Chelidonium majus L.</i> plant extract	
<i>Aleksandra Główka</i>	258
Anode material for direct borohydride fuel cell	
<i>Małgorzata Graś</i>	259
The effect of electrode modification on the electrochemical capacitor performance	
<i>Małgorzata Graś</i>	260
The application of coalescing plate for separating water and oil in water treatment plant in the petroleum industry by utilizing CFD simulation	
<i>Soran S. Ibrahim</i>	261
Research on structural properties of antimony-silicate glasses doped with thulium ions	
<i>J. Zmojda</i>	262
Structural and luminescence properties of germanate glasses modified by aluminium oxide	
<i>Renata Jadach</i>	263
Esterification reactions conducted in the presence of sulfonated mesoporous silica	
<i>Sylwia Jarmolińska</i>	264
Platinum supported on mesoporous silica of MCM-41 type – synthesis and characterization procedures	
<i>Sylwia Jarmolińska</i>	265
Application of galinstan film electrode for determination of thallium (I) traces using anodic stripping voltammetry	
<i>Katarzyna Jedlińska</i>	266
The renewable galinstan film metal based electrode for voltammetry	
<i>Katarzyna Jedlińska</i>	267

The thermodynamic properties of the liquid crystal stationary phase <i>Justyna Jonik</i>	268
The Raman spectroscopy and X-ray photoelectron spectroscopy as the methods of graphene analysis <i>Justyna Jonik</i>	269
Laser additive manufacturing of composites based on tungsten carbide <i>Magdalena Karpowicz</i>	270
Size enlargement and recovery of some cinchona-based organocatalysts applying organic solvent nanofiltration <i>Péter Kisszékelyi</i>	271
Ionic liquids additives for nickel electroplating <i>Łukasz Kolanowski</i>	272
Heteroatom-doped carbons for electrochemical applications <i>Łukasz Kolanowski</i>	273
Removal of organic contaminants from water systems by using hybrid process <i>Kacper Koczyński</i>	274
Ionic liquids as additives for lead-acid battery <i>Kacper Koczyński</i>	275
Analysis of the effect of shaping the plate of plate heat exchanger on the effectiveness of its work <i>Marcin Kos</i>	276
Investigation of the integrated reactive adsorption process <i>Tomasz Kotkowski</i>	277
Synthesis and application of cinchona-squaramide organocatalyst supported on polybenzimidazole membrane <i>Petra Kozma</i>	278
Potential toxic effects of selected nanoparticles on pulmonary surfactant system <i>Katarzyna Kramek-Romanowska</i>	279
New, simple method of determining necessary conditions of dead zone formation in catalyst pellet <i>Grzegorz Król</i>	280
The influence of classic pore precursors on a morphology and mechanical properties of polyesters membranes for tissue engineering <i>Aleksandra Kruk</i>	281
Characterization and modification of FePd thin films deposited on SiO ₂ /Si(001) <i>Magdalena Krupska</i>	282
Ion beam mixing and interdiffusion in magnetite thin films after Ar ⁺ ion irradiation <i>Magdalena Krupska</i>	283
Preparation of synthetic metalloporphyrins and their application in biomimetic oxidations of drugs in flow systems <i>József Kupai</i>	284
Interferometric fibre sensor for rotational seismology application	

<i>Anna Kurzych</i>	285
The four-channel polarimeter to examining the selected optical elements	
<i>Marlena Kwiatkowska</i>	286
Hydrodynamic studies of magnetically assisted external loop air-lift	
<i>Joanna Lechowska</i>	287
The effect of addition of various Ti powders on the zirconia matrix composite	
<i>Paula Maria Łada</i>	288
Effect of modification of carbon paste electrodes pasted on the quality of the analytical signal	
<i>Agnieszka Grzybowska</i>	289
Dopamine detection used to glassy carbon electrode modified by conductive polymer with nanopowders of TiO ₂	
<i>Lukasz Magda</i>	290
New application of gassy carbon electrode modified by material composed of ceramic nanopowder and conductive polymers	
<i>Lukasz Magda</i>	291
Investigating the possibility of manufacturing the composite from nanocrystalline hydroxyapatite and silk fibers and study of its selected properties	
<i>Maria Małysa</i>	292
Investigating the possibility of manufacturing the composite from nanocrystalline hydroxyapatite and silk fibers and study of its selected properties	
<i>Maria Małysa</i>	293
Influence of different materials on light propagation in tapered optical fiber	
<i>Joanna Moś</i>	294
Aluminosilicates as an effective filler for epoxy resin composites	
<i>Jolanta Nieroda</i>	295
The preliminary characterization of amorphous metal surface for power industry application	
<i>Jolanta Nieroda</i>	296
ZnS nanowires as a new acceptor material for the photovoltaic cells	
<i>Elżbieta M. Nowak</i>	297
Preparation of poly(vinyl alcohol)/graphene composites	
<i>Maksymilian Nowak</i>	298
The influence of the addition of ZrO ₂ on the surface parameters of a porcelain glazes	
<i>Katarzyna Pasiut</i>	299
The influence of the addition of ZrO ₂ on the technological parameters of a porcelain glazes	
<i>Katarzyna Pasiut</i>	300
Study of selected aspects in microalgae <i>Chlorella vulgaris</i> cultivation in laboratory conditions	
<i>Agnieszka Patyna</i>	301

Monitoring of domestic sewage treatment plant <i>Monika Pawlita-Posmyk</i>	302
Encapsulation of linalool in solid lipid nanoparticles <i>Irina Pereira</i>	303
Improving of nitrate sensors parameters by applying graphene-based intermediate layers <i>Magdalena Pięk</i>	304
Comparison of influence of used nanomaterials on Na ⁺ -ISEs parameters <i>Magdalena Pięk</i>	305
The environmental impact of installations for depolymerization of plastic waste <i>Paulina Pięta</i>	306
Electrooptic properties of nematic liquid crystal mixtures doped with gold nanoparticles <i>Natalia Przybysz</i>	307
Effective methods of selective filling of the air holes in the polarization-maintaining photonic crystal fiber <i>Natalia Przybysz</i>	308
Synthetic pathways of novel high fluorinated C4-C4 dialkylphenyltolanes <i>Marta Pytlarczyk</i>	309
New nematic liquid crystals with long conjugated π electronic system <i>Marta Pytlarczyk</i>	310
Microstructural changes of cast nickel alloys induced by laser beam <i>Łukasz Rakoczy</i>	311
Optimization of instrumental parameters for voltammetric determination of 4-chloro-3-methylphenol using Bi-CCE <i>Justyna Robak</i>	312
The influence of bismuth oxide nanoparticles on electrochemical properties of carbon ceramic electrode <i>Justyna Robak</i>	313
Entire volume modification of carbon ceramic electrode using zeolite <i>Justyna Robak</i>	314
Ultrasonic Coating as a Method of Medical Implants Surface Modification with Bioactive Nanoparticles <i>Julia Rogowska-Tylman</i>	315
Solidification of hazardous solid waste incineration bottom ash <i>Piotr Rożek</i>	316
Stability of water silica suspension with polymer addition <i>Diana Rymuszka</i>	317
Preparation of methyl ester of L-serine <i>Agnieszka Sebai</i>	318
Future of Flywheels Technology in Transportation <i>Albasher Shareif</i>	319

Potential of remote sensing data for detection of hydrographic features of lowland river: meandering and oxbow lakes shape changes and water quality. The Biebrza River case study	
<i>Małgorzata Ślapińska</i>	320
Carbon black as a modification layer for high sensitive melatonin determination	
<i>Joanna Smajdor</i>	321
Use of the renewable mercury film electrode for sensitive determination of selected hormones	
<i>Joanna Smajdor</i>	322
Modification layers used in voltammetric measurements	
<i>Joanna Smajdor</i>	323
Is chemometrics and voltammetry a great couple for food profiling and authenticity?	
<i>Wanda Sordoń</i>	324
Voltammetric determination of antioxidants	
<i>Wanda Sordoń</i>	325
Determination of CMC values of the surfactant solutions	
<i>Magdalena Szaniawska</i>	326
Influence of solid concentration on rheological properties of the suspensions	
<i>Adriana Szydłowska</i>	327
External mass transfer limitation of heterogeneous processes for various types of hydrodynamics	
<i>Jakub Szyman</i>	328
Comparison of micellar and alcohol extraction of flavonoid	
<i>Anna Taraba</i>	329
Influence of hot dip galvanizing on the microstructure and hardness of heat-treated construction steel	
<i>Lechosław Tuz</i>	330
Characterization of sol-gel derived glasses from binary system SiO ₂ -CaO containing cerium ions	
<i>Aleksandra Wajda</i>	331
Synthesis and analysis of oxidised graphite	
<i>Tomasz Wawer</i>	332
Elimination of environmental sample matrix interferences by using XAD-7 resin in voltammetric determination of Mo(VI)	
<i>Krzysztof Węgiel</i>	333
Conditioning of bismuth bulk electrode for the characterization of clothianidin and its determination in selected samples by DPV	
<i>Krzysztof Węgiel</i>	334
Electrochemical properties of riboflavin at a metallic annular band electrodes	
<i>Krzysztof Węgiel</i>	335
Voltammetric determination of Mo(VI) at the in situ regenerated BiABE electrode	

<i>Krystian Węgiel</i>	336
Investigation of the rate of oxygen absorption in a wave-type agitated single-use bioreactor	
<i>Kamil Wierzchowski</i>	337
Adsorption of benzo[a]pyrene on natural and synthetic materials	
<i>Katarzyna Wilkosz</i>	338
Recovery of zinc(II) from chloride solutions using hollow fibre contactor with pyridine derivatives extractant	
<i>Aleksandra Wojciechowska</i>	339
Recovery of iron(III) from chloride solutions	
<i>Aleksandra Wojciechowska</i>	340
Microwave solvothermal synthesis and characterization of ZnO nanoparticles co-doped with Co ²⁺ and Mn ²⁺ ions	
<i>Jacek Wojnarowicz</i>	341
Research on the size control mechanism of ZnO nanoparticles obtained in microwave solvothermal synthesis	
<i>Jacek Wojnarowicz</i>	342
Long Periods Fibers Grating made by filament heating	
<i>Renata Wonko</i>	343
Ultrasonic coating technology for improving bone implants	
<i>Bartosz Woźniak</i>	344
Electrodeposition of the calcium-phosphate coatings on titanium for bone tissue engineering	
<i>Bartłomiej Wysocki</i>	345
D-limonene-loaded Solid Lipid Nanoparticles (SLN) as innovative delivery system for pharmacy and cosmetic industries	
<i>Aleksandra Zielińska</i>	346
Synthesis of solid lipid nanoparticles and nanostructured lipid carriers for pharmaceutical and cosmetic purposes	
<i>Aleksandra Zielińska</i>	347
Voltammetric profiling of tea infusions	
<i>Justyna Zuziak</i>	348
Voltammetric strategies of aluminium traces determination	
<i>Justyna Zuziak</i>	349
Fabrication of Al ₂ O ₃ -Ni composites via centrifugal gel casting	
<i>Justyna Zygmuntowicz</i>	350
Index	351

Introduction

Since the very beginning of European Young Engineers Conference, since the first meeting of Students Scientific Club in 2011, we were wondering, how we can develop our work and how to provide a new, attractive and easy way to exchange knowledge and experience between young people. People who, like us, are passionate for creation, search for answers, create innovative solutions for current issues. In short – people of Science.

It may sound pompous, after all, there are many other conferences for young scientists, but we believe that, thanks to EYEC's scope, friendly atmosphere and high level of presented research, it is the best way to start or continue your scientific career.

It is already 6th edition of EYEC and we still did not materialized half of our ideas. Every year we try to give you something new: interesting guest speakers, additional workshops or accompanying contests. It is also 4th time we give you our EYEC Monograph. In this book you can find the most promising, important and reviewed papers of European Young Scientists. We hope, that this book you are holding right now, will be the first step in great career of each and every of participants of our conference.

The Monograph, as well as conference, covers following matters:

- process engineering,
- chemical engineering,
- biomedical & bioprocess engineering,
- nanotechnologies & nanomaterials,
- material engineering,
- process apparatus,
- process kinetics and thermodynamics,
- environmental protection,
- other engineering disciplines.

We hope you will find the papers within this book highly interesting and important, as we do.

Organizing Committee
Editorial Team of EYEC Monograph

Scientific Committee

The Editorial Team of EYEC Monograph is extremely grateful for the effort and work of Scientific Committee put on the reviewing process of all the manuscript published in this book. Right after authors, without Your work this book would not be created. Thank you.

Organizing Committee
Editorial Team of EYEC Monograph

Prof. Eugeniusz Molga, PhD (WUT, Poland) – Chairman

Prof. Tomasz Ciach, PhD

(WUT, Poland)

Prof. Marc-Oliver Coppens, PhD

(UCL, UK)

Prof. Paweł Gierycz, PhD

(WUT, Poland)

Prof. Leon Gradoń, PhD

(WUT, Poland)

Prof. Marek Henczka, PhD

(WUT, Poland)

Prof. György Marosi, PhD

(BME, Hungary)

Prof. Wojciech Piątkiewicz, PhD

(ISTe-NRI, Poland)

Prof. Tomasz Sosnowski, PhD

(WUT, Poland)

Prof. Andrzej Stankiewicz, PhD

(TU Delft, Holland)

Anna Adach, PhD (WUT, Poland)

Agata Bąk, PhD (WUT, Poland)

Alessandro Benedetti, PhD

(Mareco CNR-IENI, Italy)

Marta Bojarska, PhD (UDE, Germany)

Jakub Bujalski, PhD

(Yara Int., Norway)

Robert Cherbański, PhD

(WUT, Poland)

Katarzyna Dąbkowska, PhD

(WUT, Poland)

Jakub Gac, PhD (WUT, Poland)

Anna Jackiewicz, PhD (WUT, Poland)

Magdalena Jasińska, PhD

(WUT, Poland)

Joanna Jankowska-Śliwińska, PhD

(IBBE-PAS, Poland)

Naresh Kasoju, PhD (IBME, UK)

Zoltan Kovacs, PhD (BME, Hungary)

Andrzej Krasiński, PhD

(WUT, Poland)

Piotr Machniewski, PhD

(WUT, Poland)

Łukasz Makowski, PhD (WUT, Poland)

Artur Malolepszy, PhD (WUT, Poland)

Marta Mazurkiewicz-Pawlicka, PhD

(WUT, Poland)

Marcin Odziomek, PhD (WUT, Poland)

Wojciech Orciuch, PhD (WUT, Poland)

Agata Penconek, PhD (WUT, Poland)

Maciej Pilarek, PhD (WUT, Poland)

Bruno Bastos Sales, PhD

(Avans, Holland)

Paweł Sobieszuk, PhD (WUT, Poland)

Piotr Wieciński, PhD (WUT, Poland)

Anna Zalewska, PhD (WICHiR, Poland)

Scientific Commission

Łukasz Makowski, PhD DSc

He graduated from the Faculty of Chemical and Process Engineering of the Warsaw University of Technology in 1997. In 2003 he has received a PhD degree in Chemical Engineering, PhD thesis was titled “Application of the closure hypothesis and CFD for description of complex chemical reactions in the systems with turbulent flow”. In 2013 he has received DSc (habilitation) in Chemical Engineering titled „Effects of mixing in selected problems of product engineering processes”. During of his work he was



repeatedly manager or participant in many research grants funded by public resources for science or industry, for instance: State Committee for Scientific Research and National Science Centre as well as projects in 6th and 7th Framework Programme of the European Union, Bayer Technology Services GmbH, Unilever, CIECH Group Companies – ZACHEM, OLPP, Miejskie Przedsiębiorstwo Wodociągów i Kanalizacji w m.st. Warszawie, Cosmetic Packaging Factory Pollena S.A. He is co-author of 72 papers published in periodicals and conference materials.

Anna Jackiewicz-Zagórska, PhD

She graduated from the Faculty of Chemical and Process Engineering of the Warsaw University of Technology in 2004. Her master thesis was appreciated by the Award of the Ignacy Łukasiewicz Grant Fund of PGNiG S.A. for the best Master’s thesis. In November 2010, she received a PhD degree and her Doctoral thesis entitled “Investigation into filtration of aerosol particles in inhomogeneous fibrous filters” was distinguished by the Faculty Council and by the jury awarding the Fiat grants. Dr Anna Jackiewicz has been employed by the Warsaw University of Technology as Assistant Professor since 2011. She is the supervisor of the filtration laboratory at the Department of Integrated Processes Engineering.



Dr Anna Jackiewicz is co-author of 55 papers published in periodicals and conference materials. She has presented her research results at 15 international and 11 national conferences. She received scholarships for distinguished Ph.D. students in the field of science and research and scholarship for young scientists awarded by the

Centre for Advanced Studies, Warsaw University of Technology, and by the Marshal of the Mazowieckie province. In 2011, she was granted an individual Award of the Rector of the Warsaw University of Technology for scientific achievements. Her profile was presented at the exhibition entitled “Maria Skłodowska-Curie in the Service of Science Yesterday and Today” at the European Parliament in Brussels. Since 2012 Dr Jackiewicz is the manager of the Leader III project from the National Centre for Research and Development. She was awarded first place in the project called “Internship as a success of a scientist”, intended to strengthen the cooperation between researchers and enterprises.

Her scientific interests: separation processes of gas-solid and liquid particles, filtering media design, modeling of filtration in fibrous filters, techniques for aerosol generation and detection, materials science.

Oleksandr Ivashchuk, PhD

Lecturer of the Department of Chemical Engineering at Lviv Polytechnic National University (Lviv, Ukraine).

He received his PhD degree in 2008 for the research of the catalytic liquid-phase cyclohexane oxidation – he has developed effective catalytic systems for the process (binary system, catalytic complex solutions and individual catalysts).

For ten years he has been worked on the implementation of 6 research themes of the organic products technologies (researching of catalytic oxidization of liquid hydrocarbons, sonochemistry intensification of catalytic oxidization of cyclohexane, development of homogeneous catalysts, intensification of diesel fuel with organic compounds etc.) at Lviv Polytechnic National University (Lviv, Ukraine). In 2012 he has received an academic status of Senior Research Fellow. Now he works with computer simulation in the chemical technology and engineering.



Dr. Ivashchuk is a co-author of 78 scientific works, including 3 patents and 5 electronic textbooks. He is a Secretary of scientific conferences «Chemistry and Chemical Technology», «Chemical Technology and Engineering» (Lviv Polytechnic National University, Ukraine).

Dr. Ivashchuk is also the Head of Young Scientists' Council of the Institute of Chemistry and Chemical Technologies at Lviv Polytechnic National University.

Aldona Zalewska, PhD

I am an assistant professor of Chemistry since July 2014. I have been employed in the Department of Inorganic Chemistry and Solid State Technology of the Faculty

of Chemistry of Warsaw University of Technology as research and teaching assistant professor since 1997, when I earned my PH.D.

My scientific-research activity covers many issues connected with polymer electrolytes for application in lithium batteries, as well as research methods. My scientific achievements constitute 37 papers of the ISI Master Journal List of the Institute of Scientific Information. In total, I participated in the realization of 8 research projects as a contractor, main contractor and Project Manager. My teaching activity is associated with the Faculty of Chemistry of Warsaw University of Technology and covers giving lectures and supervising class exercises, laboratory courses and diploma theses. I received common awards for scientific activities such as scholarship from the Foundation of Polish Science in 1997, Rector's of the WUT collective (in 1999) and personal award (in 2001) for scientific achievements, personal award for didactical achievements (in 2008/2009), "Złota kreda" award for the best academic teacher granted by Student Self government on WUT.

Alessandro Benedetti, PhD

Researcher in the MARECO CNR-IENI sea marine station, located in Bonassola (SP, Liguria, Mediterranean sea) also responsible for management of the CePAS-Bonassola office, a public structure by the Bonassola Municipality and CNR-IENI for the divulgation of sea environment peculiarities consisting in stormy waves formation and watching.

He received his PhD in Environmental Science from Università degli Studi di Milano). Dr Benedetti's research is currently related to surface and material behavior in different seawater environments (e.g. effects of different seawater environments on superhydrophobic surfaces, Al and Fe alloys, cathodic protection of steel in shallow euphotic seawater).

He is also involved in the 'wave watching' activity which links science and education. He took part in research related to development of high resolution models for description/forecast of meteomarine dynamics of the Bonassola bay (cooperation with Univeristy of Genoa) and sea-wave motion measurement by accelerometric/sysmologic techniques (collaboration with National Geophysical and Vulcanology Institute).

Beside a number of scientific papers he also published a book "Wave Watching – lo spettacolo delle mareggiate in Liguria" (S. Gallino, A. Benedetti, L. Onorato. Ed. Hoepli, 2011).



Jakub Bujalski, PhD

He graduated in 1997 from University of Nottingham, (UK) with a MEng in Chemical Engineering. In 2003 he received his PhD in Chemical Engineering from University of Birmingham (UK), titled: “Computational fluid dynamic modelling of stirred reactors: power, baffle stresses, mixing times and semi-batch precipitation”. From 2003 to 2006 he joined the CFD group at CSIRO Minerals (Australia) as a Post Doc Researcher where he worked on CFD modelling of hydrometallurgical mineral extraction processes.



From 2006 he is based in Norway as a Principal Engineer in the Process Modelling and Control Department at the Yara International’s Innovation Research and Development Centre. His current focus is on the use of CFD in the fertiliser process industry to optimise the existing plants as well as new equipment design. He is an author of over 100 internal research reports focusing on improvements in the production of fertilisers and a number of conferences and journal publications. His current research interests are in CFD modelling of large scale industrial processes with a special focus on the nitrophosphate fertiliser process.

Organizing Committee

Members of the Scientific Club of Chemical and Process Engineering
and Foundation of Young Science

Head of Committee

Zuzanna Bojarska, BSc

Anna Dmowska, BSc

Eliza Grzymkowska, BSc

Klaudia Jaworska

Izabela Szczur

Piotr Grochowiecki

Bartosz Nowak, MSc

Kinga Kurowska, PhD

Aneta Gawryszewska, BSc

Jacek Lewicki, PhD

Michał Wojasiński, MSc

Patrycja Wierzba, MSc

Łukasz Werner, MSc

Nina Borzęcka, BSc

Krystian Jędrzejczak

Paweł Antkowiak

Kinga Kalkowska

Piotr Cendrowski, BSc

Agnieszka Hahaj

Mateusz Bartczak

Magdalena Tomczak

Joanna Kobek

Natalia Karaszewska

Kamila Bańkowska

Marcin Winnik

Łukasz Sołtan

Special Guests

Prof. Jörg Vienken, PhD

Jörg Vienken graduated in Chemical Engineering at the Technical University of Darmstadt and received a Doctoral Degree in Biophysics and Bioengineering from the Technical University of Aachen, both in Germany. He was then appointed the position of an Associate Professor at the Institute for Biotechnology of the University of Würzburg, Germany.



In 1985, he switched to the medical device industry and worked for 11 years at AKZO NOBEL Membrana in Wuppertal as Director for Clinical Research and Science Services, followed 1996 by a position as Vice President BioSciences in Fresenius Medical Care in Bad Homburg, Germany which he held until his retirement in 2013. From 2013 – 2015 he served as Board Member of Nephro-Solutions AG in Hamburg and is working since 2016 as a Freelance Advisor for the Medical Device Industry.

He has been awarded the “Emil-Bücherl-Award” for life-time achievement in the realm of Artificial Organs from the European Society for Artificial Organs (ESAO) and is a distinguished fellow of ERA-EDTA, the European Dialysis and Transplantation Association.

Jörg Vienken is Past President of the International Federation of Artificial Organs (IFAO, representing the umbrella organisation of the continental societies from Europe (ESAO), the USA (ASAIO) and Japan (JSAO)). He was a long lasting Board member of the European Society for Artificial Organs (ESAO) and served as its secretary treasurer between 1998 and 2006. He is also Past President of the Association of German Biotech Companies (VBU- DECHEMA).

Jörg Vienken still teaches Biomaterials and Artificial Organs at several German and European Universities and has published more than 300 scientific publications and book chapters as well as 8 books.

David vs Goliath – Bacteria, endotoxins and biofilms

Once, medical devices are introduced to the market place, they have to be free of both, bacteria (sterility) and their endotoxic components (absence of pyrogens). This is of paramount importance because we currently observe an increasing threat of multiresistent germs, when standard antibiotics have lost their killing activity. The manufacturing staff of medical devices, physicians and nurses should also focus on precise and careful techniques of handwashes to avoid cross-contamination. Microbial germs may, e.g., survive due to inadequate hand drying after handwash or an incautious exchange of protecting collars.

Bacteria and endotoxins In general, bacterial strains differ in the composition of their cell wall and as a consequence show different results in the germ-staining assay introduced by the Danish scientist Hans Christian Gram (1853–1938). This staining characterizes microbial cells as Gram[+] and Gram[-] cells. Their potential outweighs by far the properties of other biological cells in terms of their numbers, growth rates, shapes and flexibility to survive even odd situations. The growth rate of bacteria considerably depends on environmental conditions, i.e. temperature and nutrient conditions. The main toxic compound of bacterial cells are endotoxins (from Gram[-] cells) and exotoxins (from Gram[+] cells. Endotoxins (ETs) derive from the external cell membrane of Gram[-] germs and consist of a lipophilic head group (Lipid A) and a polysaccharide tail. This is, why they are also called „lipopolysaccharides (LPS)“. It is interesting to note, that the toxic behaviour increases with a branching of the polysaccharide chain. Endotoxin contamination can be assessed by either the Limulus Amoebocyte Lysate test (LAL-test) or by the release of cytokines after contact of ETs with mononuclear white blood cells. Both assays are described in many national Pharmacopoeias. They show that a direct general relationship between germ count and amount of possibly released endotoxins does not exist. Thus, endotoxin analyses without the simultaneous determination of present germ strains is invalid.

Biofilms When bacteria adhere to infaces (solid/liquid; liquid/gas, gas/solid) they actively produce a mucous extracellular polymeric matrix (EPS) consisting of > thousand different compounds. This protects germs from antibacteridal agents and promotes the exchange of information between neighbouring cells, based on a phenomenon called „*Quorum sensing*“. Bacterial biofilms are a common cause of persistent infections and The desintergration of biofilms is extremely difficult. Treatment with chemical agents is mostly unsuccessful, and may even increase the the concentration of released endotoxins due to a degradation of bacteria. Under normal conditions only physical forces may help fort he removal of biofilms.

Artificial Membranes for Life Sciences: Lessons learnt from dialysis applications

Membranes for haemodialysis represent a unique success in medical device application. It spans a time frame from haemodialysis as an experimental therapy to today's routine application. In the early 1980ies, the number of dialysis patients worldwide depended on the availability/production capacity of dialysis membranes and increased accordingly. Today, due to the continuous increasing patient numbers, reaching a figure of 2,5 million in 2016, capillary membranes for dialysis have become a commodity with an annual production of more than 600 million km. This is equivalent to four times the distance between the Earth and the Sun. During the optimisation of membrane production and application, a series of learning curves had to be adopted which might yield some information for the use of membranes in other realms of clinical application.

Membrane performance: Recent years have seen a shift in the dialysis market from low- to high flux membranes. They differ in their ultrafiltration coefficient (UFC) or their hydraulic permeability. This can be explained by the still unknown profile of uremic retention solutes to be removed. The target of current concepts is, therefore, the removal of molecule families rather than of individual moieties. High ultrafiltration rates using the principle of solvent drag are, thus applied with hemodiafiltration as a major treatment modality. Blood compatibility of dialysis membranes has been successfully achieved by the selection of appropriate polymers. It is interesting to note, that polymers bearing hydroxyl-groups provoke the activation of the complement system and may stimulate adverse events. The golden polymer standard for haemodialysis has turned out to be poly-sulfone and its derivatives. All membrane manufactures in the world are now using this polymer due to its versatile character.

Membrane leachables: Survival of patients suffering from end stage kidney disease and treated by haemodialysis therapy has increased in recent years. Thus, the long term and repeated exposure of patient blood to foreign surfaces, i.e. membranes, tubing and device housing opens the door for leachables from the polymer bulk to be eluted to blood circulation. Among them are plasticizers and polymer compound, such as bis-phenols. These molecules are also called endogenous hormones, because they may interfere with receptors for sexual hormones and initiate unwanted signals to cells and tissue. Research focus of recent years has been directed towards their removal or avoidance.

Membrane sterilisation procedures: Membranes belong to the category of medical devices and have to be sterile and pyrogen free prior to final clinical application. Five sterilisation techniques are currently used for this purpose, i.e., ethylene oxide, steam, γ - and β -irradiation, as well as aldehydes (formalin, glutardialdehyde). Clinical adverse events have been observed when some sterilisation techniques have interfered

with individual membrane polymers. Knowledge on these possible adverse events is thus crucial.

Membranes, as scaffolds for biological cells: Current *in vitro* and *in vivo* research is directed towards the development membrane devices to be used as 3D scaffolds for the culture of biological cells. As a consequence, investigations of surface properties, in terms of polymer purity, membrane design and 3D geometry are of paramount importance.

Membranes for the use in haemodialysis have proven their versatility for many different applications. Results and related experience of *in vitro* investigations and of clinical application on such devices may serve as a common background for membrane applications in life sciences.

Prof. Tomasz Sosnowski, PhD

Vice-Dean for Scientific Affairs of the Faculty of Chemical and Process Engineering at Warsaw University of Technology.

He received his PhD (in 1997) and DSc degree (habilitation, 2006) from Warsaw University of Technology for the research related to dynamic interfacial phenomena and their relevance for hydrodynamics and mass transfer in the human respiratory system. He was a post-doc fellow at Lovelace Respiratory Research Institute in Albuquerque, USA (1999-2000) where he worked on aerosol systems for drug delivery by inhalation. From that time problems of chemical engineering applications in biomedicine have remained his main field of scientific activity. Prof. Sosnowski is an author of more than 60 scientific papers in JCR journals and more than 200 other scientific publications (journal papers, book chapters, conference communications). In 2010 he published a book “Respirable aerosols and inhalers” (in Polish; 2nd edition in 2012) which was focused on the application of engineering methods in designing medical inhalers, analysis of aerosol flow and particle-lung interactions. He is a co-author of 3 granted patents and several patent applications. He is also a scientific expert of European Medicines Agency (EMA – London), a member of the Managing Committee of the European Initiative COST MP1106, and a member of the Committee of Chemical and Process Engineering, Polish Academy of Sciences (PAN).



Aerosol and health – the engineer’s perspective

Aerosols present in the atmosphere are often responsible for adverse health effects. Particulates with various sizes, known as PM₁₀, PM_{2.5} and PM₁, contribute to formation of environmental smog which has significant social and economic consequences. Protection of the respiratory system against inhaled aerosols becomes a vital issue although it cannot totally reduce the risk of lung diseases, which must be then effectively treated. Such therapy often uses the same way of drug delivery, that is the inhalation of medical aerosols. All mentioned issues can be controlled only by gaining knowledge on aerosol flow, regional deposition inside air filters and in the respiratory system, and, finally, on the mechanism of direct interactions of deposits with the lung surface. These problems remain within the domain of physics and engineering, therefore must be identified and solved by scientific methodology of these disciplines.

The lecture will highlight all above-mentioned issues. Starting from the basic knowledge on aerosol dynamics, the essential information on the impact of physical parameters on aerosol particles’ deposition (both inside air filter and lungs) will be demonstrated. Then the interactions between inhaled particles and lung fluids (surfactant and mucus) will be discussed to show the importance of particles properties for the health response. Finally, the essential information on aerosol drugs delivered to the lungs will be given, indicating some engineering strategies which should be applied to increase the efficiency of aerosol therapy.

Acknowledgement:

Part of this work is related to NCN project No. 2014/13/B/ST8/00808 “Specific aspects of physicochemical phenomena and mass transfer in lung fluids in the presence of inhaled micro- and nanoparticles with complex properties”.

Prof. Shinji Sakai, PhD

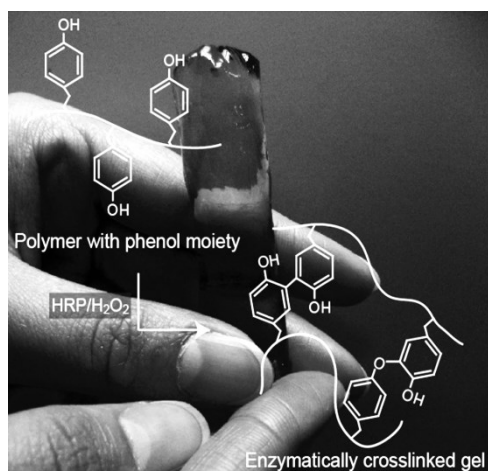
He is a full professor at the Department of Engineering Science, Faculty of Chemical Engineering of the Osaka University (Japan). Prof. Sakai received his PhD (2002) from Kyushu University (Japan). He has 110 scientific publications in international journals since 2000, mainly in the field of biomaterial. He received Young Scientist Award of Chemical Engineering Society of Japan for a development of novel cell-encapsulation process using laminar flow in 2008. He studied in Warsaw University of Technology for 4 months in 2015 (Prof. Tomasz Ciach's Lab).



His current work is a development of novel hydrogels and the processes using the hydrogels for biomedical applications. Especially, He is enjoying bio-printing using his hydrogels.

Tissue engineering using enzymes

Recently, enzyme-mediated cross-linking attracts attention as a useful route for obtaining hydrogels under mild condition for cells, e.g., at neutral pH, at physiological temperature, and with negligible heat generation. Among the enzymes catalyzing hydrogelation, horseradish peroxidase (HRP) has been vigorously studied



Photograph of hydrogel obtained from carboxymethyl cellulose derivative possessing phenolic hydroxyl moieties through HRP-catalyzed cross-linking.

because of the rapid hydrogelation after the report for hydrogelation of aqueous solution of hyaluronic acid derivative. HRP catalyzed the coupling of phenol and aniline derivatives using hydrogel peroxidase as an oxidant (Figure 1). An attractive point of the hydrogelation of using HRP is a possibility of preparing hydrogels from derivatives of varieties of polymers by introducing phenolic hydroxyl moieties to them. In this presentation, I will talk for our studies of using enzymes, not only HRP but also other enzymes, for fabrication of tissues such as spherical tissues, tubular tissues, and the tissues containing vascular-like network (1-4).

References:

- [1] S. Sakai, S. Ito, Y. Ogushi, I. Hashimoto, N. Hosoda, Y. Sawae and K. Kawakami, "Enzymatically fabricated and degradable microcapsules for production of multicellular spheroids with well-defined diameters of less than 150 μm ", *Biomaterials*, 30:5937(2009).
- [2] S. Sakai, H. Inagaki, K. Inamoto and M. Taya, "Wrapping tissues with a pre-established cage-like layer composed of living cells", *Biomaterials*, 33:6721(2012).
- [3] S. Sakai, Y. Liu, M. Sengoku and M. Taya, "Cell-selective encapsulation in hydrogel sheaths via biospecific identification and biochemical cross-linking", *Biomaterials*, 53:494(2015).
- [4] Y. Liu, S. Sakai and M. Taya, "Engineering tissues with a perfusable vessel-like network using endothelialized alginate hydrogel fiber and spheroid-enclosing microcapsules", *Heliyon*, 2, e00067 (2016).

Prof. Ilya Vorotyntsev, PhD

Ilya Vorotyntsev received his M.S. and PhD degrees in Physical Chemistry from Lobachevsky University (Russia). He spent several years in industry working on the products launch of ultra-high purity gases for semiconductors industry. In 2005, he joined Nizhny Novgorod State Technical University n.a. R.E.



Alekseev (NNSTU) to continue his teaching and research in the membrane area. In 2013, he became a Professor in NNSTU. His research activity covers material science, membrane gas separation, hybrid and integrated process. In 2016, his research group was awarded «Green Chemistry for Live», sponsored by UNESCO's International Basic Sciences Program (IBSP) and PhosAgro in close cooperation with IUPAC.

Perspective of membrane gas separation applications

The membrane technologies are highly demands in a wide range of practical application, especially in water treatment, food industry production (wine, beer, juice, milk etc.) The membrane gas separation is a technology with a high potential for implementation to the chemical industry connected with separation and purification.

The advantages of membrane gas separation make it desirable as a technology with the high potential for implementation to the chemical industry connected with separation and purification, i.e. energy-efficiency, simplicity of scalability and low material consumption. Moreover, the same mass-exchange apparatus could be used for different processes just by change the membrane inside.

The membrane gas separation is developed by two approaches, first is new membrane materials synthesis, and the second is improvements of operating system design, including membrane cascade schemes. In our group, we are realizing both. For the first time, it has been experimentally and theoretically shown that novel pulsed retentate approach during membrane gas separation provides higher separation efficiency as compared to traditional steady-state operation at the same productivity [1]. Through the example of polar gases high purification, it has been obtained that novel method of rectification under elevated pressure in conjunction with membrane gas separation allows significantly decrease energy intensity of the process and increase product yield, reducing the environmental load of the technology. The promising approach of acidic gases separation based on utilization of supported liquid membranes containing ionic liquids (ILs) as an absorbent [2]. And there where realized the combination of both approach in one membrane apparatus which lead us to the better results.

Acknowledgments

This work was financially supported by the Russian Science Foundation (project 15-19-10057) and Grant of the President of the Russian Federation for early stage researchers (MD-5415.2016.8).

References:

- [1] M.M. Trubyanov, etc. //Journal of Membrane Science. 2017. DOI: 10.1016/j.memsci.2017.01.064
- [2] Akhmetshina A.I. etc. //Separation and Purification Technology. 176 (2017) 176. 92-106. DOI: 10.1016/j.seppur.2016.11.074

Assist. Prof. Masaki Nakahata, PhD

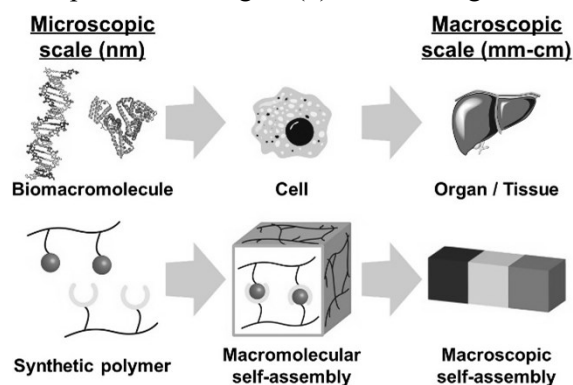
He is an assistant professor at Department of Engineering Science, Faculty of Chemical Engineering, Osaka University (Japan). He received his PhD (2015) from Department of Science, Osaka University. He has 13 publications in international journals since 2011, mainly in the fields of supramolecular chemistry and materials science. He received 9 awards including JSPS Ikushi Prize (2015) and Inoue Research Award for Young Scientists (2016). His current research interest includes engineering new biomaterials based on smart molecular design.



Engineering functional polymeric materials cross-linked by intermolecular interactions

In biological systems, biomacromolecules such as DNA and protein self-assemble via various kinds of molecular recognition. They form functional self-assemblies from microscopic to macroscopic scale in a hierarchical manner. Inspired by biological systems, researchers in the field of supramolecular chemistry have developed a series of functional self-assemblies formed by synthetic polymers. Especially, polymers modified with molecular recognition moieties have been studied intensively in recent years (Fig. 1).

This work focuses on functional polymer gels cross-linked by various kinds of molecular recognition via intermolecular interaction such as host-guest interaction, hydrogen bonds, anion-cation interaction, and dynamic covalent bonds. Polymers or polymeric gels modified with molecular recognition moieties exhibit various functions such as (1) formation of a supramolecular gel, (2) self-healing due to reversible nature of the interaction, (3) macroscopic motion due to stimuli-responsiveness, (4) adhesion between gels via specific interaction, and (5) unique mechanical properties such as flexibility and toughness. This lecture provides an overview of recent “supramolecular polymeric materials”, an emerging field in materials science and engineering.



Functional self-assemblies in biological systems and artificial systems

Marta Mazurkiewicz-Pawlicka, PhD

Dr. Marta Mazurkiewicz-Pawlicka works at the Graphene Laboratory at the Faculty of Chemical and Process Engineering, Warsaw University of Technology. She finished her PhD in 2015 at the Faculty of Materials Science and Engineering, Warsaw University of Technology. Her thesis entitled “Preparation and characterization of palladium catalysts deposited on multi-walled carbon nanotubes for use in a direct formic acid fuel cell”. She is a co-author of 27 publications in international journals mainly on the topic of carbon nanomaterials. Her research activity focuses on the preparation, modification and applications of different carbon nanomaterials (including carbon nanotubes, graphene oxide and carbon nanofibers) in alternative energy sources.



Carbon nanomaterials for energy storage and conversion applications

The global population is growing very fast resulting in an increase for energy consumption. It has been estimated that the demand for energy will double by 2050 and triple by 2100. The growing consumption of energy increases the emission of greenhouse gases and environmental pollution. The supplies of the fossil fuels decrease drastically. In order to overcome the environmental problems and to meet the demand for energy, alternative solutions are being considered. Therefore, energy storage (supercapacitors, batteries, etc.) and conversion (solar cells, fuel cells, etc.) technologies have been in the main interest of many research groups. Their main activities focus on developing high performance and lower cost materials for these applications. Carbon nanomaterials, due to their excellent mechanical, electrical, thermal and optical properties are promising materials for these technologies.

This presentation will focus on the recent advancements and future possibilities of carbon nanomaterials, such as fullerenes, carbon nanotubes, or graphene in the energy storage and conversion applications, especially in fuel cells, supercapacitors, batteries and solar cells.

Articles

Sorption of heavy metal cations using natural zeolites

*Kamila Brylewska^{1,2}

¹Faculty of Materials Science and Ceramics, AGH University of Science and Technology, Krakow, POLAND

²Faculty of Chemistry, Jagiellonian University, Krakow, POLAND

e-mail: kamilaaa@agh.edu.pl

Keywords: *zeolites, heavy metal cations, IR studies, sorption, environmental protection*

ABSTRACT

The ongoing degradation of the natural environment, connected mostly with human activity, has been a significant issue for some time now. The contamination of soil, water, and air is related mainly to the presence of heavy metal cations and inorganic anions as well as pollutants such as municipal or industrial wastewater. These contaminants have adverse effects on both animal and plant life, and their constantly rising levels have become an increasingly significant issue. The technologies used to purify waste need to be both efficient and environmentally friendly. For this reason, widely available, inexpensive and natural mineral materials with advantageous sorption properties are highly desired. In this regard, zeolites are very promising, as they can be applied to immobilize both heavy metal cations and certain inorganic anions. Volatile organic compounds (VOCs), which constitute 60% of all substances that pollute the atmosphere (including smog), pose an additional threat. Zeolites appear to be the perfect sorption material in the protection of both water and air.

The paper presents a literature review on sorption performed using natural zeolites, in particular natural clinoptilolite.

INTRODUCTION

The problem of environmental pollution

Recently, there is a growing trend of environmental degradation related predominantly to human activity. Pollutants such as municipal or industrial wastewater contribute to the contamination of soil, water, and air. Toxic and environmentally hazardous materials include most heavy metals and some inorganic anions. These substances adversely affect the environment, especially living organisms, causing numerous diseases. Volatile organic compounds (VOCs), which constitute 60% of all atmospheric pollutants, present yet another issue; 73% of such substances have been classified as carcinogenic compounds. They are also responsible for the formation of smog. These substances include combustion products such as aliphatic and aromatic hydrocarbons, among others. This is why it is extremely

important to find a solution which would allow the adverse effects connected with epicenters of pollution to be limited and to purify the already contaminated underground waters. This entails finding a solution to the problem of the simple and environmentally safe removal of the aforementioned pollutants, without excessive interference with the environment, and at the lowest viable cost. There are numerous methods of limiting the contamination of water, ranging from the application of a permeable reactive barrier (PRB), which can offer an alternative to passive and balanced in-situ remediation of groundwater, to the application of sorbents such as metallic iron [1], active carbon [2], or zeolite materials [3].

Zeolites

Zeolites are a subgroup of crystalline aluminosilicates, which have many catalytic, adsorption, molecular-sieve and ion-exchange properties. Owing to these properties, they have found application in many areas of industry, including the petrochemical industry [4], sorption processes [5], and environmental protection [6]. The last of these applications is very important because of the progressive degradation of the environment caused by human activity. The properties of these materials – especially sorption properties – stem from their structure, which is based on a three-dimensional framework of superimposed alumina $[AlO_4]^-$ and silica $[SiO_4]$ tetrahedra linked by shared oxygen atoms. The zeolite skeleton features a system of channels and cavities [7] arranged in an ordered way; their dimensions range from 4 to 12 Å. For this reason, these materials are classified as nanoporous materials; gas molecules or metal cations can freely diffuse through their structure. One of the possible arrangements of cavities of zeolite X can be seen in Fig. 1.

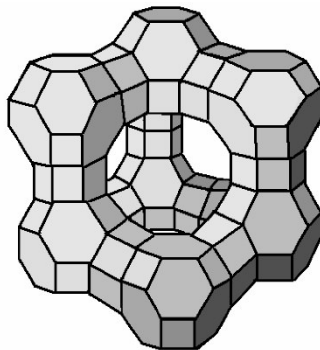


Fig. 1. Cavities of X zeolite [8].

There are numerous ways of classifying aluminosilicates, and one such division – natural vs. synthetic – is based on their origin. So far, the existence of 67 natural zeolites has been confirmed. They are found mainly in igneous and sedimentary rock. Although most natural zeolites are scarce, some are found in deposits that are sufficiently large to allow mining. These include clinoptilolite, mordenite, chabazite, analcime, erionite, phillipsite, and ferrierite.

Zeolites as adsorbents

Of the many different properties of zeolites, their sorption and ion-exchange capacity are the most important in the context of the present work. As a result of the Al→Si substitution in the tetrahedral positions, the net charge of the aluminosilicate skeleton is negative, which is compensated by the presence of calcium, magnesium, sodium or potassium cations as exchangeable cations. Because of the relatively loose structure of the afore-mentioned skeleton, these cations have great mobility and can be easily removed or replaced with other cations that exhibit a stronger affinity for the negatively charged structure of the materials, e.g. heavy metal cations (lead, cadmium, nickel, copper, etc.) [9] or ammonium ions [10]. This phenomenon is known as cation exchange.

Consequently, cations with this ability are called exchangeable cations to distinguish them from the Si and Al atoms that constitute part of the skeleton and do not undergo exchange under standard conditions. The ion-exchange capacity of natural zeolites is almost twice as high as that of clay minerals and can reach a level as high as 4 meq per 1 g of zeolite [11]. Due to their high cation-exchange capacity (CEC), these materials are widely used in processes such as the removal of heavy metals from aqueous solutions or the neutralization of radioactive waste. The natural zeolite clinoptilolite is an example of a zeolite which has excellent cation-exchange capacity. Its potential applications include the removal of cations from aqueous solutions via sorption, e.g. in the desalination of water and purification of drinking water [12]. As research has shown [13], clinoptilolite also strongly adsorbs the nitrogen in the ammonium molecule (NH₄-N) in water; however, the contaminants found on the surface of this material or in its channels may restrict its application.

Sorption mechanisms

In the case of zeolites, sorption processes occur mainly in a solid-liquid system and involve several mechanisms, including adsorption and ion exchange [14].

Adsorption is connected with changes in the concentration of a substance on the surface of the adjoining phases. These changes can be connected with the strength of intermolecular interactions (physical adsorption – Fig. 2.) or determined by the development of chemical bonds (chemisorption). Physical adsorption is generally a reversible process with a relatively high rate, and can result in the formation of more than one layer of adsorbed ions on the zeolite surface. On the other hand, in the case of chemisorption, the binding strength of ions on the external surface of the zeolite is related to the formation of chemical bonds, while the process involves the formation of stable inner-sphere complexes. Ions form a stable bond with surface functional groups – mostly OH⁻. It is assumed that chemisorption is an irreversible process.

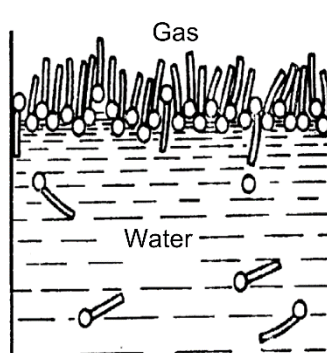


Fig. 2. The scheme of physical adsorption [15].

The second sorption mechanism is ion exchange, which involves the substitution of exchangeable ions weakly bound within the zeolite framework with metal ions present in the solution. This is possible due to the negative charge generated by the substitution of Si^{4+} with Al^{3+} in tetrahedral positions. As a result of the effect of the negative charge of the framework on the cations surrounded by water molecules, unstable outer-sphere complexes are formed; these complexes are attracted to the zeolite skeleton via electrostatic interactions [16].

Regardless of the mechanism, sorption is an equilibrium process, and the state of equilibrium can be represented graphically using adsorption isotherms, i.e. plots illustrating the dependence of the amount of adsorbed substance on the adsorbent concentration in a solution at a given temperature [17]. Any point of the isotherm corresponds to the equilibrium concentration of ions in the solution and the zeolite.

DISCUSSION

Sorption of heavy metal cations

Many research groups have extensively studied the issue of heavy metal sorption using zeolites [18]. The cation-exchange capacity of aluminosilicates is one of their most useful properties, allowing them to be used for heavy metal removal. Although this process involves both adsorption and ion exchange, the high sorption capacity of these materials can be attributed primarily to the latter phenomenon. The sorption capacity of zeolites has a tendency to decrease with increasing concentrations of heavy metals in water, and their selectivity is strongly affected by pH [18].

Despite the fact that sorption processes involving zeolites are relatively well-known and extensively described, some issues remain unsolved. These include the mechanisms that control the binding and release of metal cations, the determination of the strength of chemical bonds formed by specific ions, and the influence of various factors on the process in question. One of the main mechanisms observed in the sorption of heavy metals is ion exchange, which is defined as a stoichiometric, balanced exchange of ions in the solid phase or a balanced exchange of ions in the liquid phase. Chemisorption or intraspheric complexation are other

examples of such mechanisms. The ratio of the amount of heavy metal ions exchanged to the amount adsorbed on the surface of the zeolite depends mostly on the type of heavy metal. The sorption of heavy metals using natural clinoptilolite has been given considerable attention. Literature data [19] indicates that in the case of the sorption of lead(II) and chromium(III) by means of this zeolite, chemisorption is the dominant sorption mechanism, while in the case of nickel(III) and cadmium(II), ion-exchange and chemisorption both contribute to the same degree. On the other hand [6], investigations of the sorption of Pb^{2+} , Ni^{2+} , Zn^{2+} and Cd^{2+} cations using clinoptilolite and erionite have proven the higher sorption efficiency of erionite, which exhibited the following selectivity: $Pb^{2+} > Ni^{2+} > Zn^{2+} > Cd^{2+}$. This fact can be explained by the higher sorption capacity of erionite, while this particular selectivity is related to erionite's ionic radius and its electronegativity [6].

Sorption studies are often conducted for modified materials. Panayotova [20] used a natural zeolite found in Bulgaria and its modified versions to conduct a series of experiments aimed at removing metal ions. Modifying the zeolite with CH_3COONa and $NaCl$ solutions improved its ability to adsorb Ni^{2+} ions by 25-30%. In the presence of Ca^{2+} and Mg^{2+} ions, the adsorption of Cd^{2+} became much less effective, while zeolites modified with $NaCl$ and CH_3COONa exhibited the highest sorption capacity. Other studies [21] have shown that lead ions are strongly immobilized by the zeolite's structure, both in soft and hard water, and that modifying the zeolite with an $NaCl$ solution leads to accelerated immobilization.

In addition to natural zeolites, active sorbents also include iron oxides. Research on the synthesis of a mixture of iron oxide and clinoptilolite shows that they are capable of absorbing high concentrations of inorganic compounds [22]. According to Doula's reports [12,23], clinoptilolite doped with iron is effective at removing copper and manganese from drinking water. Studies have shown that doping clinoptilolite with amorphous iron oxides significantly improves its sorption capacity. Similar effects were observed in the case of clinoptilolite doped with Mg , $Mn(IV)$, or Al . The modified samples exhibited very desirable sorption properties vs. nitrate ions present in aqueous solutions [24].

Infrared spectroscopy as a tool for studying zeolites

Of the many research methods used to characterize the structure of aluminosilicate materials, oscillation spectroscopy deserves a special mention [25]. Numerous attempts have been made to apply this method to describe the structure of zeolites. However, the detailed interpretation of the measured spectra is a very difficult task. The introduction of selected ions and molecules affects the chemical, molecular-sieve and catalytic properties of a given zeolite structure and changes the effective dimensions of pore systems. Subsequently, changes in the IR spectra of the investigated materials should also be observed. The comparison of spectra before and after the sorption of selected ions makes it possible to determine their influence on the

structure of the sorbents and may facilitate the description and elucidation of the phenomena taking place during sorption processes.

Research conducted thus far shows that changes in the spectra in the range of bands corresponding to the lattice and pseudo-lattice vibrations induced by the sorption of heavy metal cations may play the role of an indicator of sorption processes [26]. For example, the introduction of heavy metal cations into the structure of mordenite [27] results mainly in a change in the integral intensity of a band at ca. 460 cm^{-1} , connected with occurrence of 5 member-rings (Fig. 3.). Similar changes have been observed for natural clinoptilolite [28]. It has been assumed that changes in the oscillation spectra will allow the influence of cations on the structure of sorbents to be determined, and will facilitate the description and elucidation of the phenomena that occur during sorption processes.

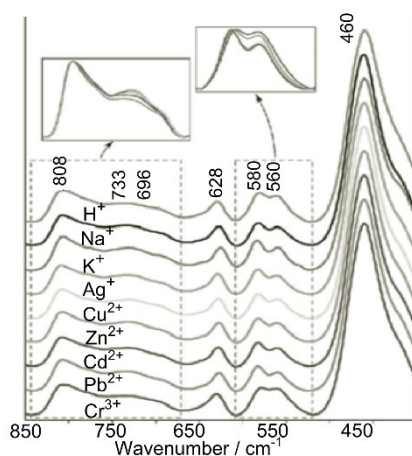


Fig. 3. MIR spectra of mordenite after the sorption of heavy metal cations [27].

Due to the complexity of zeolite structures, a detailed interpretation of the vibrational spectra requires the use of certain computational methods that allow the accurate assignment of bands to different types of vibrations. Theoretical *ab initio* calculations are often performed for model structures, and may provide valuable information as to the manner in which the analyzed metals are bound and distributed in the zeolite structure and, subsequently, on the shape of the spectra [25]. Based on these results, it is possible to obtain spectra for theoretical model units and identify their specific oscillations and corresponding bands in IR and Raman spectra [29]. Identification of ring vibrations typical of supertetrahedral structural elements (secondary building units, SBUs) is important with regard to obtaining information on the zeolite skeleton. Based on the correlation between the computational and experimental spectra of real zeolites, it is possible to determine which ring bands are associated with vibrations specific to SBUs in the zeolite structure [30]. It is also possible to obtain information about the impact of exchangeable cations introduced into the structure during sorption processes on the recorded spectra.

CONCLUSIONS

In summary, the unique properties of zeolite materials can be utilized in numerous applications. In addition, the fact that some deposits of these materials are available and their acquisition is not associated with large financial investments is not insignificant. Zeolites, especially natural ones, are very good sorbents of heavy metal cations.

ACKNOWLEDGMENTS

This work was financially supported by the National Science Centre in Poland as part of grant no. 2016/21/N/ST8/01332.

REFERENCES

- [1] Moraci N., Calabro P.S., Heavy metals removal and hydraulic performance in zero-valent iron/pumice permeable reactive barriers, *Journal of Environmental Management*, 2010, 91, 11, 2336-2341, DOI: 10.1016/j.jenvman.2010.06.019
- [2] Mansour M.S., Ossman M.E., Farag H.A., Removal of Cd(II) ion from waste water by adsorption onto polyaniline coated on sawdust, *Desalination*, 2011, 206, 301-305, DOI: 10.1016/j.desal.2011.01.037
- [3] Misaelides P., Application of natural zeolites in environmental remediation: A short review, *Microporous and Mesoporous Materials*, 2011, 144, 15-18, DOI: 10.1016/j.micromeso.2011.03.024
- [4] van Donk S., Janssen A.H., Bitter J.H., de Jong K.P., Generation, characterization, and impact of mesopores in zeolite catalysts, *Catalysis Reviews*, 2003, 45, 2, 297-319, DOI: 10.1081/CR-120023908
- [5] Wu Z., Zhao D., Ordered mesoporous as adsorbents, *Chemical Communications*, 2011, 47, 3332-3338, DOI: 10.1039/C0CC04909C
- [6] Tangkawanit S., Rangriwatananon K., Dyer A., Ion exchange of Cu²⁺, Ni²⁺ and Zn²⁺ in analcime (ANA) synthesized from Thai perlite, *Microporous and Mesoporous Materials*, 2005, 79, 1-3, 171-175, DOI: 10.1016/j.micromeso.2004.10.040
- [7] Taffarel S.R., Rubio J., Adsorption of sodium dodecyl benzene sulfonate from aqueous solution using a modified natural zeolite with CTAB, *Minerals Engineering*, 2010, 23, 10, 771-779, DOI: 10.1016/j.mineng.2010.05.018
- [8]http://www2.chemia.uj.edu.pl/dydaktyka/Procesy_Sorpcyjne.pdf (available: 18.01.2017)
- [9] Bektas N., Kara S., Removal of lead from aqueous solutions by natural clinoptilolite: equilibrium and kinetic studies, *Separation and Purification Technology*, 2004, 39, 3, 189-200, DOI: 10.1016/j.seppur.2003.12.001
- [10] Karadag D., Tok S., Akgul E., Turan M., Ozturk M., Demir A., Ammonium removal from sanitary landfill leachate using natural Gördes clinoptilolite, *Journal of Hazardous Materials*, 2008, 153, 1,2, 60-66, DOI: 10.1016/j.jhazmat.2007.08.019
- [11] Ulmanu M., Chapter in the book: Mineralogy of Natural Zeolites, *Handbook of Natural Zeolites*, Bentham Science Publisher, 2012

- [12] Doula M.K., Removal of Mn^{2+} ions from drinking water by using clinoptilolite and a clinoptilolite-Fe oxide system, *Water Research*, 2006, 40, 70, 3167-3176, DOI: 10.1016/j.watres.2006.07.013
- [13] Mackinnon I.D.R., Millar G.J., Stolz W., Low temperature synthesis of zeolite N from kaolinites and montmorillonites, *Applied Clay Science*, 2010, 48, 4, 622-630, DOI: 10.1016/j.clay.2010.03.016
- [14] Zhao G., Wu X., Tan X., Wang X., Sorption of Heavy Metal Ions from Aqueous Solutions: A Review, *The Open Colloid Science Journal*, 2011, 4, 1, 19-31, DOI: 10.2174/1876530001104010019
- [15] <http://absta.pl/adsorbatem-a-substancja-na-ktrej-ten-proces-zachodzi--adsorben.html> (available: 18.01.2017)
- [16] Doula M.K., Ioannou A., The effect of electrolyte anion on Cu adsorption-desorption by clinoptilolite, *Microporous and Mesoporous Materials*, 2003, 58, 2, 115-130, DOI: 10.1016/S1387-1811(02)00610-8
- [17] Sarbak Z., Chapter in the book: *Adsorpcja i adsorbenty. Teoria i zastosowanie*, Wydawnictwo Naukowe Uniwersytetu im. Adama Mickiewicza, Poznań, 2000.
- [18] Inglezakis V.J., Loizidon M.D., Grigoropoulou H.P., Ion exchange of Pb^{2+} , Cu^{2+} , Fe^{3+} and Cr^{3+} on natural clinoptilolite: selectivity determination and influence of acidity on metal uptake, *Journal of Colloid and Interface Science*, 2003, 261, 1, 49-54, DOI: 10.1016/S0021-9797(02)00244-8
- [19] Mozgawa W., Bajda T., Spectroscopic study of heavy metals sorption on clinoptilolite, *Physics and Chemistry of Minerals*, 2005, 31, 10, 706-713, DOI: 10.1007/s00269-004-0433-8
- [20] Panayotova M., Kinetics and thermodynamics of removal of nickel ions from wastewater by use of natural and modified zeolite, *Fresenius Environmental Bulletin*, 2001, 10, 3, 267-272.
- [21] Panayotova M., B. Velikov, Kinetics of heavy metal ions removal by use of natural zeolite, *Journal of Environmental Science and Health Part A-Toxic/Hazardous Substance*, 2002, 37, 139-147, DOI: 10.1081/ESE-120002578
- [22] Dimirkou A., Ioannou A., Kalliannou Ch., Synthesis-identification of hematite and kaolinite-hematite (k-h) system, *Communications in Soil Science and Plant Analysis*, 1996, 5-8, 27, 1091-1106.
- [23] Doula M., Synthesis of a clinoptilolite-Fe system with high Cu sorption capacity, *Chemosphere*, 2007, 67, 4, 731-740, DOI: 10.1016/j.chemosphere.2006.10.072
- [24] Pavlovic J., Milenkovic J., Stojakovic D., Rajic N., Surface modification of the natural clinoptilolite for its potential use for the nitrate removal from water media, *Serbian-Croatian-Slovenian Symposium on Zeolites – 5 th Edition Proceedings*, 2013, 112-115.
- [25] Mikuła A., Król M., Koleżyński A., The influence of the long-range order on the vibrational spectra of structures based on sodalite cage, *Spectrochimica Acta Part A-molecular and Biomolecular Spectroscopy*, 2015, 144, 273-280, DOI: 10.1016/j.saa.2015.02.073

- [26] Król M., Mozgawa W., Jastrzębski W., Barczyk K., *Application of IR spectra in the studies of zeolites from D4R and D6R structural groups*, *Microporous and Mesoporous Materials*, 2012, 156, 181-188, DOI: 10.1016/j.micromeso.2012.02.040
- [27] Król M., Mozgawa W., Barczyk K., Bajda T., Kozanecki M., Changes in the vibrational spectra of zeolites due to sorption of heavy metal cations, *Journal of Applied Spectroscopy*, 2013, 80, 5, 644-650, DOI: 10.1007/s10812-013-9821-5
- [28] Mozgawa W., Król M., Bajda T., Application of IR spectra in the studies of heavy metal cations immobilization on natural sorbents, *Journal of Molecular Structure*, 2009, 924-926, 427-433, DOI: 10.1016/j.molstruc.2008.12.028
- [29] Mozgawa W., Handke M., Jastrzębski W., Vibrational spectra of aluminosilicate structural cluster, *Journal of Molecular Structure*, 2004, 704, 1-3, 247-257, DOI: 10.1016/j.molstruc.2004.01.059
- [30] Mozgawa W., Jastrzębski W., Handke M., Cation-terminated structural clusters as a model for the interpretation of zeolite vibrational spectra, *Journal of Molecular Structure*, 2006, 792-793, 163-169, DOI: 10.1016/j.molstruc.2005.12.056

Preparation, characterization and antitubercular activity of polymeric nanoformulation of isoniazid

*Monika Budnicka¹, Agnieszka Gadomska-Gajadur¹, Paweł Ruśkowski¹

¹Technological Processes Laboratory, Faculty of Chemistry, Warsaw University of Technology, Warsaw, POLAND

e-mail: mbudnicka@ch.pw.edu.pl

Keywords: *nanospheres, emulsion solvent evaporation method, drug delivery system, isoniazid, tuberculosis*

ABSTRACT

In this article, the experimental results of the preparation of polymeric nanoparticles with isoniazid (INH) were presented. The impact of agitation rate and the tacticity of the polylactide on obtained nanospheres size was examined. Antitubercular activity of obtained particles was studied.

Poly(L-lactide), poly(DL-lactide), a lactide and ϵ -caprolactone block copolymer, polycaprolactone nanospheres with INH were received. The greater agitation rate, the bigger size of obtained nanospheres. It was noted that the more D entities content in polylactide, the larger size of the obtained spheres. The resulting polymer nanospheres have antitubercular activity.

INTRODUCTION

The tuberculosis recurrence caused great interest of scientists in many research centers [1-4]. The disease can be controlled using the known active pharmaceutical ingredient (API), namely correcting their release profile, while allowing the same to improve their therapeutic index and ultimately the overall effectiveness of treatment. A drug delivery system (DDS) using existing antituberculosis substances is a possible solution against tuberculosis. Generally DDS system enables the circulation time of API in blood prolongation, as well as therapeutic protection against rapid metabolism and side effects reduction [5-7]. Nanoparticles of active substances - one of DDS forms are of great interest [8-10]. Polymer nanospheres are promising form of DDS [11]. Due to the small size they can be administered intravenously without the risk of blood clots, easily penetrate the smallest capillaries, tissues and cells [12-14].

Because of the need for invention effective but safe, short term and comfortable therapy our team decided to develop new therapeutic system consisting of polymeric nanospheres with antitubercular substance - isoniazid (INH). The aims of this study were to obtain a polymer nanospheres containing isoniazid, to determine the effect of input variables on the process of encapsulation. Then to examine INH release profile from nanospheres and to determine INH biological activity in the polymer matrix. A method of nanospheres preparation emulsion solvent evaporation

was selected, because of its simplicity, lack of sophisticated equipment and the possibility of obtaining spheres of relatively small size [15-18].

MATERIALS AND METHODS

Materials

Poly(L-lactide) (PLLA) of M_n 4 000 g·mol⁻¹, poly(DL-lactide) (PDLA) of M_n 19 000 g·mol⁻¹ (30% D centers content), M_n 18 000 g·mol⁻¹ (50% D centers content), poly(lactide-b-co- ϵ -caprolactone) of M_n 16 500 g·mol⁻¹, poly- ϵ -caprolactone of M_n 16 000 g·mol⁻¹ were produced by Faculty of Chemistry of Warsaw University of Technology. Dichloromethane of analytical reagent grade was produced by POCH. Isoniazid (pyridine-4-carbohydrazide, 99%) was purchased from Fluco Analysis. Casein was produced by Sigma Aldrich. Poly(vinyl alcohol) (PVA) of M_w 31 000 g·mol⁻¹ (PVA 4_88), M_w 130 000 g·mol⁻¹ (PVA 18_88) were obtained from Mowiol. Poly(ethylene glycol) (PEG) of M_w 400 g·mol⁻¹, M_w 4000 g·mol⁻¹ were produced by Fluca. Gelatin was purchased from Gellwe. Ultrapure water with 18.2 M Ω cm conductivity was obtained using MiliQ device.

Polymeric spheres preparation procedure

Isoniazid (0.023 g) was dissolved in a solution of stabilizer (100 mL of a 0.01% or 0.1% or 1% wt. in water) in 250 mL round-bottom flask. The flask was stirred constantly at 300 or 600 or 900 rpm at 25°C. Then the polymer solution (5 mL of a 1% w/v in dichloromethane) was added dropwise to the flask over approx. 15 minutes. The flask was left open at 30°C for 1 h to evaporate the organic solvent. The aqueous spheres solution was filtered through a 3G Schott filter. Spheres size was estimated using DLS measurements.

Analytical methods

Spheres size measurements were performed using a Zetasizer Nano from Malvern Instruments, provided by the Chemistry and Polymer Technology Department, Faculty of Chemistry, Warsaw University of Technology.

Antitubercular activity of INH in the polymer matrix testing procedure

Polymer spheres suspensions of a concentration 230; 115; 57.5; 28.8; 14.4; 7.2 μ g/mL in water were prepared. INH solutions of a 100; 50; 25; 12.5; 6.2; 3.1 μ g/mL in water were prepared. 1 ml (suspension of spheres in water or INH solution in water) of each dilution was added to 20 mL of a tuberculosis bacteria (TB) medium. The minimum inhibitory concentration (MIC) was tested in Yumansa liquid medium with a 10% serum content. Strains height was read after 21 days of incubation. The study was performed at the Institute of Tuberculosis and Lung Diseases in Warsaw.

RESULTS AND DISCUSSION

Polymeric nanospheres with INH preparation using different polymers

Single emulsion method (o/w) was used to obtain polymeric nanospheres containing INH. The impact of agitation rate on the spheres preparation process was examined. Spheres were made of different polymers: poly(L-lactide) (PLLA), poly(DL-lactide) with 30% D centers content (PDLLA 3:7), poly(DL-lactide) with 50% D centers content (PDLLA 1:1), poly(lactide-b-co- ϵ -caprolactone) (PLA-b-PCL), poly- ϵ -caprolactone (PCL). The influence of the type of polymer on the spheres size was checked (Tab. 1.). INH concentration in the experiments was kept constant at approx. 50% by weight relative to the polymer. Process was carried out at constant temperature (25°C). For each experiment 5 mL of a 1% w/v polymer solution in dichloromethane was used. The concentration of the stabilizer was 0.1% w/v, the average molecular weight of poly(vinyl alcohol) was 130 000 g·mol⁻¹.

Tab. 1. The scope of the variables investigated in the INH encapsulation using different polymers.

Variable type	Variable value
Polymer	PLLA, PDLLA (3:7 D:L), PDLLA (1:1 D:L), PLA-b-PCL, PCL
Agitation rate	300, 900 [rpm]

Effect of agitation rate on the polymer spheres size

The agitation rate impact (300 or 900 rpm) to the spheres diameter was examined. As a polymer matrix was used: PDLLA (3:7) M_n 19 000 g·mol⁻¹, PDLLA (1:1) M_n 18 000 g·mol⁻¹, PLA-b-PCL M_n 16 500 g·mol⁻¹, PCL M_n 16 000 g·mol⁻¹. The constants were: temperature (25°C), PVA molecular weight (M_w 130 000 g·mol⁻¹). The resulting spheres size was compared to the results obtained in previous work for the PLLA spheres (M_n 4000 g·mol⁻¹) [19-20].

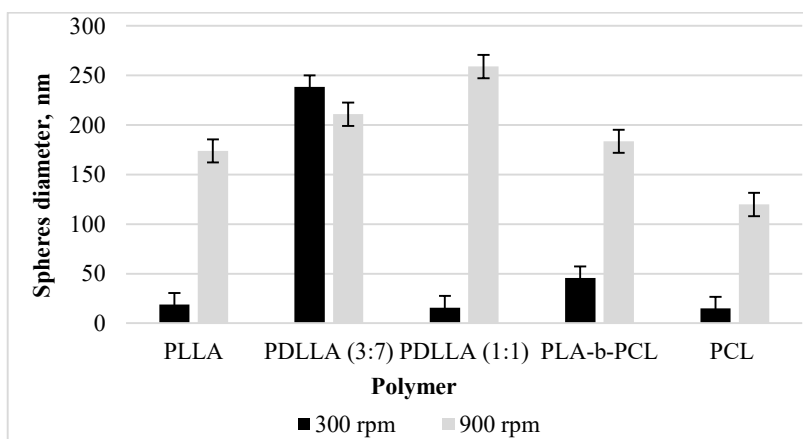


Fig. 1. Dependence of the spheres diameter on the type of polymer (PLLA, PDLLA (3:7), PDLLA (1:1), PLA-b-PCL, PCL) and agitation rate (300 or 900 rpm).

In all cases, spheres with a diameter not exceeding 270 nm were received (Fig. 1.). The increasing agitation rate, the bigger size of obtained particles. An exception was the PDLLA (3:7) spheres. The relationship confirms the compatibility of the results derived in previous work (for PLLA spheres).

The polylactide chain construction influence on the spheres size

The impact of polylactide tacticity on spheres size was examined. The constants were: temperature (25°C), PVA molecular weight (M_w 130 000 g·mol⁻¹). Variable was a mixing speed (300 and 900 rpm). Polylactides of three different stereochemical structure was applied:

- All units had the configuration L, M_n 4000 g·mol⁻¹,
- the ratio of D:L is 3:7, M_n 19 000 g·mol⁻¹,
- the ratio of D:L is 1:1, M_n 18 000 g·mol⁻¹.

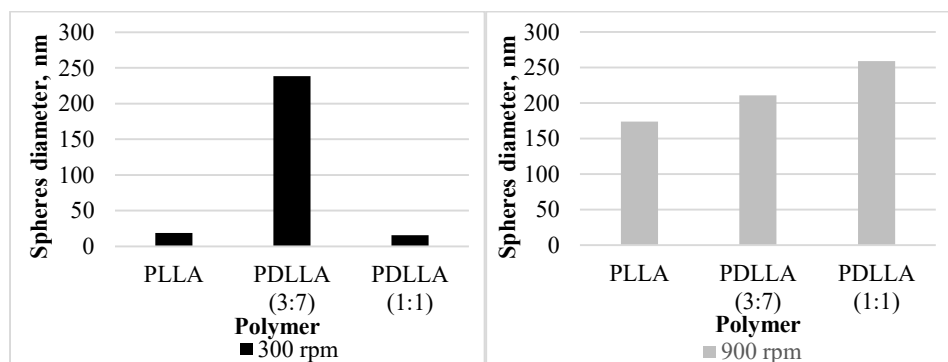


Fig. 2. The polylactide chain construction and polymer spheres size dependence at stirring rate of 300 and 900 rpm.

It is difficult to conclude how the construction of the PLA affects the particles size for a stirring rate of 300 rpm, due to the lack of a clear trend (Fig. 2.). In case of the agitation rate of 900 rpm, the more D units content, the bigger spheres size.

Stability studies of polymeric nanospheres with INH slurry using various emulsion stabilizers

Because of polymeric nanospheres with INH slurry instability after preparation in previous work, what complicates further spheres characterisation, it was decided to perform stability studies of nanospheres slurry using various emulsion stabilizers.

Preliminary studies of nanospheres preparation using various emulsion stabilizers

PLLA, PDLLA (3:7), PCL spheres with INH preparation preliminary studies was conducted using a single emulsion (o/w) method. Three emulsion stabilizers: casein, poly(ethylene glycol) (M_n 400 g·mol⁻¹ (PEG 400), and M_n 4000 g·mol⁻¹ (PEG

4000)), gelatin was examined. Aqueous solutions of stabilizers were used. Casein was solubilized with the addition of sodium carbonate (weight ratio of casein:sodium carbonate 2:1), due to the low solubility of casein in water. INH concentration in the experiments was kept constant at approx. 50% by weight relative to the polymer. The process temperature was kept constant at 25°C, stirring rate of 600 min⁻¹. 5 mL of a 1% w/v polymer solution in dichloromethane was used. The volume of stabilizer solution was 100 mL. The concentration of stabilizer was 0.1% or 1% w/v (Tab. 2.).

Tab. 2. Variables ranges in the INH encapsulation using various emulsion stabilizers.

Variable type	Variable value
Stabilizer concentration	0.1 or 1 [% w/v]
Stabilizer	casein, poly(ethylene glycol), gelatin

The results were compared to the outcomes gained in previous work, where for spheres preparation poly(vinyl alcohol) with a M_w of 30 000 g·mol⁻¹ (4_88 PVA) was used.

Stability study of nanospheres slurry using a poly(vinyl alcohol) as stabilizer

The stability of the nanospheres with INH suspension made of PLLA, PDLLA (3:7), PCL was examined. 0.1% (w/v) aqueous solution of poly (vinyl alcohol) (M_w 30 000 g·mol⁻¹, PVA 4_88) as a stabilizer was used.

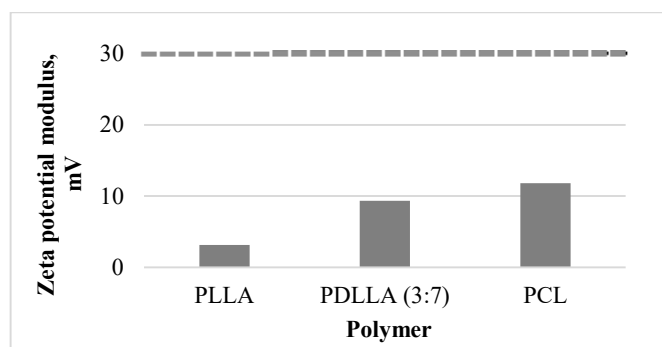


Fig. 3. Zeta potential modulus of PLLA, PDLLA (3:7), PCL nanospheres with INH suspensions using PVA of M_w of 30 000 g·mol⁻¹ as stabilizer (0.1% PVA v/w solution in water).

Zeta potential modulus of suspensions of nanospheres of all tested polymers had values less than 30 mV. In all cases the emulsions were not stable (Fig. 3.).

Poly(vinyl alcohol) did not allow to obtain a stable polymer nanospheres emulsion. Therefore it was decided to explore other stabilizers. As the polymer matrix in subsequent studies PLLA was chosen, which had been used in previous work.

The impact of emulsion stabilizer type on the PLLA nanospheres with INH suspensions stability

The contribution of the emulsion stabilizer (casein, gelatin, poly(ethylene glycol)) on the stability of the PLLA nanospheres with INH suspensions was examined. The stabilizer concentration was 0.1% and 1% v/w. In order to test the effect of sodium carbonate (used to improve the solubility of casein) on the stability of a PLLA spheres suspension, the solution of casein in a weight ratio casein:sodium carbonate of 2:1 and 1:1 were prepared.

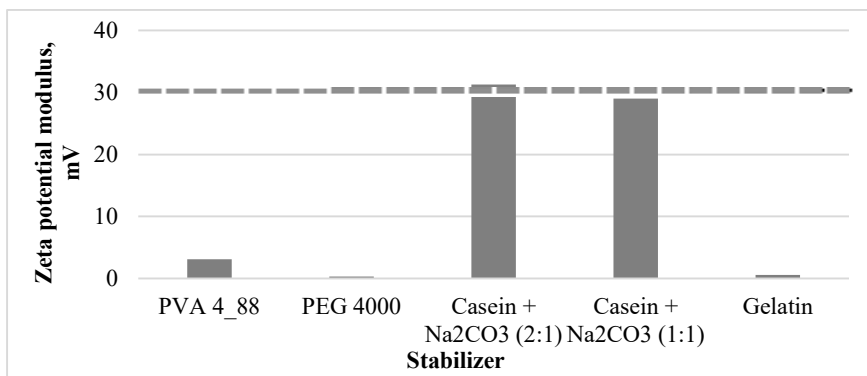


Fig. 4. Zeta potential modulus of PLLA nanospheres with INH emulsions stabilized with 4_88 PVA, PEG 4000, casein, gelatin (0.1% w/v stabilizer solution in water).

Where the stabilizers at a concentration of 0.1% w/v were used, only casein allowed to obtain a stable spheres emulsion (Fig. 4.). Other stabilizers e.g. PEG 4000, gelatin, PVA 4_88 gave unsatisfactory results. Using greater amounts of sodium carbonate (Na_2CO_2 + casein in a weight ratio of 1:1) had no significant improvement in stability. Therefore it was not used in the stabilizers examination at a concentration of 1% w/v.

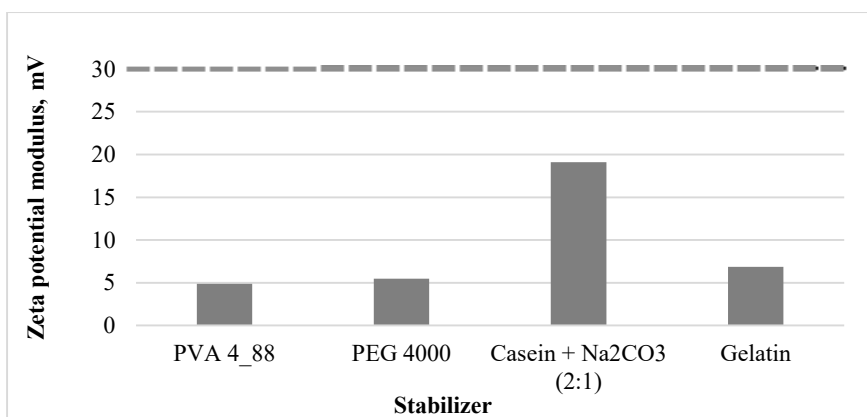


Fig. 5. Zeta potential modulus of PLLA nanospheres emulsions stabilized with 4_88 PVA, PEG 4000, casein, gelatin (1% w/v stabilizer solution in water).

Where the stabilizers at a concentration of 1% v/w were used, casein stabilized nanospheres suspension in contrast to other stabilizers showed increased stability. However, none of the stabilizers allowed to obtain stable nanospheres emulsion (Fig. 5.).

Casein solution made it possible to obtain a stable suspension of PLLA nanospheres with INH. It was decided to check, whether it is possible to obtain stable polymer spheres dispersions using other polymers.

Receiving of casein stabilized polymer nanospheres

Polymer nanospheres of PLLA, PDLLA (3:7), PDLLA (1:1), PLA-b-PCL, PCL with INH dispersed in the polymer matrix were received by a single emulsion (o/w). Aqueous solution of casein (emulsion stabilizer of 0.01% or 0.1% or 1% w/v) with sodium carbonate (weight ratio casein to sodium carbonate 2:1) was used. The process temperature was kept constant at 25°C, stirring rate of 600 min⁻¹. 5 mL of a 1% w/v polymer solution in dichloromethane was used. The stabilizer solution volume was 100 mL, the concentration of INH was approx. 50% by weight relative to the polymer. The effect of casein on the nanospheres suspensions stability and the nanospheres size was examined.

Casein impact on the stability of obtained polymer nanospheres dispersions

The impact of an aqueous solution of casein plus sodium carbonate to the stability of nanospheres suspensions from PDLLA (3:7), PDLLA (1:1), PLA-b-PCL, PCL was examined. The results were compared to PLLA. Stabilizer concentrations of 0.1% and 1% w/v were used.

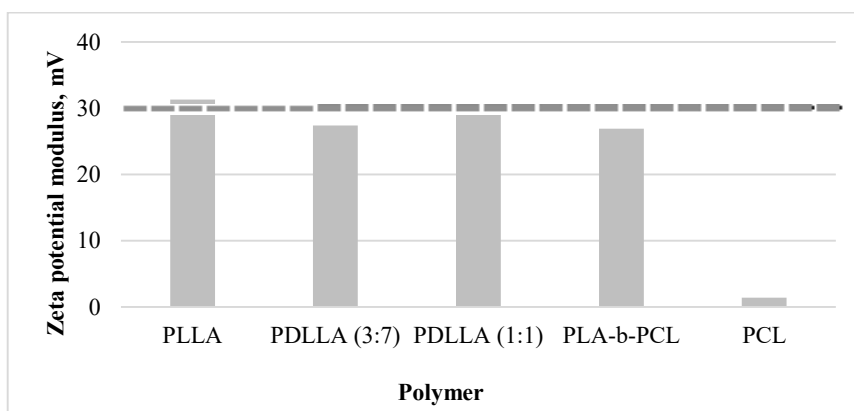


Fig. 6. Zeta potential modulus of PLLA, PDLLA (3:7), PLA-b-PCL, PCL nanospheres with INH emulsion stabilized with casein (0.1% w/v solution in water).

Using 0.1% w/v aqueous solution of casein as a stabilizer there was polylactide and PLA-b-PCL nanospheres with INH suspensions stability improvement. It was not observed for polycaprolactone spheres (Fig. 6.). In addition

to the PLLA nanospheres, PDLLA (1:1) nanospheres suspension met the stability condition.

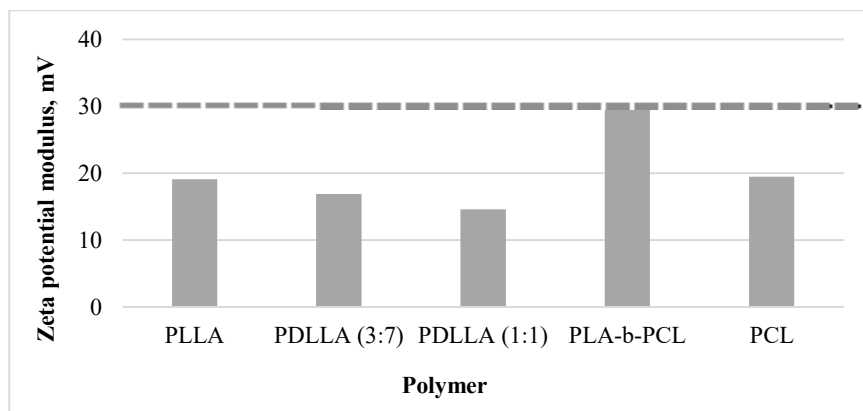


Fig. 7. Zeta potential modulus of PLLA, PDLLA (3: 7), PLA-b-PCL, PCL nanospheres emulsion stabilized with casein (1% w/v solution in water).

Using 1% w/v aqueous solution of casein, there was noticed polylactide nanosphere suspensions stability deterioration, and PLA-b-PCL nanosphere suspension stability improvement (Fig. 7.). PLA-b-PCL nanospheres suspension met the stability condition.

The influence of the casein concentration on the obtained polymer nanospheres size

The impact of an aqueous casein solution containing sodium carbonate on the size of the nanospheres obtained from PDLLA (3:7), PDLLA (1:1), PLA-b-PCL, PCL was examined. The results were compared to PLLA nanospheres. The casein concentration of 0.01% or 0.1% or 1% w/v was examined.

The use of an 0.01% w/v casein aqueous solution did not support the nanospheres receiving. Finally there was visible precipitated polymer flakes.

With an increase of casein aqueous solution concentration, the nanospheres size growth was observed. The exception was the PLLA nanospheres (Fig. 8.).

Both the aqueous solution of casein at a concentration of 0.1% and 1% w/v, there was nanoparticle size growth with an increasing D units content in the polylactide chain. These observation supports previous conclusions, as the poly (vinyl alcohol) as emulsion stabilizer was used.

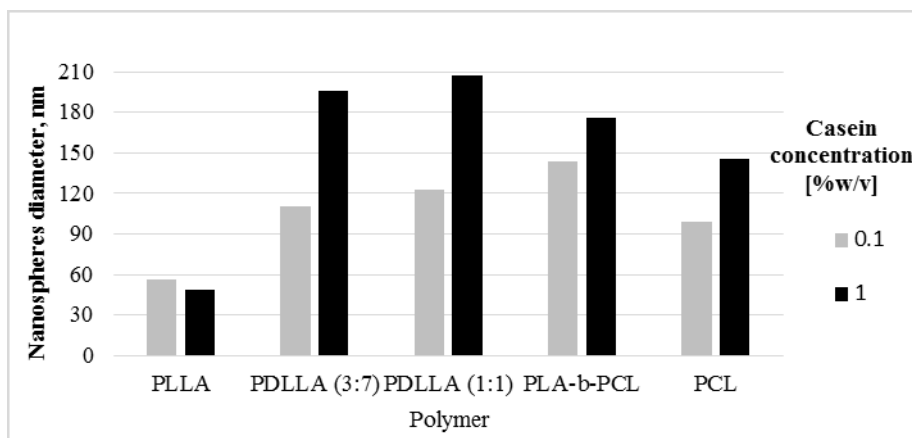


Fig. 8. PLLA, PDLLA (3:7), PDLLA (1:1), PLA-b-PCL, PCL nanospheres size dependence on the stabilizer concentration (aqueous casein solution of 0.1 or 1% w/v).

Antimycobacterial activity tests of polymer nanospheres with INH

Antimycobacterial polymer nanospheres tests were carried out on three strains of *M. tuberculosis*: H₃₇R_v, resistant to isoniazid No. 210, sensitive to isoniazid No. 192. The research was conducted at the Institute of Tuberculosis and Lung Diseases in Warsaw.

There was prepared eight samples of polymeric nanospheres with isoniazid suspensions using various polymers and stabilizers (Tab. 3.). The concentration of isoniazid in the samples after preparation was 230 µg/mL.

Tab. 3. Stabilizers and polymers used for the nanospheres preparation for activity testing (formulations 1-8).

No.	Stabilizer	Polymer
1	Casein + Na ₂ CO ₃ (2:1 w/w)	Polycaprolactone
2	Casein + Na ₂ CO ₃ (2:1 w/w)	Poly(DL-lactide)
3	Casein + Na ₂ CO ₃ (2:1 w/w)	Poly(lactide-b-caprolactone)
4	Casein + Na ₂ CO ₃ (2:1 w/w)	Poly(L-lactide)
5	PVA 4_88	Polycaprolactone
6	PVA 4_88	Poly(DL-lactide)
7	PVA 4_88	Poly(lactide-b-caprolactone)
8	PVA 4_88	Poly(L-lactide)

Aqueous spheres formulations in a concentrations of (INH concentration in the samples): 230; 115; 57.5; 28.8; 14.4; 7.2 mg/mL were prepared. For comparison the activity of the INH solution in water at concentrations of 100; 50; 25; 12.5; 6.2; 3.1 mg/mL was tested.

Because it was screening, there was made not all spheres samples dilutions (ie. 3.1 mg/mL) compared to INH alone. Strains growth was read after 21 days of incubation (Tab. 4.).

In each of the nanospheres formulations inhibitory concentration of both resistant and susceptible to INH strains is less than 7.2 mg/mL. MIC of INH alone for sensitive to INH strains was less than 3.1 mg/mL and for resistant to INH was about 6.2 mg/mL.

The activity of nanospheres samples at a concentration of 3.1 mg/mL was not examined, therefore it cannot be said that their activity is worse than the activity of INH alone. As the test results indicate that the formulations of nanospheres with INH are active against *M. tuberculosis*, accurate test will be carried out.

Tab. 4. Minimal inhibitory concentrations (MIC) of *M. tuberculosis* strains ($\mu\text{g/ml}$) (for samples 1-8 and INH alone).

Sample	Minimal Inhibitory Concentration ($\mu\text{g/ml}$)		
	<i>M. tuberculosis</i> H ₃₇ R _v	<i>M. tuberculosis</i> resistant to INH (No. 210)	<i>M. tuberculosis</i> sensitive to INH (No. 192)
1	5.8	5.8	5.8
2	<7.2	<7.2	<7.2
3	<7.2	<7.2	<7.2
4	<7.2	<7.2	<7.2
5	<7.2	<7.2	<7.2
6	<7.2	<7.2	<7.2
7	<7.2	<7.2	<7.2
8	<7.2	<7.2	<7.2
INH	<3.1	6.2	<3.1

CONCLUSIONS

Nanospheres with isoniazid were received. As a polymer matrix of spheres different polymers were used: poly(L-lactide), poly(DL-lactide), lactide and ϵ -caprolactone block copolymer, polycaprolactone. In all cases spheres with a diameter not exceeding 270 nm were obtained. It was checked that with the increase of the agitation rate, increases the size of obtained particles.

The influence of polylactide tacticity on the spheres size was checked. At a stirring rate of 900 min⁻¹, it is noted that with increasing D unit content, there is spheres size growth.

The effect of stabilizer type (poly(vinyl alcohol), casein, poly(ethylene glycol), gelatin) on the polymeric nanospheres emulsion stability was examined. It was possible to improve the stability of poly(L-lactide), poly(DL-lactide), a block copolymer of lactide and ϵ -caprolactone nanosphere suspensions. There was not achieved the desired impact on the polycaprolactone nanospheres suspension. It was studied that the more concentrated casein solution, the bigger nanospheres size. An exception was poly(L-lactide).

Antitubercular activity test results showed that the obtained nanospheres with INH were active against *M. tuberculosis*.

ACKNOWLEDGMENTS

The research was covered under the statutory activities of the Laboratory of Technological Processes, Faculty of Chemistry, Warsaw University of Technology (504 / P / 1021/0444/000).

REFERENCES

- [1] du Toit L.C., Pillay V., Danckwerts M.P., Tuberculosis chemotherapy: current drug delivery approaches, *Respiratory Research*, 2006, 7, 118-35. DOI: 10.1186/1465-9921-7-118
- [2] Getahun H., Gunneberg C., Granich R., Nunn P., HIV infection-associated tuberculosis: the epidemiology and the response, *Clinical Infectious Diseases*, 2010, 50, 3, S201-7. DOI: 10.1086/651492
- [3] Caminero J.A., Sotgiu G., Zumla A., Migliori G.A., Best drug treatment for multidrug-resistant and extensively drug-resistant tuberculosis, *Lancet Infectious Diseases*, 2010, 10, 9, 621-9 DOI: 10.1016/S1473-3099(10)70139-0
- [4] Ma Z., Lienhardt C., McIlleron H., Nunn A.J., Wang X., Global tuberculosis drug development pipeline: the need and the reality, *Lancet*, 2010, 375, 9731, 2100-9 DOI: 10.1016/S0140-6736(10)60359-9
- [5] Hoffman A., The origins and evolution of “controlled” drug delivery systems, *Journal of Controlled Release*, 2008, 132, 3, 153-63 DOI: 10.1016/j.jconrel.2008.08.012
- [6] Jain K.K, Chapter in the book: Current Status and Future Prospects of Drug Delivery Systems, *Drug Delivery Systems*, Springer, 2014 DOI: 10.1007/978-1-4939-0363-4
- [7] Jain K.K., Drug delivery systems - an overview, *Methods in Molecular Biology* 2008, 437, 1-50 DOI: 10.1007/978-1-59745-210-6_1
- [8] Nagavarma B.V., Yadav H.K.S., Ayaz A., Vasudha L.S., Shivakumar H.G., Different techniques for preparation of polymeric nanoparticles - a review, *Asian Journal of Pharmaceutical Clinical Research Supplement*, 2012, 5, 3, 16-23
- [9] Xie S., Tao Y., Panc Y., Biodegradable nanoparticles for intracellular delivery of antimicrobial agents, *Journal of Controlled Release* 2014, 187, 101-17 <http://dx.doi.org/10.1016/j.jconrel.2014.05.034>
- [10] Szymańska E., Winnicka K., Mikrosfery – nowoczesna postać leku do oczu o kontrolowanym uwalnianiu, *Farmacja Polska*, 2009, 65, 5, 378-86
- [11] Kumari A., Yadav S.K., Yadav S.C., Biodegradable polymeric nanoparticles based drug delivery systems, *Colloids and Surfaces B: Biointerfaces*, 2010, 75, 1, 1-18 DOI: 10.1016/j.colsurfb.2009.09.001
- [12] Gref R., Minamitake Y., Peracchia M.T., Trubetskoy V., Torchilin V., Langer R., *Science*, 1994, 263, 5153, 1600-3. DOI:10.1126/science.8128245
- [13] Singh A., Garg G., Sharma P.K., Nanospheres: a novel approach for targeted drug delivery system, *International Journal of Pharmaceutical Sciences Review and Research*, 2010, 5, 3, 84-8

- [14] Budnicka (Łątka) M., Gadomska-Gajadhur A., Sebai A., Chapter in the book: Nanosfery polilaktydowe z izoniazidem – nowa metoda leczenia gruźlicy, *Interdyscyplinarność badań naukowych*, Oficyna Wydawnicza Politechniki Wrocławskiej, 2016
- [15] Gadomska-Gajadhur, A., Ruśkowski, P., Synoradzki, L., Warych, I., Przybysz, A., Bijak, V., Sposób wytwarzania nanosfer polilaktydowych z substancją farmaceutycznie czynną, *PL 225920*, 2016
- [16] Gadomska, A., Warych, I., Ruśkowski, P., Synoradzki, L., Otrzymywanie nanosfer polilaktydowych, *Przemysł Chemiczny*, 2014, 93, 1011-10014 DOI: dx.medra.org/10.12916/przemchem.2014.1311
- [17] Gadomska-Gajadhur, A., Mierzejewska, J., Ruśkowski, P., Synoradzki, L., Otrzymywanie sfer polilaktydowych zawierających paracetamol, *Przemysł Chemiczny*, 2015, 94, 10, 1676-1678 DOI: 10.15199/62.2015.10.3
- [18] Sebai, A., Gadomska-Gajadhur, A., Ruśkowski, P., Optymalizacja procesu otrzymywania nanosfer proleku polilaktydu z chlorofenezyną, *Inżynieria i Aparatura Chemiczna*, 2016, 55, 5, 201-202
- [19] Budnicka (Łątka) M., *Optimization of encapsulation of isoniazid – drug for the treatment of tuberculosis*, engineering thesis, Faculty of Chemistry, Warsaw University of Technology, Warsaw 2015
- [20] Budnicka (Łątka) M., Gadomska-Gajadhur A., Sebai A., Chapter in the book: Otrzymywanie nanosfer polilaktydowych z izoniazidem, *Postępy w naukach technicznych i informatycznych oraz współczesne metody nauczania*, Wydawnictwo Naukowe Tygiel sp. z o.o., 2016.

The parameters of helicoidal structure of liquid crystals

*Anna Drzewicz, Marzena Tykarska

Faculty of Advanced Technologies and Chemistry, Military University of Technology, Warsaw, POLAND

e-mail: anna.drzewicz@wat.edu.pl

Keywords: liquid crystals, ferroelectric phase, antiferroelectric phase, helical pitch, helical twist sense

ABSTRACT

Liquid crystalline materials are used in photonics because of their special optical properties. The display market is dominated by nematic liquid crystals, however ferroelectric and antiferroelectric smectic liquid crystals are also used. They allow to build displays characterized by shorter times of record information and by better angle of imaging than nematics. It is necessary to know the parameters of helicoidal structure – the helical pitch and the helical twist sense for using liquid crystals. The knowledge of these values allows to use liquid crystalline cells at respectively selected thicknesses.

INTRODUCTION

Liquid crystal state was discovered in 1888 by Austrian botanist Friedrich Reinitzer during heating benzoate cholesterol [1]. He observed that an obscure liquid was produced after the molten substance, which in higher temperature was a clarified liquid. Further research on this compound was performed by the German physicist Otto Lehman [2]. He stated that this obscure liquid is an anisotropic center. Phase having such properties is called a mesophase. At that time the birefringence was a phenomenon typical of crystalline centers, whence derives the name of the state of matter – liquid crystals.

Liquid crystalline state combines the features of liquids, such as the viscosity and the ability to create a free surface, and of solids, like anisotropy of physical properties [3]. One of the most important properties is a high optical activity, which is easily controlled by external interaction of electrical, thermal, magnetic and mechanical fields. In practice widely used feature of liquid crystals is the selective light reflection phenomenon. It is analogical to the Bragg law of solid crystals. The macroscopic chiral helix reflects the electromagnetic radiation. The helical pitch is the parameter, which allows to use liquid crystal mixtures in displays. The main factor that determines the value of the helical pitch for the system is the temperature [4].

The application of liquid crystals is closely connected with their electrooptical properties, so that they can be used for imaging information. The presence of liquid crystals enabled the miniaturization of devices, which are characterized by simplicity of design and reliability [5].

The aim of this work is to review the parameters of the helicoidal structure of chiral smectic phases and the most common research methods used to determine these parameters.

SMECTIC PHASES

The orientational and positional arrangement in smectic phases is performed. The first type of arrangement is connected with the rotational of molecules and the second type – with the translational of molecules [6]. The order parameter of smectic liquid crystals is described by the formula:

$$S = \frac{1}{2} \left\langle \cos \left| \frac{2z}{a} \right| \cos^2 \gamma - 1 \right\rangle \quad (1)$$

where z is the value of coordinate directed normal to the plane of the layer, a is the smectic layer thickness and γ is the angle between the long axis of molecule and the director.

The smectic phases are noted by symbol Sm and large letters of the alphabet (A, B, C, etc.). In the smectics the molecules are arranged in layers of a certain thickness, which is comparable to the length of the molecule. The eleven basic smectic phases have been obtained. They are orthogonal phases A, B, L, E and their oblique equivalents C, I, J, K, F, G, and H [7]. In this work only SmC phase is described.

The SmC phase is an oblique analogue of orthogonal SmA phase (Fig. 1). It is characterized by the arrangement of the molecules in the layers. These molecules are additionally inclined by an angle θ from the normal to the layer. The preferred orientation of the molecule relative to the plane is defined by the director [8].

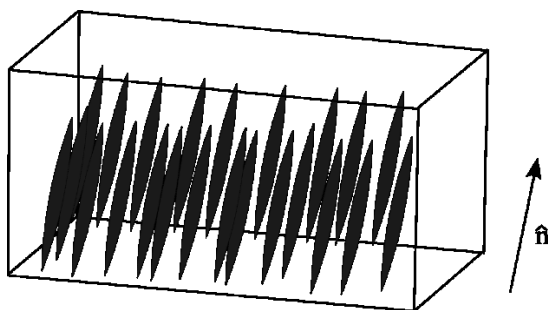


Fig. 1. The SmC liquid crystalline phase.

CHIRAL LIQUID CRYSTALLINE PHASES

The presence of chiral phases in liquid crystals is directly related to the structure of the molecule, which may not have a plane of symmetry. The appearance at least one asymmetric center (eg. tetragonal, substituted by four different substituents, carbon atom) causes the disappearance of the plane of symmetry. Another way to create the chiral liquid crystal is to add an optically active dopant to the non-chiral liquid crystal material (called liquid crystal base). The chiral phases are marked with a star put the letter assigned to a particular type of phase [9].

Ferroelectric phases

The ferroelectric SmC^* phase is an equivalent of the synclinic SmC phase, whose structure is shown in Fig. 2a.

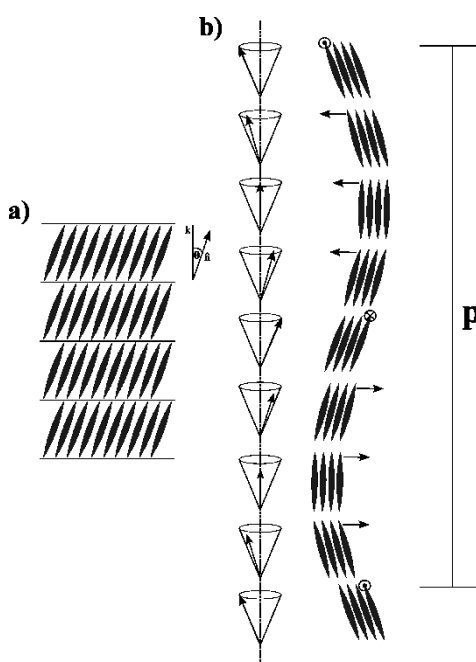


Fig. 2. The arrangement of molecules in:
a) synclinic SmC phase; b) ferroelectric SmC^* phase.

The twice axis C_2 is the only type of symmetry for this structure and causes the appearance of the local spontaneous polarization \vec{P}_S in the smectic layers along the C_2 axis by the sum of the dipole moments of the individual molecules in these layers. The helicoidal structure of SmC^* phase causes the disappearance of spontaneous polarization at the transition to the subsequent layers at the distance equal to the length of the helical pitch (Fig. 2b).

Meyer was the first researcher who proved experimentally ferroelectric properties of SmC^* phase in (S)-3-[4-(4-decyloxy-benzylideneamino)-phenyl]-acrylic

acid 2-methyl-butyl ester (DOBAMBC) by developing the helicoidal structure using electric current [10].

Antiferroelectric phases

The antiferroelectric SmC_A^* phase is an equivalent of the anticlinic SmC_A phase (Fig. 3a), wherein directors in adjacent layers are inclined by the same angle (θ , $-\theta$) with respect to the normal to the layer, but in opposite directions.

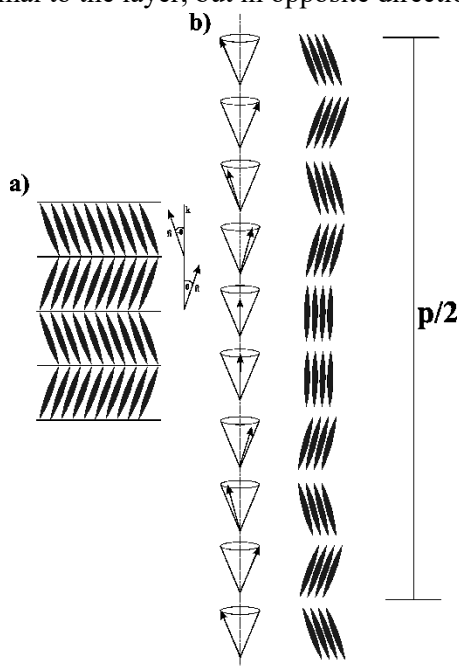


Fig. 3. The arrangement of molecules in:
a) anticlinic SmC_A phase; b) antiferroelectric SmC_A^* phase.

In the SmC_A^* phase the director also rotates relative to the normal to the layer to form a macroscopic helicoidal structure, as in the SmC^* phase. However in contrast to the ferroelectric phase the spontaneous polarization removes in the microscale (within the two smectic layers). It is caused by the opposite orientation of spontaneous polarization vectors in adjacent layers (Fig. 3b).

The first compound (4'-octyloxy-biphenyl-4-carboxylic acid 4-(1-methyl-heptyloxycarbonyl)-phenyl ester, MHPOBC) with the antiferroelectric phase was obtained by professor Furukawa [11].

PARAMETERS OF HELICOIDAL STRUCTURE

The helix is one of the most representatives chiral forms in nature. It is characterized by two parameters – helical pitch and helical twist sense. The values of these parameters determine different possible applications of the chiral phases. In the following sections the parameters of helix and methods of measurements them will be described.

Helical pitch

The distance, at which director rotates 360° during the transition to the next liquid crystal layer, is the helical pitch (p). The helical pitch dependence of the temperature in the chiral smectic phases is important in both the thermodynamic description and in the possibilities of applications of these phases in displays [12-14]. The value of helical pitch influences the electrooptical properties and determines the use of cells with different thicknesses.

According to the work of Ji Li and others [15], the helical pitch is dependent on the temperature in different way in the liquid crystalline materials (Fig. 4).

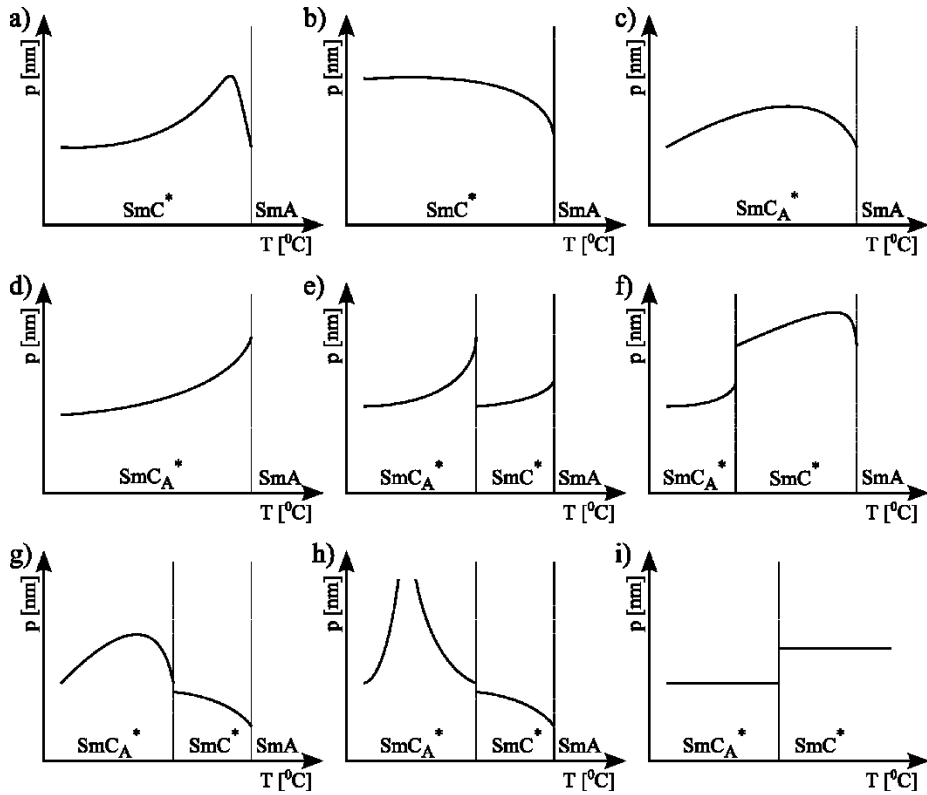


Fig. 4. The helical pitch dependence on the temperature for liquid crystal materials [15].

The value of helical pitch may rapidly increase during the transition from SmA phase to SmC^* , then decreases slowly (Fig. 4a) or after rapidly growth the helical pitch may not change with decreasing temperature (Fig. 4b). In the direct transition from SmA phase to SmC_A^* reduction of the temperature causes increase of the helical pitch in the antiferroelectric phase and then after passing through a maximum causes decrease of this value (Fig. 4c). Another case shows that after the transition from SmA to SmC_A^* the value of the helical pitch decreases during cooling (Fig. 4d). The helical pitch in the liquid crystal materials with a phase sequences $SmA - SmC^* - SmC_A^*$ changes in many different ways with temperature. The helical pitch may suddenly appear in the ferroelectric phase and then it decreases with

decreasing temperature (Fig. 4e) or in the initial phase increases and upon cooling decreases (Fig. 4f) or increases with decreasing temperature (Fig. 4g). In all of these cases there is rapidly change of the value of helical pitch in the antiferroelectric phase. In the SmC_A^* phase may be a discontinuity of the helical pitch which is a phenomenon associated with the inversion of helical twist sense (Fig. 4h). The value of helical pitch can also be independent of the temperature in the SmC^* and SmC_A^* phases (Fig. 4i).

Helical twist sense

The other parameter characterizing the helicoidal structure is the helical twist sense, which is defined as positive for a right-handed or clockwise twist (Fig. 5b) and negative for a left-handed or anticlockwise twist (Fig. 5a).

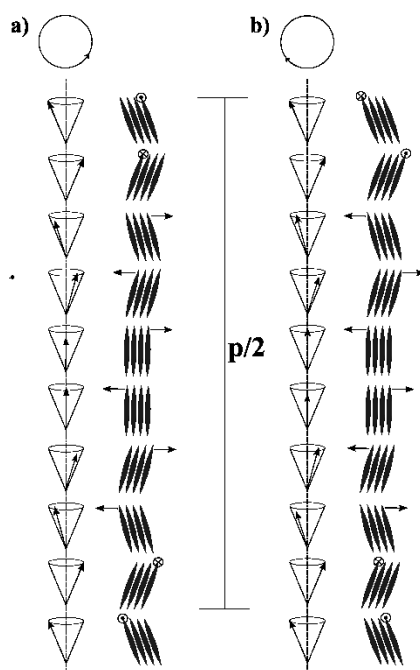


Fig. 5. The helical twist sense: a) left-handed; b) right-handed.

The helical twist sense of the chiral liquid crystalline phases depends on the absolute configuration of the asymmetric carbon atom and its position relative to the rigid core of molecule. According to the Gray and McDonnell theory [16] the carbon atom at R-type of absolute configuration in the odd position relative to the rigid core rotates the polarization plane to the right (dextra) – Rod. A similar situation is obtained for S-type of absolute configuration in the even position – Sed. However, the left-handed helix will be created, when the asymmetric carbon atom has R (S)-type of absolute configuration in, respectively, the even (odd) position – Rel (Sol). This theory was extended by Goodby and Chin [17] who combined the helical twist sense with the spontaneous polarization.

These theories are general in nature, but there are exceptions to them. It is connected with the inversion of the helical twist sense phenomenon depending on the temperature. There are few theoretical explanations of the helical twist sense inversion within one phase of a single compound. The most popular is that the change of the concentration of different conformers promote opposite handedness [18-22].

METHODS OF MEASUREMENTS

The measurements of the helicoidal structure parameters in chiral smectic phases are the most difficult measurements for this class of materials. In this work the most popular methods of measuring the helical pitch and the helical twist sense will be described: based on the selective light reflection phenomenon and based on the polarimetry technique, respectively.

Measurement of helical pitch

The phenomenon of selective light reflection for chiral liquid crystals is similar to the X-ray reflection for solid crystals. The Bragg's law is:

$$m\lambda = 2d\sin\theta \quad (2)$$

where m is a positive integer, λ is the wavelength of incident wave, d is the interplanar distance and θ is the scattering angle.

The macroscopic helicoidal structure presented in the chiral liquid crystals has the ability to selectively reflecting electromagnetic waves (Fig. 6).

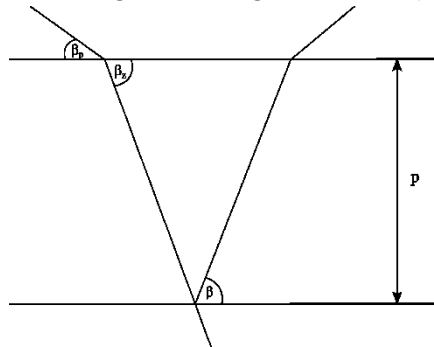


Fig. 6. The geometry of electromagnetic wave scattering in a layer of chiral liquid crystal. β_i is the angle of incidence, β_r is the angle of refraction, β is the angle of scattering and p is the helical pitch.

The interplanar distance is replaced with the helical pitch, so the Bragg's formula for the selective light reflection phenomenon is:

$$m\lambda = 2p\sin\beta \quad (3)$$

The electromagnetic wave passing through a layer of chiral liquid crystal refracted. The angle of scattering is dependent on the refractive index according with the Snell's law:

$$\sin\beta = n\sin\beta_p \quad (4)$$

Hence, the equation of the Bragg's law for the chiral liquid crystals is:

$$m\lambda = 2np\sin\beta_p \quad (5)$$

Assuming the order of reflection and that the electromagnetic wave is the parallel to the helicoidal axis, the equation is:

$$\lambda = 2np \quad (6)$$

In the case of antiferroelectric smectic phase, due to the overlap condition of the reflectance of the pitch $\left(\frac{p}{2}\right)$, the formula is:

$$\lambda = np \quad (7)$$

The average refractive index for liquid crystals is about 1.5 [23].

Prof. Kuczyński [24] noted the strong influence of the surface forces (anchoring forces) for helicoidal structure in the case of methods based on the planar arrangement of molecules. In such system the interaction of molecules with the boundary surface is very high. In this method the homeotropic arrangement of molecules is used. This situation is much more favorable, since the anchoring forces are weaker and have smaller influence on the helicoidal structure.

Measurement of helical twist sense

The helical twist sense measurement for chiral smectic liquid crystals is based on the phenomenon of twisting the polarization light plane by the chiral liquid crystal with the helix axis parallel to the light beam. This method was described by Kuczyński and coworkers [25] and illustrated in Fig.7.

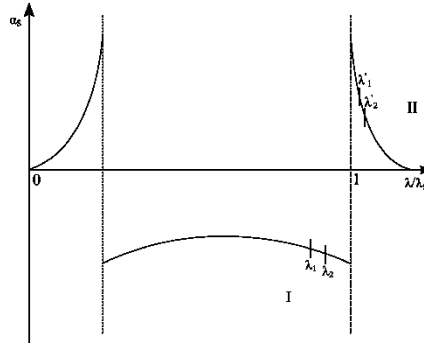


Fig. 7. The angle of rotation of plane polarized light (α_s) as a function of the electromagnetic wavelength (λ), where λ_s is the wavelength of selective reflection. For $\lambda > \lambda_s$ rotation of the plane of polarized light is in accordance with the helical twist sense (area II).

For $\lambda < \lambda_s$ situation is reserved (area I) [25].

The knowledge of the selective reflected wavelength for the tested chiral liquid crystal is very important in this method. For $\lambda < \lambda_s$ the right-handed helix selectively reflects right-handed circular polarized light and transmits left-handed part. However for $\lambda > \lambda_s$ situation is reversed. The problem is, when the selective reflected wavelength is close to the wavelength of an electromagnetic radiation source. In this case the angle of the

twisting polarized plane for two electromagnetic wavelengths smaller or larger than the selective reflected wavelength (λ_1, λ_2 for area II or λ'_1, λ'_2 for area I) must be examined. In the case of the area I: $|\alpha_S(\lambda_1)| < |\alpha_S(\lambda_2)|$, and for the area II: $|\alpha_S(\lambda'_1)| > |\alpha_S(\lambda'_2)|$.

The homeotropically aligned material is putted between crossed polarizers and the top polarizer is rotated relative to the bottom one. The clockwise rotation indicates a left-handed helix, and anticlockwise causes right-handed helix [26].

CONCLUSIONS

The described methods of measurements of helical pitch and helical twist sense are the best for chiral smectic liquid crystals (ferroelectric SmC* and antiferroelectric SmC_A*) because of their helicoidal structures and the necessity of the homeotropic arrangement. These methods are characterized by the smallest impact of the boundary surfaces to the helix of molecules, good reproducibility of results and the availability of research equipment. The knowledge of the helicoidal parameters of liquid crystalline materials is very important and used in the creation of displays.

REFERENCES

- [1] Reinitzer F., Beiträge zur Kenntniss des Cholesterins, *Monatshefte für Chemie*, 1888, 9, 421-441, DOI: 10.1007/BF01516710
- [2] Lehmann O., Über fließende Krystalle, *Zeitschrift für Physikalische Chemie*, 1889, 4, 462-472
- [3] Adamczyk A., *Niezwykły stan materii – Ciekłe kryształy*, Wiedza Powszechna, Warszawa, 1981
- [4] Tykarska M., Czerwiński M., Miskurka J., Influence of temperature and terminal chain length on helical pitch in homologue series nH6Bi, *Liquid Crystals*, 2010, 37, 4, 487-495, DOI: 10.1080/02678291003686880
- [5] Dąbrowski R., Żmija J., *Ciekłe kryształy*, WAT, Warszawa, 1984
- [6] Grey G.W., *Molecular structure and properties of liquid crystals*, Academic Press, London, 1962
- [7] Friedel M.G., Les états mésomorphes de la matière, *Annales de Physique*, 1922, 18, 273-474
- [8] Tykarska M., *Faza antyferroelektryczna indukowana i rozszerzona*, WAT, Warszawa, 2010
- [9] Demus D., *Types and classification of liquid crystals: Liquid Crystals Applications and Uses*, Utopia Press, Signapore, 1990
- [10] Meyer R.B., Liebert L., Strzelecki L., Keller P., Ferroelectric liquid crystals, *Journal Physique Letter*, 1975, 36, 69-71, DOI: 10.1051/jphyslet:0197500360306900
- [11] Inukai T., Furukawa K., Terashima K., Saito S., Isogai M., Kitamura T., Mukoh A., *Abstract Book of Japan Domestic Liquid Crystal Meeting*, Kanazawa, 1985, 172

- [12] Emelyanenko A.V., Osipov M.A., Theoretical model for the discrete flexoelectric effect and a description for the sequence of intermediate smectic phases with increasing periodicity, *Physical Review E*, 2003, 68, 5, DOI: 10.1103/PhysRevE.68.051703
- [13] Piecek W., Perkowski P., Raszewski Z., Morawiak P., Żurowska M., Dąbrowski R., Czupryński K., Long pitch orthoconic antiferroelectric binary mixture for display applications, *Molecular Crystals and Liquid Crystals*, 2010, 525, 160-172, DOI:10.1080/15421401003796223
- [14] Kurp K., Tykarska M., Drzewicz A., Lapanik V., Sasnouski G., Effect of ferroelectric liquid crystalline quaterphenyl structure and handedness on helical pitch length in bicomponent mixtures, *Liquid Crystals*, 2016, DOI: 10.1080/02678292.2016.1226975
- [15] Li J., Takezoe H., Fukuda A., Novel Temperature Dependences of Helical Pitch in Ferroelectric and Antiferroelectric Chiral Smectic Liquid Crystals, *Japanese Journal of Applied Physics*, 1991, 30, 3, 532-536, DOI: 10.1143/JJAP.30.532
- [16] Gray G.W., McDonnell D.G., The Relationship Between Helical Twist Sense, Absolute Configuration and Molecular Structure for Non-Sterol Cholesteric Liquid Crystals, *Molecular Crystals and Liquid Crystals*, 1976, 34, 9, 211-217, DOI: 10.1080/15421407708083708
- [17] Goodby J.W., Chin E., Helical Twist and Spontaneous Polarization Direction in Ferroelectric Smectic Liquid Crystals, *Journal of the American Chemical Society*, 1986, 108, 4736-4742, DOI: 10.1021/ja00276a009
- [18] Kašpar M., Górecka E., Sverenyák H., Hamplová V., Glogarová K., Pakhomov S.A., Helix twist inversion in ferroelectric liquid crystals with one chiral centre, *Liquid Crystals*, 1995, 19, 589-594, DOI: 10.1080.02678299508031072
- [19] Cieplak B., Kocot A., Merkel K., Wrzalik R., Praniuk R., Dielectric and Optical Studies of FLC Sample with Helix Inversion, *Ferroelectrics*, 2004, 311, 83-95, DOI: 10.1080/00150190490511275
- [20] Czerwiński M., Tykarska M., Helix parameters in bi- and multicomponent mixtures composed of orthoconic antiferroelectric liquid crystals with three ring molecular core, *Liquid Crystals*, 2014, 41(6), 850-860, DOI:10.1080/02678292.2014.884248
- [21] Tykarska M., Czerwiński M., Żurowska M., The temperature and concentration dependence of helical pitch in the mixtures of antiferroelectric compounds with the opposite helical twist sense, *Liquid Crystals*, 2011, 38(5), 561-566, DOI:10.1080/02678292.2011.558217
- [22] Tykarska M., Czerwiński M., The inversion phenomenon of the helical twist sense in antiferroelectric liquid crystal phase from electronic and vibrational circular dichroism, *Liquid Crystals*, 2016, 43(4), 462-472, DOI: 10.1080/02678292.2015.1118769

- [23] Raszewski Z., Kędzierski J., Perkowski P., Piecek W., Rutkowska J., Kłosowicz S., Zieliński J., Refractive indices of the MHPB(H)PBC and MHPB(F)PBC antiferroelectric liquid crystals, *Ferroelectrics*, 2002, 276, 289-300, DOI: 10.1080/00150190214411
- [24] Kuczyński W., Behavior of the helix in some chiral smectic C* liquid crystals, *Physical Review E*, 2010, 81, DOI: 10.1102/PhysRevE.81.021708
- [25] Kuczyński W., Lagerwall S.T., Matuszczyk M., Skarp K., Stebler B., Wahl J., Fast-Switching Low-Temperature Liquid Crystal Mixtures, *Molecular Crystals and Liquid Crystals*, 1987, 146, 173-187, DOI: 10.1080/00268948708071812
- [26] Shtykov N.M., Vij J.K., Lewis R.A., Hird M., Goodby J.W., Dielectric and optical rotatory power investigations of an antiferroelectric liquid crystal 12OF1M7 in a homeotropic cell: implications for models of the structure of ferrielectric phases, *Liquid Crystals*, 2001, 28, 1699-1704, DOI: 10.1080/02678290110068974

A new method to compare micromixedness results obtained in iodide-iodate method using different reactant concentrations

*Michał Fedoryk, Manfred Kraut

Institute for Micro Process Engineering, Karlsruhe Institute of Technology, Karlsruhe, GERMANY

e-mail: michalfedoryk@gmail.com

Keywords: *Villermaux-Dushman, micromixedness ratio, cyclone type micro mixers*

ABSTRACT

Micromixing investigations are conducted using different experimental methods. One of them is the iodide-iodate reaction method, so-called Villermaux-Dushman method. Due to reaction kinetics, which is not fully known, usually one 'standard set' of reactants concentrations is applied. Subsequently, optical densities of obtained mixtures are compared.

The proposed approach is based on experimental results of optical densities of mixtures generated by the cyclone type micro mixer. Mixing was investigated using different concentration sets at the same hydrodynamic conditions. Molar ratios of reactants were maintained. Obtained results allowed calculating values of micromixedness ratio. Application of higher concentrations of reactants ended up in lower apparent micromixedness ratio.

This paper presents the new protocol to compare micromixedness ratios obtained using different concentrations of reactants. The presented method is applicable for continuous-flow systems in microdevices where different reactants concentrations have been used. It was found that calculated micromixedness ratio is a function of the concentration ratio to the power of -3.73 .

Thanks to the presented protocol it is possible to broaden the range of investigated hydrodynamic conditions: higher reactants concentrations at higher flows as well as lower ones when mixing is less intensive can be applied and still calculated micromixedness ratios are comparable. The method allows the calculation of exit iodine concentrations, without the explicit knowledge of the actual kinetic data.

INTRODUCTION

Mixing is one of processes used de facto in every branch of industry. It is defined as the reduction of inhomogeneity in order to achieve a desired process result [1], where inhomogeneity can be observed in temperature, concentration and phase distribution. Mixing is investigated not only because of its significant cost in chemical and related industries, which process with huge amounts of bulk materials, to reduce operating costs, but also because of the influence of mixing on selectivity. Micromixing has also an impact in precipitation processes, where it can lead to variation of the geometric parameters in the obtained crystals [2]. These can be crucial criteria in the formulation of pharma products.

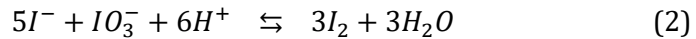
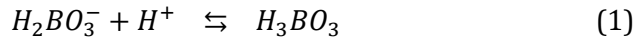
The iodide iodate reaction method is used widely to investigate mixing not only in laboratory-scale apparatus [3–5] but also in microdevices [6–8]. Since the measured optical density cannot describe mixing quantitatively [9–10], in many investigations the same concentrations of reactants have been applied in different hydrodynamic cases. Therefore the range of measureable cases has been limited by chosen concentration set often denoted as ‘standard’

In this paper the procedure of comparing results obtained using continuous flow micromixers with different reactant concentrations is described.

MATERIALS AND METHODS

Iodide-iodate reaction method

Among several chemical reactions systems used to investigate mixing [11–12], the iodide iodate reaction method seems to be relatively cheap, as for reactants cost, and fast in application. This method [13] uses different reaction rates of neutralization (Eq. 1) and comproportionation, so-called Dushman reaction (Eq. 2), which occur in parallel.



Neutralization is supposed to be so fast as to appear instantaneous, while comproportionation is a fast reaction, but slow in comparison to neutralization. Thus, efficient mixing results preferably in neutralization (Eq. 1); therefore, more iodine is created in non-ideal mixing processes.

Iodine reacts with iodide excess (Eq. 3) to form triiodide, which is measured spectrophotometrically.

Cyclone type micro mixers

The structure of cyclone type mixers manufactured at the IMVT is shown in Fig. 1. The drawing presents the shape of the hole in the mixing inlay. Firstly, feed solutions flow into inlet pockets (1) which are located opposite to the end of the flange connection. Fluid bends there and enters the inlet channel (2), of the cross-section of a square $200 \text{ } [\mu\text{m}] \times 200 \text{ } [\mu\text{m}]$, which is tangentially connected with the cylindrical mixer chamber (3) of the diameter equal $500 \text{ } [\mu\text{m}]$ and the height equal $4 \text{ } [\text{mm}]$. Thanks to that localization, a swirl motion is created inside the mixing chamber to improve the mixing process. Afterwards, the mixture flows out through the tangential outlet channel (4) of the cross-section of a square $300 \text{ } [\mu\text{m}] \times 300 \text{ } [\mu\text{m}]$ and the outlet pocket (5).

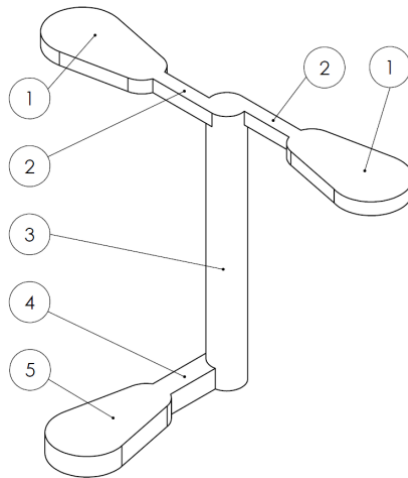


Fig. 1. A sketch of investigated mixer: 1 – inlet pocket, 2 – inlet channel, 3 – mixing chamber, 4 – outlet channel, 5 – outlet pocket.

Simplicity of the design allows varying structural parameters of this class of mixers such as height and diameter of mixing chamber, number and width of inlets, angle of connection inlet channel–mixing chamber, and number of mixing chambers. That makes cyclone type mixers very flexible and broadens their possible application. An influence of some of mentioned parameters has been investigated and compared with results of CFD simulations [14].

Experimental set-up

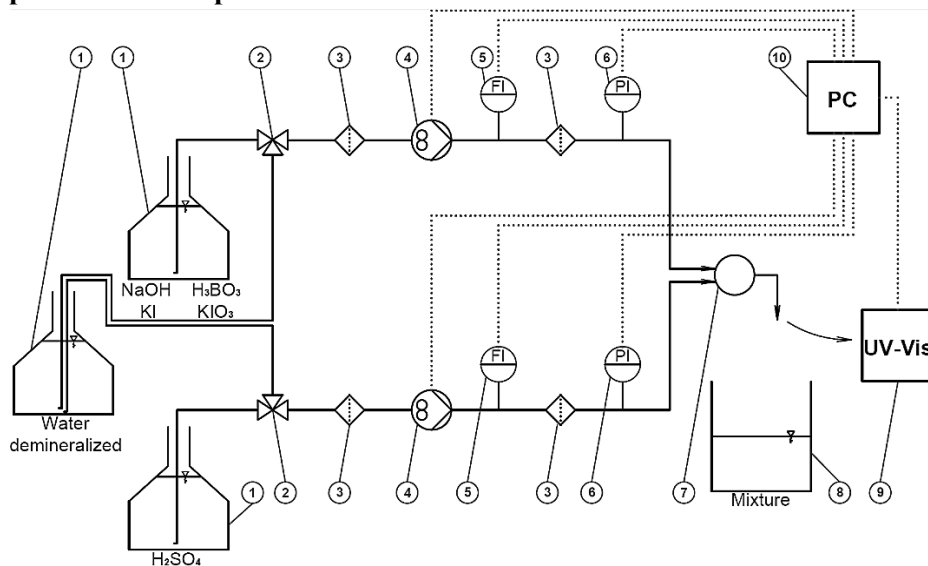


Fig. 2. Scheme of the set-up; numbering described in the text.

Mixing experiments were conducted using dedicated set-up, which scheme is shown in Fig. 2. Buffered solution of iodide and iodate salts (hereinafter *Villermoux solution*) as well as acid solution have been prepared fresh every day. Reactants are

kept in separate vessels (1). Demineralized water allows rinsing the set-up by switching two valves (2). Four 40 [μm] filters (3) prevent pumps and the mixer from solid parts. Solutions are pumped by two independently operated micro-gear pumps (4) (mzr-7206, HNP Mikrosysteme). The flow generated by one pump has an influence on the other pump; therefore, both voltages are adjusted parallelly and recurrently. First amounts of solutions flowing through the Coriolis mass flow meter (5) (Promass 63, Endress+Hauser) allow achieving densities of liquids and, after simply calculation, mass flow rates corresponding with declared volumetric flow rates. Pressure is measured on-line by pressure transducers (6) (Type E913, Bourdon Haenni) located approx. 0.5 [m] before the mixer. The mixture outflowing from the micromixer (7) is collected in a vessel (8). Absorbance of resulting mixture is measured ex-situ. For each steady state, a few milliliters of outflowing mixture is collected in quartz cuvette to be analyzed by spectrophotometer (9) (HP 8453) connected with the computer (10). Results (i.e. absorbance spectra) are sent in a digital form to the dedicated software, where the maximal value of the optical density of the peak located around a wavelength of 353 [nm] is determined by the operator of the experimental set-up.

Obtained optical density as raw data to further calculations

Determination of the triiodide ion concentration $c_{I_3^-}$

Obtained values of absorbance were used to calculate concentrations of triiodide ion in resulting mixtures $c_{I_3^-}$. According to the Beer-Lambert law, optical density OD is proportional to optical path length l , molar extinction coefficient ε_{OD} , and concentration of substance c . It can be written as Eq. 4:

$$OD = \varepsilon_{OD} \cdot l \cdot c_{I_3^-} \quad (4)$$

where:

OD	[-]	optical density,
ε_{OD}	[$\text{dm}^3/(\text{mol} \cdot \text{cm})$]	molar extinction coefficient,
l	[cm]	optical path length,
$c_{I_3^-}$	[mol/dm^3]	concentration of triiodide.

A concentration of triiodide ion is to be calculated; therefore, Eq. 4 should be rearrangement into form of Eq. 5:

$$c_{I_3^-} = \frac{OD}{\varepsilon_{OD} \cdot l} \quad (5)$$

Values of optical density and optical path length are known for each measurement. The value of molar extinction coefficient of triiodide ion ε_{OD} at peak located around wavelength equal approx. $\lambda \approx 353$ [nm] was determined by several teams of researchers, whose results are available in literature. Some reports are listed in Tab. 1.

Tab. 1. Values of molar extinction coefficients of triiodide ion obtained by different authors.

Year	Reference	λ [nm]	ε_{OD} [dm ³ /(mol·cm)]
1951	[15]	353	26400
1984	[16]	350	25750
2005	[17]	350	23200
2011	[8]	353	26047
2012	[18]	352	27600
2015	[19]	353	25750

As can be seen (Tab. 1), values of molar extinction coefficient obtained by different groups differ, as well as the chosen wavelength of the center of the peak. Due to this fact, an average value of molar extinction coefficient equal $\varepsilon_{OD} = 25791$ [dm³/(mol·cm)] was used in further calculations.

Determination of the segregation index X_S and micromixedness ratio α

In order to describe micromixing quantitatively, known concentrations of chemicals were used to calculate segregation index X_S and further – micromixedness ratio α .

Segregation index is a quantity whose values lie between 0 and 1. One can distinguish two extreme cases: total segregation, when $X_S = 1$ and perfect mixing on molecular level, when $X_S = 0$. All other cases are described as partial segregation and values of segregation index can be calculated from general relation (Eq. 6) [4]:

$$X_S = \frac{Y}{Y_{ST}} \quad (6)$$

where:

X_S	[-]	segregation index,
Y	[-]	yield of iodine
Y_{ST}	[-]	iodine yield in theoretical reference case of total segregation.

The value of Y is described by Eq. 7 [4]:

$$Y = \frac{2 \cdot (n_{I_2} + n_{I_3^-})}{n_{H^+O}} \quad (7)$$

where:

n_i	[mol]	mole number of i -th chemical.
-------	-------	----------------------------------

Subscript 0 indicates initial value, before mixing.

For the continuous flow system used for investigation of mixing process in microstructured cyclone type mixer, Eq. 7 can be rewritten:

$$Y = \frac{2 \cdot \dot{V}_{Villiermaux} (c_{I_2} + c_{I_3^-})}{\dot{V}_{acid} \cdot c_{H^+O}} \quad (8)$$

where:

\dot{V}_i [m³/s] volumetric flow rate of the solution,
 c_i [mol/m³] concentration of i -th chemical.

The value of Y_{ST} can be calculated using a method by Guichardon[4]: In fact Y_{ST} would be a function of the geometry of the mixing vessel, but for simplicity this formula, given by Guichardon was used:

$$Y_{ST} = \frac{\frac{6 \cdot c_{IO_3^-}_0}{c_{H_2BO_3^-}_0}}{\frac{6 \cdot c_{IO_3^-}_0}{c_{H_2BO_3^-}_0} + 1} = \frac{6 \cdot c_{IO_3^-}_0}{6 \cdot c_{IO_3^-}_0 + c_{H_2BO_3^-}_0} \quad (9)$$

The micromixedness ratio α is simply connected with segregation index X_S (Eq. 10). The model for α is to divide the entire volume into two parts: one which is perfectly mixed ($c_{I_2} = 0$) and the other one which is completely segregated. Their ratio then is a measure of the mixing deficit. The micromixedness ratio α is defined therefore as [20]:

$$\alpha = \frac{V_{PM}}{V_{ST}} = \frac{1 - X_S}{X_S} \quad (10)$$

where:

α [-] micromixedness ratio,
 V_{PM} [-] volume fraction of perfectly mixed fluid,
 V_{ST} [-] volume fraction of fluid with total segregation.

Determination of the iodine concentration c_{I_2}

Concentration of iodine c_{I_2} is necessary to determine the value of Y and thus X_S and α . It can be calculated thanks to mass balance and knowledge of the equilibrium constant. Mass balance of iodine (chemical element) based on reaction of comproportionation (Eq. 2) is shown in Eq. 11:

$$c_{I^-} = c_{I^-}_0 - \frac{5}{3} \cdot (c_{I_2} + c_{I_3^-}) - c_{I_3^-} \quad (11)$$

On the other hand, the equilibrium constant for reaction (Eq. 3) is described by Eq. 12:

$$K_B = \frac{c_{I_3^-}}{c_{I_2} \cdot c_{I^-}} \quad (12)$$

where:

K_B [dm³/mol] equilibrium constant.

The dependence of this constant of temperature has been determined [16]. Values of equilibrium constant can be calculated using Eq. 13:

$$K_B(T) = 10^{\left(\frac{555}{T} + 7.355 - 2.575 \cdot \log_{10}(T)\right)} \quad (13)$$

In Eq. 13 temperature values should be given in Kelvins [K].

By combining mass balance equation (Eq. 11) and equilibrium equation (Eq. 12), one can obtain a quadratic equation (Eq. 14) with concentration of iodine c_{I_2} as the unknown:

$$-\frac{5}{3} \cdot c_{I_2}^2 + \left(c_{I^-_0} - \frac{8}{3} \cdot c_{I^-_3} \right) \cdot c_{I_2} - \frac{c_{I^-_3}}{K_B} = 0 \quad (14)$$

The solution of Eq. 14, easy obtainable analytically, must be positive and must make physical sense. Thus, the concentration of iodine c_{I_2} can be calculated according to Eq. 15:

$$c_{I_2} = \frac{-\left(c_{I^-_0} - \frac{8}{3} \cdot c_{I^-_3} \right) - \sqrt{\left(c_{I^-_0} - \frac{8}{3} \cdot c_{I^-_3} \right)^2 - 4 \cdot \left(-\frac{5}{3} \right) \cdot \left(-\frac{c_{I^-_3}}{K_B} \right)}}{2 \cdot \left(-\frac{5}{3} \right)} \quad (15)$$

$$c_{I_2} = 0.3 \cdot c_{I^-_0} - 0.8 \cdot c_{I^-_3} - 0.3 \cdot \sqrt{\left(c_{I^-_0} - \frac{8}{3} \cdot c_{I^-_3} \right)^2 - \frac{20 \cdot c_{I^-_3}}{3 \cdot K_B}}$$

Steps described above allow the calculation of the segregation index X_S and micromixedness ratio α using known parameters of raw solutions as well as measured absorbance of the outflowing mixture.

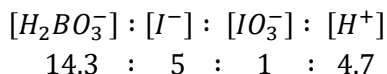
Concentrations of mixed solutions

Five pairs of solutions have been mixed using microstructured cyclone type. Concentrations of inlet solutions have been standardized by Institute for Micro Process Engineering, Karlsruhe Institute of Technology [10]. Standard set of concentration, abbrev. IMVT-1SC, (Tab. 2) is the basis of this system. Sets of other concentrations could be obtained by multiplying the amount of each chemical by the same number. For example, set IMVT-3SC used for this work contains chemicals of concentrations three times higher than declared in IMVT-1SC. NaH_2BO_3 has been made from equimolar mixture of sodium hydroxide (NaOH) and boric acid (H_3BO_3).

Tab. 2. Standard concentration sets. Values in [mol/dm³].

	Solution 1			Solution 2
	NaH_2BO_3	KI	KIO_3	H_2SO_4
IMVT-1 SC	0.0455	0.0159	0.0032	0.0150
IMVT-3 SC	0.1364	0.0478	0.0095	0.0450
IMVT-3.5SC	0.1591	0.0558	0.0111	0.0525
IMVT-4 SC	0.1818	0.0638	0.0127	0.0600
IMVT-4.5SC	0.2046	0.0717	0.0143	0.0675
IMVT-5 SC	0.2273	0.0797	0.0159	0.0750

As can be seen, molar ratios of reactants are as follows:



Equal volumetric streams have been applied to maintain equal molar streams of reactants. Solutions have been mixed in room temperature equal approx. 20 [°C].

RESULTS AND DISCUSSION

For each experiment the absorbance per 1 [cm] at peak near wavelength equal $\lambda=353$ [nm] has been recorded. For each measurement concentrations of reactants in the feed solutions and their densities have been known. What is more, the way of mixer and flange assembling has been noticed. Due to negligible difference in viscosity μ and density ρ of feeds, and constant width of inlet channels d and velocity of the liquid v on mixer inlet caused by application the same volumetric flow rates, it can be assumed, that Reynolds number $Re = \rho dv/\mu$ for inlets channels is equal for each case, and further, hydrodynamic conditions inside mixing chamber is the same for each case.

Experimental results

The set-up described in before was investigated using aqueous solutions, using different concentrations sets: IMVT-3SC, IMVT-3.5SC, IMVT-4SC, IMVT-4.5SC, and IMVT-5SC. Due to lengths of available cuvettes for spectrophotometer, it has not been possible to use lower concentrations (height of the peak comparable with measuring error while using the longest cuvette) as well as higher ones (optical density higher than 1 [-] while using the shortest one). Five equal volumetric streams have been applied: 2×0.5 [dm³/h], 2×1.0 [dm³/h], 2×1.5 [dm³/h], 2×2.0 [dm³/h], and 2×2.5 [dm³/h]. Hydrodynamic conditions in the mixing chamber have been investigated using different concentration sets; therefore different optical densities have been measured. Thanks to obtained results, micromixedness ratios α have been calculated according to the procedure described above and are presented in Fig. 3.

As can be seen (Fig. 3), observed α is not independent of concentration. Possible explanation of this phenomenon is the fact that the yield of iodine is not correlated with reactants concentration by linear function, since the order of reaction (Eq. 2) is higher than 1 [21]. However, we attempt to show a way to compare α values observed with different concentration sets.

It can be seen that obtained micromixedness ratios lies on the straight lines of different slopes, but of zero value around 0.6 [dm³/h]. Five hydrodynamics cases have been described by micromixedness ratios which have been dependent on the used concentrations set. It can be observed, that difference in calculated α is decreasing with increasing concentrations. To check the influence of reactants concentration on results, obtained data are presented on the plot with a concentration factor on the abscissa (Fig. 4). The concentration factor indicates how many times concentration of

every reactant has been raised in comparison to standard concentration set IMVT-1SC. In other words, it is the number n in notation $IMVT-nSC$. Both axes present logarithms of described values.

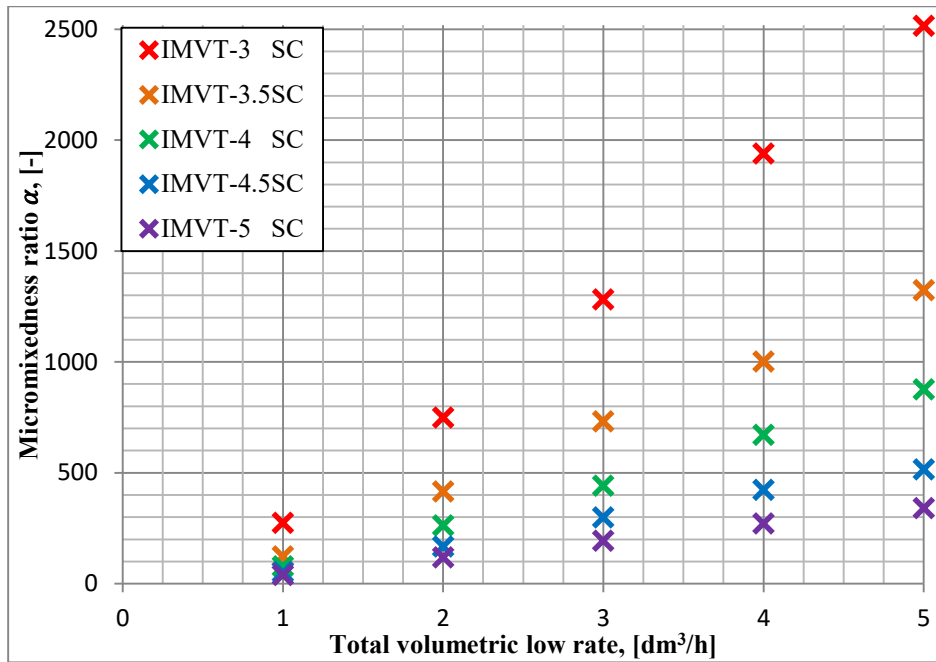


Fig. 3. Micromixedness ratios obtained using different concentrations sets.

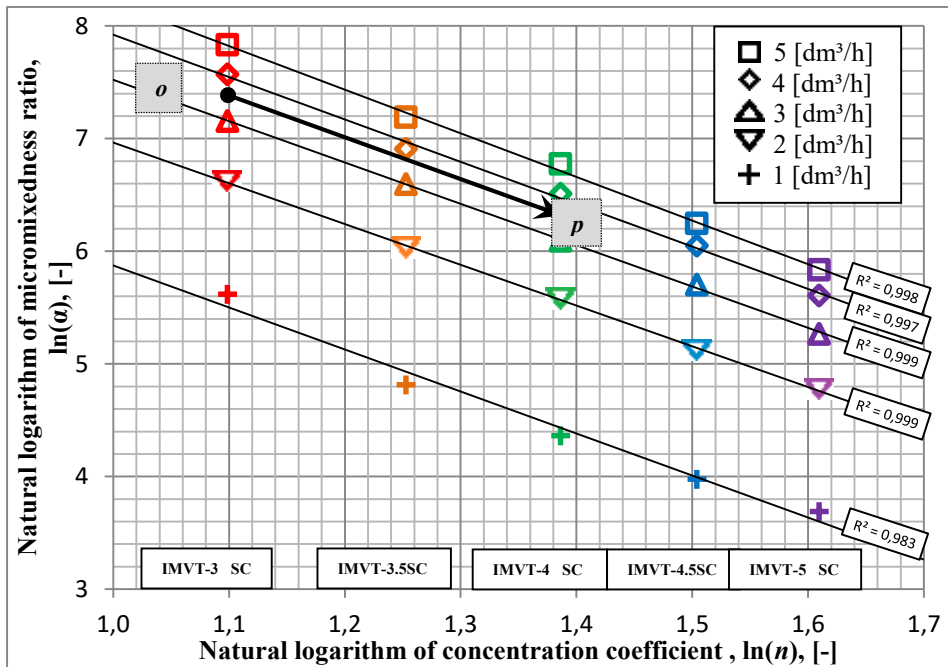


Fig. 4. Concentration influence on micromixedness ratio.

The fact that lines showing dependency of logarithm of micromixedness ratio $\ln(\alpha)$ on the concentration are parallel allows introducing the method of prediction of α in other concentration set than used. For example, the black arrow in Fig. 4 shows the prediction of micromixedness ratio obtained thanks to feed solutions with reactants concentrations described as IMVT-3SC (marked *o*—observed) to the situation, when IMVT-4SC would have been applied (marked *p*—predicted).

Correlation between results obtained using different concentrations

As can be seen in Fig. 4, points can be approximated using linear regression. The calculated average coefficient of determination R^2 is equal 0.995. Points representing higher flows fit better to straight lines ($R^2 = 0.997$ and more) than for the lowest flow rate ($R^2 = 0.983$). It can be pointed out, that measuring errors could have been higher while the lowest flow rate has been investigated. The accuracy of mass flow meters decreases when measured flow is lower than 0.1% of nominal [22], but remains of order of magnitude of few percent. Applied mass flow meters have been characterized by nominal flow of 100 [kg/h]. More significant impact could have been induced by uneven work of pumps which have been operated at very low voltages. The operating voltage change of the smallest possible unit has caused flow change sometimes of 0.02 [kg/h]. As a result, the relative error between indicated and obtained flow rates could have been larger, and asymmetry of flows could have caused larger relative error.

When approximating every series independently, 5 slightly different slopes k are obtained, which average is equal $k = -3.729$ with standard deviation of 0.087 (2.3% of mean value). To confirm this result, all series has been also estimated parallelly in order to try to obtain a better fitted slope value. For this reason, all points have been calculated using the formulas of straight lines with one slope. Using *Solver* in *MS Excel* the sum of squared residuals has been minimized to obtain the new slope value, which was the same as for 3 significant figures. Values calculated in described method have been compared with measured ones (Fig. 5.). What is more, mentioned transformation from IMVT-3SC into IMVT-4SC has been presented in this figure. Due to this operation result obtained using IMVT-3SC can be compared with results obtained using IMVT-4SC.

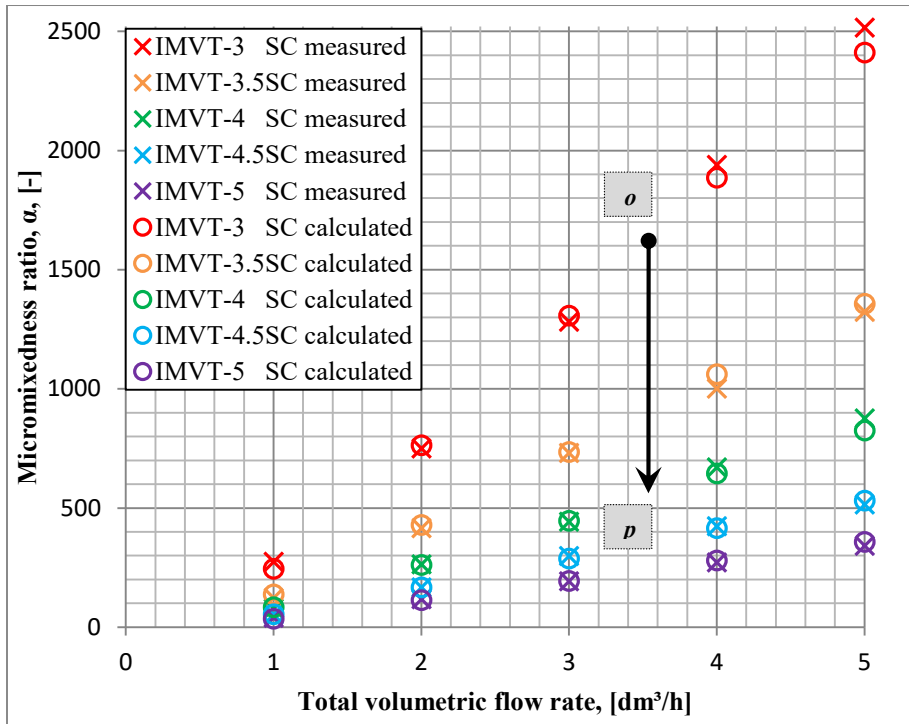


Fig. 5. Comparison of measured micromixedness ratio and estimated averaged values.

Average differences between measured and approximated values have been presented in Tab. 3. The most significant residua can be observed for the lowest flow rate. One of possibilities that could explain this phenomenon is lower accuracy of measured micromixedness ratio, as discussed above.

Tab. 3. An accuracy of data approximation.

Total volumetric flow rate	[dm³/h]	5	4	3	2	1	
Average residuum	[% of measured value]	4.1	3.5	1.6	2.1	8.1	3.9 mean

Obtained slope can be used to predict micromixedness ratios in different concentration set. Let us assume that subscript p denotes predicted value in new concentration set, while subscript o denotes obtained or used value. The symbol n denotes concentration coefficient described above. The linear dependency between old and new micromixedness ratio presented in log-log plot can be written as Eq. 16:

$$\ln(\alpha_p) - \ln(\alpha_o) = k \cdot [\ln(n_p) - \ln(n_o)] \quad (16)$$

Using logarithm properties, Eq. 16 can be written as Eq. 17:

$$\ln\left(\frac{\alpha_p}{\alpha_o}\right) = k \cdot \ln\left(\frac{n_p}{n_o}\right) \quad (17)$$

Eq. 17 can be rearranged in order to obtain an equation to predict micromixedness ratio value for different concentration sets (Eq. 18):

$$\alpha_p = \alpha_o \left(\frac{n_p}{n_o} \right)^k \quad (18)$$

with $k = -3.73$ determined above.

Inlet configuration impact

While operation, the mixer inlay is enclosed inside the dedicated flange adapter made of stainless steel. Outlet from the mixing inlay is located asymmetrically and, as a result, the inlay can be connected with the bottom part of the adapter only in one way. Due to symmetry of the inlet side of the mixer inlay (two same-shaped inlet chambers located opposite one another) it is possible to adjust the top adapter connector in two ways. Additionally, two feeds can be supplied alternatively to two flange inlets. As a result, it is possible to mount the mixing unit in four configurations, which are schematically presented in Fig. 6. Numbering of used configurations is detailed in Tab. 4. These were named in order to check if any inlet configuration impact can be observed.

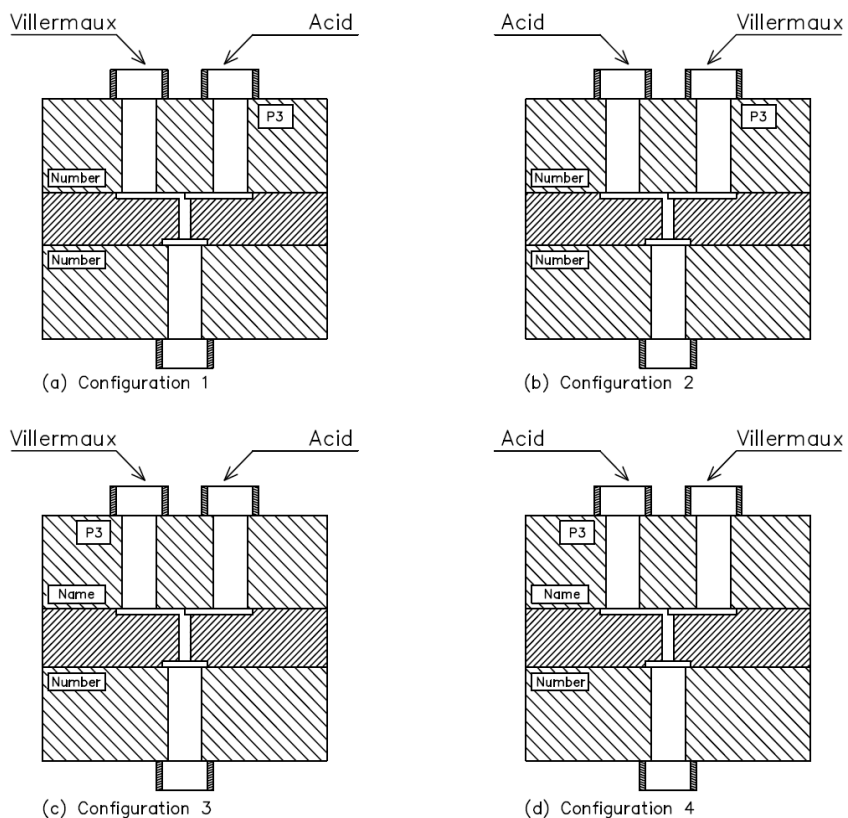


Fig. 6. Possible inlet configurations caused by the symmetries in mixer inlay and flange adapter.

Tab. 4. Numbering of inlet configurations.

Configuration 1	Acid solution in inlet P3	number opposite to the number
Configuration 2	Villiermaux solution in inlet P3	number opposite to the number
Configuration 3	Villiermaux solution in inlet P3	number opposite to the name
Configuration 4	Acid solution in inlet P3	number opposite to the name

For each point value of micromixedness ratio has been calculated according to the way presented in chapter “Obtained optical density as raw data to further calculations”. Values obtained in four different configurations have been averaged and the obtained mean value has been used in further calculations. Possible inlet configuration impact in that type of apparatus was described in detail in [14]. In this work none significant systematic error was observed.

CONCLUSIONS

Presented method to compare micromixedness ratios has been developed based on results of investigation of mixing in the cyclone type micromixer with iodide iodate reaction method. It is applicable for continuous-flow systems in microdevices where different reactants concentrations have been applied. One of requirements of the usage is maintaining molar ratios of reactants.

The method allows the calculation of exit iodine concentrations, without the explicit knowledge of the actual kinetic data.

Optical densities obtained using differently assembled mixing unit have been averaged to calculate mean micromixedness ratio for each flow and concentration set. It was applied in order to avoid configuration impact.

Thanks to presented protocol it is possible to broaden the range of investigated hydrodynamic conditions: higher reactants concentrations at higher flows as well as lower ones when mixing is less intensive can be applied and still calculated micromixedness ratios are comparable.

One using described method should keep in mind that the larger difference between used concentrations, the higher possible error.

ACKNOWLEDGEMENTS

This work was supported by the European Union via the program *Erasmus+*.

NOTATIONS

α	[-]	micromixedness ratio
ϵ_{OD}	[dm ³ /(mol·cm)]	molar extinction coefficient
μ	[Pa·s]	fluid viscosity
ρ	[kg/m ³]	fluid density
c_i	[mol/m ³]	concentration of i -th chemical
d	[m]	width of the inlet channel
K_B	[dm ³ /mol]	equilibrium constant of reaction (Eq. 3)
k	[-]	coefficient or exponent in micromixedness ratios comparison (constant)
l	[cm]	optical path length
n	[-]	concentration factor (in notation IMVT- n SC)
n_i	[mol]	number moles of i -th chemical
o	[-]	observed value of α
OD	[-]	optical density
p	[-]	predicted value of α
Re	[-]	Reynolds number
T	[K]	temperature
v	[m/s]	velocity of the liquid in the inlet channel
\dot{V}_i	[m ³ /s]	volumetric flow rate of the solution
V_{PM}	[-]	volume fraction of perfectly mixed fluid
V_{ST}	[-]	volume fraction of fluid with total segregation
X_S	[-]	segregation index
Y	[-]	the ratio of acid mole consumed in reaction of comproportionation (Eq. 2), which is equal the yield of iodine
Y_{ST}	[-]	iodine yield in theoretical reference case of total segregation

REFERENCES

- [1] Paul, E.L., Atiemo-Obeng, V.A., Kresta, S.M. (Ed.), *Handbook of Industrial Mixing*, Wiley Interscience, Hoboken, NJ, USA, 2004.
- [2] Pohorecki, R., Bałdyga, J., *The effects of micromixing and the manner of reactor feeding on precipitation in stirred tank reactors*, Chem. Eng. Sci., 1988, 43, 8, 1949–1954. DOI:10.1016/0009-2509(88)87067-2.
- [3] Fournier, M.-C., Falk L., Villermaux J., *A new parallel competing reaction system for assessing micromixing efficiency—determination of micromixing time by a simple mixing model*. Chem. Eng. Sci., 1996, 51, 5187–5192. DOI:10.1016/S0009-2509(96)00340-5.
- [4] Guichardon, P., Falk, L., *Characterisation of micromixing efficiency by the iodide-iodate reaction system. Part I: experimental procedure*. Chem. Eng. Sci., 2000, 55, 4233–4243. [http://dx.DOI.org/10.1016/S0009-2509\(00\)00068-3](http://dx.DOI.org/10.1016/S0009-2509(00)00068-3).
- [5] Nouri, L., Legrand, J., Benmalek, N., Imerzoukene, F., Yeddou, A.-R., Halet, F., *Characterisation and comparison of the micromixing efficiency in torus and batch stirred reactors*, Chem. Eng. J., 2008, 142, 78–86. DOI:10.1016/j.cej.2008.01.030.
- [6] Panić, S., Loebbecke, S., Tuercke, T., Antes, J., Boškovic, D., *Experimental approaches to a better understanding of mixing performance of microfluidic devices*. Chem. Eng. J., 2004, 101, 409–419. DOI:10.1016/j.cej.2003.10.026.
- [7] Men Y., Hessel V., Löb P., Löwe H., Werner B., Baier T., *Determination of the segregation index to sense the mixing quality of pilot- and production-scale microstructured mixers*, Chemical Engineering Research and Design, 2007, 85(A5), 605–611. DOI:10.1205/cherd06172.
- [8] Commerge, J.-M., Falk, L., *Villermaux–Dushman protocol for experimental characterization of micromixers*. Chemical Engineering and Processing, 2011, 50, 979–990. DOI:10.1016/j.cep.2011.06.006.
- [9] Bourne, J., *Comments on the iodide/iodate method for characterizing micromixing*, Chem. Eng. J., 2008, 140, 638–641. DOI:10.1016/j.cej.2008.01.031.
- [10] Kölbl, A., Kraut, M., Schubert, K., *The iodide iodate method to characterize microstructured mixing devices*. AIChEJ, 2008, 54, 639–645. DOI:10.1002/aic.11408.
- [11] Bourne, J., *Mixing and the Selectivity of Chemical Reactions*, Organic Process Research & Development, 2003, 7, 471–508. DOI:10.1021/op020074q.

- [12] Jasińska, M., *Test reactions to study efficiency of mixing*, Chem. Process Eng., 2015, 36, 2, 171–208. DOI:10.1515/cpe-2015-0013.
- [13] Villermaux, J., Falk, L., Fournier, M.C., *Potential use of a new parallel reaction system to characterize micromixing in stirred reactors*. [in:] Tatterson, G.B. (Ed.) *Industrial Mixing Technology: Chemical and Biological Applications*. AIChE Symposium Series, 1994, 299, 90, 50–53.
- [14] Kölbl, A., Kraut, M., Wenka, A., *Design parameter studies on cyclone type mixers*. Chem. Eng. J., 2011, 167, 444–454. DOI:10.1016/j.cej.2010.08.092.
- [15] Awtrey A., Connick R., *The Absorption Spectra of I_2 , I_3^- , I^- , IO_3^- , $S_4O_6^{2-}$ and $S_2O_3^{2-}$. Heat of the Reaction $I_3^- = I_2 + I^-$* , J. Am. Chem. Soc., 1951, 73, 4, pp 1842–1843. DOI:10.1021/ja01148a504.
- [16] Palmer D., Ramette R., and Mesmer R., *Triiodide Ion Formation Equilibrium and Activity Coefficients in Aqueous Solution*, Journal of Solution Chemistry, 1984, Vol. 13, No. 9. DOI:10.1007/BF00650374
- [17] Wei YG, Liu CG, Mo LP, *Ultraviolet absorption spectra of iodine, iodide ion and triiodide ion*, Guang Pu Xue Yu Guang Pu Fen Xi, 2005, 25(1), 86–8.
- [18] Burgess A., Davidson J., *A Kinetic–Equilibrium Study of a Triiodide Concentration Maximum Formed by the Persulfate–Iodide Reaction*, J. Chem. Educ., 2012, 89, 814–816. DOI:10.1021/ed200055t.
- [19] Thompson K. C., Gillespie S., Goslan E., *Disinfection By-products in Drinking Water*, RSC, 2015.
- [20] Villermaux, J. *Micromixing phenomena in stirred reactors*. [in:] *Encyclopedia of fluid mechanics*. Houston: Gulf Publishing Company, 1986.
- [21] Kölbl, A., Kraut, M., Dittmeyer, K., *Kinetic investigation of the Dushman reaction at concentrations relevant to mixing studies in microstructured cyclone type mixers*. Chem. Eng. Sci., 2013, 101, 454–460. DOI:10.1016/j.ces.2013.07.008.
- [22] O'Banion, *Coriolis: The Direct Approach to Mass Flow Measurement*, AIChE, CEP, 2013.

New, simple method of determining necessary conditions of dead zone formation in catalyst pellet

*Grzegorz Król¹, Mirosław Szukiewicz¹

¹Faculty of Chemistry, Rzeszow University of Technology, Rzeszow, POLAND

e-mail: ich_gk@prz.edu.pl

***Keywords:** dead zone in catalyst pellet, necessary conditions of dead zone formation in catalyst pellet*

ABSTRACT

New, simple method of determining necessary conditions of dead zone formation is proposed. The method was compared with a procedure discussed earlier in literature. The method efficiency was tested on a basis of few well know reaction systems (one-reagent reaction, multi-reagent reaction, consecutive reaction, parallel reaction and consecutive – parallel reaction) with power law and Langmuir-Hinshelwood kinetic equations. The new method application is simpler than the formers and allows to detect and fill some gaps in presented in literature results. Due to simplicity the method can be especially recommended for complex reactions systems.

INTRODUCTION

Great number of organic and inorganic compounds is manufactured on solid-state catalysts. In these heterogeneous reaction systems, mass transfer of reactants first takes place from the bulk fluid to the external surface of the pellet. Then the reactants migrate from the external surface into and through the pores within the pellet, with reaction taking place only on the catalytic surface of the pores. So that both transfer of the reactants into a catalyst pellet and reaction rate have an influence on a rate of processes running on solid-state catalyst [1]. If diffusion is much slower than reaction rate, i.e. diffusional resistances are large, concentration of reactants towards the pellet center decreases rapidly. For sufficiently strong diffusional limitations, concentration of a reagent in a pellet center drops down to zero – in a pellet center appears zone without reaction (so called 'dead zone')[2,3,4]. In consequence, efficiency of catalyst process decreases. So that it is significant task to predict operation conditions of reactor for which such zone could appear in catalyst pellet.

Determination of the conditions of dead zone formation is quite hard task, for this reason they have not been fully formulated. Sufficient conditions can be determined only for few simplest cases. Therefore, most frequently necessary conditions have been presented [5,6,7]. If they are not satisfied, dead zone cannot be formed. Despite, that fulfilling of necessary condition does not guarantee that dead zone appears, knowledge of necessary conditions is very important from practical point of view. It enables to exclude the cases for which dead zone cannot be formed.

Andreev [8] developed general method of determining necessary conditions of dead zone formation and applied them to few well know reaction systems (one-reagent reaction, multi-reagent reaction, consecutive reaction, parallel reaction and consecutive – parallel reaction) with power law and Langmuir-Hinshelwood kinetic equations. His procedure seems to be a bit complex. So that recently we developed our own procedure [9] of determining necessary conditions of dead zone formation. It will be called further “integral” method, because it bases on testing convergence of integrals.

Our method was tested for the same reaction systems as has been presented by Andreev. Obtained results were in most cases the same as those presented in [8]. It confirm that our conception was errorless and it can be used for other reaction systems which have not been considered in literature so far. But we detected also an exception. Application of our algorithm for multi-reagent systems allowed to obtain more precise relationships. This case will be described in details in present paper.

NECESSARY CONDITIONS OF DEAD ZONE FORMATION FOR TWO-REAGENT REACTION

Further considerations will focus on two-reagent reaction of the form:



with kinetic equation related to compound A:

$$R_A = k \cdot C_A^n \cdot C_B^m \quad (2)$$

For mentioned reaction rate of vanishing of compound B could be write as follow:

$$R_B = \frac{b}{a} \cdot k \cdot C_A^n \cdot C_B^m \quad (3)$$

Concentration of compound A and compound B can drop down to zero inside the pellet, so that dead zone can be formed by A or by B or by both compounds simultaneously. To simplify our investigations, let's assume now that only necessary conditions of dead zone formation by compound A would be further considered.

Prater-like relationship between concentrations of compounds A and B

It is purposeful to present Prater-like relationship between concentrations of compound A and B at first.

Steady-state mass-balance set of equations for components A, B in pellet of various geometry ($\alpha=0$ flat, $\alpha=1$ cylindrical, $\alpha=2$ spherical) has a form:

$$\left\{ \begin{array}{l} D_{eA} \cdot \frac{1}{r^\alpha} \cdot \frac{d}{dr} \left(r^\alpha \cdot \frac{dC_A}{dr} \right) = k \cdot C_A^n \cdot C_B^m \\ D_{eB} \cdot \frac{1}{r^\alpha} \cdot \frac{d}{dr} \left(r^\alpha \cdot \frac{dC_B}{dr} \right) = \frac{b}{a} \cdot k \cdot C_A^n \cdot C_B^m \end{array} \right. \quad (4)$$

with boundary conditions on external surface of catalyst:

$$C_A(R) = C_{A,S}, C_B(R) = C_{B,S} \quad (5),(6)$$

where:

D_A, D_B – effective diffusivities of reagents respectively A i B,

r – position in the pellet,

R – pellet radius.

Assuming that concentration of compound A vanishes to zero at r_0 (dead zone for compound A form the range $r_0 \geq r \geq 0$), following conditions for concentration of compound A at point r_0 should be fulfilled:

$$C_A(r_0) = 0, \left. \frac{dC_A}{dr} \right]_{r=r_0} = 0 \quad (7),(8)$$

Because reaction does not occur in the range $r_0 \geq r \geq 0$, concentration of compound B does not change in this range. So that following condition for compound B is also fulfilled:

$$\left. \frac{dC_B}{dr} \right]_{r=r_0} = 0 \quad (9)$$

Equations set (4) with conditions (5),(6),(7),(8),(9) completely describe dead zone formation by compound A in this system.

We can transform set (4) to:

$$\begin{cases} D_{eB} \cdot \frac{D_{eA}}{D_{eB}} \cdot \frac{b}{a} \cdot \frac{1}{r^\alpha} \cdot \frac{d}{dr} \left(r^\alpha \cdot \frac{dC_A}{dr} \right) = \frac{b}{a} \cdot k \cdot C_A^n \cdot C_B^m \\ D_{eB} \cdot \frac{1}{r^\alpha} \cdot \frac{d}{dr} \left(r^\alpha \cdot \frac{dC_B}{dr} \right) = \frac{b}{a} \cdot k \cdot C_A^n \cdot C_B^m \end{cases} \quad (10)$$

Than from set (10) we derive:

$$D_{eB} \cdot \frac{D_{eA}}{D_{eB}} \cdot \frac{b}{a} \cdot \frac{1}{r^\alpha} \cdot \frac{d}{dr} \left(r^\alpha \cdot \frac{dC_A}{dr} \right) = D_{eB} \cdot \frac{1}{r^\alpha} \cdot \frac{d}{dr} \left(r^\alpha \cdot \frac{dC_B}{dr} \right) \quad (11)$$

Dividing equation (11) by $D_{eB} \cdot r^\alpha$ and integrating it from r_0 to r gives:

$$\frac{b}{a} \cdot \frac{D_{eA}}{D_{eB}} \cdot \int_{r_0}^r \frac{d}{dr} \left(r^\alpha \cdot \frac{dC_A}{dr} \right) dr = \int_{r_0}^r \frac{d}{dr} \left(r^\alpha \cdot \frac{dC_B}{dr} \right) dr \quad (12)$$

Next, introducing Eq (8), (9) to (12) leads to:

$$\frac{b}{a} \cdot \frac{D_{eA}}{D_{eB}} \cdot r^\alpha \cdot \frac{dC_A}{dr} = r^\alpha \cdot \frac{dC_B}{dr} \quad (13)$$

and after dividing by r^a and second integrating it from R to r we obtain:

$$\frac{b}{a} \cdot \frac{D_{eA}}{D_{eB}} \cdot \int_R^r \frac{dC_A}{dr} dr = \int_R^r \frac{dC_B}{dr} dr \quad (14)$$

Introduction of Eq (5),(6) into equation (14) gives:

$$\frac{b}{a} \cdot \frac{D_{eA}}{D_{eB}} \cdot (C_A - C_{A,S}) = C_B - C_{B,S} \quad (15)$$

Equation (15) is an analog of well-known Prater equation.

It could be rewritten as follow:

$$\frac{b}{a} \cdot \frac{D_{eA}}{D_{eB}} \cdot \frac{C_{A,S}}{C_{B,S}} \cdot (C_A \cdot \frac{C_{B,S}}{C_{A,S}} - C_{B,S}) = C_B - C_{B,S} \quad (16)$$

Denote:

$$W_A = \frac{D_{eA}}{D_{eB}} \cdot \frac{C_{A,S}}{C_{B,S}} \cdot \frac{b}{a} \quad (17)$$

Finally we can write down relations between concentration of compound B and concentration of compound A:

$$C_B = W_A \cdot \frac{C_{B,S}}{C_{A,S}} \cdot C_A + (1 - W_A) \cdot C_{B,S} \quad (18)$$

For $r = r_0$ we obtain:

$$C_B(r_0) = (1 - W_A) \cdot C_{B,S} \quad (19)$$

We can draw some interesting conclusions:

- if $W_A > 1$, $C_B(r_0) < 0$ – so that this case has no physical meaning
- if $W_A = 1$, $C_B(r_0) = 0$ – it means that concentration of compounds A, B simultaneously vanishes to zero at r_0
- if $W_A < 1$, $C_{B(r_0)} > 0$, concentration of compound B is always greater than zero inside pellet.

Integral method

Our procedure in general form was described in [9] in details. Now we will present fundamentals of integral method on the basis of two-reagent reaction.

Mass balance equation for compound A (first equation in set (4)) could be rewritten in dimensionless form, as follows:

$$\frac{1}{x^\alpha} \cdot \frac{d}{dx} (x^\alpha \cdot \frac{dC_A^\#}{dx}) = \phi^2 \cdot C_A^{\#n} \cdot C_B^{\#m} \quad (20)$$

where:

$$x = \frac{r}{R}, C_A^\# = \frac{C_A}{C_{A,S}}, C_B^\# = \frac{C_B}{C_{B,S}}, \text{ Thiele modulus: } \phi = \sqrt{\frac{R^2 \cdot k \cdot C_{A,S}^n \cdot C_{B,S}^n}{C_{A,S} \cdot D_{eA}}}$$

Next, relation between dimensionless concentrations of compounds B and A could be written on a basis of equation (18), as follows:

$$C_B^\# = W_A \cdot C_A^\# + (1 - W_A) \quad (21)$$

After introducing equation (21) to equation (20), one can finally obtain:

$$\frac{1}{x^\alpha} \cdot \frac{d}{dx} \left(x^\alpha \cdot \frac{dC_A^\#}{dx} \right) = \phi^2 \cdot C_A^{\#n} \cdot [(1 - W_A) + W_A \cdot C_A^\#]^m \quad (22)$$

where:

$$R(C_A^\#) = C_A^{\#n} \cdot [(1 - W_A) + W_A \cdot C_A^\#]^m \quad (23)$$

is dimensionless reaction rate in terms of compound A concentration.

One can now derived necessary conditions of dead zone formation by compound A in two-reagent system from convergence of following integrals:

$$I_{1p} = \int_0^{C_A^\#} (C_A^\#)^n \cdot [(1 - W_A) + W_A \cdot C_A^\#]^m dC_A^\# \quad (24)$$

$$I_{2p} = \int_0^1 \frac{dC_A^\#}{\sqrt{\int_0^{C_A^\#} (C_A^\#)^n \cdot [(1 - W_A) + W_A \cdot C_A^\#]^m dC_A^\#}} \quad (25)$$

In our opinion, the comparison test [10] is the simplest way of examination of convergence of integrals (24) and (25).

If $W_A < 1$, it is easily to show that integrals (24) and (25) are converged if and only if:

$$1 > n > -1 \quad (26)$$

So that for this case necessary conditions obtained by Andreev. [8] remain valid.

However, if $W_A = 1$ will be assumed, equation (22) and integrals (24) and (25) can be easily simplified to (27), (28) and (29), respectively:

$$\frac{1}{x^\alpha} \cdot \frac{d}{dx} \left(x^\alpha \cdot \frac{dC_A^\#}{dx} \right) = \phi^2 \cdot (C_A^\#)^{n+m} \quad (27)$$

$$I_{1p} = \int_0^c (C_A^\#)^n \cdot C_A^{\#m} \cdot dC_A^\# \quad (28)$$

$$I_{2p} = \int_0^1 \frac{dC_A^\#}{\sqrt{\int_0^c (C_A^\#)^n \cdot C_A^{\#m} \cdot dC_A^\#}} \quad (29)$$

In this case integrals (28) and (29) are convergent if and only if when:

$$1 > n + m > -1 \quad (30)$$

One can notice that for $W_A = 1$:

- dimensionless concentrations of compound A and B is equal through whole pellet (see equation (21))
- compound A and B simultaneously form dead zone
- necessary conditions of dead zone formation for this case should have a form of inequalities (30), rather than (26)

Eq. (30) shows that if $W_A = 1$, conditions of dead zone formation significantly differs from those for $W_A < 1$. Andreev [8] completely omitted the case of $W_A = 1$. In our opinion, the mentioned gap appeared, because an isolation of particular cases by Andreev's method is quite hard task. To show it, let's present Andreev's algorithm.

Andreev's method

Andreev evolved his method by applying mean-value theorem to mas- and thermal-balance equations of catalyst pellet. In this way he obtained procedure based on calculations of two appropriate function limits [8]. After application of this general procedure to kinetic equation (2), one can obtain following formulas:

$$\lim_{C_A \rightarrow 0, C_B \rightarrow C_B^*} \frac{1}{C_A \cdot (k \cdot C_A^n \cdot C_B^m)} = \infty \quad (31)$$

$$\lim_{C_A \rightarrow 0, C_B \rightarrow C_B^*} \frac{k \cdot C_A^n \cdot C_B^m}{D_{eA} \cdot C_A} = \infty \quad (32)$$

where C_B^* is a compound B concentration at a position in catalyst where $C_A=0$.

After reorganization formulas (3) and (4) take a form:

$$\lim_{C_A \rightarrow 0, C_B \rightarrow C_B^*} \frac{1}{k \cdot (C_A^{n+1} \cdot C_B^m)} = \infty \quad (33)$$

$$\lim_{C_A \rightarrow 0, C_B \rightarrow C_B^*} \frac{k \cdot C_A^{n-1} \cdot C_B^m}{D_{eA}} = \infty \quad (34)$$

Next, assuming that $C_B^* > 0$, conditions (33) and (34) could be rewritten as follows:

$$n + 1 > 0 \quad (35)$$

$$n - 1 < 0 \quad (36)$$

and finally:

$$1 > n > -1 \quad (37)$$

Eq. (37) correspond to (26) and this is the only condition presented in [8] for multi-reagent reaction. However, more detailed analysis of relations (5) and (6) shows that if C_B^* would be equal to 0, exponent m would have also an influence on fulfillment of these equalities. $C_B^* = 0$ means that both compounds should form dead zone simultaneously. Such situation was not included in Andreev's investigations.

In our opinion, the weak side of Andreev's procedure lies in fact that particular cases of solution can be easily omitted, if we consider more complex process. We showed, that the Andreev's method allows to detect the case of $W_A=1$, but its detection is more difficult. Finding of the particular cases was much more easier when integral method was used. For this reason, the integral method can be especially recommended for complex reactions systems.

CONCLUSIONS

The analysis of obtained result leads to the following conclusions:

- Integral procedure is simple, precise and fast method to examine necessary conditions of dead zone formation.
- Integral method is easier in application than presented earlier in literature.

ACKNOWLEDGEMENTS

This work was supported by grant no. 2015/17/B/ST8/03369 of the National Science Centre, Poland.

REFERENCES

- [1] Jayaraman V.K., Doraiswamy L.K., Some aspects of diffusional interference in catalytic reactions, *Current Science*, 1983, 52, 7, 280-290.
- [2] Thiele E. W., Relation between catalytic activity and size of particle, *Industrial & Engineering Chemistry*, 1939, 31,7, 916-920.
- [3] Temkin M. I., Diffusion effects during the reaction on the surface pores of a spherical catalyst particle, *Kinetic and Catalysis*, 1975, 16, 104-112.
- [4] Aris R., *Mathematical theory of diffusion and reaction in permeable catalyst*, Clarendon Press, Oxford University Press, London, 1975.
- [5] Fedotov V. Kh., Alekseev B. V., Koltsov N. I., "Dead zone" in porous catalyst grain for reactions with slightly nonmonotonic kinetic, *Reaction Kinetics and Catalysis Letters*, 1985, 29, 1, 71-77.

- [6] Garcia-Ochoa F., Romero A., The dead zone in a catalyst particle for fractional-order reactions. *AIChE Journal*, 1988, 34, 1916-1918, DOI: 10.1002/aic.690341120.
- [7] York R.L., Bratlie K.M., Hile L.R., Jang L.K., Dead zones in porous catalysts: Concentration profiles and efficiency factors, *Catalysis Today*, 2011, 160, 1, 204-212, DOI: 10.1016/j.cattod.2010.06.022.
- [8] Andreev V. V., Formation of a “dead zone” in porous structures during processes that proceeding under steady state and unsteady state conditions, *Review Journal of Chemistry*, 2013, 3,3, 239-269, DOI: 10.1134/S2079978013030011.
- [9] Król G., Szukiewicz M., Conditions of dead zone forming in porous catalyst pellet, *The 22nd Polish Conference of Chemical and Process Engineering*, Conference Proceedings, 2016, 615-623.
- [10] Buck, R. C., *Advanced Calculus (2nd ed.)*, New York: McGraw-Hill, 1965.

The influence of the classic pore precursors on the morphology of polyesters membranes for tissue engineering

*Aleksandra Kruk¹, Agnieszka Gadomska-Gajadur¹, Paweł Ruśkowski¹, Karolina Łojek¹, Urszula Stodulska¹, Ludwik Synoradzki¹

¹Faculty of Chemistry, Warsaw University of Technology, Warsaw, POLAND

e-mail: akruk@ch.pw.edu.pl

Keywords *tissue engineering, scaffolds, polylactide, poly-ε-caprolactone, biodegradable polymers*

ABSTRACT

The results of the preparation of semi-permeable membranes using inversion phase method were presented. The membranes were made of poly-L-lactide or poly-ε-caprolactone. The influence of classic pore precursor on the morphology of membranes was analysed. The results showed that addition of pore precursor promotes the growth of the number and size of pores. The influence of the kind of pore precursor for each polyesters is different. For this reason, for each of the polyesters should be selected suitable pore precursor.

INTRODUCTION

In the recent years, the most interesting field of tissue engineering are scaffolds. There are three-dimensional structures, which are used for regenerate damaged tissues [1–3]. Exist many form of scaffolds, very popular are nano-non-wovens, self-assembly hydrogels scaffolds, acellural scaffolds and porous scaffolds [4, 5]. Porous scaffolds are solid materials, which frequently occur in form of semi-permeable membranes. This form allow to delivery of nutrients to the cells and evacuation of metabolites outside the scaffold [6–8].

Popular materials for production of porous scaffolds are polymers, natural and synthetic [10, 11]. In first group, are polymers naturally occurring in organisms, e.g. gelatin, chitozan or collagen. Second group, includes mainly biodegradable polymers, e.g. polylactide (PLA), poly-ε-caprolactone (PCL), polyglycolide (PGA) or their copolymers. This polyesters are characterised by biocompatibility and biodegradability and are well-tolerated by organisms [12, 13]. Moreover, these compounds and their degradation products are non-toxic to the organism cells. Additionally, they are subject to hydrolytic decomposition, first to the building monomers which are physiologically present in organisms of mammals and subsequently to CO₂ and water, products of physiological metabolism which are easily excreted from the organism. These polyesters differ in degradation time which, for a given polymer, increases with the length of carbon chain. Thanks to this characteristic, it is possible to control, to some extent, degradation time of the whole scaffold by choosing appropriate polymer with a specific molecular weight [13–14].

The main role of the scaffolds is mimic to natural extracellular matrix (ECM). ECM is a necessary element of tissue, it provides support for cells. The properties of scaffolds must be similar to properties of ECM of regenerated tissue. For this reason, the morphology and mechanical properties of scaffold must be adjust to the type of treated tissue [15, 16].

Exist many method of obtaining porous scaffolds. One of the most popular is inversion phase method. This technique is based on pouring of the membrane-forming polymer solution onto an inert base (e.g. glass plate) and on subsequent immersion thereof in coagulation bath consisting of insoluble polymer. After polymer coagulation, the membrane is taken out of the coagulation bath and dried. Variant of this method is addition of pore precursors to polymeric solution. For this purpose, other polymers (e.g. polyvinylpyrrolidone, poly(ethylene glycol)) or non-organic salts with appropriate crystal diameter are mainly used. Pore precursors are washed out from the structure of the already coagulated membrane [17–19].

In this work, the influence of pore precursors which are common used in the inversion phase method on the morphology of the polyesters membranes were compared. Shown that in this method there is not universal pore precursor and for the each polymer, proper pore precursor should be selected. In the literature we can find many works about inversion phase method, but they don't show comparison of influence of pore precursors on the morphology of the membranes depending on used polyesters.

MATERIALS AND METHOD

Materials

Poly-L-lactide (PLLA) of M_n 86 000 g/mol NW 2003D was distributed by Nature Works. Poly- ϵ -caprolactone (PCL) of M_n 80 000 g/mol was distributed by Sigma Aldrich. Polyvinylpyrrolidone (PVP) of M_n 10 000 g/mol, poly(ethylene glycol) (PEG) of M_n 20 000 g/mol and Pluronic® F-127 were distributed by Sigma Aldrich. Chloroform and methanol were distributed by POCh SA. Ultrapure water with 18.2 M Ω cm conductivity was obtained using MiliQ device.

Preparation of the membrane-forming solution

The solutions of poly-L-lactide or poly- ϵ -caprolactone with the addition of pore precursors (PVP, PEG, Pluronic® or NaCl) and without them, were prepared. Firstly, solution of polyesters in chloroform with 350 cP viscosity were obtained. Polymers were dissolved in organic solvent during 24 h with constant stirring using a magnetic stirrer without heating. Pore precursors (in 1:1 weight ratio to polymer) were added after complete dissolution of polyesters. Subsequently the stirring was continued for the next 24 h. In the case of addition of NaCl, firstly crystals of salts were crushed in a mortar.

Preparation of membranes

The polyester solutions in chloroform with addition of pore precursors and without it, were poured onto a glass base. Thickness of solution on a base was 0,4 mm. The membranes were gelled in methanol and subsequently washed in water. The membranes were dried after polymer coagulation and removal of pore precursor.

Analytical methods

The viscosity of polylactides solutions in chloroform was analysed using viscosimetric method in a capillary viscometer. The viscosity was measured by a flow time of a given quantity of liquid by a suitably calibrated capillary tubes with a known pressure difference.

The morphology of cross-sections for membranes and both surfaces was analysed using Scanning Electron Microscopy (SEM) Hitachi TM1000. Samples of the membranes were immersed in ethanol and then fractured in liquid nitrogen. After drying, the membrane samples were coated with 7–10 nm thick gold layer using K550X Sputter Coater. Samples coated with gold were analysed in 300x magnifications using 15 kV acceleration voltage.

RESULTS

Semi-permeable membranes made from poly-L-lactide or poly- ϵ -caprolactone were obtained. For the each polyester influence of classic pore precursors on morphology of the membranes was examined. As a pore precursors polyvinylpyrrolidone, poly(ethylene glycol), Pluronic® and NaCl were used.

Membranes obtained without addition pore precursors

The membranes obtained from PLLA without pore precursors (Fig. 1) on the lower surface (located on the side of the glass plate used as a base) contain rare pores, 2–5 μm in diameter. In the cross-section were observed pores, in size 5–15 μm . At the lower surface, pores were smaller, about 5 μm . At the upper surface, pores were bigger, 10–15 μm in diameter. The upper surface was more porous, than lower one. The pores were in size 3–10 μm . On the both surfaces pores were coated with a thin covering layer.

On the lower surface of the PCL membranes obtained without addition of pore precursors (Fig. 2) were observed rare pores, in size 1–5 μm . In the cross-section were observed pores, 15–25 μm in diameter. On the lower surface, pores were bigger, 20–30 μm . The upper surface was more porous, than lower one. Moreover, the pores were bigger, their size were in range 15 to 25 μm . The other pores on this surface were coated with a thin covering layer.

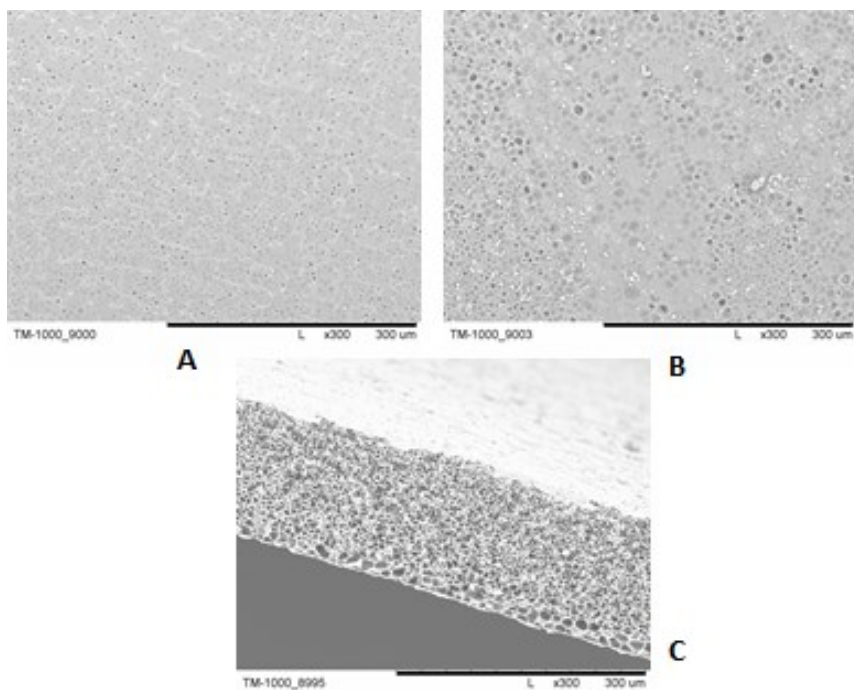


Fig. 1. SEM photomicrographs of PLLA membranes obtained without pore precursor. A – lower surface, B – upper surface, C – cross-section

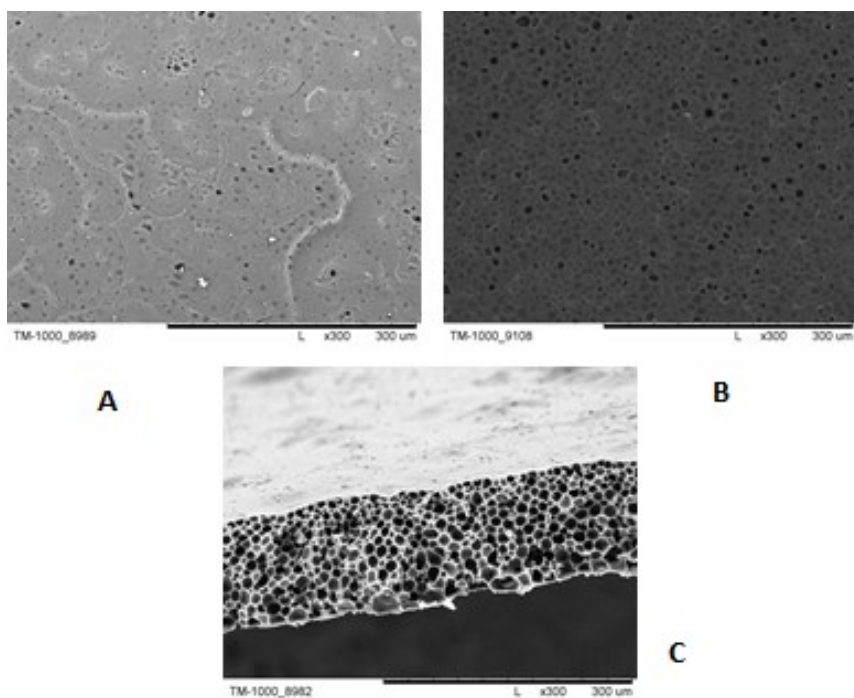


Fig. 2. SEM photomicrographs of PCL membranes obtained without pore precursor. A – lower surface, B – upper surface, C – cross-section.

Membranes obtained with addition of PVP

The PLLA membranes obtained with addition of PVP as a pore precursor (Fig. 3) on the lower surface contained rare pores, about 5 and 25–40 μm in diameter. In the cross-section were observed pores in size 15–20 μm . At the both surfaces pores were bigger, 20–30 μm . On the upper surface occurred multiple pores, in size 5–10 and 15–20 μm .

The PCL membranes obtained with addition of PVP as a pore precursor (Fig. 4) on the lower surface contained rare pores, about 5 and 25–40 μm in diameter. In the cross-section were observed pores in size 30–60 μm . At the lower surface pores were bigger, 55–75 μm , and at the upper surface smaller, 20–30 μm . The upper surface pores was more porous than lower one, size of the pores was in range 5–15 μm .

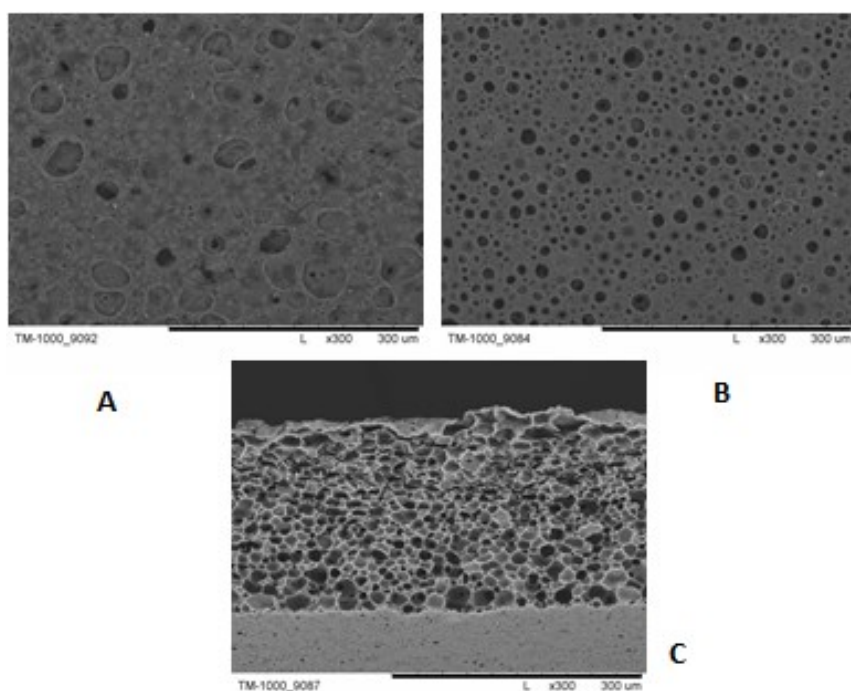


Fig. 3. SEM photomicrographs of PLLA membranes obtained with addition of PVP. A – lower surface, B – upper surface, C – cross-section.

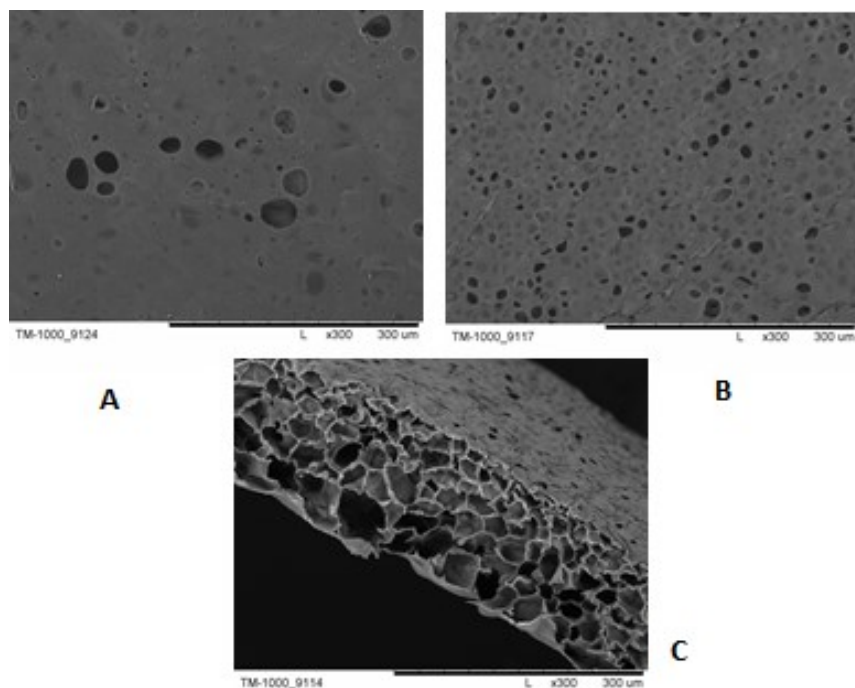


Fig. 4. SEM photomicrographs of PCL membranes obtained with addition of PVP. A – lower surface, B – upper surface, C – cross-section.

Membranes obtained with addition of PEG

The PLLA membranes obtained with addition of PEG as a pore precursor (Fig. 5), on the lower surface contained pores coated with a thin covering layer. In the cross-section were observed pores in size 5–10 μm . At the lower surface pores was bigger, in size about 15 μm . Between them occurred smaller pores, below 5 μm in diameter. The upper surface contain multiple pores in size 5–10 μm . Part of the pores was covered with a thin covering layer.

On the lower surface of the PCL membranes obtained with addition of PEG (Fig.6) pores were coated with a thin covering layer. In the cross-section size of the pores was 15–30 μm . At the lower surface pores were bigger, 55–70 μm in diameter. At the upper surface pores were smaller, in size 15–20 μm . On the upper surface were observed rare pores, 10–25 μm in diameter. Most of these pores were coated with a thin covering layer.

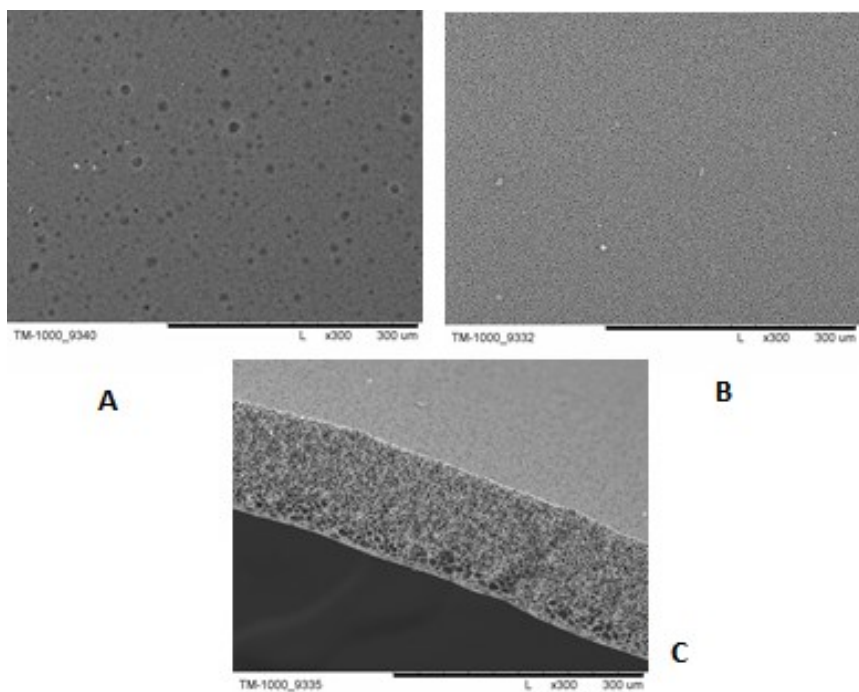


Fig. 5. SEM photomicrographs of PLLA membranes obtained with addition of PEG. A – lower surface, B – upper surface, C – cross-section.

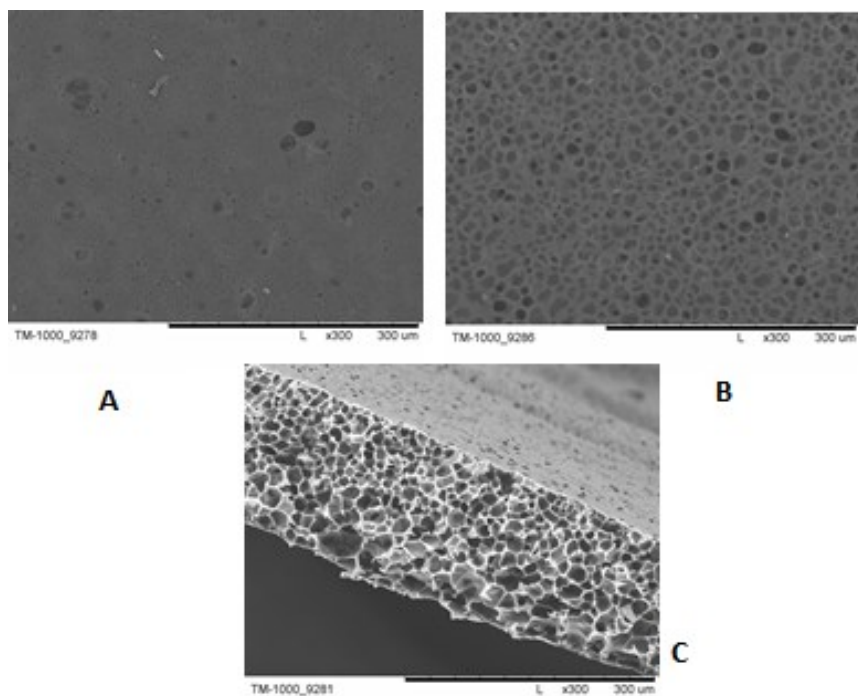


Fig. 6. SEM photomicrographs of PCL membranes obtained with addition of PEG. A – lower surface, B – upper surface, C – cross-section.

Membranes obtained with addition of Pluronic®

The PLLA membranes obtained with addition of Pluronic® as a pore precursor (Fig. 7) on the lower surface contained rare pores, in size 5–15 μm . Other pores on this surface were coated by covering layer. In the cross-section were observed pores 5–15 μm in diameter. At the lower surface pores were bigger, in size 20–30 μm . The upper surface contained multiple pores, 5–15 μm in diameter.

The PCL membranes obtained with addition of Pluronic® as a pore precursor (Fig. 8) on the lower surface contain rare pores, in size about 5 and 15–30 μm . In the cross-section were observed pores, 15–25 μm in diameter. At the lower surface pores were bigger, in size 30–50 μm and were oblong in shape. The upper surface contained pores 10–15 μm in diameter.

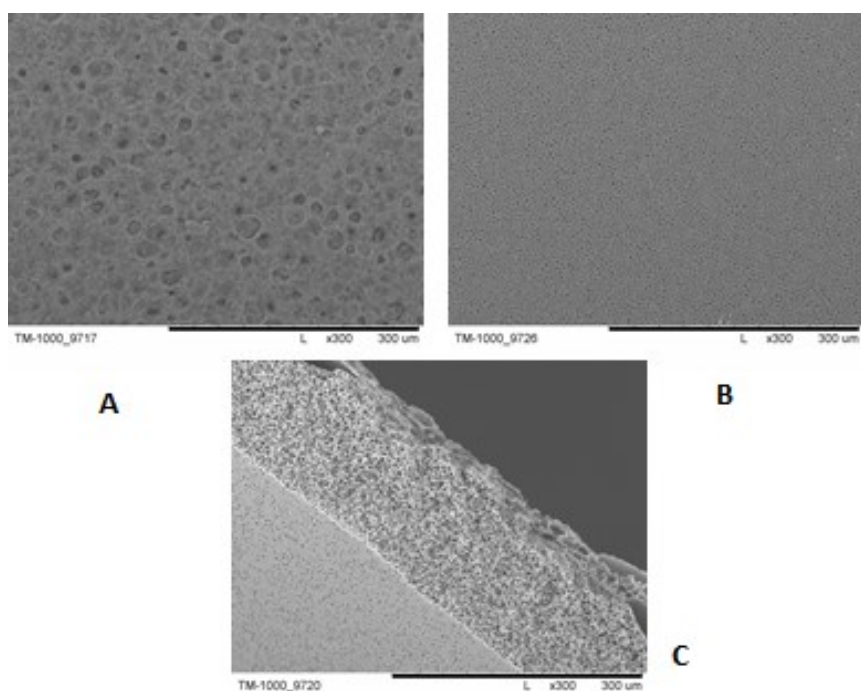


Fig. 7. SEM photomicrographs of PLLA membranes obtained with addition of Pluronic®. A – lower surface, B – upper surface, C – cross-section.

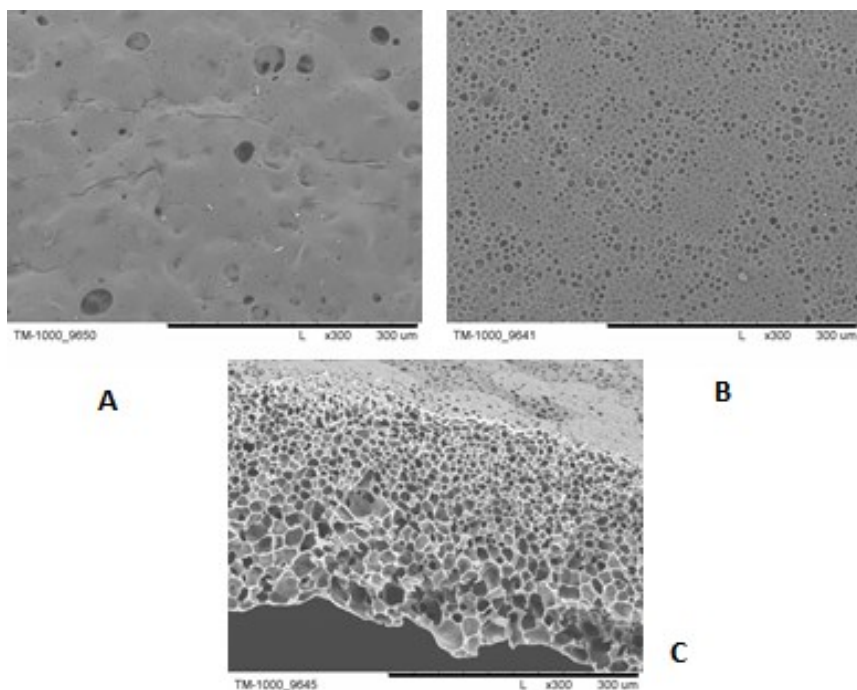


Fig. 8. SEM photomicrographs of PCL membranes obtained with addition of Pluronic®. A – lower surface, B – upper surface, C – cross-section.

Membranes obtained with addition of NaCl

The PLLA membranes obtained with addition of NaCl as a pore precursors (Fig. 9) on the lower surface contained rare pores, 10–15 μm in diameter. Other pores on this surface were coated with a thin covering layer. In the cross-section pores were in size 5–10 μm . Between them was observed pores 30–40 μm in diameter. On the upper surface occurred rare pores, in size 10–15 μm .

On the lower surface of PCL membranes obtained with addition of NaCl as a pore precursor (Fig. 10) occurred rare pores, about 30 μm in diameter. Other pores on this surface were covered with a thin covering layer. In the cross-section were observed pores in size 10–15. Between them were present bigger pores, 30–50 μm in diameter. The upper surface contained pores in size 5 –15 and about 30 μm .

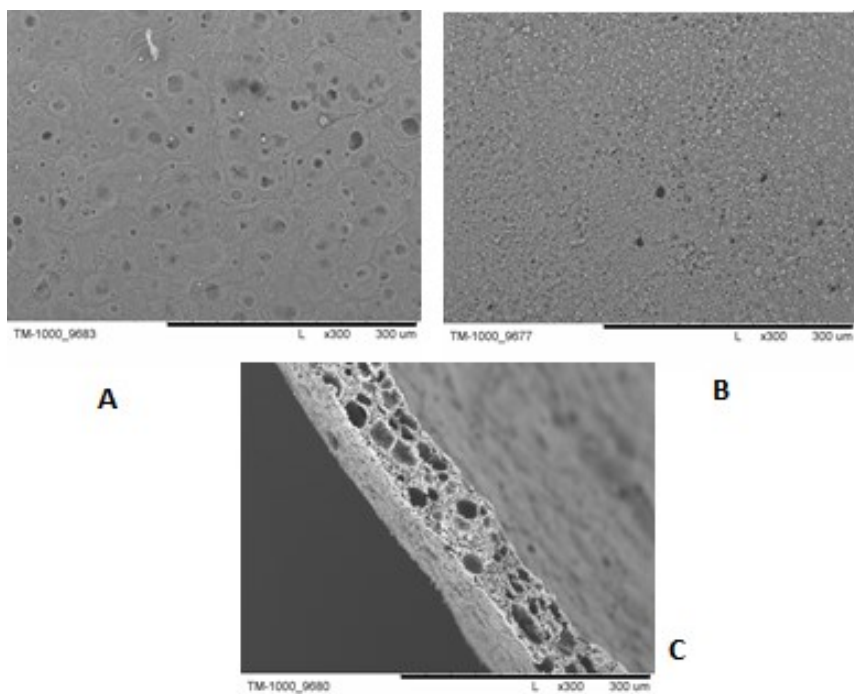


Fig. 9. SEM photomicrographs of PLLA membranes obtained with addition of NaCl. A – lower surface, B – upper surface, C – cross-section.

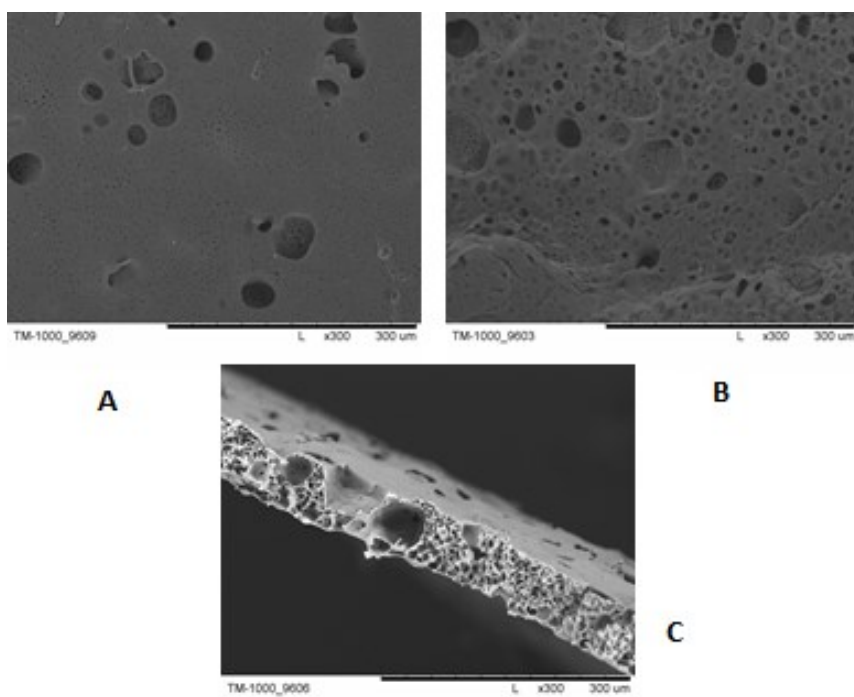


Fig. 10. SEM photomicrographs of PCL membranes obtained with addition of NaCl. A – lower surface, B – upper surface, C – cross-section.

DISCUSSION

The all results, contained size of the pores on the both of surfaces and in the cross-section were summarized in the Table 1.

Table 1. Morphology of the membranes in dependence on used pore precursor.

	PLLA			PCL		
	lower surface	cross-section	upper surface	lower surface	cross-section	upper surface
without pore precursors	rare pores, 2–5 μm	5–15 μm	3–10 μm	rare pores, 1–5 μm	15–30 μm	15–25 μm
PVP	rare pores, ~5 and 25–40 μm	15–30 μm	5–20 μm	~5 and 25–40 μm	20–75 μm	5–15 μm
PEG	practically no pores	5–15 μm	5–10 μm	practically no pores	15–70 μm	10–25 μm
Pluronic®	rare pores, 5–15 μm	5–30 μm	5–15 μm	rare pores 15–30 μm	15–50 μm	10–15 μm
NaCl	rare pores, 10–15 μm	5–10 and 30–40 μm	10–15 μm	rare pores, ~30 μm	10–15 and 30–50 μm	5–15 and ~30 μm

The polyesters membranes obtained by inversion phase method are characterised by asymmetric structure. The lower surface is not very porous. In the cross-section occurred multiple pores. The upper surface is more porous than lower one. This structure prevents the falling out of the cells by less porous surface and allows entry of cells into the porous cross-section by porous surface.

Effect of one kind of pore precursor on morphology of membranes for each polyester is different. Addition of poly(ethylene glycol) for PCL membranes favor the formation of bigger pores, while for PLLA promotes the formation smaller pores, compared to the method without pore precursor.

The addition of PVP as a pore precursor is favorable for the morphology of the PLLA and PCL membranes. In the membranes obtained with the addition of PVP, the upper surface is much more porous, than lower one. Moreover, the pores in the cross-section are larger in size. In the case of PCL membranes good results give too addition of PEG as a pore precursor. Effect of addition of other pore precursors is disadvantageous, porosity of surface and size of the pores in cross-section of the membranes are insufficient for cell cultures.

CONCLUSION

The influence of the addition of the pore precursors on the morphology of semi-permeable membranes was examined. The membranes were made from poly-L-lactide or poly- ϵ -caprolactone.

The results show that membranes obtained without pore precursor have insufficient morphology for tissue engineering. The cross-section should contain open pores about the diameter above 10 μm . Surfaces, expect on of them should have

multiple pores about diameter, because it allow for entry of cells to cross-section of the membranes. In membranes obtained without pore precursor one of the surfaces is not enough porous and cells have difficultly access to inside of the membranes. For this reason it is necessary to modify the methods for the preparation of membranes, which consists of addition of a pore precursor.

For each polyester should be selected kind of used pore precursor. Certain pore precursor for one polyester could promote occur bigger pores, and for other polymer – smaller pores (e.g. PEG and PLLA and PCL membranes).

The PCL membranes, compare to the PLLA contain bigger pores in cross-section, either in the case of using addition of pore precursor or not. This polyesters differ in mechanical properties and degradation rate, therefore depending on desired properties should be selected polymer. The studies of mechanical properties and degradation rate of discussed membranes are continued.

REFERENCES

- [1] O'Brien F. J., Biomaterials & scaffold for tissue engineering, *Mater. Today*, 2011, 14, 88–95 DOI:10.1016/S1369-7021(11)70058-X
- [2] Ma P. X., Scaffolds for tissue fabrication, *Materials Today*, 2004, 7, 30–40 DOI:10.1016/S1369-7021(04)00233-0
- [3] Grolik M., Tissue engineering – new tool in tissue reconstruction [in Polish], *Scientific papers of the society PhD*, Jagiellonian University Science, 2011, 3, 33–40.
- [4] Kruk A., Gadomska-Gajadhur A., Ruśkowski P., Chwojnowski A., Synoradzki L., Preparation of polylactide scaffolds with spongy structure for cell cultures – preliminary studies and optimization [in Polish], *Polimery*, 2017, 2, 118–127 dx.doi.org/10.14314/polimery.2017.118
- [5] Chan B. P., Leong K. W., Scaffolding in tissue engineering: general approaches and tissue-specific considerations, *Eur. Spine J.*, 2008, 17, 467–479 DOI 10.1007/s00586-008-0745-3
- [6] Dhandayuthapani B., Yoshida Y., Maekawa T., Kumar D. S., Polymeric scaffolds in tissue engineering application: A review, *Int. J. Polym. Sci.*, 2011, 19, 1687–9422 doi:10.1155/2011/290602
- [7] Kruk A., Gadomska-Gajadhur A., Ruśkowski P., Chapter in the book: Modern trends in medicine [in Polish], Applications of bioresorbable scaffolds for tissue engineering [in Polish], *Wydawnictwo Tygiel*, 2015.
- [8] Chwojnowski A., The semi-permeable polysulfone membranes [in Polish], *The team of printing and publishing of IBIB PAS*, 2011
- [9] Gołębiowski J., Gibas E., Malinowski R., Selected biodegradable polymers - synthesis, properties, applications [in Polish], *Polimery*, 2008, 53, 799–807
- [10] Lakshmi S., Laurencin C. T., Biodegradable polymers as biomaterials, *Prog. Polym. Sci.*, 2007, 32, 762–798 DOI:10.1016/j.progpolymsci.2007.05.017
- [11] Gunatillake P. A., Adhikari R., Biodegradable synthetic polymers for tissue engineering, *Eur. Cells Mater.*, 2003, 5, 1–16 DOI: 10.22203/eCM.v005a01

- [12] Ulery B. D., Nair L. S., Laurencin C. T., Biomedical Applications of Biodegradable Polymers, *J. Polym. Sci. Polym. Phys.*, 2011, 49, 832–864 DOI: 10.1002/polb.22259
- [13] Gupta A.P., Kumar V., New emerging trends in synthetic biodegradable polymers Polylactide: a critique, *Eur. Polym. J.*, 2007, 43, 4053–4074 DOI: 10.1016/j.eurpolymj.2007.06.045
- [14] Nowak B., Pająk J., Biodegradation of polylactide (PLA) [in Polish], *Arch. Gosp. Odpad. Ochr. Środ.*, 2010, 12, 1–10
- [15] Hinderer S., Layland S. L., Schenke-Layland K., ECM and ECM-like materials — Biomaterials for applications in regenerative medicine and cancer therapy, *Adv. Drug Deliv. Rev.* 2016, 97, 260–269 dx.doi.org/10.1016/j.addr.2015.11.019
- [16] Geckil H., Xu F., Zhang X., Moon S., Demirci U., Engineering hydrogels as extracellular matrix mimics, *Nanomedicine*, 2010, 5, 469–484 doi: 10.2217/nmm.10
- [17] Kruk, A. Gadomska-Gajadhur, P. Ruśkowski, L. Synoradzki, A. Chwojnowski, The method for preparing three-dimensional bilayer polylactide scaffold for culture of skin equivalents [in Polish], *Patent Application P-413603*
- [18] Lan Levengood S., Zhang M., Chitosan-based scaffolds for bone tissue engineering, *J. Mater. Chem. B*, 2014, 2, 3161–3184 DOI: 10.1039/C4TB00027G
- [19] Wen Y., Lian F., Ren Y., Guan H., Enhanced electrochemical properties of a novel polyvinyl formal membrane supporting gel polymer electrolyte by Al₂O₃ modification, *J. Polym. Sci. Pol. Phys.*, 2014, 52, 572–577 DOI: 10.1002/polb.23448

Investigation of high-temperature resistant optical fiber elements for sensor construction

*Anna Kurzych

Faculty of New Technology and Chemistry,
Military University of Technology, Warsaw, POLAND
e-mail: anna.kurzych@wat.edu.pl

Keywords: sensor, interferometer, optical fiber coupler, temperature, polarization state

ABSTRACT

The paper presents a laboratory investigation of high-temperature resistant optical fiber couplers and interferometers for an application in interferometric optical fiber sensors constructions. The measured optical fiber couplers as well as Mach-Zehnder interferometers have been performed to operate in a wide temperature range up to 750°C. In order to test their main parameters a special measuring system has been constructed. Requirement of high-temperature resistant fiber optic sensors operating properly up to the temperature equals 750°C is dictated by industry needs. Mechanical or electronic systems are not able to function in such wide range of the temperature.

INTRODUCTION

Rapid growth of a fiber optic telecommunication definitely has exceeded an optimistic prediction of many scientists. A new generation of sensors has emerged due to the telecommunication and optoelectronics development. The fiber optic sensors represent a family of the optoelectronic devices that can be used to measure a lot of physical quantities, for instance: displacement, pressure, temperature, flow rate and chemical composition of substances [1 - 3].

The requirement of the high-temperature fiber optic sensors operating properly up to the temperature equals 750°C is dictated by industry needs. The mechanical or electronic systems are not able to function in such wide range of the temperature. Widespread piezoelectric sensors used to measure vibration, acceleration or substance flow have limitations due to, inter alia, the Curie temperature. For instance, the power plants requires liquid flow sensors which operate stable and properly in cooling circuits or driving a turbine generator. Diameters of the pipes, electromagnetic field generated by a generator, vibrations caused by the operation of equipment should not effect on the measurements correctness. Sensors operating in such environmental conditions have to be stable in the wide temperature range.

The wide operating temperature range of the sensor affects its versatility, it simplifies system design and reduces the number of components used to measurements. Instead of using two different sensors (for the low and high

temperature range) it is more advantageous to assembly one stable sensor system. It simplifies control, calibration as well as collected data analysis.

The analysis of the optical components for optical fiber sensors based on the Mach-Zehnder interferometer demands taking into account lots of factors which influence on the device operating. The optical fiber couplers have to assure an precise 50% distribution of the beam and do not change the parameters of the beam polarization. However, the output polarization state depends on beam's birefringence, its rate-of-turn, optical fiber orientation as well as modes coupling anisotropy [4]. The conditions of interference have to be fulfilled in order to obtain maximal value of an interference fringes contrast. The most significant interference conditions are following: coherence of interfering waves, properly selected optical paths in the interferometer arms as well as Fresnel-Arago conditions [5] regarding the polarization state of the interfering beams.

In the paper the investigation of the high-temperature optical fiber couplers and interferometers have been presented. The measurements have been carried out in the temperature range from 23°C to 800°C. The analysis of the carried out experimental tests gave opportunity to verify thermal stability of the selected elements and their application in the high-temperature resistant interferometric sensors.

INVESTIGATED OPTICAL FIBER COMPONENTS

Two types of the optical fiber couplers and two types of the optical fiber Mach-Zehnder interferometers operating in the various range of temperature have been investigated. As the low-temperature resistant optical fiber coupler (Fig. 1) operating in the temperature range between -40°C to 85°C the commercially available coupler X (FIBRAIN, Poland) has been used with following parameters [6]: coupling ratio: 50%, wavelength: 780 nm, channels directionality: ≤ 0.7 dB, maximal insertion loss: ≤ 3.7 dB, work temperature: -40°C - 85°C. Its construction consist of a standard single mode fiber. An area of coupling have been protected by a metal tube with dimensions: length $L=55$ m, diameter $\varphi = 3$ mm. The single mode fiber was connected using a glue EPO-TEK. Additionally, an interior of the tube is filled by a silicone elastomer set of Sylgard- operating range -45°C - 200°C [7].



Fig. 1. Low-temperature resistant commercial fiber optic coupler.

The second type of the coupler – high-temperature resistant optical fiber coupler (Fig. 2) – has been constructed using glass elements, a special glue characterized by operating temperature up to 1371°C and a single-mode optical fiber covered by a copper. The copper cover was applied in order to a thermal protection [8-10].

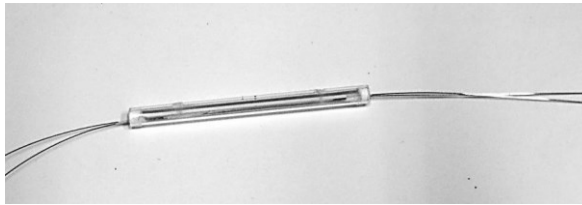


Fig. 2. High-temperature resistant optical fiber coupler used during measurements.

The measured Mach-Zehnder interferometers have been constructed using the above described low-and high-temperature resistant optical fiber couplers.

MEASURING SETUP

In order to determine the coupling ratio, insertion losses as well as interference fringes contrast of the optical fiber elements in function of the temperature and input beam polarization state the special measuring system has been constructed. This system consist of (Fig. 3): computer (gathering and processing of collected data), polarimeter (observation of polarization state of the beam launched into coupler/interferometer as well as optical power meter), induction heater (it allowed to obtain the temperature range of 23°C - 800°C), programmable temperature controller with thermoelement (control of the temperature inside the heater chamber), two FC/APC adapters (optical fibers connection minimalizing back reflections, maximal value of attenuation – 0.15 dB [11]), polarization adjuster (adjustment of the various polarization state of the input beam), semiconductor laser Vertical Cavity Surface Emitting Laser (VCSEL) (source of light, 850 nm wavelength), power supplier (laser power supply), function generator (modulation of the optic fiber interferometers), oscilloscope (observation of the sinusoidal signal of the interferometers), photodetector (measurement of the optical power of output interferometer).

The electromagnetic radiation emitted by the VCSEL is transmitted through the optical fiber terminated with the FC/APC adapter. Then, using the fiber optic adapter the beam is launched into the fiber polarization adjuster. The polarization adjuster consists of the optical fiber wound on the three loops and a special controller frame (Thorlabs). It enables to change the polarization state by changing positions of the loops. The polarization state is controlled by the polarimeter. After the selected polarization state obtainment the optical fiber is connected to one of the X coupler port or interferometer arm. The measured optical fiber element is placed in the induction heater. The outputs of the optical elements are connected to the polarimeter (in case of optical fiber couplers measurements)/photoedetector and oscilloscope (in case of optical fiber interferometers measurements) in order to measure the output optical power as well as observe polarization state/sinusoidal signal.

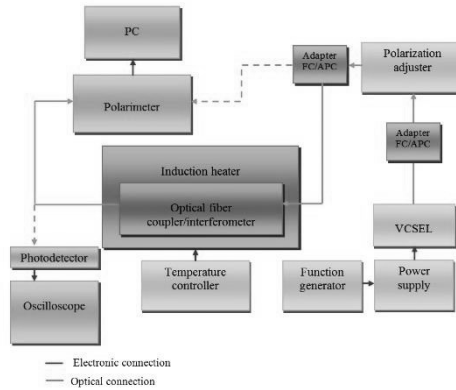


Fig. 3. Block diagram of the measuring setup.

The modulation by wavelength of the light source has been applied during the Mach-Zehnder interferometers investigation. The frequency change of the laser emission (ν) causes a phase shift in an output signal of interferometer [2]. It is well known that frequency of the laser emission can be change in a small range by the supplying current change. The phase shift (ϕ) induced by the change of the laser emission frequency can be described by the following dependence [2]:

$$d\phi = \frac{2\pi\Delta L n_{ef}}{c} d\nu \quad (1)$$

where: n_{ef} – the effective refractive index of the mode, ΔL – optical path length difference of the interferometer, c – speed of light in vacuum. The function generator allows to modulate the supplying current of the VCSEL. The modulation was performed using sawtooth curve with 1 kHz frequency.

The described above measuring setup allows to determine the temperature and polarization characteristics of the optical fiber couplers and interferometers. Fig. 4 presents particular steps of the research. During the measurements one applied the six selected polarization states: left-handed circularly, right-handed circularly, vertically linear, horizontally linear, left-handed elliptical and right-handed elliptical polarized light.

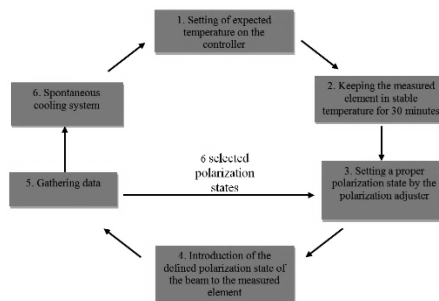


Fig. 4. Block diagram of the carrying out measurements algorithm.

RESULTS

The major parameters of the optical fiber coupler, regarding their technical application, are the coupling ratio and insertion losses (simplifying - losses). A good quality commercial optical fiber coupler is characterized by the losses lower than 1 dB. The operation of the optical fiber sensors without any disturbances requires the stability of coupling ratio in entire work temperature range.

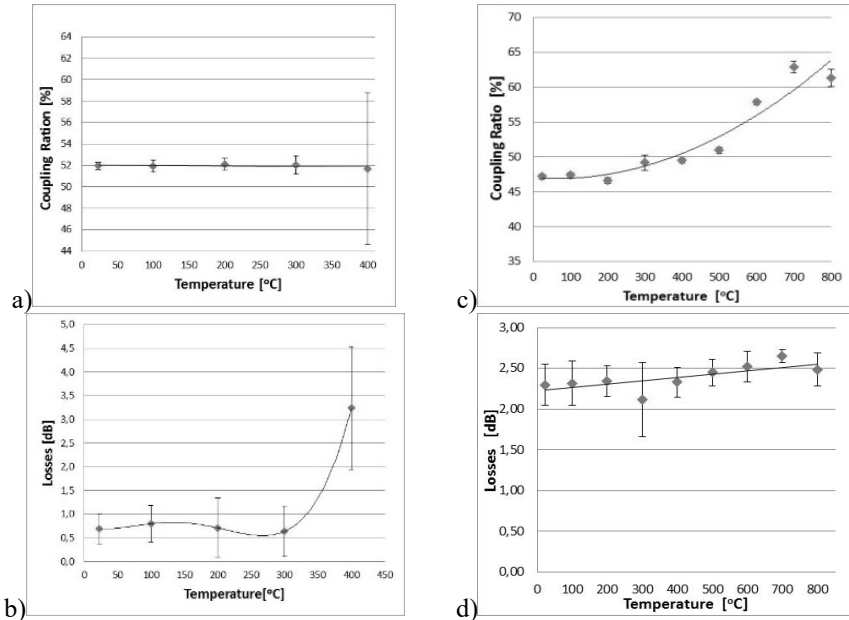


Fig. 5. Coupling ratio and losses versus temperature for the: a),b) low-temperature resistant coupler; c),d) high-temperature resistant coupler.

Fig. 5. presents the temperature characteristics of the low-and high-temperature resistant optical fiber couplers. The obtained characteristics for the low-temperature coupler (Fig. 5a and 5b) indicated that the coupler had 52% coupling ratio and about 1 dB value of losses up to the temperature equals 300°C. The coupler has been damaged in the temperature equals 400°C. The experimentally obtained operating temperature (approximately 300°C) in comparison to manufacturer's data (85°C) had exceeded the assumed value.

Many elements used in optical systems is characterized by dependency of losses versus polarization of the optical signal. This phenomenon is named Polarization Dependent Loss (PDL) [12]. The measuring system presented in the Fig. 3 allowed to change the polarization state of the input signal. The low-temperature coupler have not shown the dependency of polarization state both in the case of the coupling ration and the value of measured losses. The determined mean square deviation of the coupling ratio and losses is lower than 5% during various polarization state of input beam (excluding temperature equals 400°C when the coupler was damaged).

The temperature characteristics for the high-temperature resistant coupler has been presented in the Fig. 5c,5d. In the temperature range from 23°C to 500°C the

coupling ratio is equal approximately to 50%. Nevertheless, after the temperature equals 500°C the coupling ratio evidently increased. It is the temperature at which the intense oxidation process of the copper occurs. The characteristic of the coupling ratio versus temperature above the temperature 500°C can be explained by the damage of the optical fiber protective copper layer which introduces the high thermal stresses.

The losses dependence as well as values of the mean square deviation indicated that the polarization state does not influence on the high-temperature resistant coupler’s parameters. The value of losses in the temperature range from 23°C to 800°C varies in the range from 2.11 dB to 2.65 dB. For the commercial coupler the losses did not exceed 1 dB up to the temperature equals 300°C. The higher value of the losses is caused by stresses introduced the by high-temperature glue. The glue introduced additional stresses and microbending in the area of gluing.

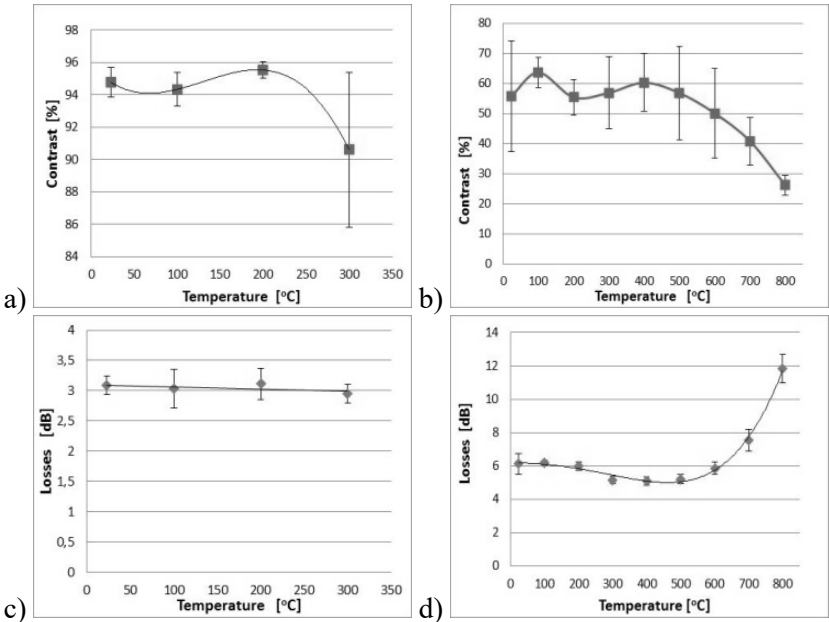


Fig. 6. Interference fringes contrast and losses versus temperature for the: a),b) low-temperature resistant interferometer; c),d) high-temperature resistant interferometer.

Interferometric fiber optic sensors designed to detect external physical factors are characterized by the high sensitivity. The effect named polarization-induced fading (PIF) [13] can be observed when an interferometer is constructed using a standard optical fiber. This phenomenon causes the fading by the polarization state fluctuations. It can produce wide limitations. Therefore, the thermal and polarization characteristic of the Mach-Zehnder optical fiber interferometers have been determined and presented in Fig. 6. The low-temperature resistant interferometer obtained value of interference fringes contrast in range of 89.99% –95.52% which is acceptable value. The contrast does not depend on the temperature in the range from 23°C to 200°C where mean square deviation does not exceed 2% during various input polarization state. It indicated that contrast is not depend on polarization state.

The measured losses of the low-temperature resistant interferometer do not exceed 3 dB which is the acceptable value taking into account that low-temperature resistant optical fiber coupler had losses about 1 dB. The temperature equals 300°C caused damage of the interferometer.

In case of the high-temperature resistant interferometer the value of contrast is on the same level (about 55%) up to the 500°C temperature. The rapid and linear decrease of the contrast one can observe after the temperature equals 600°C. The values of mean square deviation distinctly exceeded the value of the measurement by 50% which is caused by various input polarization state of the beam. This phenomenon can be explained by application of the high-temperature resistant glue which induced the birefringence of the single-mode optical fiber by introducing stresses.

The graph in Fig. 5d can be split into two characteristic ranges. The first one including the temperature range from 23°C to 500°C has linear course and the losses are equal about 6dB. The course of the second one including the temperature range from 500°C to 800°C increases exponentially to the value 11.82 ± 0.83 dB for $T = 800^\circ\text{C}$. The low value of the mean square deviation (lower than 10%) indicated that the various polarization states do not have effect on the losses of the high-temperature resistant interferometer. The losses of the high-temperature resistant interferometer are higher than the losses of low-temperature resistant interferometer it can be caused by the special high-temperature glue which could introduce microbending.

CONCLUSION

The main parameters of the optical fiber couplers and Mach-Zehnder interferometers have been investigated. The thermal and polarization characteristics for low-and high-temperature resistant optical elements have been drawn. The curve of coupling ratio versus temperature for the low-temperature resistant optical coupler in the temperature range of 23°C - 300°C has linear course and the value of the coupling ratio equals 52%. The low-temperature resistant coupler showed thermal stability and lack of input polarization state influence on the main parameters. The high-temperature resistant optical coupler was stable up to the temperature 500°C. The output optical power fluctuated in the temperature above 500°C due to the oxidation of the copper which covered the optical fiber for the protection. The parameters of the both couplers did not change during the various polarization states of the input beam.

The low-temperature resistant interferometer operated without fluctuations in the temperature range from 23°C to 300°C. The interference fringe contrast had value in the range from 89.99% to 95.52%. This interferometer was stable during the temperature and polarization state changes. The contrast and losses characteristics were not disturbed to the temperature equals 300°C and by various input polarization states.

The high-temperature resistant interferometer was very sensitive to the polarization state of the input signal due to the induced birefringence of the optical fiber. The birefringence of optical fiber (in the place of glue impact) causes arbitrary changes of the propagating light. It causes disturbances of the interference conditions and consequently influences on the value of the interference fringes contrast.

In order to eliminate polarization influence on the interferometer operation it is possible to apply a special photonic optical fiber or an automatic polarization controller.

The paper pointed out the main disadvantages of the high-temperature resistant elements for the sensor construction which have to be eliminated before their application in industry. Nevertheless, the investigated optical fiber elements give promising opportunity to construct a new high-temperature resistant optical fiber sensors.

REFERENCES

- [1] Szustakowski M., Jachowicz R. S., Jaroszewicz L., *Electronic and fiber sensors and their applications, IV National School of Optoelectronics*, Waplewo (in Polish), 1990
- [2] Szustakowski M., Turczyński K., Turczyński Z., *Fiber optic/interferometric sensors, 1th National School of Optoelectronics*, Uniście (in Polish), 1987
- [3] Ziętek B., *Optoelectronics, Scientific Publishing Nicolaus Copernicus University*, Toruń (in Polish), 2005
- [4] Jaroszewicz L., *Analysis of polarization in a fiber optic gyroscope, Doctoral thesis*, Warsaw (in Polish), 1988
- [5] Goldstein D., *Polarized Light*, Marcel Dekker Inc., 2003
- [6] <http://fibrain.com/> 16.01.2016
- [7] http://ncnc.engineering.ucdavis.edu/pages/equipment/Sylgard_184_data_sheet.pdf, 06.11.2015
- [8] Me' Ndez A., *Specialty Optical Fibers Handbook, Photonics Center*, Boston University, Boston, Massachusetts 2007
- [9] Bogatyjtjov V.A., Dianov E.M., Biriukov A.S. , Sysoliatin A.A., Voronov V.V., Khitun A.G., Hyun Do M., Han Kim J., *Performance of high-strength Cu-coated fibers at high temperatures, Conference on Optical Fiber Communications*, 1997 OSA Technical Digest Series (Optical Society of America, 1997), paper WL20
- [10] Biriukov A. S., *Reliability and optical losses of metal-coated fibers at high temperatures, Symposium Proceedings*, San Francisco 1998
- [11] <http://www.555.pl/index.php?act=2334> 14.01.2016
- [12] Perlicki K., *Measurements in optical telecommunication systems*, Publisher of Communications and Communications, Warsaw (in Polish), 2002
- [13] Kersey A. D., Marrone M. J., Dandridge A., Tveten A. B., *Optimization and Stabilization of Visibility in Interferometric Fiber-optic Sensors Using Input-Polarization Control*, *Journal of Lightwave Technology*, 10(6), 1988

Experimental results of the vertical-cavity surface-emitting laser for optical fiber sensors application

*Anna Kurzych

Faculty of New Technology and Chemistry,
Military University of Technology, Warsaw, POLAND
e-mail: anna.kurzych@wat.edu.pl

Keywords: semiconductor laser, threshold current, wavelength modulation, VCSEL

ABSTRACT

The paper presents theoretical and experimental studies of selected parameters of a promising laser for an optical fiber sensor application. Main advantages of the vertical-cavity surface-emitting lasers (VCSELs) include extremely low threshold current (below 1 mA), low cost, single transversal and longitudinal mode operation, an ability to use an operating current for a wavelength modulation. These features made the laser sources very attractive for application in interferometric fiber optic sensors (in contradiction to edge emitting semiconductor lasers). In the paper Author presented laboratory results which confirm an opportunity to modulate VCSELs' wavelength by the operating current. Moreover, the VCSELs' polarization stability has been verified due to their future application in interferometric optical fiber sensors application.

INTRODUCTION

A standard optical fiber interferometric sensor consists of three basic elements: source of the light, interferometer and electronic detection system [1]. An industrial application of these sensors requires not only a high sensitivity but also a minimization of costs and dimensions. Unique properties and parameters of the semiconductor lasers - VCSELs - such as low threshold current (below 1 mA), mass production, opportunity to modulate wavelength by operating current make VCSELs appropriate sources of light for the optical fiber sensors construction in comparison to other standard lasers [2-4]. Moreover, VCSELs offer quasi-single mode operation, high efficiency, easy integration with electronic circuits as well as high power per unit area. The dimension minimization of sensors by using VCSELs is big advantage as well [2,4,5]. VCSELs are commonly used for a keyboard mouse construction which obtained much higher speed than standard optical keyboard mice. There are also an narrow area of production of specialized VCSELs for spectroscopy [6]. The application of VCSELs in the interferometric optical fiber sensors [7-10] requires an assumption that the environmental and work conditions do not effect on their parameters. Polarization state or wavelength changes induced by the temperature or operating current could be adversely affect a performance of the sensor and introduce incorrect recordings [1]. The paper reviews theoretically and experimentally an operating current influence on the wavelength and polarization state of the VCSELs

output signal. The aim of the studies is to confirm the VCSELs' polarization stability as well as wavelength modulation by the operating current. The polarization state of laser output beam is very significant in the interferometric sensors in order to fulfill the Fresnel-Arago [7] conditions what reflect an interference fringes contrast. The sensitivity in the interferometric sensors depends on the fringes contrast. The polarization switching in VCSELs is commonly observed between the two orthogonal linearly polarized states in a fundamental mode [11, 12]. This phenomenon is result of their cylindrical symmetry and surface emission. Nowadays, there are solutions to control the polarization of VCSELs output light by affecting the transverse guiding and/or introducing mode-selective loss or gain as well as introducing different kinds of anisotropy [13, 14]. In order to verify the polarization stability the two VCSELs have been investigated, one of them was with "polarization locking" and the second one was without this option. Presented investigation verifies the VCSELs' application for the optical fiber sensors construction which requires polarization stability.

THEORETICAL BACKGROUND

Definition of a threshold current

Threshold current is a current flowing through a laser diode at which laser's amplification achieves value sufficient for a lasing. When the current is lower than the threshold value, the recombination of electrons and electron holes will not cause the lasing and the emitting light is incoherent.

Emission spectrum of semiconductor lasers

The laser emission spectrum depends mostly on the temperature and the operating current [15]. The changes of the temperature strongly effect on the behavior of the laser that it has become the method of a tuning. In order to obtain a narrow spectrum and reduce the number of modes the operating current must first increase above the threshold, below which the spectrum is broad (Fig. 1). A pumping signal increase causes moving the wavelength to the red part of the spectrum.

The operating current increase causes a heating of the junction, and it produces refractive index growth, moving the gain to the longer wavelengths. The higher temperature increases the wavelength, so that it contributes to the decline in the width of band gap (Fig. 2).

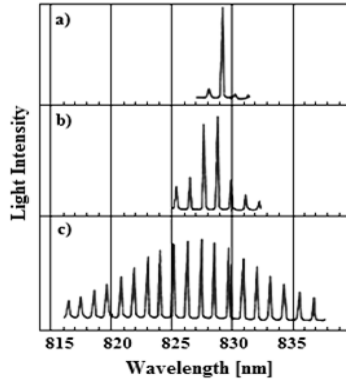


Fig. 1. Light intensity of a semiconductor laser depending on the operating current: [4]
a) $I = 100 \text{ mA}$, $P = 10 \text{ mW}$, b) $I = 80 \text{ mA}$,
 $P = 4 \text{ mW}$ c) $I = 67 \text{ mA}$, $P = 67 \text{ mW}$.

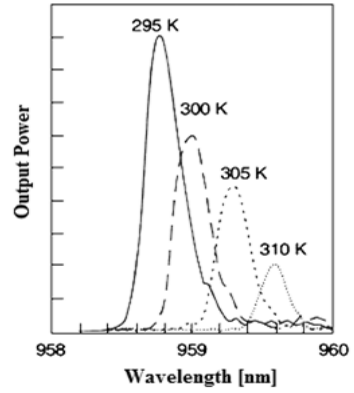


Fig. 2. Spectrum of semiconductor laser versus temperature [4].

Mathematical description of the polarization beam

Definition of the fundamental parameters defining the polarization of the light beam

An ellipticity e is determined as a quotient of minor and major axis of an polarization ellipse $e = a/b$. The ellipse describes propagation of the light wave in z direction. The angle of the ellipticity is more universal value which is defined by the following relationship [7]:

$$\varepsilon = \arctan\left(\frac{b}{a}\right) \quad (1)$$

For circular polarization, $|\varepsilon| = 45^\circ$. The azimuth is the angle between the E_x axis and the major axis of the ellipse.

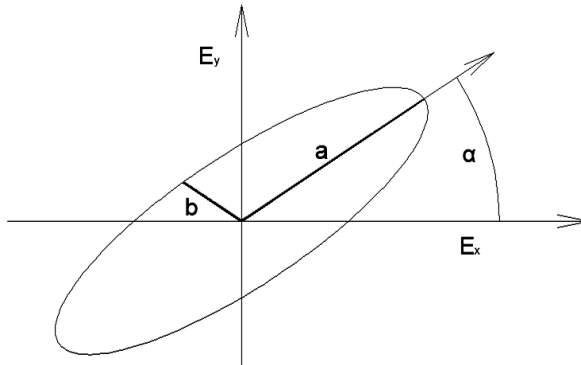


Fig. 3. Definition of azimuth and ellipticity in the polarization description [16].

Another very important parameter describing the light polarization is the degree of polarization (DOP). It is defined as the quotient of the polarized light beam intensity to the total intensity of the light beam.

$$DOP = \frac{I_p}{I_0} \quad (2)$$

where: I_p – intensity of the polarized light beam, I_0 – total intensity of the light beam.

MATERIALS AND METHODS

The two types of VCSLEs have been selected for experimental studies. They operate at the wavelengths around 850 nm and have manufactured by ULM Photonics based on GaAs/AlGaAs quantum-well. In the paper they are named VCSEL-1 and VCSEL-2. “Polarization locking” is the basic difference between them. The VCSEL-1 is equipped with “polarization locking” and should have stable polarization of the output beam. Tab.1 presents the main parameters of the investigated VCSELs.

Tab. 1. Main parameters of the investigated VCSELs.

Parameter	Unit	Manufacturer's data	
		VCSEL-1	VCSEL-2
Threshold current	mA	0.99	0.65
Max. optical power	mW	0.35	0.44
Max. operating current	mA	2.87	3.02
Temperature	°C	25	25
Wavelength	nm	850	850

The lasers were coupled to the standard SMF-28 single mode optical fiber. The integrated structure of the VCSEL with the optical fiber is shown in Fig. 4a. Fig. 4b presents the construction diagram of the coupling module.

a)



b)

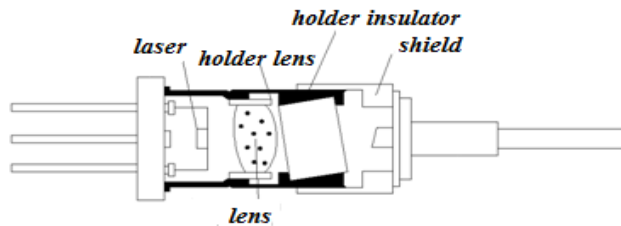


Fig. 4. Laser coupling module: a) Technical realization of coupling laser module with the optical fiber, b) Schematic diagram of the laser coupling module with the optical fiber.

THE MEASURING SYSTEM

There was constructed the measuring system shown in Fig. 5 in order to measure the changes in polarization features and wavelength of emitted light by the VCSELs.

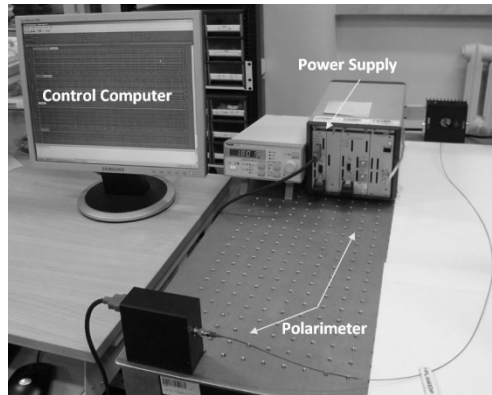
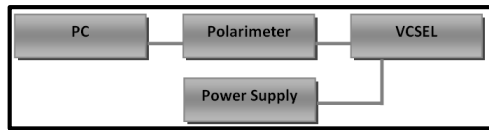


Fig. 5. Block diagram of the measurement system to study the polarization features of VCSEL.

It consists of: computer (gathering and processing of collected data), polarimeter (observation of polarization state of the beam), VCSEL (source of light, 850 nm wavelength), power supplier (laser power supply). In order to determine the dependence of laser wavelength as a function of the operating current the polarimeter was replaced by the Optical Spectrum Analyzer (OSA). Polarimeter (ThorLabs) has precision values of ellipticity and azimuth \pm . The optical unit of the polarimeter consists of the: rotating quarter-wave plate, fixed polarizer, and photodiode (see Fig. 6). The wave plate transforms the input polarization depending on the actual rotating angle. Then, the polarizer only transmits the portion of the light with its polarization parallel to the transmission axis. As a result, the polarization modulation is converted into an amplitude modulation. The photodetector supplies a current that is proportional to the optical power. The Fourier transformation is used to calculate accurately all polarization relevant parameters like SOP, DOP, azimuth, ellipticity, Stokes vectors, etc.

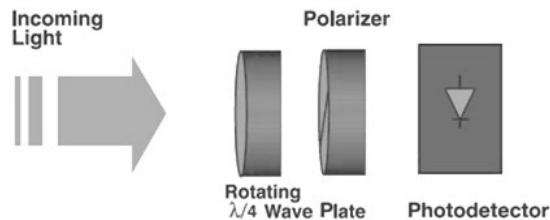


Fig. 6. Scheme of rotating wave plate technique [17].

The external sensor head IR1 type enables measurements in the range wavelength from 700 ÷ 1000 nm. The measured laser was connected to the polarimeter with the aid of FC/PC connector. The optical fiber was put freely in order

to eliminate stresses and bends which could cause micro-crack and introduce damping.

Changing of the passage of current through the VCSEL structure provided the possibility of adjusting the generator power (ThorLabs). Range of measurement: from 0.2 ÷ 2.0 mA.

RESULTS

Dependence of laser wavelength as a function of the operating current

VCSEL emission spectrum depends considerably on the current flowing through the structure. It is also a method of tuning the wavelength of these devices. The most significant aspect is to exceed the threshold current, which gives considerable stability and more efficient operation of the lasers. It is a requirement to obtain the laser's action, which gives coherent electromagnetic radiation.

Both lasers (VCSEL-1 and VCSEL-2) have demonstrated similar dependence of wavelength as a function of the operating current at temperature equals 20°C. Graphs have a linear character in the range from 1.1 ÷ 2.0 mA and 1.5 ÷ 2 mA for VCSEL-1 and VCSEL-2, respectively (Fig. 7). Changes in wavelengths are in the range of 0.02 ÷ 0.05 nm/100 μ A.

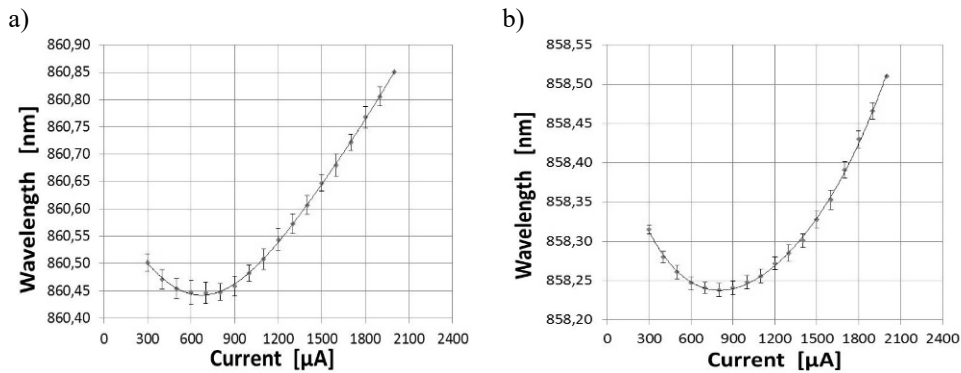


Fig. 7. Dependence of wavelength as a function of the operating current at temperature 20°C for: a) VCSEL-1, b) VCSEL-2.

Changes of polarization parameters of VCSELs as function of the operating current

The VCSEL application in the sensor-systems basing on the interferometer requires linear and stable polarization state of the output beam. Measurements of the VCSELs' polarization features are very significant due to the polarization switching in VCSELs which is commonly observed between the two orthogonal linearly polarized states in fundamental mode. Polarization experimental characteristics obtained for the VCSEL-1 are presented in Fig. 8 and Fig. 9. In Fig. 8 are shown changes of the degree of polarization, while in Fig. 9a and Fig. 9b are shown the changes of parameters describing the polarization ellipse.

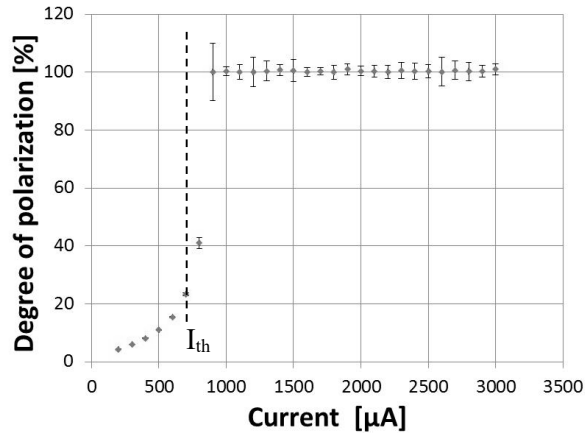


Fig. 8. Degree of polarization of VCSEL-1 depending on the operating current.

The degree of polarization is at first very low, not exceeding 50 %. Then the value increases. One can observe jump this value when the operating current is 900μA. There is the point where stimulated laser emission prevails over absorption and spontaneous emission, the laser action begins. This point has considerably higher value of the measurement uncertainty. There is the highest instability of the VCSEL. This indicates that the laser during the transition from incoherent recombination emission to the emission of coherent and polarized laser light shows the highest instability. After crossing 900 μA the characteristic is stable and has linear course.

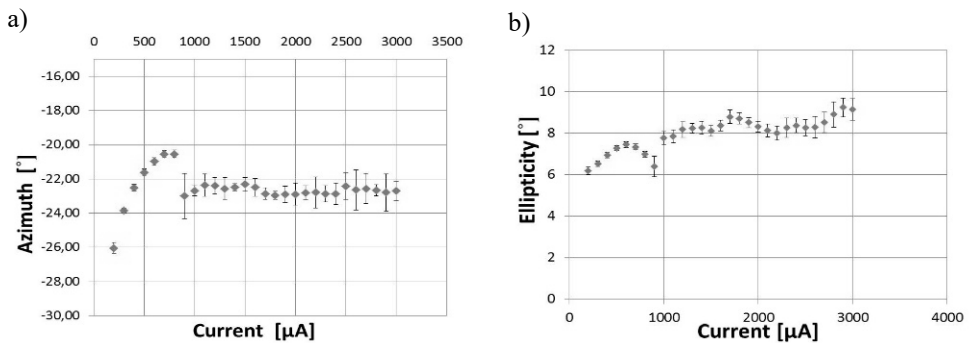


Fig. 9. Influence of the operating current on the polarization state for VCSEL-1: a) azimuth, b) ellipticity.

In Fig. 9a and 9b there are the same distinctive ranges as presented in Fig. 8. The initial changes of polarization are caused by majority of the spontaneous emission over stimulated emission. The characteristics are stable when the operating current has value over 900 μA. Discrepancies in characteristics, however, are not big and occur in the range between 8° for azimuth and 4° for ellipticity.

The experimental results for laser VCSEL-2 are presented in Fig. 10 and in Fig. 11. The characteristics of the parameters polarization for the second laser have different courses than for the previous one.

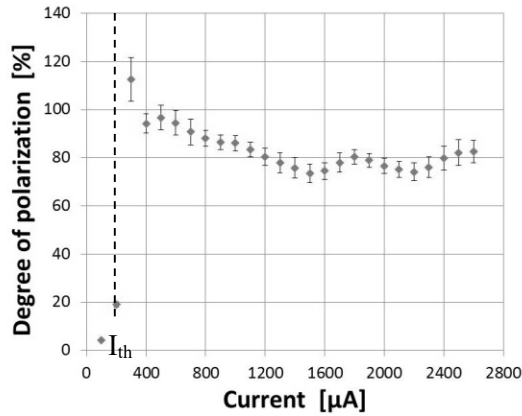


Fig. 10. Degree of polarization of VCSEL-2 depending on the operating current.

The characteristic of degree of polarization for VCSEL-2 has also clearly two ranges of laser operation, below and above the threshold current. Above threshold current, the value of degree of polarization changes with increasing of the operating current and reaches about 80%. One of the reason of this behavior may be a coexistence a few wavelengths for this laser.

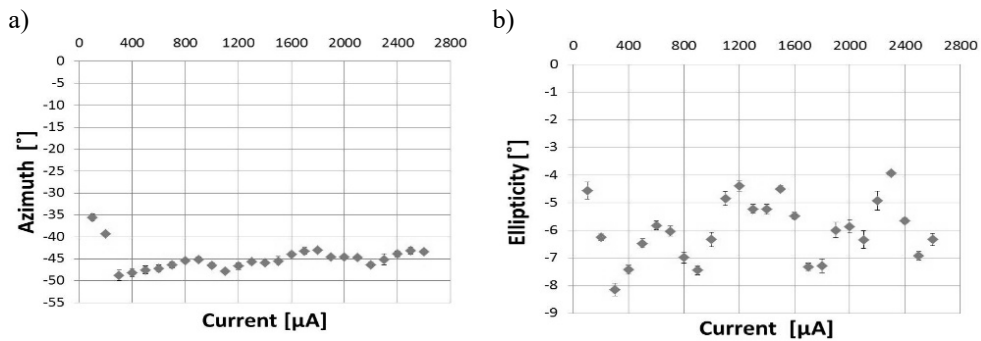


Fig. 11. Influence of the operating current on the polarization state for VCSEL-2: a) azimuth, b) ellipticity.

In Fig. 11a one can indicate the characteristic point when the laser exceeded the threshold, i.e. 300 μA . The further course of the characteristics of the azimuth is stable, the maximal changes reach 7°. However, characteristic of ellipticity is very irregular. These differences could be due to the use of the longer input optic fiber of the second laser or richer emission spectrum. Moreover, many scientists attributed the VCSEL's polarization switching to thermal effects induced by the self-heating of the laser's current [11]. In the case of VCSEL-1 during long-term operation in various operating current polarization instability was not observed. Therefore, VCSELs with “polarization locking” property can be used for optical fiber mass construction.

CONCLUSIONS

In this work the theoretical and experimental analysis of the innovative semiconductor source of the light have been presented. Nowadays the VCSEL is highly appreciated and used in a wide application field. These devices offer high efficiency and opportunity for improving capabilities, such as: lower value of operating current, higher optical power per area unit, higher reliability ($>10^7$ h MTTF), possibility to operate in high temperature range, scalability, low costs, increasing the efficiency of coupling fiber, possibility to integrate the 1 - and 2-dimensional array for parallel optical interconnects.

Measurements carried out indicated that the VCSELs can be modulated by operating current changing. The obtained changes of the wavelength are in the range of $0.02 \div 0.05$ nm/100 μ A.

The laser with the polarization locking (VCSEL-1) has stable 100% degree of polarization during operation, while the laser without polarization locking (VCSEL-2) has unstable 80% DOP. VCSELs equipped with "polarization locking" allow for commercial fiber sensors mass constructions. Results of the research indicated that VCSELs are appropriate light sources for the optical fiber sensors construction only when they are equipped with polarization control. Moreover, the modulation of wavelength by the operating current is possible. Author reported the optimized (concerning polarization stability, efficiency and low power consumption) working conditions of the tested VCSELs allowing for their low-cost commercial application in optical fiber sensors.

REFERENCES

- [1] Bahrapour A. R., Tofighi S., Bathaee M, Farman F., Optical Fibe Interferometers and Their Applications, Interferometry - Research and Applications in Science and Technology, Padron I. (Ed.), ISBN: 978-953-51-0403-2, *InTech*, 2012, Available from: <http://www.intechopen.com/books/interferometry-research-and-applications-in-science-and-technology/optical-fiber-interferometer-and-their-applications>.
- [2] Bugajski M., Technology of semiconductor nanostructures applied to the production of photonic devices, *VII Scientific Conference "Electron Technology" ELTE*, Polanica Zdrój (in polish), 2000, 589-597.
- [3] Sarzała R., Czystanowski T., Wasiak M., Dems M., Piskorski Ł., Nakwaski W., Panajotov K., Numerical Self-Consistent Analysis of VCSELs, *Advances in Optical Technologies*, 2012, 2012, doi:10.1155/2012/689519.
- [4] Ziętek B., Lasers, *Scientific Publishing Nicolaus Copernicus University*, Toruń (in Polish), 2009.
- [5] Ziętek B., Optoelectronics, *Scientific Publishing Nicolaus Copernicus University*, Toruń (in Polish), 2005.
- [6] Zappe H. P., Monti di Sopra F., Gauggel H. P., Gulden K. H., Hovel R., Moser M., High-spectral-purity VCSELs for spectroscopy and sensors, *Laser Diodes and LEDs in Industrial, Measurement, Imaging, and Sensors Applications II; Testing*,

Packaging, and Reliability of Semiconductor Lasers V - Proc. SPIE 3945, 2000, 106, doi:10.1117/12.380526.

[7] Goldstein D., *Polarized Light*, Marcel Dekker Inc., 3rd edition, ISBN 9781439830406, 2010.

[8] Culshaw B., Dakin J. Eds., *Optical Fiber Sensors: Systems and Applications*, Artech House, Boston, 1989, 2.

[9] Grattan K., Meggit B., *Optical fiber sensors technology. Fundamentals*. Kluwer Academic Publishers, Boston, Dordrecht, London, 2000, 1-44.

[10] Ghatak A., Thyagarajan K., *An Introduction to Fiber Optics*, Cambridge University Press, 1st edition, ISBN 9781139174770, 1998.

[11] Yen Tsu-Chiang, Li Yueh-Chen, Wu Yu-Heng, *Analogy between the Ising Model and the Polarization Switching of Vertical-cavity Surface-emitting Lasers*, *PIERS Proceedings*, Prague, Czech Republic, 2015, 2069- 2073.

[12] Tan M. P., Kasten A. M., Strand T. A., Choquette K. D., *Polarization Switching in Vertical-Cavity Surface-Emitting Lasers With Anisotropic Cavity Geometry and Injection*, *IEEE Photonics Technology Letters*, 2012 24, 9.

[13] Ostermann J. M., Michalzik R., *Polarization Control of VCSELs*, *Springer Series in Optical Sciences*, 2012, 166, 147-179.

[14] Gustavsson J.S., Haglund A., Soderberg E., Vukusic J., Modh P., Jedrasik P., Larsson A., *Mode and polarisation control in VCSELs using shallow surface structures*, *IET Optoelectron.*, 2007, 1, 5.

[15] Islam Khan N., Hayder Choudhury S., Ahmed Roni A., *A comparative study of the temperature dependence of lasing wavelength of conventional edge emitting stripe laser and vertical cavity surface emitting laser*, *International Conference on Data Communication Networking and Optical Communication System*, 141-1452011, DOI: 10.5220/0003512101410145.

[16] Azzam R. M., Bashara N.M., *Ellipsometry and Polarized Light*, North Holland Publication, Amsterdam, 1979.

[17]<http://www.jaybao-eo.com/image/page/download/Polarimeter.pdf>, 20.03.2017.

The four-channel polarimeter to examining the selected optical elements

Marlena Kwiatkowska

Institute of Technical Physics. Faculty of New Technologies and Chemistry. Military University of Technology. Warsaw. POLAND

e-mail: marlena.kwiatkowska@wat.edu.pl

Keywords: *polarimetry. polarimeter. Stokes vector. Mueller matrix*

INTRODUCTION

The study of polarization parameters of various types of optical materials is a very important step in enabling their more late application. Full information describing a set of polarization properties of any material contained in the so-called Mueller matrix. Full information describing a set of polarization properties of any material contained in the Mueller Matrix. It requires obtaining measurements of Stokes vectors six distinctive polarization states. At this target polarimetric system are applied. One such system is a four-channel polarimeter that allows you to measure the Stokes vector elements of different centers and optical elements using the system of four photodetectors. The most important feature built the four-polarimeter is possible to register the state and degree of polarization of the light beam passing through the test elements in a moment of time. Cannot be used in most measuring devices. An essential element of verification of the quality of operation of this system is its proper calibration and comparative studies of the system standard. Therefore the present study will be presented measurement calibration system built with commercially available from Thorlabs polarimeter acting based upon the quarter-rotating.

THEORERICAL BASES AND THE DESCRIPTION OF MEACURING METHOD

The source of much optical information is rating polarization properties of the various optical elements based on the determination of the Mueller matrix of the optical element. Implementing the vector of Stokes S is necessary for the definition of the Mueller matrix. This vector describes the properties of polarized light beam and stores it in the following form [1]:

$$S = \begin{pmatrix} S_0 \\ S_1 \\ S_2 \\ S_3 \end{pmatrix} \quad (1)$$

Every components of this vector informs about the intensity of the light beam: S_0 the quantity of the intensity included in wave with horizontal or vertical polarization, S_1 the quantity of the intensity move in polarization about angle $+45^\circ$ and -45° , S_2 the quantity of the intensity connected with polarization right and left

circular. In order to connect elements of this vector with parameters of the polarization of the light beam one should introduce him in the following form:

$$S = \begin{pmatrix} S_0 \\ S_0 P \cos 2\psi \cos 2\chi \\ S_0 P \sin 2\psi \cos 2\chi \\ S_0 P \sin 2\chi \end{pmatrix} \quad (2)$$

Where: P is a symbol of the degree of polarization and ψ, χ define state of polarization and they are associated with the measured vector S in the following way:

$$P = \frac{\sqrt{S_1^2 + S_2^2 + S_3^2}}{S_0} \quad 0 \leq P \leq 1 \quad (3)$$

$$\psi = \frac{1}{2} \arctan \left(\frac{S_2}{S_1} \right) \quad 0 \leq \psi \leq \pi \quad (4)$$

$$\chi = \frac{1}{2} \arcsin \left(\frac{S_3}{S_0} \right) \quad -\frac{\pi}{4} \leq \chi \leq \frac{\pi}{4} \quad (5)$$

Knowing the above definition of the Stokes vector and a method for identifying the parameters of the polarization of the light beam it is possible to present as the input Stokes vector S is transformed by optical element. This element is represented by the Mueller matrix producing the Stokes vector output S'. [2,3], S'= M·S.

It is assumed that the relationship between the respective components of the vector S and the elements of the matrix M are linear. Mueller matrix is a sixteen-element square matrix which from the point of view of measurement of optical components contains information about the basic parameters of the optical medium [3].

In this work to determine the elements of the Stokes vector four-channel polarimeter and polarimeter of the ThorLabs company has been used. Position for the measurement was composed of a light source a generator of the state polarization the polarization analyser and detector. Between the generator and the analyser there was set up an examined element what was shown in the picture 1. In case of the examination liquid crystal cell system is equipped with the functional generator for controlling the liquid crystal by the electric field. Four-channel polarimeter consist of three beam-splitter cubes. three polarizers oriented at an angle of + 45° and one at 90° quarter-wave plate oriented at an angle 90° and four detector at the end of each channel. The detector is a semiconductor sensor for converting the signal light into an electric signal. This property allows the measurement of the intensity of the light beam at the output of the system.

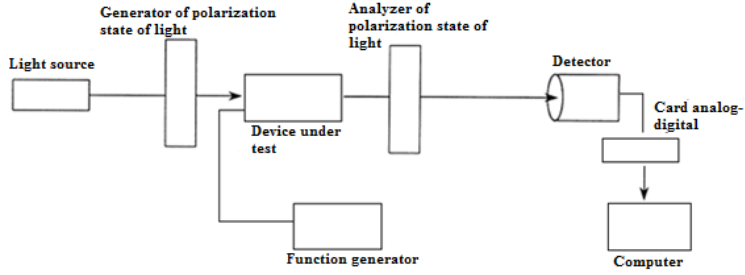


Fig. 1. The measurement station to determine the parameters of Stokes vector.

Principle effect of the above arrangement is following: the beam emitted from helium-neon laser illuminates the generator of the state of the polarization which is used for a synthesis of the desired state of the polarization. Generated state of the polarization of the light after the passage through the examined element is changing. These changes are being measured by the appropriately built system of the analyser of the polarization. Each detector is connected to an analogue card company Natural Instrument. This card has four separate analog inputs what the allowing simultaneous reading of results from each of them. The use of various optical elements for building each channel of polarimeter is used to get the complete Stokes vector of the analysed light beam. The intensity of the beam measured on each channel is proportional to the Stokes parameter - S_0 . In addition the second channel contains information about the parameter S_1 , third parameter S_2 and S_3 , and the fourth channel of S_3 . These relations are described below [4, 6]:

$$I_{D1} = a_0 S_0 \quad (6)$$

$$I_{D2} = b_0 S_0 + b_1 S_1 \quad (7)$$

$$I_{D3} = c_0 S_0 + c_1 S_2 + c_2 S_3 \quad (8)$$

$$I_{D4} = d_0 S_0 + d_1 S_3 \quad (9)$$

Where: I is the intensity of light beam measured on individual detectors. a , b , c , d – are coefficients of proportionality. S_0 , S_1 , S_2 , S_3 - parameter of Stokes.

From appointed parameters of Stokes were calculated Mueller matrices for the selected optical elements. The individual elements of the matrix were calculated from the following formulas [7]:

$$m_{00} = \frac{I_{1H} * S_{0H} + I_{1V} * S_{0V}}{S_{0H} + S_{0V}}$$

$$m_{10} = \frac{I_{1H} * S_{1H} + I_{1V} * S_{1V}}{S_{0H} + S_{0V}}$$

$$m_{01} = \frac{I_{1H} * S_{0H} - I_{1V} * S_{0V}}{S_{0H} + S_{0V}}$$

$$m_{11} = \frac{I_{1H} * S_{1H} - I_{1V} * S_{1V}}{S_{0H} + S_{0V}}$$

$$\begin{aligned}
m_{02} &= \frac{I_{1(+45)} * S_{0(+45)} - I_{1(-45)} * S_{0(-45)}}{S_{0(+45)} + S_{0(-45)}} & m_{12} &= \frac{I_{1(+45)} * S_{1(+45)} - I_{1(-45)} * S_{1(-45)}}{S_{0(+45)} + S_{0(-45)}} \\
m_{03} &= \frac{I_{1R} * S_{0R} - I_{1L} * S_{0L}}{S_{0R} + S_{0L}} & m_{13} &= \frac{I_{1R} * S_{1R} - I_{1L} * S_{1L}}{S_{0R} + S_{0L}} \\
m_{20} &= \frac{I_{1H} * S_{2H} + I_{1V} * S_{2V}}{S_{0H} + S_{0V}} & m_{30} &= \frac{I_{1H} * S_{3H} + I_{1V} * S_{3V}}{S_{0H} + S_{0V}} \\
m_{21} &= \frac{I_{1H} * S_{2H} - I_{1V} * S_{2V}}{S_{0H} + S_{0V}} & m_{31} &= \frac{I_{1H} * S_{3H} - I_{1V} * S_{3V}}{S_{0H} + S_{0V}} \\
m_{22} &= \frac{I_{1(+45)} * S_{2(+45)} - I_{1(-45)} * S_{2(-45)}}{S_{0(+45)} + S_{0(-45)}} & m_{32} &= \frac{I_{1(+45)} * S_{3(+45)} - I_{1(-45)} * S_{3(-45)}}{S_{0(+45)} + S_{0(-45)}} \\
m_{23} &= \frac{I_{1R} * S_{2R} - I_{1L} * S_{2L}}{S_{0R} + S_{0L}} & m_{33} &= \frac{I_{1R} * S_{3R} - I_{1L} * S_{3L}}{S_{0R} + S_{0L}}
\end{aligned}$$

Results of measurements

To build a four-channel polarimeter and the establishment of procedures for determining the Stokes parameters will examine the impact of the light beam from the selected optical elements. In the course of the study examined how they look Mueller matrix for elements such as a polarizer quarter-wave plate. Matrix are appointed from the parameters the Stokes obtained from four-channel polarimeter and polarimeter of Thorlabs company.

Polarizer

The designated matrix shows that the polarizer does not change phase as the parameters m_{22} , m_{23} , m_{32} , m_{33} take the oscillating close to zero. It is possible to notice also that the examined polarizer is a linear polarizer. Significant values appear in the first two columns of the matrix. Values in the first two columns are calculated from the Stokes parameters related to the state of linear polarization of the vertically and horizontally.

Tab. 1. Mueller matrix for polarizer.

Mueller Matrix (four-channel polarimeter)	Mueller Matrix (ThorLabs polarimeter)
$ \begin{pmatrix} \mathbf{0.404} & \mathbf{0.407} & \mathbf{-0.020} & \mathbf{-0.001} \\ \mathbf{0.422} & \mathbf{0.422} & \mathbf{-0.022} & \mathbf{0.011} \\ \mathbf{-0.125} & \mathbf{-0.153} & \mathbf{0.010} & \mathbf{-0.012} \\ \mathbf{-0.012} & \mathbf{-0.103} & \mathbf{-0.120} & \mathbf{-0.001} \end{pmatrix} $	$ \begin{pmatrix} 0.430 & 0.429 & 0.034 & 0.004 \\ 0.429 & 0.429 & 0.034 & 0.004 \\ -0.002 & -0.002 & -0.005 & -0.004 \\ -0.018 & -0.018 & 0.003 & -0.005 \end{pmatrix} $

Quarter-wave plate

Tab. 2. Mueller matrix for quarter-wave plate.

Mueller Matrix (four-channel polarimeter)	Mueller Matrix (ThorLabs polarimeter)
$\begin{pmatrix} 0.967 & -0.001 & 0.009 & -0.124 \\ 0.026 & 0.001 & -0.017 & 0.949 \\ -0.137 & -0.005 & 0.875 & -0.044 \\ -0.006 & -0.912 & -0.127 & -0.024 \end{pmatrix}$	$\begin{pmatrix} 0.892 & 0.024 & 0.013 & -0.001 \\ -0.037 & -0.033 & -0.083 & 0.917 \\ 0.018 & -0.011 & 0.914 & 0.088 \\ -0.026 & -0.895 & 0.002 & -0.039 \end{pmatrix}$

From the calculated Mueller matrix can be deduced what angle relative to the incident beam has been set quarter-wave plate. The location of significant values shows that the test element is set at an angle of -45° . For such a case the significant values appear in m_{00} , m_{13} , m_{22} , m_{31} and the last parameter is with the minus sign.

EXAMINATION OF THE IMPACT OF THE LIQUID CRYSTAL CELL ON THE STATE OF POLARIZATION OF LIGHT

Four-channel polarimeter built to test how the properties of polarized light beam after passing through the liquid crystal. Measuring station for testing a liquid crystal cell it is not converted in relation to the previously performed measurements. It consists of a generator and analyzer of the polarization state of light. Analyzer of the polarization state are four-channel polarimeter and polarimeter of Thorlabs. Examine the liquid crystal requires the preparation of a special measuring cell (a scheme of the cell shown in the following figure). During the experiment used cells measuring a thickness of $15 \mu\text{m}$.

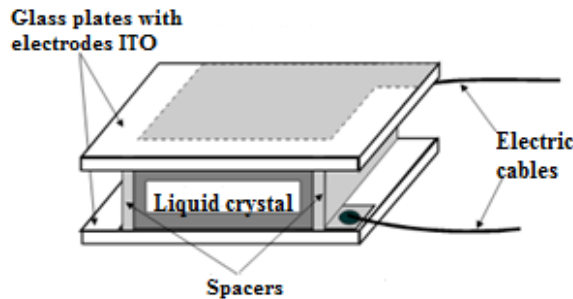


Fig. 2. Scheme of the liquid crystal cell [5].

In the nematic liquid crystal the molecules form a localized area with a specific orientation. When the electrodes will connected to a voltage less than 5V the liquid crystal molecules will be arranged with their long axes at an angle (from 0° to 90°) to the direction of the electric field. When application of a maximum allowable voltage (5V) causes the molecules are arranged in parallel with the electric field vector. When the forces of the electric field is removed the molecules of the substance nematic return to their initial order. [5]

Therefore to make the appropriate measurements had to be measuring cell filled with nematic liquid crystal connected to functional-arbitrary generator in order to work with external electric field. Designated Stokes vectors for the light beam after passing through the measuring cell allowed to determine the Mueller matrix. Matrices have been determined for each voltage electric field. Obtained so twenty-eight matrix which graphically presented on Fig. 3.

Analyzing the graphs which are graphical presentation of Mueller matrix it can be seen that the measurements made using four-channel polarimeter are very close to measurements measured using a reference polarimeter.

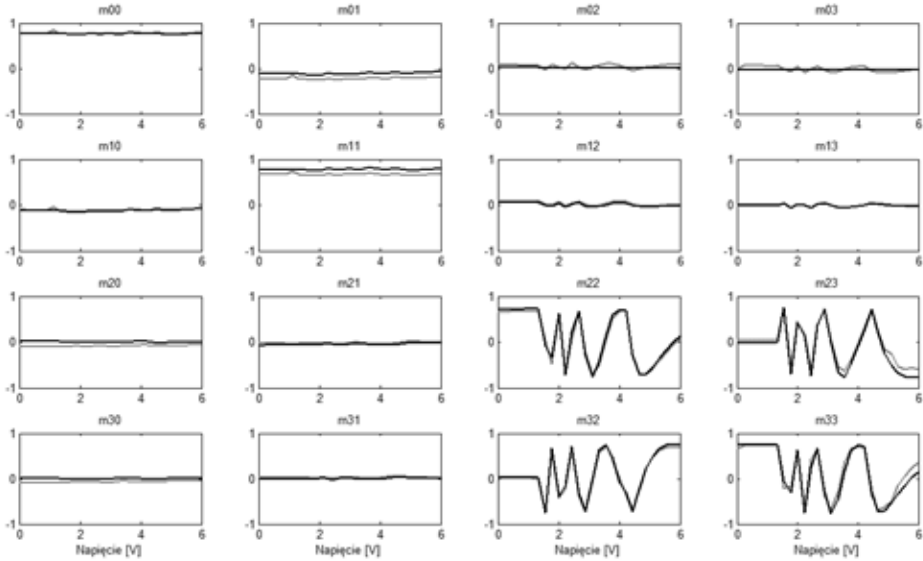


Fig. 3. Graphical representation of Mueller matrix calculated from the Stokes parameters measured by the four-channel polarimeter (black line) and polarimeter ThorLabs (grey line).

CONCLUSION

Analysing of the results of measurements made using a built polarimeter four-channel for testing of selected optical elements can provide the following conclusions: examine the impact of individual components of the four-channel polarimeter on the change the polarization of the light beam it helped build a system capable of providing the full Stokes vector for the analyzed light beam from the get intensity from four detectors of the polarimeter. At using the four-channel polarimeter was examined influence of optical elements so as the polarizer and quarter-wave plate for the change of the polarization of the light beam through by them. The impact of individual centers on the optical beam of light was presented in the form of a Mueller matrix. Built measuring system made it possible to examine the liquid crystal cells in a static mode. Obtained in measuring Mueller matrix are presented in graphical form. Analysis of the results from the measurement of static allowed noted that the liquid crystal to change the phase of the light beam passed therethrough. Matrices designated from

Stokes parameter set for a four-channel polarimeter compared with the results of reference polarimeter allowing to note that these results are in good agreement.

REFERENCES

- [1] D. Goldstein. Polarized Light: Second Edition. Revised and Expanded. Nowy Jork. 2003.
- [2] F. Ratajczyk. Dwójłomność i polaryzacja optyczna. Oficyna Wydawnicza Politechniki Wrocławskiej. Wrocław. 2000.
- [3] E. Collett. Polarized light in fiber optics. The PolaWave Group. New Jersey. 2003.
- [4] M. Bass. E.W. Van Stryland. D.R. Williams. Polarization. Handbook of optics. 2001. vol.1. s. 247 – 274.
- [5] G. Derfel. Podstawy fizyki i zastosowań ciekłych kryształów. Instytut Fizyki Politechniki Łódzkiej. Łódź. 2006.
- [6] E. Collett. The Description of Polarization in Classical Physics. American Journal of Physics. 1968. vol. 36.
- [7] E. Compain, S. Poirier, General and self-consistent method for the calibration of polarization modulators, polarimeters, and Mueller-matrix ellipsometry, Applied Optics, 1999, vol. 38.
- [8] O. Arteaga, J. Freudenthal, Mueller matrix polarimetry with four photoelastic modulators: theory and calibration, Applied Optics, 2012, vol. 51.

Hydrodynamic studies of magnetically assisted external loop airlift

*Joanna Lechowska^{1,2}

¹West Pomeranian University of Technology in Szczecin, Faculty of Chemical Technology and Engineering, POLAND

²Students' Scientific Association of the Institute of Chemical Engineering and Environmental Protection Processes, Faculty of Chemical Technology and Engineering, West Pomeranian University of Technology in Szczecin, Szczecin, POLAND

e-mail: lechowska.joanna@zut.edu.pl

Keywords: *airlift reactor, hydrodynamic, rotating magnetic field*

ABSTRACT

The hydrodynamic studies of the novel construction of external loop airlift reactor were presented. The novel approach for hydrodynamic processes in the airlift reactor was based on the application of the rotating magnetic field (RMF). The values of the mixing time and the liquid circulation velocity were obtained using the tracer response method. The main aim of the presented work was to investigate the influence of RMF frequency, the gas flow rate and the location of the RMF generators on the hydrodynamic parameters.

INTRODUCTION

The airlift reactors are classified as one of the important group of bubble devices. These apparatus are commonly applied for gas-liquid processes, such as production of organic acids, manufacturing pharmaceuticals, antibiotics and enzymes or water purification [3]. The airlift reactors have a wide range of applications in both chemical engineering and biotechnology processes such as sulfur dioxide absorption [4], production of bacterial cellulose [6], biomass production from natural gas [18], bio-oxidation of minerals [15], antibiotics production [2], nitrification/denitrification process [17], batch phenol biodegradation [10], gibberellic acid production [7] and gluconic acid fermentation [16]. These devices offer simple and effective mixing in two-phase systems involving gases and liquids. The airlift reactor offers advantages of no moving parts, low shear power consumption and good mixing quality.

Typically, the airlift reactor consists of two vertical regions: the riser, equipped with gas distributor, and the unaerated zone called the downcomer. These regions are connected with a gas-liquid disengagement section and a horizontal bottom section. In the case of this reactor, the liquid circulation is the result of the difference of the hydrostatic pressures between the aerated and unaerated sections.

The hydrodynamic studies are the important part of the experimental research that enable the understanding of the processes inside the airlift reactors. The experimental relations describing the hydrodynamic parameters such as mixing and

circulation time or liquid circulation velocity in the internal [11, 12] and external loop [5, 8, 18] airlift reactors are often presented in the literature.

Thus far, several studies have suggested that the magnetic field influenced the hydrodynamics in airlift reactors. Hristov [9] presented the interesting set of the examples of the magnetically assisted airlift and bubble columns. Al-Qodah and Al-Hassan [1] performed the hydrodynamic and mass transfer studies in the magneto stabilized airlift fermenter. In the later work, Al-Qodah and Lafi [2] developed the model that enabled to describe the antibiotic production in magneto three phase airlift.

The novel approach for hydrodynamic processes in the airlift reactor was based on the application of a rotating magnetic field (RMF). Rakoczy and Masiuk [14] published research results in the field of a mixing process under the action of a transverse rotating magnetic field. Przybył et al. [13] proved that the mixing system with the RMF generator may be successfully applied instead of a mixer for liquids.

The main aim of this work was to present the experimental studies of the influence of the RMF on the mixing time and liquid circulation velocity in the novel construction of the external loop airlift reactor.

MATERIALS AND METHODS

The investigations were performed using the experimental set-up shown in Fig. 1.

All the experiments were carried out in the external loop airlift reactor with the inside diameters of the riser and downcomer equal to 0.102 m and the height of 0.94 m, respectively. The disengagement section with the width of 0.285 m and the length of 0.80 m were filled with the tap water to the height of 0.05 m. Air was injected into the riser zone by means of the sparger. The gas flow rate was varied between 2 and 14 dm³·min⁻¹. The superficial gas velocity in the riser U_{GR} was changed in the range between 0.004-0.0285 m·s⁻¹. The superficial gas velocity was calculated from the ratio of the flow rate of the gas and the cross-section of the riser column (this geometrical parameter of the tested airlift column was equal to 0.0082 m²).

The hydrodynamic characteristics were obtained using tracer injection method. As a tracer, 300 ml saturated sodium chloride solution was injected on the surface of the liquid in the downcomer. The conductive probes were located in the probe taps in the downcomer section. The distance between the probes was equal to 0.65 m. The conductivity of the liquid were measured simultaneously and recorded by the multifunctional meters CX-701.

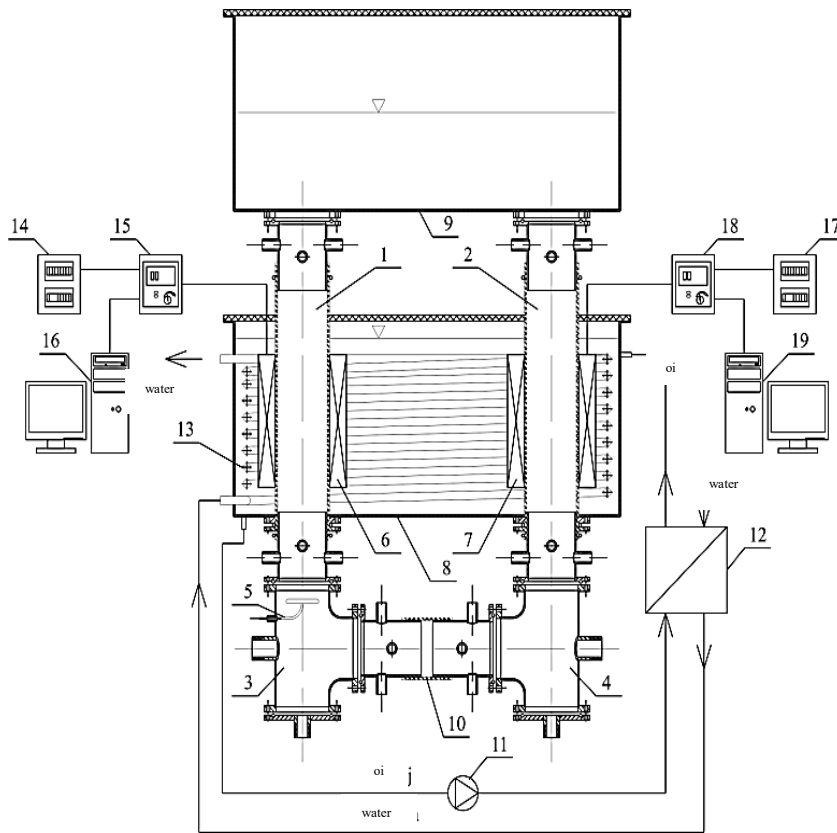


Fig. 1. Scheme of experimental apparatus: 1 – riser, 2 – downcomer, 3, 4 – T-connector, 5 – sparger, 6, 7 – RMF generator, 8 – housing, 9 – disengagement section, 10 – connector, 11 – pump, 12 – heat exchanger, 13 – internal coil, 14, 17 – electronic control box, 15, 18 – transistorized inverter, 16, 19 – personal computer.

The main part of this work was the investigation of the effect of the RMF (location of magnetic field generator and frequency) on the hydrodynamic parameters. The rotating magnetic field was generated by the stators of the three-phase asynchronous electrical engines located in the riser and the downcomer section, respectively. This kind of magnetic field induces a time-averaged azimuthal force, which drives the flow of the electrical conducting fluid in circumferential direction. The magnetic field lines rotate in the horizontal direction with the rotation frequency of the field. The RMF frequency f was changed in the range 10-50 Hz. The RMF with the magnetic induction B is controlled by means of the alternating current frequency equal to the frequency of the RMF. The values of the magnetic induction at different points inside the generator of magnetic field are detected by using the microprocessor magnetic induction sensors connected with the Hall probe and a personal computer. Basing on the records of the magnetic induction random signals the mean values of the parameter B at each sampling point was calculated. As follows from the analysis of the experimental data, the values of the magnetic induction are spatially distributed

and independent at the time. The spatial distribution of the magnetic field in the applied generator of the magnetic field is showed in Fig. 2.

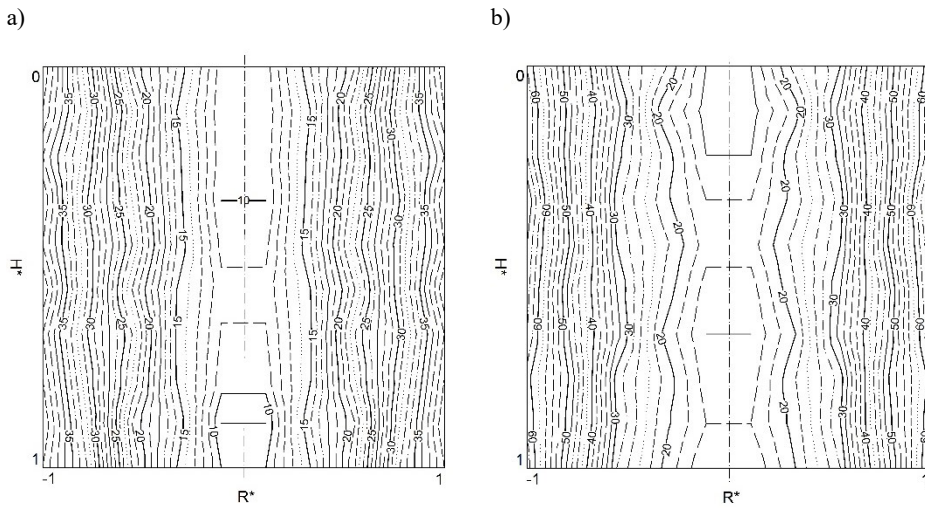


Fig. 2. The typical example of the contour patterns of the spatial distribution of the magnetic field induction in the cross-section of the RMF generator: a) $f = 10$ Hz; b) $f = 50$ Hz.

On the basis of the experimental measurements, the maximal and averaged values of the magnetic field were obtained. These values are dependent on the value of the RMF frequency (see Table 1).

Tab. 1. The maximal and averaged values of the magnetic field as a function of the RMF frequency.

RMF frequency, f	Maximal value of magnetic field, B_{\max}	Averaged value of magnetic field, B_{mean}
10 Hz	40 mT	24 mT
30 Hz	51 mT	28 mT
50 Hz	62 mT	34 mT

All hydrodynamic parameters were determined based on the tracer response curve. The example of the curve obtained from the experimental data shown in Fig. 3.

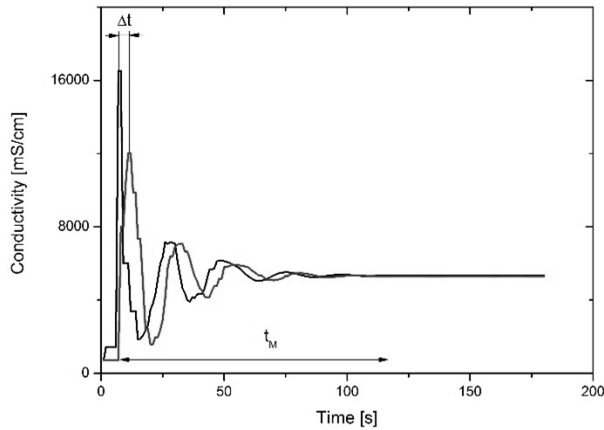


Fig. 3. The example of the tracer response curve.

The mixing time, defined as a time when the conductivity of the liquid reach the 99% homogenization. First, the values of the conductivity of liquid were normalized and obtained from the following relationship (1):

$$C_i = \frac{C(t) - C_0}{C_\infty - C_0} \quad (1)$$

where: $C(t)$ is the conductivity of the liquid in the time t , C_∞ is the final conductivity value, C_0 is the initial conductivity value of the liquid.

The data can be conveniently replotted in terms of a probe log variance as a function of time. To obtain an overall mixing time for the system, the two probe responses must be combined and the relationship for two probes were defined as (2):

$$\log \sigma^2 = \log \left\{ \frac{1}{2} [(C_1 - 1)^2 + (C_2 - 1)^2] \right\} \quad (2)$$

where: C_1 and C_2 is the normalized experimental data for the first probe and the second probe, respectively.

The liquid circulation velocity were determined as the quotient of the distance between the probe taps (0.65 m) and the time interval between the parallel peaks recorded for two conductive probes located in the downcomer. The relationship describing the liquid circulation velocity is following (3):

$$U_{LD} = \frac{\Delta s}{\Delta t} \quad (3)$$

where: Δs is the distance between the probe taps, Δt is the time interval between peaks (see Fig. 3.).

RESULTS

Liquid circulation is a consequence of the different values of bulk densities of the liquid in the riser and the downcomer section. The liquid velocity is directly related to the gas hold-up in the both sections, also size and velocity of the bubbles. Moreover, the liquid circulation velocity has a significant effect on the heat transfer coefficients, gas-liquid mass transfer, shear forces and liquid turbulence in the airlift reactors [7].

Furthermore, the mixing time is the parameter that enable the comparison of different type reactors and their hydrodynamic properties. Chaves et al. [7] proved that in the airlift reactors the mixing process consists of two components: backmixing as a result of recirculation, and axial dispersion in the riser and the downcomer due to the turbulent flow inside the reactor and different velocities of the gas and liquid phases.

Fig. 4. show the liquid circulation velocities in the downcomer and the mixing time as a function of superficial gas velocity in the riser. The graphs represent the data obtained for the measurements without the effect of the exposition of rotating magnetic field.

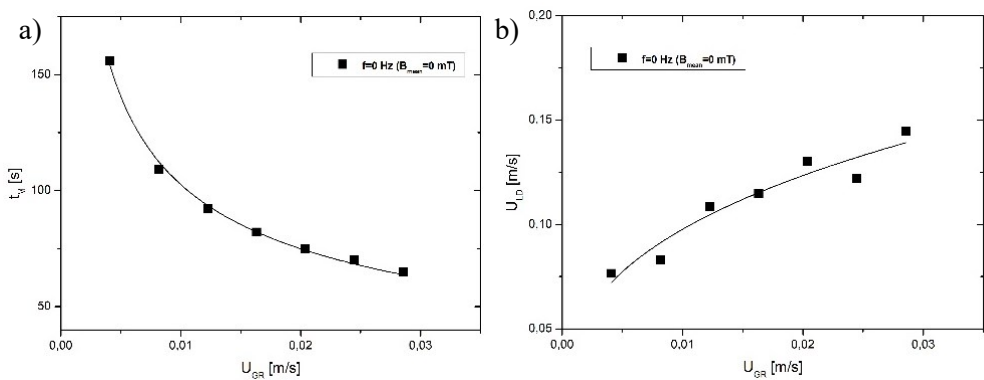


Fig. 4. The dependence of: a) $t_M = f(U_{GR})$ and b) $U_{LD} = f(U_{GR})$.

The main part of the research concerned the investigation on the effect of the localization of the rotating magnetic field generators (in the riser or the downcomer section) on the values of the mixing time and the liquid circulation velocities.

The experimental data of these parameters as a function of superficial gas velocity in the riser for the RMF frequencies varied in the range 0 – 50 Hz (the averaged values of the magnetic induction were changed in the range from 0 mT and 34 mT) were plotted and shown in the Fig. 5.

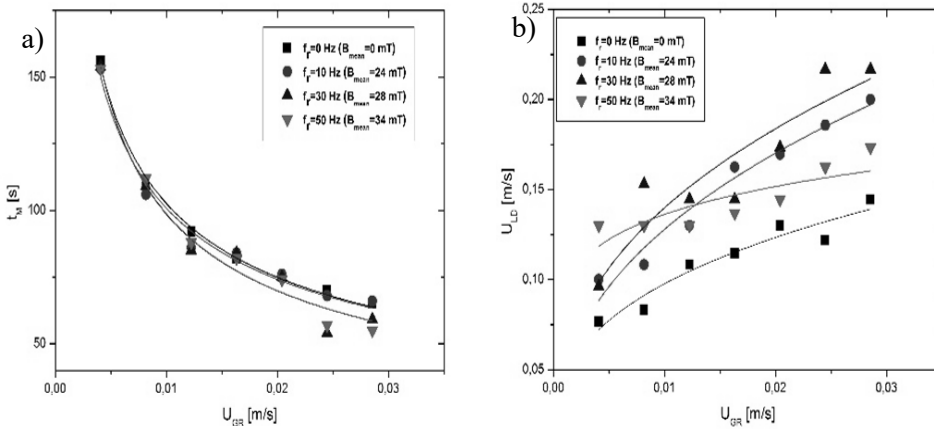


Fig. 5. The dependence of: a) $t_M = f(U_{GR})$ and b) $U_{LD} = f(U_{GR})$ for the RMF exposition in the riser section.

The strong influence of the superficial gas velocity on the tested hydrodynamic parameters is presented in Fig. 4 and 5. The rapid decrease of the mixing time and the increase of the liquid circulation velocity with the augmentation of U_{GR} were stated. Moreover, the research proved the effectiveness of the rotating magnetic field application. The decline of the mixing time (equivalent to the mixing process enhancement) results from the increase of the magnetic field intensity. The more noticeable effect of the RMF on the liquid circulation velocity measurement in the external loop airlift reactor is presented in Fig. 5b. This study showed that the maximal values of the U_{LD} were obtained for the RMF frequency in the riser section equal to 30 Hz. This effect is probably resulted from the significant volume of the gas phase in the riser section due to the injection of air that could impede the RMF influence.

The liquid circulation velocities in the downcomer and the mixing time for the RMF exposition in the riser section were fitted to the correlations summarized in the Table 2.

Tab. 2. The equations for the mixing time and liquid circulation velocity for the RMF exposition in the riser section.

Parameter	RMF frequency/averaged value of magnetic field	Equation	R ²
Mixing time t_M	0 Hz (0 mT)	$t_M = 12.70 U_{GR}^{-0.45}$	0.995
	10 Hz (24 mT)	$t_M = 13.12 U_{GR}^{-0.45}$	0.981
	30 Hz (28 mT)	$t_M = 9.95 U_{GR}^{-0.49}$	0.969
	50 Hz (34 mT)	$t_M = 9.89 U_{GR}^{-0.49}$	0.982
Liquid circulation velocity U_{LD}	0 Hz (0 mT)	$U_{LD} = 0.46 U_{GR}^{0.34}$	0.911
	10 Hz (24 mT)	$U_{LD} = 0.85 U_{GR}^{0.41}$	0.953
	30 Hz (28 mT)	$U_{LD} = 0.86 U_{GR}^{0.39}$	0.813
	50 Hz (34 mT)	$U_{LD} = 0.28 U_{GR}^{0.16}$	0.600

where: R² is the coefficient of determination

It was observed that the gas-liquid mixture in the downcomer has different flow structure than in the riser. The lower hold-up of the gas phase in the liquid, the lack of the inlet flow of air and the higher density of the fluid are the main factors determining the circulation in the airlift reactors. The observations suggested that the exposition of RMF in the downcomer can influence on the hydrodynamic parameters in another way than in the riser. The results obtained for the generation of the rotating magnetic field in the downcomer section are presented in the Fig. 6. Similarly, the RMF frequencies were varied in the range 0 – 50 Hz (the averaged values of the magnetic induction were changed in the range from 0 mT and 34 mT).

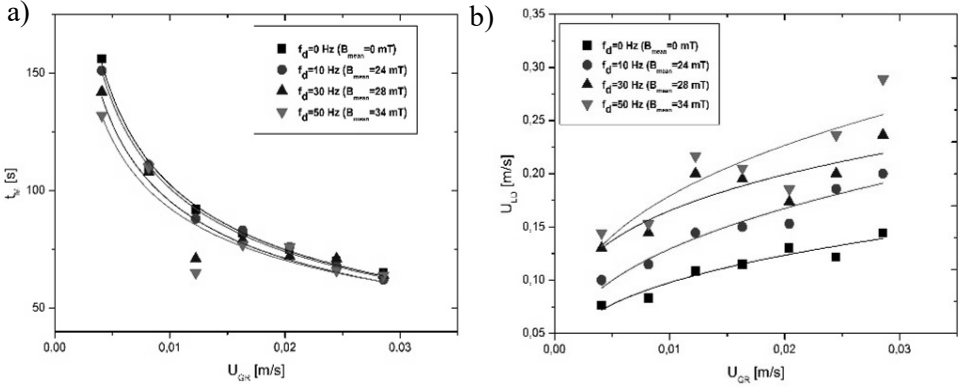


Fig. 6. The dependence of: a) $t_M = f(U_{GR})$ and b) $U_{LD} = f(U_{GR})$ for the RMF exposition in the downcomer section.

Tab. 3. The equations for the mixing time and liquid circulation velocity for the RMF exposition in the downcomer section.

Parameter	RMF frequency/averaged value of magnetic field	Equation	R ²
Mixing time t_M	0 Hz (0 mT)	$t_M = 12.70 U_{GR}^{-0.45}$	0.995
	10 Hz (24 mT)	$t_M = 12.95 U_{GR}^{-0.45}$	0.994
	30 Hz (28 mT)	$t_M = 13.48 U_{GR}^{-0.43}$	0.914
	50 Hz (34 mT)	$t_M = 15.03 U_{GR}^{-0.39}$	0.839
Liquid circulation velocity U_{LD}	0 Hz (0 mT)	$U_{LD} = 0.46 U_{GR}^{0.34}$	0.911
	10 Hz (24 mT)	$U_{LD} = 0.72 U_{GR}^{0.37}$	0.923
	30 Hz (28 mT)	$U_{LD} = 0.57 U_{GR}^{0.37}$	0.705
	50 Hz (34 mT)	$U_{LD} = 0.85 U_{GR}^{0.34}$	0.682

where: R² is the coefficient of determination

The effect of the exposition of the RMF in the downcomer section on the mixing time and the liquid circulation velocity is more evident in comparison to the results shown in the Fig. 5. This fact could be determined by the lack of the air injection in this section. The mixing time decreased with the increase of the frequency of the RMF but, above all, the liquid circulation velocity was maximalized by the application of the RMF. It was stated that the higher values of the RMF induction generated in the downcomer section, the faster liquid circulation.

In the Tab. 3. the correlation describing the mixing time and the liquid circulation velocity for the location of the RMF generators in the downcomer are presented.

CONCLUSIONS

Summarizing, the use of the RMF-assisted airlift reactor described in the current study allows to significantly increase the liquid circulation velocities. Another significant observation is the positive effect of RMF on the hydrodynamic condition in the tested reactor, confirmed by the mixing time. Therefore, it can be concluded, that the use of the RMF may provide a novel technique for improving hydrodynamic processes and when fully developed may find application in the bioprocessing applications.

REFERENCES

- [1] Al-Qodah Z., Al-Hassan M., Phase holdup and gas-to-liquid mass transfer coefficient in magneto stabilized G-L-S airlift fermenter, *Chemical Engineering Journal* 2000, 79, 41 – 52. DOI: 10.1016/S1385-8947(00)00142-X
- [2] Al-Qodah Z., Lafi W., Modeling of antibiotics production in magneto three-phase airlift fermenter, *Biochemical Engineering Journal* 2001, 7, 7 – 16; DOI: 10.1016/S1369-703X(00)00095-4
- [3] Bednarski W. Fiedurek J., Podstawy biotechnologii przemysłowej, *Wydawnictwa Naukowo - Techniczne*, Warszawa 2007.
- [4] Bekassy-Molnar E., Marki E., Majeed J.G., Sulphur dioxide absorption in airlift-tube absorbers by sodium citrate buffer solution, *Chemical Engineering and Processing*, 2005, 44, 1039 – 1046. DOI:10.1016/j.cep.2005.02.001
- [5] Bendjaballah N., Dhaouadi H., Poncin S., Midoux N., Hornut J-M., Wild G., Hydrodynamics and flow regimes in external loop airlift reactors, *Chemical Engineering Science* 1999, 54, 5211 – 5221. DOI: 10.1016/S0009-2509(99)00242-0
- [6] Chao Y., Ishida T., Sugano Y., Shoda M., Bacterial cellulose production by *Acetobacter xylinum* in a 50-L internal-loop airlift reactor. *Biotechnology and Bioengineering*, 2000, 68, 3, 345 – 352. DOI: 10.1002/(SICI)1097-0290(20000505)68:3<345
- [7] Chavez-Parga M.C., Gonzalez-Ortega O., Negrete-Rodriguez M.I.X., Medina-Torres L., Silva E.M.E., Hydrodynamics, mass transfer and rheological studies of gibberellic acid production in an airlift bioreactor, *World Journal of Microbiology and Biotechnology* 2007, 23, 651 – 623. DOI: 10.1007/s11274-006-9270-x
- [8] Guo Y.X., Rathor M.N., Ti H.C., Hydrodynamics and mass transfer studies in a novel external-loop airlift reactor, *Chemical Engineering Journal* 1997, 67, 2005 – 214. DOI: 10.1016/S1385-8947(97)00043-0

- [9] Hristov J., Magnetic field assisted fluidization – a unified approach. Part 6. Topics of Gas-Liquid-Solid Fluidized Bed Hydrodynamics, *Reviews in Chemical Engineering*, 2007, 23, 6, 373 – 526. DOI: 10.1515/REVCE.2007.23.6.373
- [10] Jia X., Wen J., Jiang Y., Liu X., Feng W., Modeling of batch phenol biodegradation in internal loop airlift bioreactor with gas recirculation by *Candida tropicalis*, *Chemical Engineering Science* 2006, 61, 3463 – 3475. DOI:10.1016/j.ces.2005.12.025
- [11] Klein J., Dolgos O., Godo S., Blazej M., Markos J., Application of a magnetic tracer method for the characterization of hydrodynamics in internal-loop airlift bioreactors, *27th International Conference of the Slovak Society of Chemical Engineering, Chemical Papers* 2000, 54, 456 – 466.
- [12] Merchuk J.C., Contreras A., Garcia F., Molina E., Studies of mixing in a concentric tube airlift bioreactor with different spargers, *Chemical Engineering Science* 1998, 53, 709 – 719. DOI: 10.1016/S0009-2509(97)00340-0
- [13] Przybył A., Rakoczy R., Konopacki M., Kordas M., Drozd R., Fijałkowski K., Investigation of mixing time in liquid under influence of rotating magnetic field. *XXII Ogólnopolska Konferencja Inżynierii Chemicznej i Procesowej – Proceedings*, 1160.
- [14] Rakoczy R., Masiuk S., Studies of a mixing proces induced by a transverse rotating magnetic field, *Chemical Engineering Science*, 2011, 66, 2298 – 2308; DOI:10.1016/j.ces.2011.02.021
- [15] Ruitenbergh R., Schultz C.E., Buisman C.J.N., Bio-oxidation of minerals in airlift loop bioreactors, *International Journal of Mineral Processes*, 2001, 62, 271 – 278. DOI: 10.1016/S0301-7516(00)00058-2
- [16] Sikula I., Jurascik M., Markos J., Modeling of fermentation in an internal loop airlift bioreactor, *Chemical Engineering Science* 2007, 62, 5316 – 5221. DOI:10.1016/j.ces.2007.01.050
- [17] Szewczyk K.W., Kuroń-Kulig A., Simultaneous nitrification and denitrification in a new airlift reactor, *Journal of Biotechnology* 2007, 131, 2, 148. DOI:10.1016/j.jbiotec.2007.07.861
- [18] Yazdian F., Shojaosadati S.A., Nosrati M., Pesaran Hajiabbas M., Vasheghani-Farahani E., Investigation of gas properties, design, and operational parameters on hydrodynamic characteristics, mass transfer, and biomass production from natural gas in an external airlift loop bioreactor, *Chemical Engineering Science*, 2009, 64, 2455 – 2465. DOI:10.1016/j.ces.2009.02.023

The influence of materials phase changes on spectral characteristic in optical fiber taper

*Joanna E. Moś, K.A. Stasiewicz, L.R. Jaroszewicz

Faculty of New Technology and Chemistry

Military University of Technology, Warsaw, POLAND

e-mail: joanna.musial@wat.edu.pl

Keywords: *tapered technology, biconical optical fiber taper, optical sensor.*

ABSTRACT

The paper presents the results of manufacturing temperature sensor of a micrometer size based on taper technology, using a standard single mode telecommunication fiber SMF28. The materials of variable state of matter dependent on temperature in order to change light beam propagation were used.. Measurements were made in the wavelength range 800-1700nm. We used a supercontinuum light source and the main conclusion is that we can use these sensors in a whole range of wavelengths. Previous studies were in a small range 1270-1370nm for superluminescent diode [1]. Achievements of external losses for such sensor are below 0.2 dB. Obtained threshold temperature is equal to the conversion temperature of used materials for whole spectrum of investigated range.

INTRODUCTION

In the past decades development of optical fiber technology gave the possibility of manufacturing new elements with the diameter of several micrometers [2, 3]. The fundamental requirement for all projected and manufactured optical fiber elements is to secure light propagation inside the arrangements and make it highly replicable. In this way the in-line elements are very useful, especially for protecting all the system miniaturization. There are many ways to obtain such results. Now many investigations are focused on photonic crystal fibers (PCF) [4-6]. Unfortunately, this technology is still expensive regarding the cost of PCF and requires the use of advanced technology to make possible the connection of PCF with most of standard measurement equipment [6]. Many of works in PCF technology are concentrated to fill the air holes with a different type of material like liquid crystal [7, 8], but it also requires an additional set-up for filling holes.

Another way to obtain satisfactory results is the implementation of an optical fiber taper technology [9,10] The tapering technology is relatively easy and gives the possibility of continuous monitoring of the changes in the light propagation through the fiber during its tapering [10, 11]. Tapering process allows to change optional boundary condition of fibers without necessity of drawing new fibers. The theoretical and experimental investigation of changing core diameter and cladding diameter, as well as refractive index profile along the taper region [9-11] shows that there is a possibility to use a biconical optical fiber taper as basic element to manufacture an

advanced sensor from different factors [12]. Since the taper allows to control light beam propagation in the fiber, it gives very interesting possibility of connecting such structure with external material characterized by variable state of concentration [1]. Thus, different interferometric temperature sensors using the phenomenon of multimodal interference in tapered region and based on an optical fiber taper have been proposed [13, 14]. Another way of sensors' designing is covering the taper waist with noble metal layers [12, 15] (platinum, gold etc.). Such case uses the principle of reflection and change of the boundary condition. Application of an additional material in the taper waist area caused increased the sensor sensitivity to detect parameters such as temperature [1, 13, 14], chemical and biological factors [15].

In this paper as an additional material we used wax and paraffin. These materials are characterized by phase transitions liquid-solid at various temperatures. The result of this combination was a threshold sensor. The purpose of this study was to verify that the sensor operates in a wide range of wavelengths 800-1700nm.

TECHNOLOGY OF TAPERED OPTICAL FIBER

This paper presents results of manufacturing the in-line threshold temperature optical fiber sensor based on biconical optical fiber technology [1, 8]. The manufactured sensor is made in a low cost technology using an SMF28 made by Corning®. As an external material which influence the propagation were chosen paraffin and wax with the melting temperature higher than 61°C. In the first part of the paper the applied technology with its main advantages is presented. This part also contains information on manufactured tapers, parameters which influence propagation properties, and characteristics of manufactured tapers, especially insertion losses. Second part of the described manufactured sensors along with description of measuring set-up using supercontinuum source Fianium secures measuring in a wide wave range between 800 nm and 1700 nm. Used as a detector the optical power meter precisely marks the melting temperature and, thus, the manufactured sensor sensitivity. Conclusions of the presented experimental results contain additional information about advantages of such sensors with special attention put on their use in mass production.

The set-up for manufacturing advanced optical fiber taper elements used elongation process of a fiber in a low-pressure gas burner. Process of elongation is provided in melting temperature obtained by a heating part of the fiber region in a propane-oxygen flame. The fiber elongation is realized by an axial stretching at two points located symmetrically to the heating point. Figure 1 presents the functional scheme and the picture of the set-up named FOTET II (Fiber-Optic Taper Element Technology) which was developed in the laboratory of the Institute of Technical Physics, Military University of Technology.

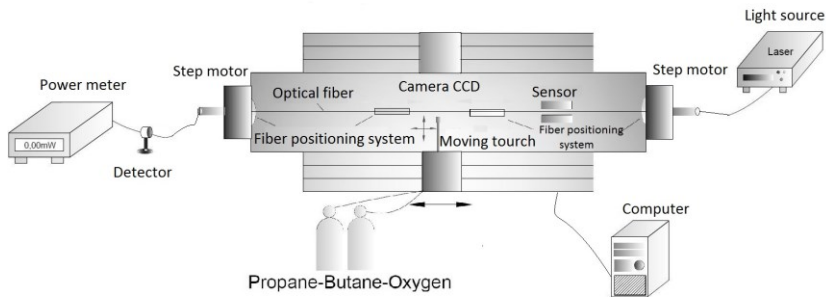


Fig. 1. The scheme of FOTET II set-up for manufacturing advanced elements based on an optical fiber taper.

The main advantage of this arrangement in comparison with commercially available stations as GPX-3400 (Vytran) and CW 5000 (Lightel) is a possibility of being used in manufacturing of different biconical tapers (with the length of the taper main region from point up to 200 mm and the waist diameter of several micrometers) [8, 10] for all types of fibers including standard telecommunication fibers, photonic crystal fibers, as well as plastic fiber. The process of the fiber elongation can be controlled by the flame movement connected with speed of two stretching engines. The system of a taper elongation was designed to avoid the fiber's damage (especially breaking) and to get a perfect biconical taper which was achieved by permanent monitoring of the light propagation through the fiber and by application of a special anti-gravitation unit for controlling the flame distance from the taper.

For our investigation's purpose the most interesting are tapers with a long taper waist region. For manufacturing temperature sensors as is schematically presented in Fig. 2, we made a taper of the whole length of elongation equal to 30.50 ± 0.16 mm. The diameter of waist region was equal to 6.0 ± 0.5 μm . The manufactured tapers were to receive very low insertion losses which can be achieved by a proper shape of the whole taper region (adiabatic type) including the area of connection of an upstretched fiber with the taper waist region. The achievement losses of the manufactured tapers were equal to 0.18 ± 0.02 dB.

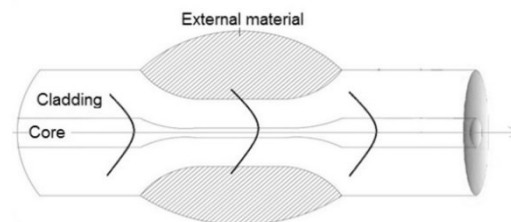


Fig. 2. Scheme of the optical fiber temperature sensor with a mark of the main elements [6].

Possibility to obtain a taper with the diameter of several micrometers (which is equal to the core of an SMF28®) makes that the optical beam is propagating in the whole taper waist region and in some parts outside of it. In the taper the air stays in a cladding. The leaking-out of beam is defined by the depth of penetration parameters

d_p . These parameters depend on a refractive index of the outside material which surrounds the taper and can be written as [14]:

$$d_p = \frac{\lambda}{\sqrt{2\pi(n_1^2 \sin^2 \theta_{\text{int}} - n_{\text{out}}^2)}} \quad (1)$$

Where n_1 , n_{out} are the refractive indices of the taper and the outside material, θ_{int} is the angle of an input wave with the wavelength λ .

Our idea was connected with the use of a leaking beam from the taper and how changing material of cladding influenced it. In order to protect in structure propagation condition, it is good to use materials with a refractive index close to the refractive index of glass and additional parameters which will be changed in a chosen temperature. For the measurement's purpose we chose very well-known materials like wax and paraffin. Both of them change their state of matter from constant to liquid in a temperature above 61°C. Such transition changes propagation parameters in an optical fiber taper. The propagation should be impossible for solid state which is connected with overall leaking of the beam from the taper region - material is non-transparent. For liquid state material is transparent and the refractive index is lower than the taper structure's which protects classic optical fiber propagation at total reflection condition.

RESULTS

All prepared structures of temperature sensors were measured several times to prove that there will be no damage during changing state of matter for heating and cooling of wax. Additionally, we used two laser source SC450 and SM1550nm and two detectors: OSA AQ6319 Yokogawa and Power Meter PM300 Thorlabs.

Below are presented the results of a manufactured temperature sensor for two most popular materials, wax and paraffin, which have different melting temperature but similar refractive index in the liquid state. In Figures 3 and 4 are presented spectral characteristics in a wide range of 800 -1700 nm (from Fianium source). From the spectra characteristics we can conclude that for the whole transmission range a threshold change of power in the presented sensors can be observed. As it can be noticed for both materials over 70°C, there is no difference of power and the sensors keep stable. In Figure 5 are presented hysteresis of change of power obtained from a single mode laser and an optical detector for wavelength 850nm, 1310 nm and 1550 nm. Rapid increase of power (change of state of matter from constant to liquid) for the temperature of 62-64°C can be observed what corresponds to the parameter of melting of chosen materials. As it can be observed for paraffin, we obtained more rapidly changes of optical transmission than in wax. A difference between chosen wavelengths may be a mistake of a measurement system OSA - time of taking whole range take few seconds in which time the temperature is changing. The difference in rapidity can also be observed in solidification process in these materials. Decrease of

optical power in cooling process is not so rapid as in heating process for wax. As for the second material – paraffin a sudden change of power from maximum to no propagation in the cooling process can be observed.

Obtained results from supercontinuum source allow us to check the influence on a wide range. As it can be noticed, the change of power is evenly for the whole range.

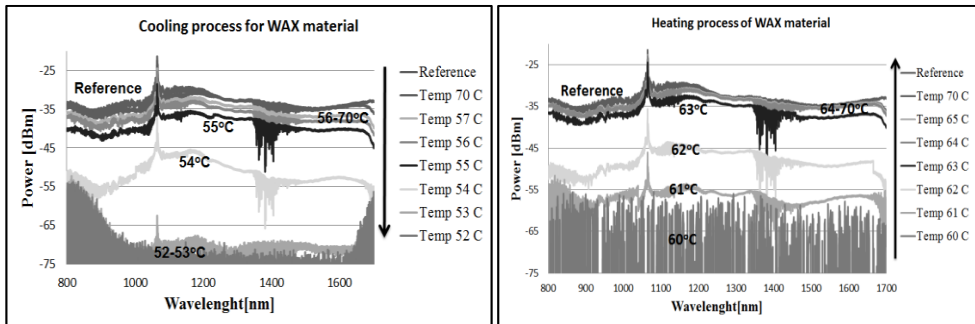


Fig 3. Spectral characteristics for the temperature sensor for SC source cooling and heating process in the range 800 – 1700 nm external material Wax.

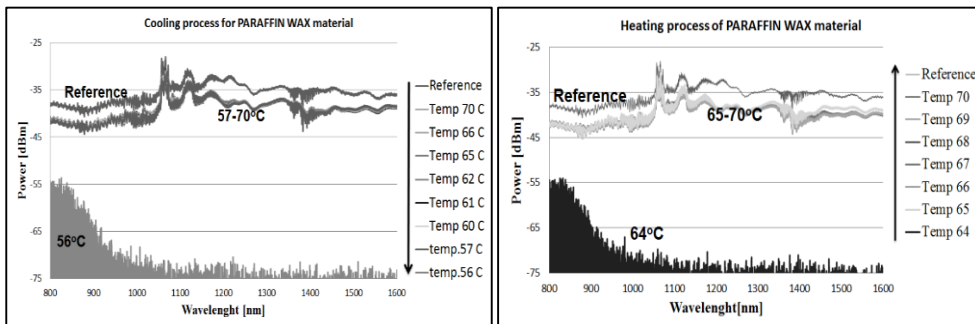


Fig 4. Spectral characteristics for the temperature sensor for SC source, cooling and heating process - external material Paraffin.

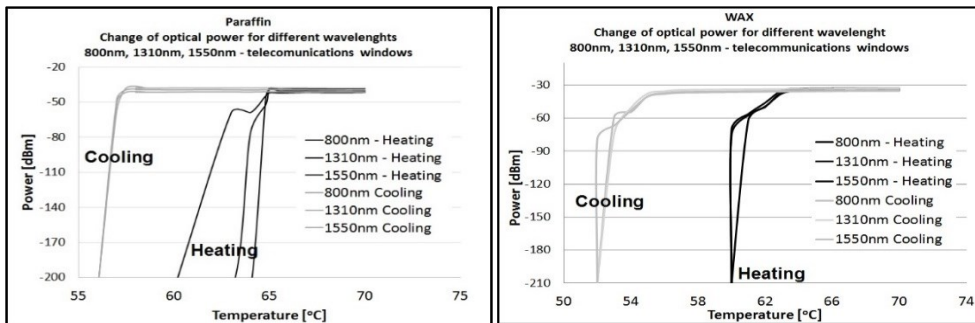


Fig 5. Hysteresis of heating and cooling of the temperature sensor with Wax and Paraffin.

CONCLUSION

Manufacturing of temperature sensor based on biconical optical fiber taper connected with material of variable state of matter is possible and allow to obtain very good results. The realized investigation shows that use of the additional material does not increase losses in width range (800-1700 nm). Results presented in this article show that by using wax or paraffin we can obtain the threshold temperature sensor. Achievement of external losses for sensor are below 0.2 dB. Obtain threshold temperature is equal to the conversion temperature of used materials. In our observation and theoretical simulation we can also predict that there is a possibility to make a whole scale of temperature sensors by using different types of material.

REFERENCE

- [1] K.A. Stasiewicz, J.E. Musial, Threshold temperature optical fibre sensors, *Optical Fiber Technology*, 2016, 32, 111-118, DOI:10.1016/j.yofte.2016.10.009
- [2] C. Tsao, Optical Fiber Waveguide Analysis, *Oxford University Press*, London, 1992
- [3] I. Kaminow, "Optical fiber telecommunication," *Academic Press*, 2008
- [4] T. Birks J. Knight, P. St. J. Russell., "Endlessly single-mode photonic crystal fibre," *Opt. Lett.*, 1997, 22, 13, 961 DOI. 10.1364/OL.22.000961
- [5] E.C. Magi P. Steinvurzel, B.J. Eggleton, Tapered photonic crystal fiber, *Optics Express*, 2004, 12, 5, 776-784, DOI.10.1364/OPEX.12.000776
- [6] S. Zhu, F. Pang, T. Wang, Single-mode tapered optical fiber for temperature sensor based on multimode interference, *SPIE-OSA-IEEE* , 2011, 8311 83112B-1, DOI: 10.1117/12.904444
- [7] T.R. Woliński, K. Szaniawska, S. Ertman, P. Lesiak, A.W. Domański, R. Dabrowski, E. Nowinowski-Kruszelnicki and J. Wojcik, Influence of temperature and electrical fields on propagation properties of photonic liquid-crystal fibers, *Proc. SPIE 5855, 17th International Conference on Optical Fibre Sensors*, 322, DOI:10.1117/12.623425
- [8] J. Kędziński, K. Garbat, Z. Raszewski, M.A. Kojdecki, K. Kowiorski, L.R. Jaroszewicz, E. Miszczyk, R. Dąbrowski, J. Zieliński, and W. Piecek, Optical properties of a liquid crystal with small ordinary and extraordinary refractive indices and small optical anisotropy, *Opto-Electronics Review*, 2014 ,22, 3, 162–165, DOI: 10.2478/s11772-014-0196-9
- [9] K.A. Stasiewicz, R. Krajewski, L.R. Jaroszewicz, M. Kujawińska, and R. Świllo, Influence of tapering process on changes of optical fiber refractive index distribution along a structure, *Opto-Electron. Rev.*, 2010, 18,1, 102-109, DOI: 10.2478/s11772-009-0030-y
- [10] T. A. Birks and Y. W. Li, The shape of fiber tapers, *J. of Lightwave Techn.* 1992, 10, 4, 432-438, DOI: 10.1109/50.134196
- [11] L. R. Jaroszewicz, M. Kujawińska, K. A. Stasiewicz, B. Siwicki, S. Wojcik, P. Marc, Enhanced interferometric methods for investigation of refractive index

- distribution changes along tapering structure in photonic crystal fibers *Proc. SPIE*, 2010, 7387, 7387-57, DOI: 10.1117/12.870785
- [12] K. Q. Kieu and M. Mansuripur, Biconical Fiber Taper Sensors, *IEEE Photonics Technology Lett.*, 2006, 18, 21, 2239 - 2241 DOI:10.1109/LPT.2006.884742
- [13] P. Lu, L. Men, K. Sooley, Q. Chen, Tapered fiber Mach-Zehnder interferometer for simultaneous measurement of refractive index and temperature, *Applied Optics*, 2009, 48, 13, 131110-131110-3 DOI:10.1063/1.3115029
- [14] S. W. Harun, K. S. Lim, S. S. A. Damanhuri, H. Ahmad, Microfiber loop resonator based temperature sensor, *Journal of the European Optical Society - Rapid publications*, 2011, 6, 11026, 1-4, DOI: 10.2971/jeos.2011.11026
- [16] Tian, Y.; Wang, W.; Wu, N.; Zou, X.; Wang, X. ,Tapered Optical Fiber Sensor for Label-Free Detection of Biomolecules, *Sensors* 2011, 11,4, 3780-3790, DOI:10.3390/s11040378

Optical properties of Photonic Crystal Fiber filled by ZnO nanoparticles fluid

Natalia Przybysz^{1,2}

¹Institute of Technical Physics, Faculty of Advanced Technologies and Chemistry, Military University of Technology, Kaliskiego St, 00-908 Warsaw, Poland

²University of Lodz, Faculty of Chemistry, Department of Materials Technology and Chemistry, Pomorska 163, 90-236 Lodz, Poland

e-mail: natalia.przybysz@wat.edu.pl

Keywords: *photonic crystal fiber, filled photonic crystal fibers, ZnO nanoparticles fluid, optical fiber threshold sensor.*

ABSTRACT

The aim of this work was synthesis and analysis ZnO nanoparticles and examination their influence on optical properties of selected photonic crystal fiber. Special attention has been focused on the synthesis of ZnO NPs. There were developed two synthesis methods of ZnO NPs, As a result of these synthesis there were obtained in propan-2-ol: monodisperse colloid I with average size of NPs 30 nm±8 nm ZnO NPs and polydisperse colloid II with ZnO NPs average size: 180, 630 and 1200 nm. Based on both colloids were prepared samples to tests. Each sample was a piece of 20-30cm long PCF filled by ZnO based nanofluid spliced on both sides with standard single mode fiber (SMF 28e Corning) and forms patch cord. The patchcord was illuminated by light from supercontinuum generator and it was measured optical power spectrum after passing the patch cord. Introducing NPS to the PCF's changed these characteristics. The light propagation in PCF filled with monodisperse ZnO colloid I in the whole spectral range was more advantageous in comparison to the propagation in PCF filled with propan-2-ol. Whereas polydisperse ZnO NPs filling resulted in a slight decrease in the transmission of light in the whole tested spectral range, however additional absorption peaks appeared at the wavelength 791nm. The presence of these peaks is probably caused by the larger size of ZnO NPs.

INTRODUCTION

Development of optoelectronics gave the transmission technology a wide variety of new opportunities. In the past few years, the rapid progress could be seen in the optical fibers' technology and optoelectronic converters. At the beginning of 20th century the filling of air opening in special optical fibers was discovered. In literature connected with the examined issues we can find many articles about the filling of air opening in special optical fibers by the following substances: alkanes [1], liquid crystals [2], water [3], liquids with nanoparticles [4], organic mixtures [5], polymers [2], immersive liquids [6]. The filling of the fibers allowed to design and manufacture photonic optical fibers' converters or sensors.

Nowadays, many studies are made in order to improve advanced sensors' systems. Miao and others [7], showed air holes filled with liquid and nanoparticles Fe_3O_4 in 10 nm size. The cross section of PCF, where the pitch was $6.36\mu\text{m}$, the average diameter of air hole was $3.67\mu\text{m}$, core diameter was $8.8\mu\text{m}$ (fabricated by Yangtze Optical Fiber and Cable Co. Ltd., China). One of the practical aims of the study is to find the potential application of this device as an intensity-modulated sensing element or a tunable all-in-fiber gain equalization filter with an adjustable slope. In this experiment made for Fe_3O_4 spectral characteristics are in the temperature range from 20 to 100°C . As a result of the experience was observed a linear relation between temperature and power transmission of PCF fiber-filled nanoparticles. Thus, it can therefore be used as the based-intensity temperature sensor, and other adjustable photonics device [7].

Moreover, the available literature contains a number of articles describing the photonic fiber filling various substances, and the spectral analysis is carried out at the selected temperature range.

Among different metal oxide nanoparticles, ZnO NPs are an attractive material because of wide band gap 3.37 eV, large bond strength, and large exciton binding energy (60 meV) at room temperature. Therefore, ZnO NPs have found many applications as gas [8], chemical and bio-sensors, storage, optical and electrical devices, window materials for displays or solar cells.

In this study, we present the analysis of the influence of the ZnO NPs filling on the light propagation in microstructured fibres in a broad spectral range. Only nanoparticles having a low and high polydisperse index were chosen as a filling of the fibre LMA-10. They were placed in photonic crystal fibres LMA-10.

EXPERIMENTAL

Materials

As single-mode photonic crystal fiber (PCF) was selected a Large Mode Area (LMA-10) fiber. According to the producer (NKT Photonics) the core and cladding material of the LMA-10 fiber was silicon coated by acrylic single layer. The LMA-10 core, outer cladding and coating diameters were $8 \pm 0.5\mu\text{m}$, $125 \pm 2\mu\text{m}$ and $250 \pm 10\mu\text{m}$, respectively. Transmission spectra and transmission power and measured for a wavelength range of 400 nm – 1700 nm.

Chemicals

Zinc acetate dihydrate 99% p.a., (from Lach-Ner); sodium hydroxide 98.8% p.a.-basic., (Chempur) and 2-Propanol 99,7% pure p. a.-basic, (Chempur) were used as received and without further purification.

Synthesis

Mono- and polydisperse ZnO nanoparticles were prepared similarly to those described in the literature [Hale2005, Jacobsson 2011]. In order to prepare mono- and

polydisperse ZnO nanoparticles two different sets of experiments have been done. In one (synthesis I), two solutions A and B were mixed at the same time, ZnO particles began to grow as monodisperse nanoparticles (colloid I). In the other set of experiments (synthesis II) A solution to B was added in portions (2.5 ml) with vigorous stirring. In this case ZnO are formed as polydisperse nanoparticles (colloid II). Both colloids were stable over one month.

In the case of the solution A preparation, 0.02 mol NaOH are dissolved in 16 mL of 2-propanol at 65°C. Then the solution was cooled in an ice bath to 0°C. In a similar way, solution B was obtained: 0.22 mmol $\text{Zn}(\text{OAc})_2 \cdot 2\text{H}_2\text{O}$ are dissolved in 16 mL of 2-propanol under vigorous stirring at 65°C. The prepared solution was diluted with 168 mL of chilled 2-propanol and cooled in an ice bath to 0°C. As described above, the solution A was added to B and slowly heated in a water bath to 65°C.

CHARACTERIZATION METHODS

Dynamic Light Scattering measurements

DLS measurements of size and size distribution of ZnO nanoparticles in the colloids were performed with the use a Nano ZS zetasizer system (Malvern Instruments). During all measurements the parameters were as follows: laser wavelength of 633 nm (He–Ne), scattering angle of 173° (fixed—without changing possibility), measurement temperature of 25°C, medium viscosity of 2.040 mPa·s (25°C), and medium refractive index of 1.377, and material refractive index of 2.000. The sample was loaded into quartz microcuvette (Hellma, the optical path length – 10.00 mm), and five measurements were performed, for which the mean result was recorded.

Scanning Electron Microscope (SEM) images

Scanning Electron Microscopy (SEM) images were performed using a Nova NanoSEM 450 Schottky Field Emission Scanning Electron Microscope (FESEM) produced by FEI. The images of LMA-10 fiber were acquired in secondary electrons mode using TLD detector (magnifications 12 000x and 20 000x). LMA-10 filling preparation and transmission spectra measurements.

Before the filling of air openings and conducting the analysis, the photonic fibre must undergo mechanical treatment and transmit introduced chemical substance on suitable distance from the front of the fibre and then it is possible to prepare photonic line. This line was constructed with the LMA 10 fibre with ZnO NPs filling and it is 2 cm long. The networks, prepared in this way, underwent the spectral examination. In order to conduct this analysis, photonic fibre, must be weld with telecommunication fibres. The two ends of the PCF are spliced to standard single-mode fibers SMF 28. The SMF 28 are spliced to light from a supercontinuum (FIANUM SC-450) source which is coupled into this devise.

The transmission spectrum is measured by an optical spectrum analyzer (ANDO AQ6315B).

RESULTS AND DISCUSSION

The results obtained for ZnO NPs colloid prepared in synthesis I are shown in Fig. 1. Analysis of the results confirms that the ZnO NPs are monodisperse. Polydisperse index (PDI) was 0.075 and the size of ZnO NPs in the investigated colloids was (30 ± 8) nm.

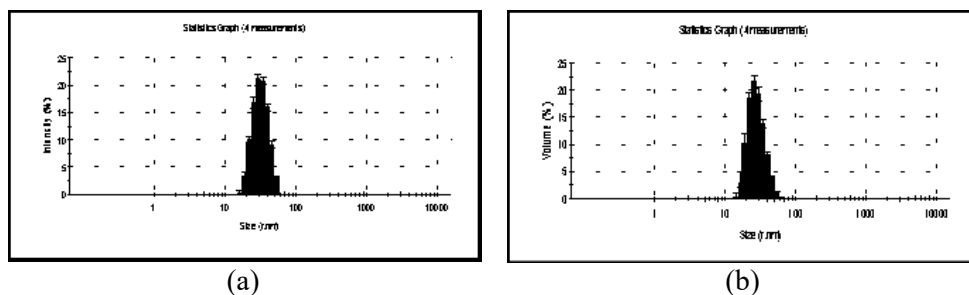


Fig. 1. Histogram ZnO NPs size depending on the intensity of the scattered light (a) and the volume of the light scattering of nanoparticles (b).

Tab. 1. DLS measurements of ZnO NPs.

ZnO NPs size d [nm]		PDI
Intensity (%)	Volume (%)	
32 ± 8 nm (100%)	28 ± 8 nm (100%)	0.075

Analysis of the size of the nanoparticles chart demonstrate that the colloid is one population of nanoparticles with average size of 30 nm. On the basis of the ratio of PDI it can be concluded that the resulting nanoparticles are monodisperse with a small size scatter

DLS measurements for ZnO NPs colloid obtained in synthesis II are not shown here. However, the PDI was 0.686 indicating that the tested colloid was polydisperse. In that case it is not possible to determine the size of the nanoparticles from DLS technique because of the presence of the larger particles which will dominate the light scattering signal and mask the presence of the smaller particles. However, the size was determined from SEM images of the LMA-10 photonic fibers cut in the presence of filling (Fig. 2 b,c,d).

SEM measurements show that the LMA-10 fiber in the place of cutting is smooth (Fig. 2a) while the LMA-10 with polydisperse ZnO NPs filling is covered with a large number of nanoparticles with different sizes (Fig. 2 b,c). A population of 100 nanoparticles of ZnO was measured from image 2c and plotted the histogram (Fig. 2d). Analysis of the obtained result indicates that in the investigated polydisperse ZnO NPs received from colloid II, three populations of nanoparticle sizes are visible: around 180 nm (the most numerous), 630 nm and 1200 nm. In the case of bigger

nanoparticles (630 nm and 1200 nm), only single nanoparticles of this size were observed on the surface of LMA-10.

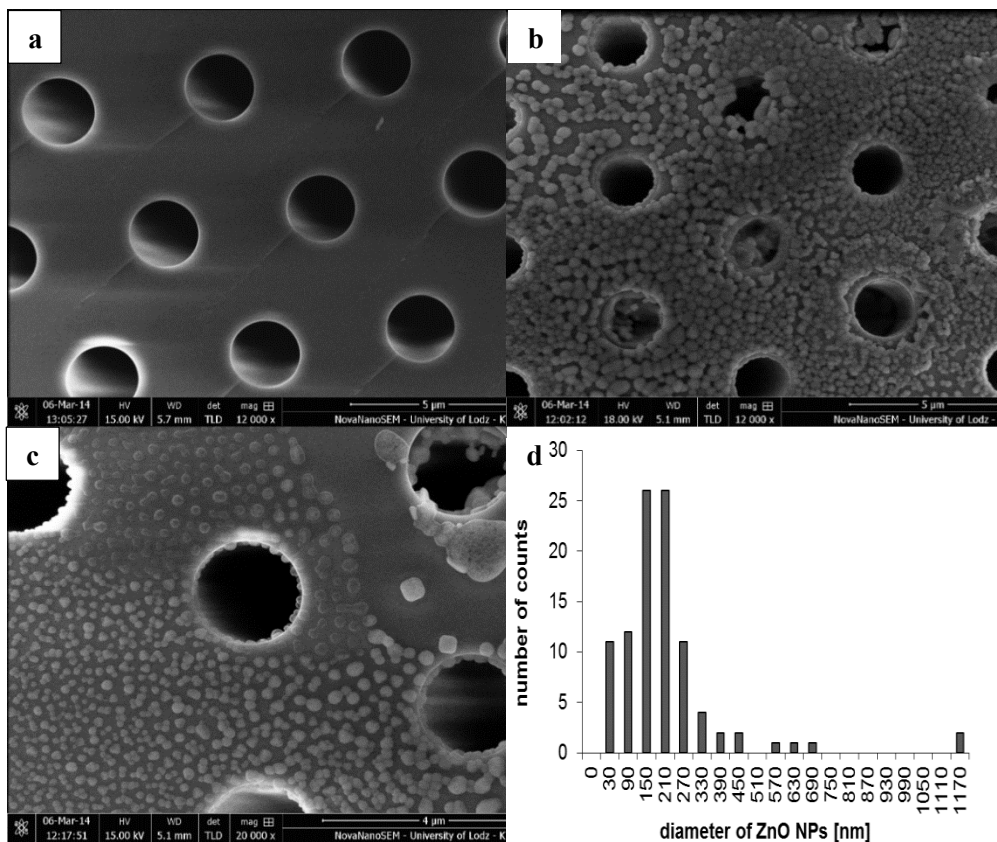


Fig. 2. SEM images of the cross sections of : **(a)** empty LMA-10 and **(b,c)** LMA-10 filled by polydisperse ZnO NPs, **(d)** ZnO NPs size distribution measured from **(c)** SEM image NPs **(b)** and **(c)** were released of LMA-10 after cutting it in the place of the filling.

Air holes of microstructured fibers can be placed various substances that affect the propagation of light waves. In the experiment, the LMA fibers 10 holes were filled with ZnO nanoparticles with low and high sizes' polydispersity ZnO NPs are three-dimensional structures, which, due to its relatively small size (100 nm) have unique optical and electrical properties.

As we can see in Fig. 3 a, structures of the spectral band are in the range of visible light. Band gaps observed for the ZnO nanoparticles with low polydispersity coincide with the size of the bands observed for the propan-2-ol, wherein the nanoparticles were synthesized (thus the absorption bands in the visible range originate from the solvent). Moreover, it should be noted that a better wave transmission for a fibre filled with ZnO NPs (low PdI) in relation to the solvent (propan-2-ol) filled photonic fiber.

However, if we examine Fig. 3 b it can be concluded that the structure is a spectral band in the visible range from 350 nm to 600 nm. Furthermore, one can

observe two distinct energy gaps in the range of 450 nm to 500 nm and in the range of 500 to 600 nm - corresponding to the energy gaps observed for propan-2-ol and two absorption peaks at a wavelength of 586 and 791 nm (Fig. 3 c), observed for ZnO NPs with a size high polydispersity of the entire sample volume. It seems that it is caused by presence of ZnO NPs in size about 630 nm. According to Struk [9] studies the thickness increasing of the ZnO layers in range from 490 to 554 nm caused the wavelength shifting from 508.95 to 555.85 nm and from 659.21 to 727.13 nm. In relation to Struk investigations we observed red shifting of absorption peaks due to larger size of ZnO NPs (630 nm) in comparison to ZnO layers (554 nm).

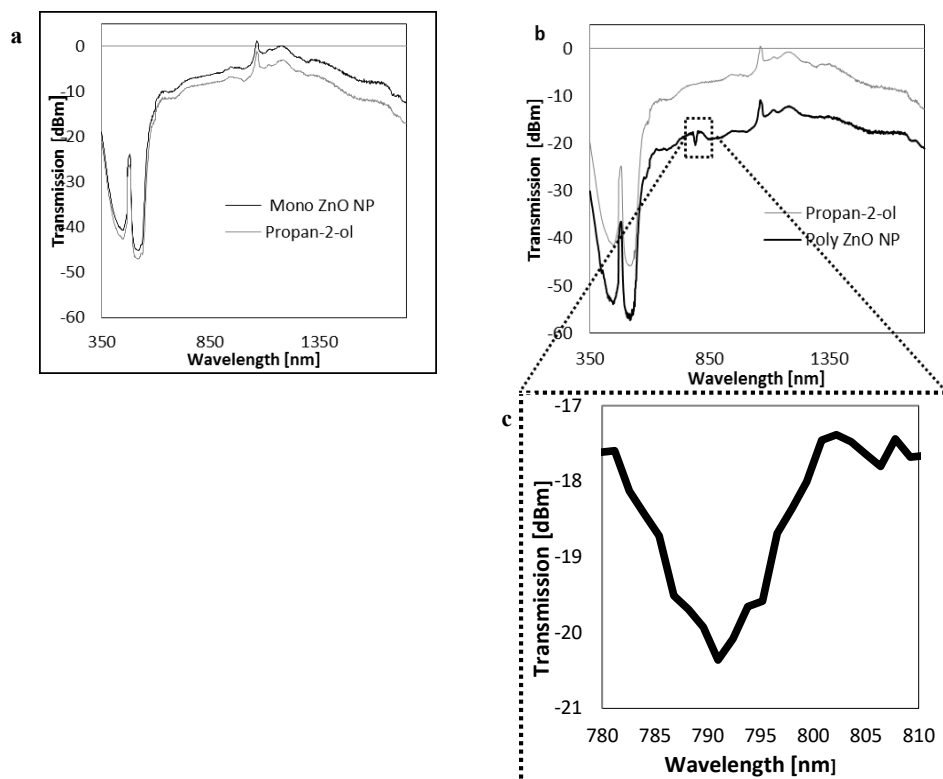


Fig. 3. A plot of the transmission wavelength for the fiber filled with ZnO NPs in propan-2-ol with: a low polydispersity size and the propan-2-ol (Fig. 3a), a high polydispersity index and the propan-2-ol (Fig. 3b) and a high polydispersity in the wavelength range of 780 nm to 810 nm.

The presence of ZnO nanoparticles in size of 30 nm inside of PCF does not result in appearance absorption peaks in investigated spectral range due to the size of ZnO NPs which coincides with the bands observed for the propan-2-ol.

Studies concerning transmission of ZnO NPs with a high PDI are the most promising because of the recorded 586 and 791 nm absorption bands in terms of application in special fibers and they require further studies related to the determination of temperature thresholds.

CONCLUSIONS

To sum up, with the increase in the size of the ZnO nanoparticles, the lowering of the transmission curve in the visible range is observed. Moreover, studies of transmission of ZnO NPs with a high PDI are more promising (registered absorption band 791 nm) from the point of view of the application of the special fibers and they require further studies related to the determination of temperature thresholds. Additional absorption band registered in the solution of nanoparticles of high PDI may be due to the large sample size polydispersity. As a result is a precise size of nanoparticles in the synthesis of ZnO with a high polydispersity could cause the appearance of additional absorption bands.

On the basis of the above analysis we can unequivocally state that the introduction of nanoparticles into the LMA 10 fiber resulted in a significant change in attenuation of the wave from 400 nm to 1700 nm, in which were carried out studies of wave propagation for all the presented above solutions of ZnO NPs.

REFERENCES AND NOTES

- [1] Marć P., Przybysz N., Stasiewicz K., Jaroszewicz L.R., Alkanes-filled photonic crystal fibers as sensor transducers, *Proc. SPIE* 9634, 96345O (2015).
- [2] Eggleton B. J., Kerbage C., Westbrook R. S., Windeler R. S., Hale A., Microstructured optical fiber devices, *Opt. Express* 9 (13), pp. 698-712, 2001.
- [3] C. Martelli, J. Canning, K. Lyytikainen, N. Groothoff, Water-core Fresnel fiber, *Opt. Exp.*, vol. 13, pp. 3890–3895, 2005.
- [4] Yinping M., Bo L., Kailiang Z., Yan L., Hao Z., Temperature tunability of photonic crystal fiber filled with Fe₃O₄ nanoparticle fluid, *Appl. Phys. Lett.* 98, p. 21103, 2011.
- [5] Marć P., Piliszek P., Murawski M., Szymanski M., Nasiłowski T., Pawlik K., Jaroszewicz L. R., Temperature threshold sensor based on optical switch with filled photonic crystal fiber, 22nd International Conference on Optical Fibre Sensors OFS-22, 15-19.10.12 Beijing, Chiny, *Proc. of SPIE*, 8421, pp. 8421-74, 2012.
- [6] Wang Y., Bartel H., Ecke W., Moerl K., Lehmann H., Schroeder K., Willsch R., Kobelke J., Rothhardt M., Spittel R., Shan L., Brueckner S., Jin W., Tan X., Jin L., Thermo-optic switching effect based on fluid-filled photonic crystal fibre, *IEEE Photonics Technology Letters*, 22 (3), pp. 88-90, 2010.
- [7] Miao Y., Liu B., Zhang K., Liu Y., Zhang H., Temperature tunability of photonic crystal fiber filled with Fe₃O₄ nanoparticle fluid, *Applied Physics Letters* 98, 021103 (2011).
- [8] Konidakis I., Androurlidaki M., Zito G., Pissadakis S., Growth of ZnO nanolayers inside the capillaries of photonic crystal fibers, *Thin Solid Films* 555 (2014) 76-80.
- [9] Struk P., Pustelny T., Opilski Z., Researches on the Spectral Transmittance of Zinc Oxide ZnO Semiconductor Layers, *Acta Physica Polonica A* 118 (2010) 1239-1241.

Synthetic pathways of 4-(alkyl-1-yn-1-yl)-bromo/chlorobenzenes as useful intermediates for highly birefringent Liquid Crystals

*Marta Pytlarczyk, Przemysław Kula

Institute of Chemistry, Faculty of Advanced Technologies and Chemistry, Military University of Technology, Warsaw, POLAND

e-mail: marta.pytlarczyk@wat.edu.pl

Keywords: *Sonogashira cross-coupling, liquid crystal, terminal acetylene*

ABSTRACT

Liquid crystalline (LC) materials are widely used in displays and photonic devices. Some applications of LC materials require high values of birefringence (Δn) [1-4]. In the case of rod-like LC molecules, designing molecules with long conjugated π electron systems can generate higher values of Δn (Fig. 1).

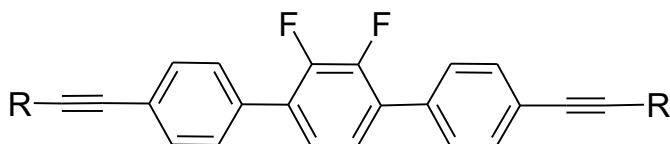


Fig. 1. General structure of 1,4-bis[4-(alkyl-1-yn-1-yl)phenyl]-2,3-difluorobenzene.

One of the molecular design approaches is based on 4-(alkyl-1-yn-1-yl)-phenyl-4-yl unit as a nonpolar terminal endcap of the molecule. 4-(Alkyl-1-yn-1-yl)-bromo/chlorobenzenes with longer alkyl part (for alkyl longer than four) can be synthesized via direct Sonogashira cross-coupling of terminal alkynes with 1-bromo-4-iodobenzene. The situation becomes more complicated in the case of shorter homologues since the terminal alkynes are gases at normal conditions and direct protocol cannot be employed.

In this work we presented short literature review of synthetic methods useful for synthesis of arylacetylenes and our preliminary results in synthesis of 4-(alkyl-1-yn-1-yl)-bromo/chlorobenzenes, either short and longer chained systems (Fig. 2.). Thus obtained intermediates are convenient semi-product in synthesis of rod-like Liquid Crystals.

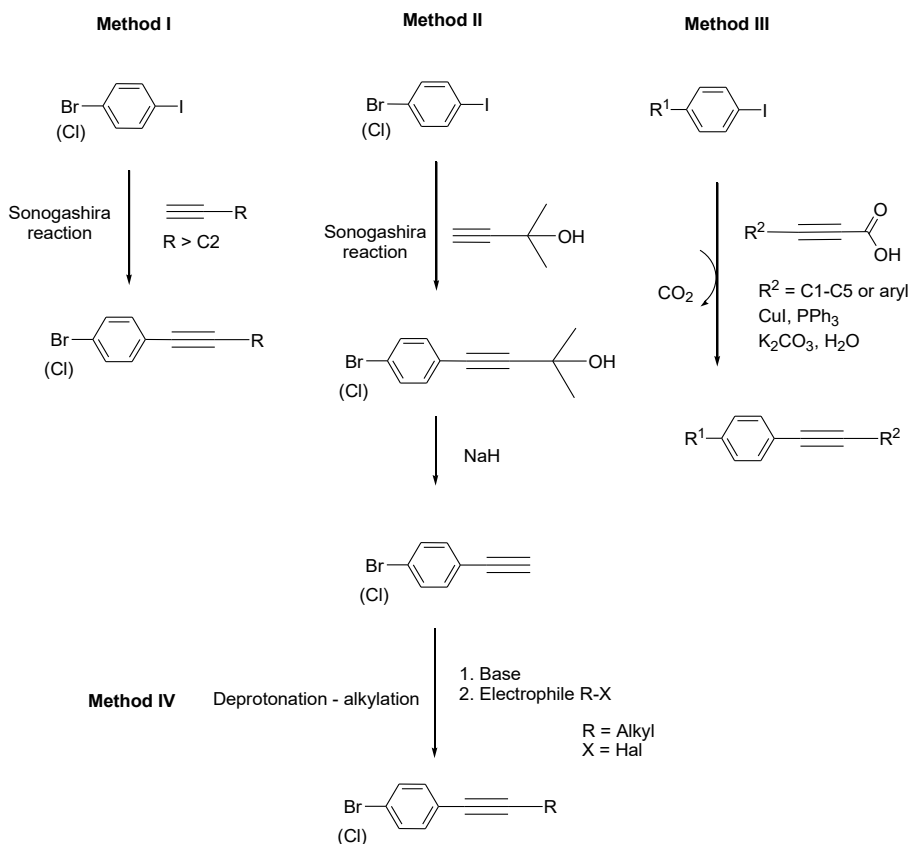
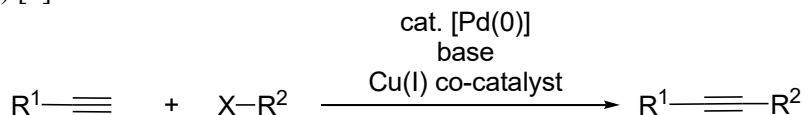


Fig. 2. Synthetic pathways of 4-(alkyl-1-yn-1-yl)-bromo/chlorobenzenes.

SYNTHETIC METHOD REVIEW

Sonogashira coupling

One of the methods of $\text{sp}^2\text{-sp}$ carbon-carbon bond formation is a Sonogashira reaction. This method was first reported in 1975 by K. Sonogashira and co-workers [5]. Nowadays, it is one of the most important reactions used in the synthesis of many useful molecules from pharmaceuticals and natural products to nanostructures [6-8]. This coupling requires an aryl or vinyl halide or triflate and a terminal alkyne as substrates and two catalysts: palladium catalyst and copper(I) iodide as a co-catalyst (Fig. 3.) [9].



$\text{R}^1 = \text{Aryl, Heteroaryl, Alkyl, SiR}_3$

$\text{R}^2 = \text{Aryl, Heteroaryl, Vinyl}$

$\text{X} = \text{I, Br, Cl, OTf}$

Fig. 3. General reaction for Sonogashira coupling.

4-(Alkyl-1-yn-1-yl)-bromo/chlorobenzenes with longer alkyl chain (for alkyl longer than four atoms of carbon) can be synthesized via direct Sonogashira cross-coupling of terminal alkyne with 1-bromo/chloro-4-iodobenzene (Method I, Fig. 2.). The reactivity difference of bromine/chlorine vs. iodine in the case of Sonogashira reaction, is sufficient to ensure effective mono-functionalization from the iodo-side. In the case of homologue C4 in alkyl chain, direct approach of Sonogashira coupling is more complicate due to gaseous state of but-1-yn at normal conditions and direct protocol cannot be employed [10]. Terminal alkynes low boiling points are presented at Fig. 4.

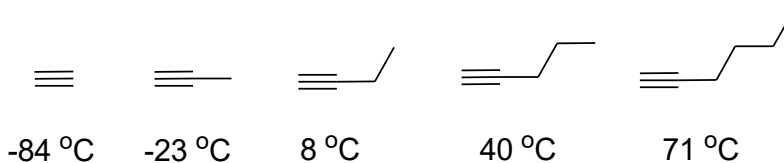


Fig. 4. Boiling points of C2-C6 terminal alkynes.

Catalytic Nitrile-Alkyne Cross-Metathesis

Only one literature report presented synthesis of this 4-(but-1-yn-1-yl)-bromobenzene (Fig. 5.) [11]. This compound was obtained only as by-product (yield 18%) in catalytic cross-metathesis reaction of an alkyne (hex-3-yne) with a nitrile (4-bromobenzonitrile) catalyzed by tungsten complex. This approach is unfavourable for multigram synthesis.

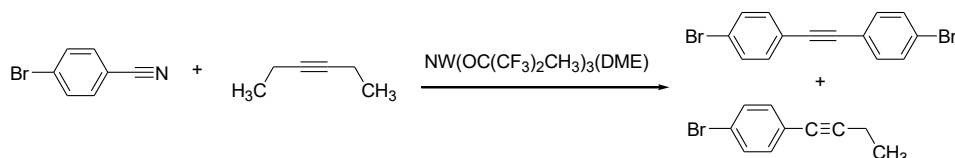


Fig. 5. Catalytic cross-metathesis reaction.

Decarboxylative coupling of $sp - sp^2$ carbons of aryl halides with alkynyl carboxylic acids.

First example of decarboxylative coupling of sp carbon and sp^2 carbon in the presence of $\text{Pd}_2(\text{dba})_3$ and phosphines ligands (e.g. dppf, P^tBu_3 , PCy_3), were reported in 2008 by S. Lee and co-workers [12, 13]. One year later Mao and co-workers described copper-catalyzed decarboxylative coupling of aryl halides with alkynyl carboxylic acids performed in water (Fig. 6., Tab. 1) [14].

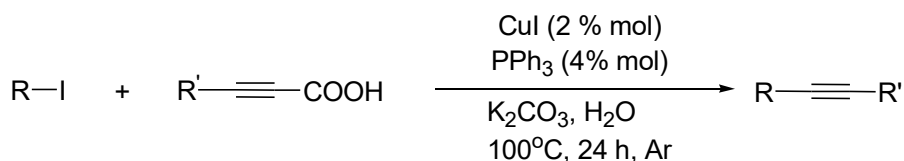
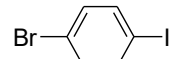
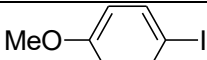
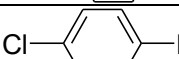
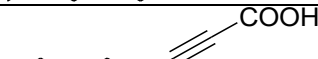
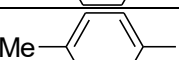
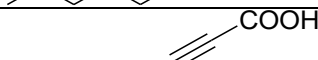
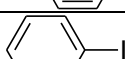
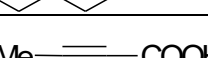
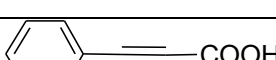
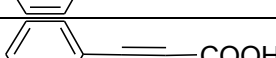


Fig. 6. General Scheme of decarboxylative coupling of aryl iodides and alkynoic acids.

Tab. 1. Scope of copper-catalyzed decarboxylative coupling of aryl iodides and alkynoic acids performed in water or DMSO [14].

Entry	R-I	R'—C≡C—COOH	Yield ^a (%)	Yield ^b (%)
1			94	92
2			99	99
3			88	94
4			95	95
5			95	89
6			86	23
7			97	72
8			99	92

Reaction conditions: aryl iodide (0,3 mmol), alkynoic acid (0,4 mmol), CuI (2 mol %), PPh₃ (4 mol %), K₂CO₃ (0,9 mmol), solvent (3 mL), 100 °C, 24 h, under Ar; a- DMSO as the solvent, b – water as the solvent.

The presented results show that high yields were obtained in almost all cases when reactions were performed in water but also in DMSO (Table 1). 2-Octynoic acid and phenylpropionic acids are excellent reagent for decarboxylative coupling. Only in one case when 2-butyne-1-carboxylic acid was used, product was obtained in 23 % yield (water as solvent) (Table 1, Entry 6). This research show many advantages of decarboxylative coupling: reactions performed in water without co-solvent, excellent comparable yields of reactions, copper catalyst system without palladium complexes. According to this research and another publications, this synthetic route is promising alternative to terminal alkynes in synthesis of 4-(alkyl-1-yn-1-yl)-phenyl-4-yl units [15]. This approach will be also considered in our work in the future.

Deprotonation – alkylation

Terminal alkynes are weak acids (pK_a=25). The use of a conjugated base lead to formation of alkynide ion. Later use of this ion as a nucleophile in nucleophilic substitution (S_N2) reaction with primary alkyl halide lead to displace a halide ion from the primary alkyl halide (Fig. 7.) [16-18].

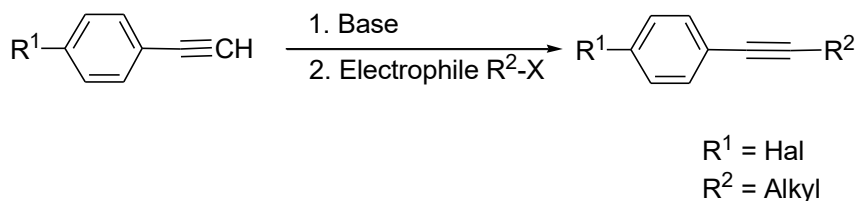


Fig. 7. General scheme of deprotonation-alkylation reaction of terminal alkyne.

RESULTS AND DISCUSSION

Bromobenzenes with alkynyl chain C5 and C6

For longer chained systems (above 4 atoms of carbon in aliphatic chain) we have used Sonogashira cross-coupling of terminal acetylenes with aryl halide (Fig. 8.) [19]. Up to this time we were able to obtain 4-(hex-1-yn-1-yl)-bromobenzene with good yield 81% and 4-(hex-1-yn-1-yl)-bromobenzene with yield 94%.

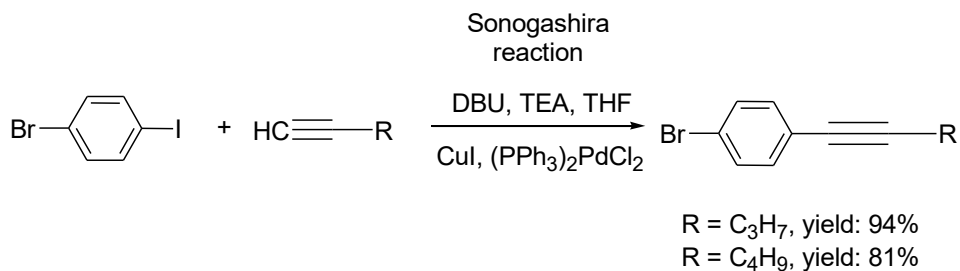


Fig. 8. Sonogashira cross-coupling reaction of terminal acetylenes with aryl halide.

Bromo/chlorobenzenes with alkynyl chain C2

1-bromo/chloro-4-ethynylbenzene was obtained with two-step synthesis (Fig. 9.).

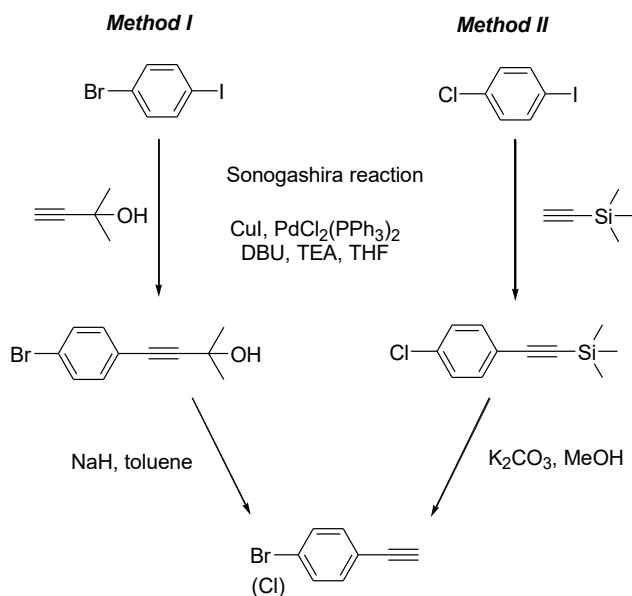


Fig. 9. Synthetic pathways of 1-bromo/chloro-4-ethynylbenzenes.

According to Method I the reaction of 1-bromo-4-iodobenzene with 2-methyl-3-butyl-2-ol leads to the formation of protected phenylacetylene derivative. Next synthetic step, that is the hydrolysis of intermediate product by catalytic amount of sodium hydride in toluene as a solvent. Method II (consist of two steps first) is Sonogashira cross – coupling of 1-chloro-4-iodobenzene with ethynyltrimethylsilane and second step is deprotection of trimethylsilyl group of an alkyne in presence of potassium carbonate and methanol as a solvent [20].

Bromo/chlorobenzenes with alkynyl chain C3 and C4

As a starting material in synthesis of bromo/chlorobenzenes with alkyl chain C3 and C4 we used 1-bromo/chloro-4-ethynylbenzenes (Fig. 10.).

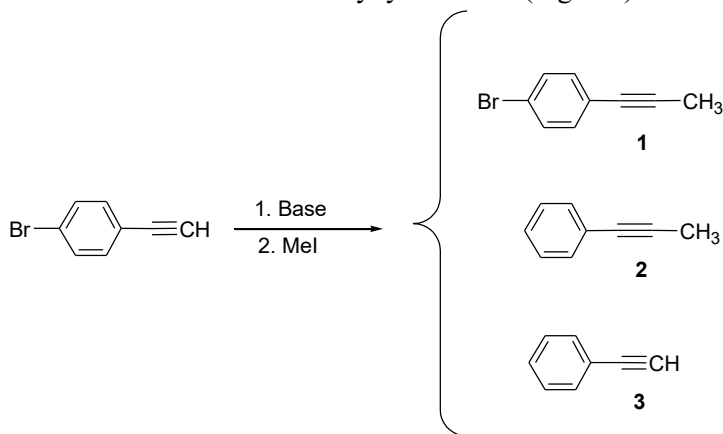


Fig. 10. Deprotonation – alkylation of 1-bromo-4-ethynylbenzenes.

Initially, our research involved four types of bases such as: lithium diisopropylamide (LDA), n-buthyllithium, sodium hydride and isopropylmagnesium bromide. Methyl iodide and ethyl bromide were used as alkyl halides. Results are presented in the Table 2 below. The best result were obtained when lithium diisopropylamide was used. For the yield improvement two equivalent of base was used (yield increased from 48% to 72 %). In the case, when n-BuLi was used, as a result of reaction we observed not only desired product 4-(1-prop-1-yn-1-yl)bromobenzene, but also terminal acetylene and debrominated product. It shows that this organolithium base is too strong for deprotonation of $-C\equiv CH$ group, the bromine/lithium exchange start to occur.

methods: a) Sonogashira cross-coupling reaction between aryl or vinyl halides or triflates and a terminal acetylenes b) decarboxylative coupling of $sp - sp^2$ carbons of aryl halides with alkynyl carboxylic acids c) in catalytic cross-metathesis reaction of an alkyne with a nitrile (only as a by-product) d) in deprotonation-alkylation reaction of terminal alkynes. For longer chained systems, above 4 atoms of carbon in aliphatic chain, Sonogashira coupling is good method to synthesis of 4-(alkyl-1-yn-1-yl)-bromo/chlorobenzenes. For shorter homologues of 4-(alkyl-1-yn-1-yl)-bromo/chlorobenzenes deprotonation – alkylation reaction is promising. In deprotonation – alkylation reaction of 1-bromo/chloro-4-ethynylbenzenes four bases were used. The best results were obtained when chloroderivative was used as a substrate. N-Buthyllithium is too strong base for deprotonation of $-C\equiv CH$ in vicinity of bromoaryl group of 1-bromo-4-ethynylbenzene but for 1-chloro-4-ethynylbenzene this base gives excellent results. Obtained intermediates are convenient semi-product in synthesis of rod-like Liquid Crystals.

REFERENCES

- [1] Kula P., Dziaduszek J., Herman J., Dąbrowski R., Highly birefringent Liquid Crystals and mixtures, SID Symposium Digest of Technical Papers, 2014, 45, 100-103, DOI: 10.1002/j.2168-0159.2014.tb00028.x
- [2] Pauluth D., Tarumi K., Advanced liquid crystals for Television, Journal of Materials Chemistry, 2004, 14, 1219-1227, DOI:10.1039/B400135B
- [3] Węglowska D, Kula P., Herman J., High birefringence bistolane liquid crystals: synthesis and properties, Royal Society of Chemistry, 2016, 6, 403-408, DOI: 10.1039/c5ra15291g
- [4] Dąbrowski R., Kula P., Herman J., High birefringence Liquid Crystals, Crystals, 2013, 3, 443-482, DOI:10.3390/cryst3030443
- [5] Sonogashira K., Tohada Y., Hagihara N., A Convenient Synthesis of Acetylenes: Catalytic Substitutions of Acetylenic Hydrogen with Bromoalkenes, Iodoarenes, and Bromopyridines, Tetrahedron Letters, 1975, 50, 4467-4470
- [6] Bakherad M., Recent progress and current applications of Sonogashira coupling reaction in water, Applied Organometallic Chemistry, 2013, 27, 125-140, DOI:10.1002/aoc.2931
- [7] Yin L., Libscher J., Carbon – Carbon Coupling Reactions Catalyzed by Heterogenous Palladium Catalysts, Chemical Reviews, 2007, 107, 133-173, DOI:10.1021/cr0505674
- [8] Sonogashira K., Development of Pd – Cu catalyzed cross- coupling of terminal acetylenes with sp^2 –carbon halides, Journal of Organometallic Chemistry, 2002, 653, 46-49, DOI: 10.1016/S0022-328X(02)01158-0
- [9] Chinchilla R., Nájera C., Recent advances in Sonogashira reaction, Chemical Society Reviews, 2011, 40, 5084-5121, DOI:10.1039/C1CS15071E

- [10] Koralovič A., Schnürch M., Mihovilovic M., Tandem Catalysis: From Alkynoic Acids and Aryl Iodides to 1,2,3-Triazoles One Pot, *The Journal of Organic Chemistry*, 2011, 76, 2613-2618, DOI:10.1021/jo1024927
- [11] Geyer A. M., Gdula R. L., Wiedner E. S., Johnson M. J. A., Catalytic Nitrile-Alkyne Cross Metathesis, *Journal of the American Chemical Society*, 2007, 129, 3800-3801, DOI:10.1021/ja0693439
- [12] Moon J., Jeong M., Nam H., Ju J., Moon J. H., Jung H. M., Lee J., One-Pot Synthesis of Diarylalkynes Using Palladium –Catalyzed Sonogashira Reaction and Decarboxylative Coupling of sp Carbon and sp² Carbon, *Organic Letters*, 2008, 10, 5, 945-948, DOI:10.1021/ol703130y
- [13] Li T., Sun P., Hailong Y., Zhu Y., Yan H., Lu L., Mao J., Copper Catalyzed decarboxylative Coupling of aryl halides with alkynyl carboxylic acids performed in water, *Tetrahedron*, 2012, 68, 6413-6419. DOI 10.1016/j.tet.2012.06.003
- [14] Moon J., Jang M., Lee S., Palladium Catalyzed Decarboxylative Coupling of Alkynyl Carboxylic Acids and Aryl Halides, *The Journal of Organic Chemistry*, 2009, 74, 1403-1406, DOI:10.1021/jo802290r
- [15] Park K., Lee S., Transition metal-catalyzed decarboxylative coupling reactions of alkynyl carboxylic acids, *RSC Advances*, 2013, 3, 14165-14182, DOI:10.1039/C3RA41442F
- [16] Clayden J., Greeves N., Warren S., Wothers P., *Organic Chemistry*, OUP Oxford, 2001
- [17] Fujihara T., Tani Y., Semba K., Terao J., Tsuji Y., Copper – Catalyzed Silacarboxylation of Internal Alkynes by Employing Carbon Dioxide and Silylboranes, *Angewandte Chemie International Edition*, 2012, 51, 11487-11490, DOI 10.1002/anie.201207148
- [18] Weiss H. M., Touchette K. M., Angell S., Khan J., The concerted addition of HBr to aryl alkynes; orthogonal pi bond selectivity, *Organic & Biomolecular Chemistry*, 2003, 1, 2152-2156, DOI: 10.1039/B300045A
- [19] Shimada T., Bajrachatya G. B., Yamamoto Y., Aqua palladium Complex: A Stable and Convenient Catalyst for the Intermolecular Hydroamination of Alkynes, *European Journal of Organic Chemistry*, 2005, 1, 59-62, DOI:10.1002/ejoc.200400568
- [20] Wang Y., Huang B., Sheng S., Cai M., A novel and efficient synthesis of terminal arylacetylenes via Sonogashira coupling reactions catalysed by MCM-41-supported bidentate phosphine palladium(0) complex, *Journal of Chemical Research*, 2007, 12, 728-732, DOI 10.3184/030823407X275928

Cracking of precipitation hardened alloys induced by Nd-YAG laser beam

*Łukasz Rakoczy¹, Anna Zielińska-Lipiec¹, Lechosław Tuz¹, Krzysztof Pańcikiewicz¹, Tomasz Góra^{1,2}

¹AGH University of Science and Technology, Faculty of Metals Engineering and Industrial Computer Science, Department of Physical and Powder Metallurgy, Team of Heat Treatment and Welding, Av. Mickiewicza 30, 30-059 Cracow

²AGH University of Science and Technology, Faculty of Mechanical Engineering and Robotics, Department of Manufacturing Systems, Team of Manufacturing Techniques

e-mail: lrakoczy@agh.edu.pl

Keywords: *Nd-YAG, laser beam, cracking, high strength materials*

ABSTRACT

The paper presents the microstructural investigation of nickel based superalloys after surface modification by Nd-YAG laser beam. Selected materials belong to the group of precipitation strengthened by intermetallic phase γ' . Light microscopy observation of alloys in as received condition showed substantially high microstructural inhomogeneity created upon crystallization of casting. During solidification, the alloying elements segregate heavily between the phases. Dendrite cores were strictly occupied by precipitations of intermetallic γ' phase surrounded by γ -matrix. In interdendritic regions eutectic island γ/γ' and primary carbides were also observed. Volume fraction of undesired eutectic islands is the greatest in the superalloy MAR-M247, which indicates that segregation of alloying elements was the highest in comparison with Rene 77 and Inconel 713C. High content of γ' -formers Al and Ti indicates that superalloys are highly susceptible to hot cracking in heat affected zone (HAZ). Analysis of induced cracking revealed liquation of γ' and primary carbides along grain boundaries that occurred during surface modification which contributed to hot cracking in HAZ.

INTRODUCTION

Certain groups of material have a remarkable ability to maintain mechanical properties at elevated service temperatures. These are the high-temperature materials. Their uses are many and varied, whereas good examples include the elements for gas turbines, rockets and heat exchangers. For these applications, the performance characteristics are limited by the operating conditions which can be tolerated by the materials used. For example, the thrust and fuel economy displayed by the modern aeroengine are strongly dependent upon, and limited by the high-temperature strength of the nickel-based superalloys used for its hottest sections [1-3]. Over the latter part of the twentieth century, a concerted period of alloy and process development enabled the performance of the superalloys to be improved dramatically. Presently, SC (single

crystal) superalloys are being used in increasing quantities in the gas turbine engine; if the very best creep properties are required, then the turbine engineers turn to them, although it should be recognized that the use of castings in the directionally solidified and equiaxed forms is still practiced in many instances. Considering the high manufacturing cost for new components, it is becoming commercially important to develop less expensive processes such as welding/joining or repair and buildup techniques for damaged parts [4-6]. It is well known that superalloys precipitation strengthened by γ' possess low weldability, due to these alloys are susceptible to microfissuring in HAZ during welding. These difficulties are connected with considerable content of γ' -formers such as aluminum and titanium (above 6% wt. Al+Ti). Moreover cracking results from competition between stress generation and material resistance to cracking. Liquation cracking in heat affected zone is caused by thermal welding strain and substantially low ductility of base metal due to melting along grain boundaries. Additionally, cracking is attributed to shrinkage stresses connected with rapid re-precipitation of intermetallic γ' -phase during cooling upon welding. According to [7] constitutional liquation of γ' has the greatest impact on liquation cracking in Inconel 738. Investigation performed in K3 nickel based superalloy revealed in turn that M_5B_3 , eutectic island γ/γ' and MC-type carbides cause liquation cracking along grain boundaries during [8]. This research was initiated to perform a study of the susceptibility to cracking of nickel based superalloys MAR-M247, Rene 77 and Inconel 713C.

MATERIALS AND METHODS

Base metals used in this research were three CC (conventionally cast) superalloys with chemical composition presented in table 1. In order to observe susceptibility to hot cracking the surface of alloys was modified by Nd-YAG laser beam. Process was carried out with the use of ALS 100 laser workstation. Subsequently metallographic samples were prepared. Observations were conducted on the face of unetched specimens and etched in 10% CrO_3 and Kalling reagent. The microstructure was examined and analyzed using Leica light microscope and FEI Nova NanoSEM scanning electron microscope. In table 2 parameters of surface modification are presented.

Tab.1. Chemical composition of investigated nickel based superalloys.

Alloy/Element	Co	Cr	Al	Mo	Ti	Ta	Hf	W	Nb	C	Ni
MAR-M247	9.92	8.4	5.58	0.64	0.92	3.12	1.11	10.19	-	0.13	Bal.
Rene 77	14.55	14.43	4.16	3.98	3.37	-	-	0.05	-	0.06	Bal.
Inconel 713C	0.27	13.31	6.13	4.2	0.89	-	-	-	2.45	0.12	Bal.

Tab.2. Selected parameters of surface modification.

Voltage [V]	Impulse time [ms]	Frequency [Hz]	Diameter of beam [mm]	Power [W]	Energy [J]
222	20	3	0.8	75,6	25,21

RESULTS AND DISCUSSION

In figure 1a-c distribution and morphology of primary carbides is presented. Chemical composition of alloys suggests that in microstructure MC-type carbides are presented. According to [9-10] carbide formers in MAR-M247 are Hf and Ta, in Rene 77 Ti, whereas in Inconel 713C Nb and Ti. The smallest volume fraction of primary carbides is observed in Inconel 713C. Generally, carbides precipitate directly from liquid during solidification process and take a form from blocky shape to chinese script. Formation of carbides along the grain boundaries aims to enhance mechanical properties, namely creep resistance at elevated service temperature. In figure 1d-f dendrite core fulfilled by γ' cubic particles and interdendritic regions are clearly visible. During solidification segregation of chemical elements took place and so in interdendritic regions carbides and eutectic γ/γ' are presented.

In figure 2 the microstructure of superalloys near fusion line is presented. Crystallization crack in fusion zone propagated along grain boundaries is observed in MAR-247 (Fig. 2a). Above mentioned area is characterized by cellular and cellular-dendritic structure with small undissolved primary carbides. Near arms of chinese script carbide in HAZ eutectic reaction occurred which is visible as re-solidified film. Microstructure of Rene 77 and Inconel 713C alloys near fusion line is shown in Fig. 2b and 2c respectively. The fragments of the fusion zone revealed cellular structure and thin layer of planar growth. The heating rate and cooling was high and so primary carbides do not dissolved similarly like in MAR-M247.

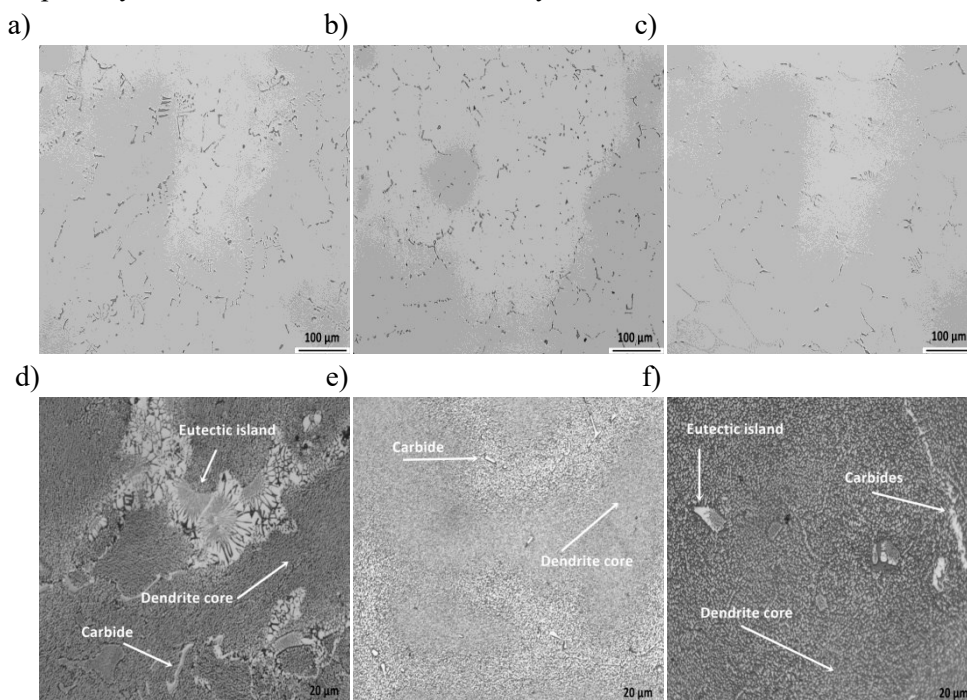


Fig.1. Base metal in as received condition: a), d) MAR-M247; b), e) Rene 77; c), f) Inconel 713C. LM.

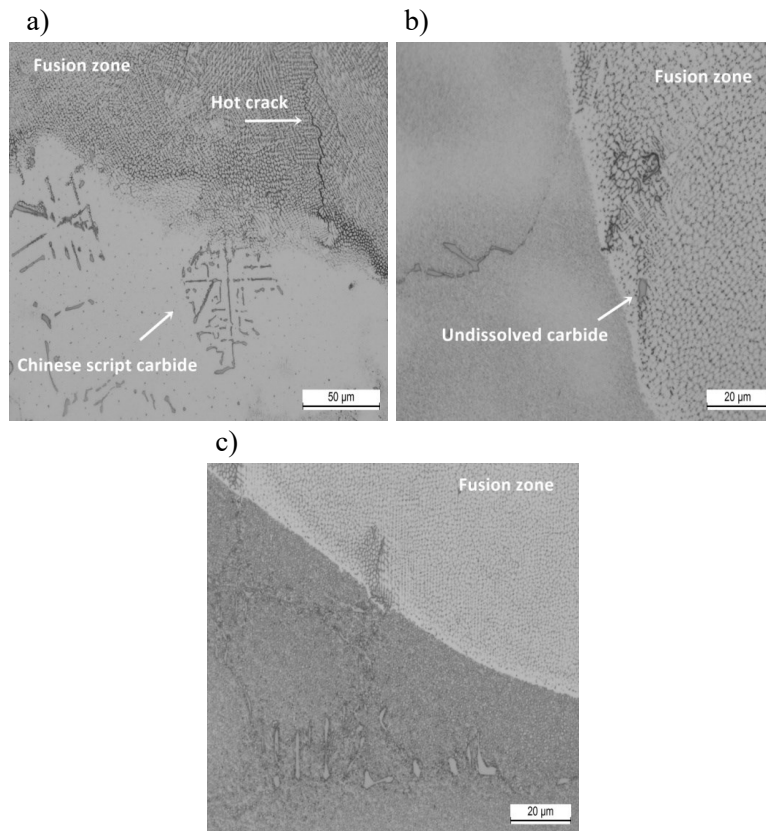


Fig. 2. Heat affected zone microstructure: a) MAR-M247; b) Rene 77; c) Inconel 713C. LM.

In fig. 3 the presence of hot cracks in fusion zone and HAZ can be observed. They ran along the grain boundaries and characterized by different length. In superalloys MAR-M247 and Rene 77 carbides along cracks edge are observed, thereby indicating that the primary carbides have been also partially dissolved. In the first alloy brittle fracture of the secondary carbides are also observed. In the alloy Inconel 713C crack was probably initiated in the fusion zone and then developed via fusion line to the HAZ. In heat affected zone cracking propagated due to weakening of the grain boundaries by non-equilibrium liquid film. The necessary condition to cracking in SWC is presence of liquid film along grain boundaries upon cooling during welding. In nickel-based superalloys liquid in HAZ is created via constitutional liquation phenomena of intermetallic phase γ' . This phenomena was firstly proposed by Pepe and Savage in 18Ni maraging steel and then observed by other investigators in nickel based superalloys. It has been attributed to liquation of second phases in alloy (below solidus temperature), due to a eutectic reaction between second phase particle and the matrix. As a result nonequilibrium film (enriched in Al and Ti) along grain boundaries is produced. Constitutional liquation of second phase takes place during rapid heating of the base metal up to eutectic temperature or higher. During cooling from welding temperatures rapid re-precipitation of γ' particles occur which induces relatively large shrinkage.

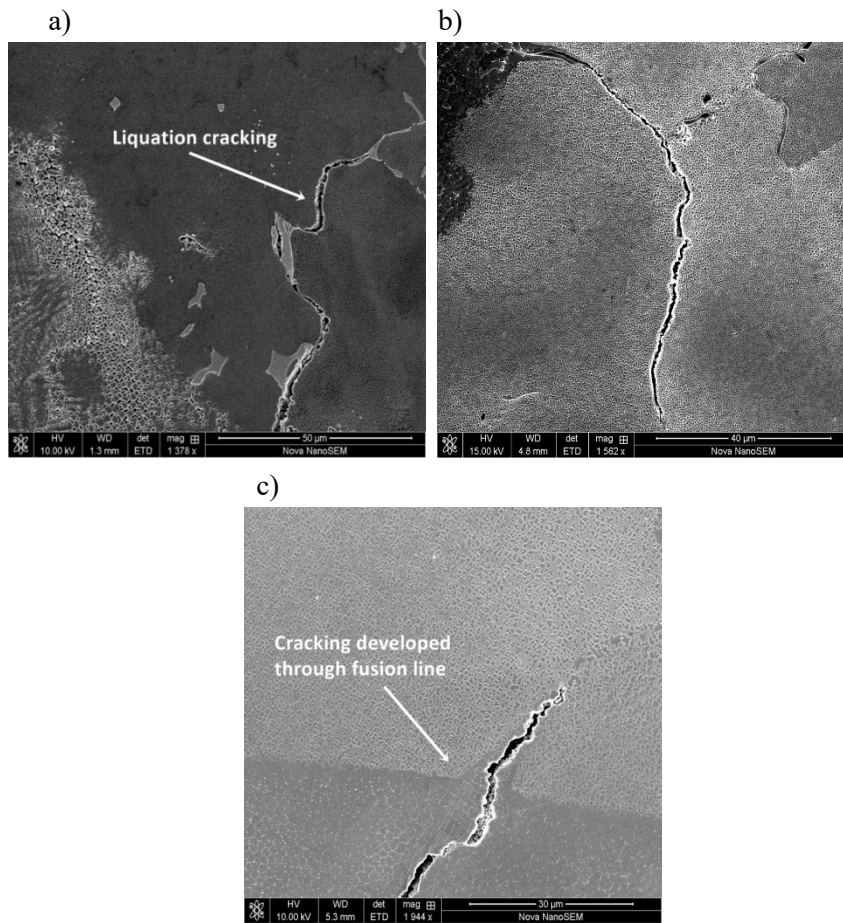


Fig. 3. Heat affected zone liquation cracking: a) MAR-M247; b) Rene 77; c) Inconel 713C. SEM.

CONCLUSIONS

The microstructure of nickel based superalloys MAR-M247, Rene 77 and Inconel 713C modified by Nd-YAG laser beam were investigated using light and scanning electron microscopy. The materials in as received condition were characterized by considerable microstructural inhomogeneities originating from the segregation of alloying elements during the casting solidification. Presence of hot cracks in gas turbine elements is definitely not acceptable as the crack may grow during long term service. Understanding of liquation phenomena and cracking morphology in HAZ could provide insight on how to improve reliability of components. Microstructural investigation allow to state that cracks in superalloys MAR-M247 and Rene 77 were initiated by the constitutional liquation phenomena of γ' phase and primary carbides. Whereas in Inconel 713C crystallization crack developed from fusion zone via fusion line and propagate along weakened grain boundaries in HAZ.

ACKNOWLEDGEMENTS

This research work was supported by the Polish Ministry of Science and Higher Education, Grant No. 11.11.110.299.

Conflicts of Interest

The authors declare no conflict of interest.

REFERENCES

- [1] Reed R., The superalloys: fundamentals and applications, *Cambridge University Press*, Cambridge, 2006
- [2] Dupond J., Lippold J., Kiser S., Welding metallurgy and weldability of nickel-base alloys, *John Wiley&Sons*, 2009
- [3] Tuz L., Pańcikiewicz K., Rakoczy Ł., Żurek Z., Evaluation of the microstructure of 600 and 617 nickel alloys subjected to arc welding, *Biuletyn Instytutu Spawalnictwa*, 2016, 6, 45-47 [in polish]
- [4] Rakoczy Ł., Zielińska-Lipiec A., Tuz L., Microstructure and properties of repair welds with the use of Hastelloy X alloy in the delivery condition and after long term service, *Przegląd Spawalnictwa*, 2016, 4, 54-56 [in polish]
- [5] Ojo O., Ding R., Chaturvedi M., Laser beam weld microstructures in directionally solidified alloy IC6, *Intermetallics*, 2008, 16, 188-197
- [6] Dannis Y., Arvieu C., Lacoste E., Larrouy T., Quenisset J.M., An investigation on thermal metallurgical and mechanical states in weld cracking of Inconel 738LC superalloy, *Materials and Design*, 2010, 31, 402-416
- [7] Montazeri M., Ghaini F.M., The liquation cracking behavior of IN738LC superalloy during low power Nd:YAG pulsed laser welding, *Materials Characterization*, 2012, 67, 65-73
- [8] Li Q., Lin X., Wang X., Yang H., Song M., Huang W., Research on the grain boundary liquation mechanism in heat affected zones of laser forming repaired K465 nickel-based superalloy, *Metals*, 2016, 6(3), 64
- [9] Editor J.R. Davis, ASM Specialty Handbook: Heat resistant materials, *ASM International*, 1997
- [10] Szczotok A., Szala J., Cwajna J., Hetmańczyk M., Selection of etching methods of primary carbides in MAR-M247 nickel-base superalloy for computer-aided quantitative metallography, *Materials Characterization*, 2006, 56, 348-354
- [11]. González M.A, Martínez D.I., Pérez A., Guajardo H., Garza A., Microstructural response to heat affected zone cracking of prewelding heat-treated Inconel 939 superalloy, *Materials Characterization*, 2011, 62, 1116-1123
- [12] Montazeri M., Malek Ghaini F., Ojo O., Heat input and the liquation cracking of laser welded IN839LC superalloy, *Welding Journal*, 2013, 92, 258-264

Stability of water silica suspension with polymer addition

*Diana Rymuszka¹, Salvador Perez Huertas¹, Konrad Terpiłowski¹, Marta Tomczyńska-Mleko²

¹Department of Physical Chemistry, Interfacial Phenomena, Faculty of Chemistry, Maria Curie-Skłodowska University, Lublin, POLAND

²Institute of Plant Genetics, Breeding and Biotechnology, University of Life Sciences, Lublin, POLAND

email: d_rymuszka@vp.pl

Keywords: *polyvinylpyrrolidone (PVP), silica, stability*

ABSTRACT

The effect of adsorption of polyvinylpyrrolidone (PVP) (with weight 55 kDa) on suspension stability was studied. The studies were carried out in different range of silica concentration (2.3%, 3.1% and 3.4%) and in the absence and presence of PVP. For stability determination of investigated systems, turbidimetry method was applied. The obtained results indicate that suspensions without polymer were characterized by the smallest stability, whereas the systems with addition of PVP and the same dilution were successively stable and had big influence on the silica stability.

INTRODUCTION

Studies on the stability of colloidal systems in the presence of polymers play a crucial role for both, theoretical and practical reasons. Polymers are characterized by stabilization-flocculation properties in colloidal systems [1-8] and therefore they are widely used in many industrial branches including chemical, pharmaceutical, food, automotive technology and electrical engineering. Such big demand for efficient stabilizers and flocculants of colloidal suspensions in industry and agriculture makes studies on the stability mechanism in the presence of macromolecular compound very relevant. Thus, it can be concluded that polymers, according to their valuable properties, offer very useful and important applications in industry.

Silica is a very good material, which because of its valuable properties like high purity, well-defined surface area, low chemical reactivity or durability enhancement of products is widely used in pharmaceutical, paint and cosmetic industry. It is also good dispersant which can be used in pigments instead of surfactants [9].

Polymer chains can modify the surface properties of colloidal particles leading to their steric stabilization or destabilization by bridging flocculation or charge neutralization. Stability of highly dispersed systems depends on not only the amount of adsorbed polymer, but mainly on the conformation of both, adsorbed on the solid surface and nonadsorbed in the bulk solution macromolecules. Among many factors influencing on polymer chains conformation, the most important is the type of polymer functional groups.

EXPERIMENTAL

Materials

The samples of silica ($M=60.08$ g/mol, $d=2.6$ g/cm³, $S_{BET}= 294.6\pm 8.7$ m²/g, adsorption average pore size by BET is 101.3Å) obtained by Chuiko Institute of Surface Chemistry, National Academy of Science of Ukraine, Kiev, Ukraine were used in the experiments as an adsorbent. The polyvinylpyrrolidone (PVP) (Sigma Aldrich, $M_w=55.00$ kDa) was used in the studies as an adsorbate. All measurements were carried out in the 37°C and pH=4.5-5.

Preparation of the suspensions

The base polymer solution was prepared by dissolving 1 g of polymer into 99 g of distilled water. For this purpose the PVP solution was placed in magnetic shaker (Magnetic Stirrer type MMG, Polamed) for about 20 min. The basic suspension of silica in water was prepared adding 1.5 g of SiO₂ to 35 cm³ of distilled water. In this case the solid content was 4.1%. Later this system was placed into ultrasounds for 5 minutes. Basic suspension was used for preparation of three system characterized by solid contents: 2.3; 3.1 and 3.4% (by dilution with water).

To obtain suspension with polymer with following solid contents: 2.3; 3.1 and 3.4% (the same as for system without PVP), 30, 13 and 8 cm³ of starting polymer solution was mixed with 35 cm³ of basic silica dispersion. Finally, all suspensions with polymer were diluted by adding 2 cm³ of distilled water. All symbols of examined systems used in manuscript are placed in Table 1. The pH of the samples with and without PVP were measured using pH meter (Seven Multi, Mettler Toledo). The average pH of the samples in the absence of PVP was 4.5, whereas that of the samples in the presence of polymer was 5.

Tab. 1. Characteristics of examined silica suspension without and with addition of polyvinylpyrrolidone (PVP).

Sample symbol	Silica content in suspension [%]	Polymer amount added to the solution [cm ³]	Suspension dillution with water
SiO ₂ _2.3	2.3	-	-
SiO ₂ _2.3/PVP	2.3	30	-
SiO ₂ _2.3/PVP/diluted	2.3	30	+
SiO ₂ _3.1	3.1	-	-
SiO ₂ _3.1/PVP	3.1	13	-
SiO ₂ _3.1/PVP/diluted	3.1	13	+
SiO ₂ _3.4	3.4	-	-
SiO ₂ _3.4/PVP	3.4	8	-
SiO ₂ _3.4/PVP/diluted	3.4	8	+

Principles of measurements

The stability measurements of the silica suspensions with and without PVP were carried out using a *Turbiscan Lab^{Expert}* with a *TLABCooler cooling module*. The apparatus possesses an electroluminescence diode which emits collimated light beam ($\lambda=880$ nm) passing through the suspension. The apparatus has two synchronized detectors. A transmission detector records light passing through a probe under angle of 0° in relation to the incident light direction. The second one is a backscattering detector registers the light scattered under angle of 135° . The obtained data are stored and converted by a computer program. The results are presented in the form of curves, which show the intensities of transmission (TS) and scattering as a function of time.

The samples were put in a flat-bottom cylindrical glass measurement cells (turbiscan bottles) and scanned from the bottom to the top. The optical properties of the dispersion along the height of the samples placed in the cell were investigated. 20 cm³ of examined suspension was introduced into turbiscan bottle (7 cm long) and then placed in the thermostated measurement chamber. The stability measurements were performed at 37°C. The changes in the suspension stability were monitored for 15 hours (single scans were collected every 15 minutes). Schematic presentation of light transmission through stable and unstable suspension is presented in Figure 2.

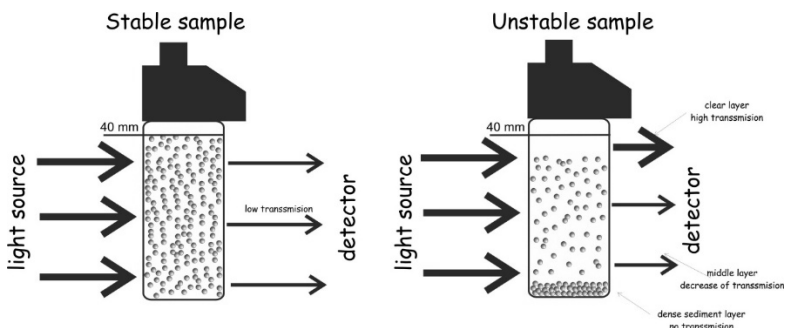


Fig. 2. Schematic representation of measuring bottle containing suspension.

Stability estimations

The samples stability can be estimated and compared using the Turbiscan Stability Index (TSI). This parameter takes into account all single measurements during experiments and the TSI value is obtained from their average. All processes taking place in the sample, including sedimentation and clear layer formation as well as particle settling, were summed up. TSI index was calculated with the special computer program, Turbiscan Easy Soft with the following formula:

$$TSI = \sqrt{\frac{\sum_{i=1}^n (x_i - x_{BS})^2}{n - 1}} \quad (1)$$

where: x_i – average backscattering for each minute of measurement, x_{BS} – average x_1 , n – number of scans (repetitions of single measurement during total time of the experiment).

The TSI values change in the range from 0 to 1. The higher the TSI value is, the more unstable system is. TSI is equal 1 for the suspension with very low stability.

Measurements of the aggregate size

The aggregate size of the examined suspension with and without polymer was measured with *Zetasizer 3000 (Malvern Instruments)*, using the microelectrophoresis method. Each result was taken from three independent measurements. Moreover, each independent measurement was consisted of five measurements of the same sample. The measurement error did not exceed 2%. The Zetasizer range provides both exceptionally high performance and entry level systems that incorporate combinations of a particle size analyzer, zeta potential analyzer, molecular weight analyzer, protein mobility and microrheology measurements.

To measure the size of the particles, samples were placed in the chamber of Zetasizer 3000 and lighted by the laser which was used as the source of light. Then, the intensity of scattering light by particles was measured and obtained data were sent to the computer which was calculating particles size. Zetasizer System is determining size of the particles measuring the speed of Brown movement of the particles using DLC technique (Dynamic Laser Scattering) and then recalculates it for the size of particles. Obtained from the measurements function of correlation is used for calculations of the particles size. Next, Zetasizer Software is using algorithms and particles size is determined.

RESULTS AND DISCUSSION

The explanation of stabilization-destabilization properties of investigated suspensions requires defining conformation of polymer chains in the bulk and adsorbed on the solid surface.

Fig. 3, 4 and 5 present the turbiscan profiles of PVP on the SiO₂ surface obtained at three examined solid concentrations 2.3; 3.1 and 3.4%. The relative position of transmission curves in different time cycles of the experimental indicate dynamic of processes occurring in the investigated systems. The level of suspension in measurement bottle is along the x axis and transmitted light intensities are along the y axis. The value of 40 mm on the x axis observed in figures is the mark to which the investigated suspension was poured in measuring bottle.

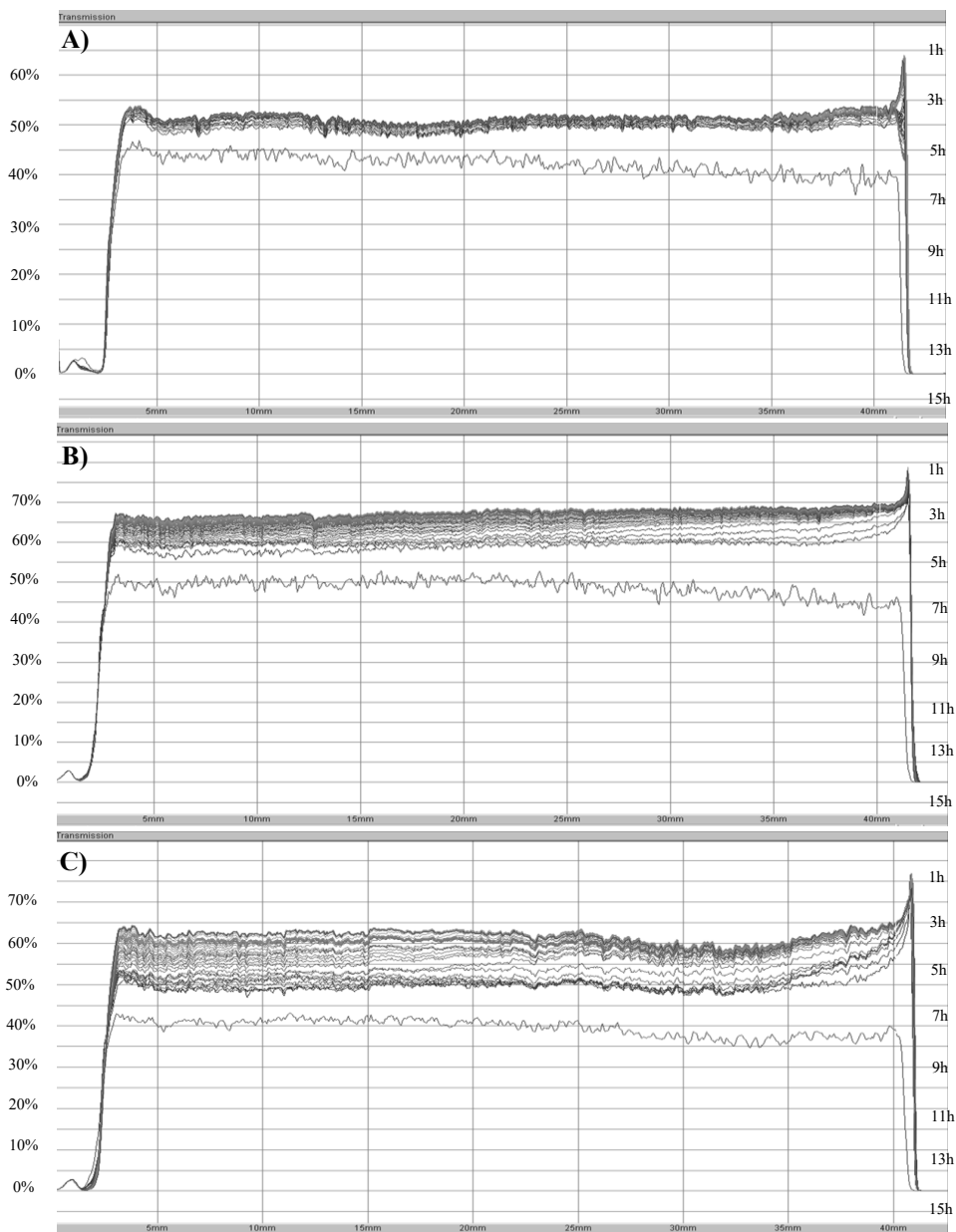


Fig. 3. Transmission curves for silica suspensions without PVP:
A) SiO₂_2.3; **B)** SiO₂_3.1; **C)** SiO₂_3.4.

Tab. 2 presents changes of the stability parameters (TSI) on the top, bottom and global of sample characterizing the systems under investigation.

Tab. 2. TSI values of silica suspensions in the absence and presence of PVP.

Sample	TSI _{global}	TSI _{top}	TSI _{bottom}
SiO ₂ _2.3	9.9	15.9	7.4
SiO ₂ _2.3/PVP	8.3	22.9	5.4
SiO ₂ _2.3/PVP/diluted	5.0	5.0	5.5
SiO ₂ _3.1	18.7	24.7	15.6
SiO ₂ _3.1/PVP	1.5	2.2	2.0
SiO ₂ _3.1/PVP/diluted	11.2	22.2	2.9
SiO ₂ _3.4	22.2	26.5	18
SiO ₂ _3.4/PVP	0.7	1.6	0.5
SiO ₂ _3.4/PVP/diluted	2.1	5.2	1.0

Based on the obtained results it can be concluded that decrease of the silica content (samples without addition of polymer) leads to increase of system stability. It is supported by TSI_{global} values which for SiO₂_2.3; SiO₂_3.1 and SiO₂_3.4 amount 9.9; 18.7 and 22.2 (Tab. 2), respectively. Figs. 3A-C show how the distance between the first and the last measurement has similar value if the silica concentration is reduced. The main mechanism occurring in those samples is flocculation which leads to the changes of particle size (Tab. 3).

Tab. 3. Sizes of silica particles in the absence and presence of PVP.

Sample	Effective aggregate size [nm]
SiO ₂ _2.3	196.3
SiO ₂ _2.3/PVP	100.5
SiO ₂ _2.3/PVP/diluted	175.8
SiO ₂ _3.1	285.7
SiO ₂ _3.1/PVP	380.3
SiO ₂ _3.1/PVP/diluted	210.9
SiO ₂ _3.4	280.0
SiO ₂ _3.4/PVP	372.3
SiO ₂ _3.4/PVP/diluted	384.6

Analyzing the lowest concentration, 2.3%, it can be observed that presence of PVP does not improve so largely the stability like in the case of other investigated systems with different concentrations. TSI_{global} for the sample without polymer amounts 9.9, whereas for SiO₂_2.3/PVP and SiO₂_2.3/PVP/diluted is lower and amounts 8.3 and 5.0 (Tab. 2), respectively. In this case the stability of SiO₂_2.3 and SiO₂_2.3/PVP are similar. The highest stability was observed for diluted suspension with addition of polymer which is about two times higher than for the sample SiO₂_2.3. In the Figs. 4A and 5A are presented scans registered by Turbiscan for samples SiO₂_2.3/PVP and SiO₂_2.3/PVP/diluted which show the formation of small

particles (flocculation) (Tab. 3) from 2 mm to 30 mm of the bottle (Fig. 4C). The TS values range from 15 to 50% what is caused by clarification process. For SiO₂_2.3/PVP/diluted (Fig. 5C) the same process occurs but observed in the turbiscan profiles changes are smaller and TS values change from 27 to 34% what is related with smaller sizes of the particles so stability of this suspension is higher than for SiO₂_2.3/PVP. With the time the changes of profiles indicate that suspensions with PVP are destabilized according to clarification process. The TSI value increases in upper part of tube (35-40 mm zone).

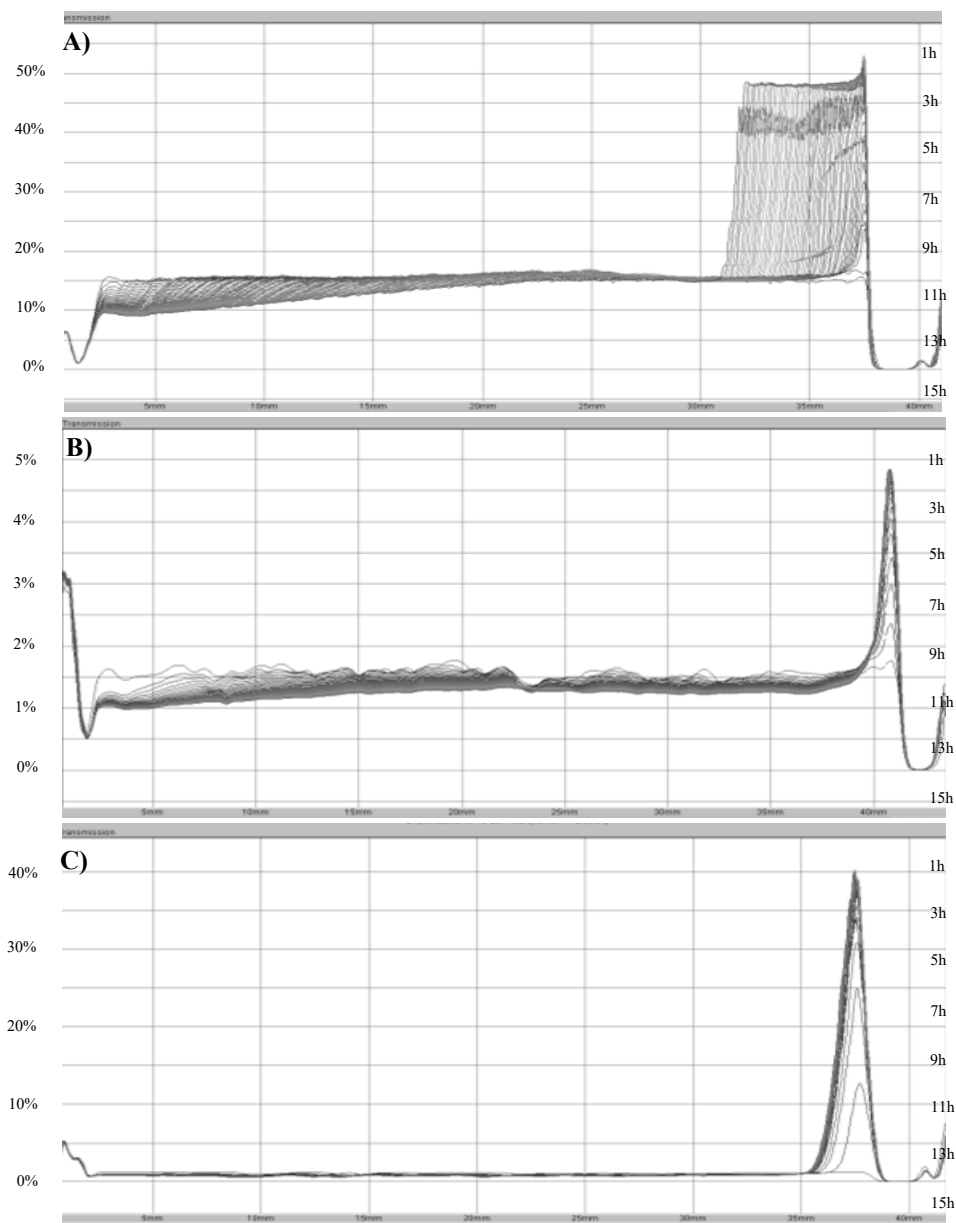


Fig. 4. Transmission curves for silica suspensions with polymer:
 A) SiO₂_2.3/PVP; B) SiO₂_3.1/PVP; C) SiO₂_3.4/PVP.

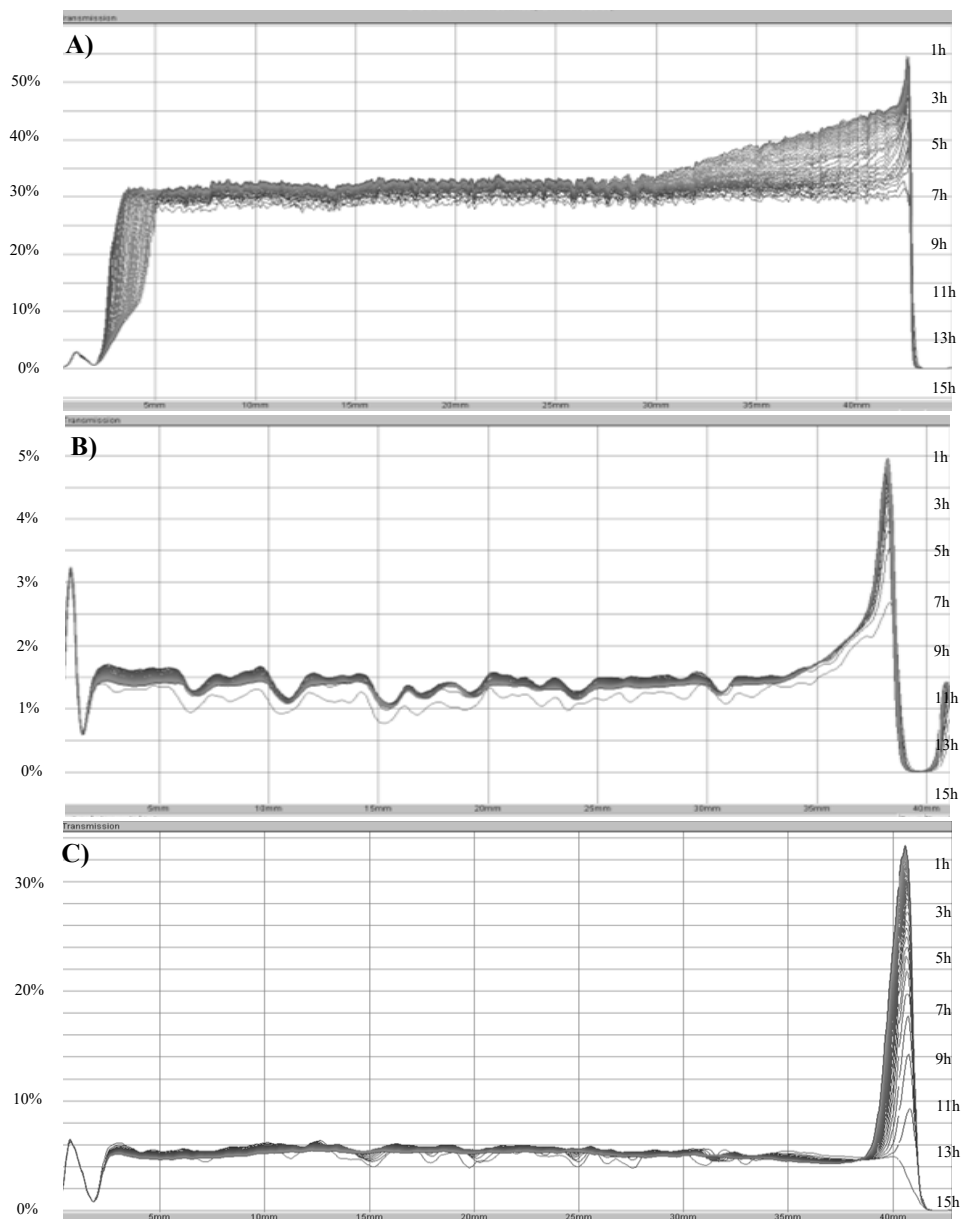


Fig. 5. Transmission curves for silica suspensions with polymer after dilution:
A) SiO₂_2.3/PVP/diluted; **B)** SiO₂_3.1/PVP/diluted; **C)** SiO₂_3.4/PVP/diluted.

The addition of PVP to SiO₂_3.1 improves stability of investigated samples. TSI changes from 18.7 (SiO₂_3.1) to 1.5 and 11.2 for SiO₂_3.1/PVP and SiO₂_3.1/PVP/diluted (Tab. 2), respectively. In Fig. 4B the average TS in the 0-35 mm zone changes only from 1 to 1.75% what indicates that the stability is high but on the top TS values are higher and change from 1.75 to 4.4%. It suggests small clarification on the top. The most stable sample was obtained for system SiO₂_3.1/PVP for which TSI vale amounts 1.5. The same suspension but diluted is

characterized by worse stability ($TSI=11.2$). On the top clarification process occurs and is similar to not diluted sample (Fig. 5B).

Taking into account $SiO_2_{3.4}$ concentration, it can be observed that the highest value of TSI_{global} , 22.2 (Tab. 2), was obtained for the sample without addition of PVP polymer. It shows that stability of this sample is the worst from all studied $SiO_2_{3.4}$ systems. Fig. 3C presents that the first measurement was registered at 40% and the last at 65%. However, completely different situation was noticed for $SiO_2_{3.4}/PVP$ suspension for which TSI_{global} value is the smallest in comparison to suspensions $SiO_2_{3.4}$ and $SiO_2_{3.4}/PVP/diluted$. It confirms that addition of polymer significantly improves stability of dispersion.

Figure 4 reports effect of PVP addition on stability of silica/polymer suspensions. All samples with addition of polymer are more stable than those with only silica content. They are stable in almost every place in the bottle particles flocculation does not appear and TS values are in the range 0.2-0.5%. On the other hand, on the top of the bottle 35 mm clarification process takes place and TS signals reaches 40%. In the case of systems with PVP but diluted it can be observed that their stability is higher than systems with the absence of polymer but worse than not diluted suspensions so addition of distilled water does not improve stability of silica/PVP systems. The TS signals (Fig. 5A) range from 4 to 7% and also at the top clarification appears.

The addition of PVP leads to the highest stability in the case of sample $SiO_2_{3.4}/PVP$ which is correlated with bigger sizes of the aggregates. On the other hand, the smallest aggregates were observed for the samples with the lowest concentration. Higher content of solid in the suspension makes collision of colloidal particles more probable and leads to aggregation.

CONCLUSIONS

The influence of the polyvinylpyrrolidone (PVP) on stabilization-destabilization properties of the silica suspensions was studied. The turbidimetric results as a form of transmission curves, as well as calculated stability parameters indicate that the solid suspension without the polymer is highly unstable at $37^\circ C$ and $pH=5$. The most stable sample was $SiO_2_{3.4}/PVP$ for which the lowest value of TSI_{global} and big size of the aggregates about 372 nm were obtained. On the other hand, dilution of suspensions only in the case of $SiO_2_{3.4}/PVP/dilution$ leads to stability improvement. For samples with higher concentrations the opposite effect is observed. The studies showed that for the lowest concentration 2.3%, the main observed phenomena of destabilization was flocculation with bigger size particles and further clarification. For concentration 3.1%, both, clarification and flocculation processes occurred indicating changes in particle size in the system. On the other hand, for 3.4% the main mechanism of destabilization was clarification observed on the top.

REFERENCES

- [1] Pettersson A., Marino G., Pursiheimo A., Rosenholm J.B., Electrosteric stabilization of Al(2)O(3), ZrO(2), and 3Y-ZrO(2) suspensions: Effect of dissociation and type of polyelectrolyte, *Journal of Colloid and Interface Science*, 2000, 228, 73.
- [2] Mewis J., Vermant J., Rheology of sterically stabilized dispersions and latices, *Progress in Organic Coatings*, 2000, 40, 111.
- [3] Guldborg-Pedersen H., Bergström L., Stabilizing ceramic suspensions using anionic polyelectrolytes: adsorption kinetics and interparticle forces, *Acta Materialia*, 2000, 48, 4563.
- [4] Das K.K., Somasundaran P., A kinetic investigation of the flocculation of alumina with polyacrylic acid, *Journal of Colloid and Interface Science*, 2004, 27, 102-109.
- [5] Kamibayashi M., Ogura H., Otsubo Y., Viscosity behavior of silica suspensions flocculated by associating polymers, *Journal of Colloid and Interface Science*, 2005, 290, 592.
- [6] Runkana V., Somasundaran P., Kapur P.C., A population balance model for flocculation of colloidal suspensions by polymer bridging, *Chemical Engineering Science*, 2006, 61, 182-191.
- [7] Yu J., Wang D., Ge X., Yan M., Yang M., Flocculation of kaolin particles by two typical polyelectrolytes: A comparative study on the kinetics and floc structures, *Colloids and Surfaces A: Physicochemical and Engineering Aspects*, 2006, 290, 288-294.
- [8] Kamibayashi M., Ogura H., Otsubo Y., Shear-thickening flow of nanoparticle suspensions flocculated by polymer bridging, *Journal of Colloid and Interface Science*, 2008, 321, 294-301.
- [9] Wawrzkiwicz M., Wiśniewska M., Gun'ko V.M., Zarko V.I., Adsorptive removal of acid, reactive and direct dyes from aqueous solutions and wastewater using mixed silica-alumina oxide, *Powder Technology*, 2015, 278, 306-315.
- [10] Haaf F., Sanner A., Straub F., Polymers of *N*-vinylpyrrolidone: Synthesis, characterization and uses, *Polymer Journal*, 1985, 17, 143-152.
- [11] Roos A., Creton C., Novicov M.B., Feldstein M.M., Viscoelasticity and tack of poly(vinyl pyrrolidone)-poly(ethylene glycol) blends, *Journal of Polymer Science Part B*, 2002, 40, 2395.
- [12] Majumdar D., Blanton N.T., Schwark W.D., Clay-polymer nanocomposite coatings for imaging application, *Applied Clay Science*, 2003, 23, 265.
- [13] Shively L.M., Droplet size distribution within oil-in-water emulsions prepared from solid state dispersions, *Journal of Colloid and Interface Science*, 1993, 155, 66.
- [14] Hou Y., Kondoh H., Shimojo M., Kogure T., Ohta T., High-yield preparation of uniform cobalt hydroxide and oxide nanoplatelets and their characterization, *Journal of Physical Chemistry B*, 2005, 109, 19094.
- [15] Gao Y., Wang F., Liao S., D.Yu, Sun N., Active catalyst for the hydrodechlorination of perchlorobenzene, *Reactive and Functional Polymers*, 2000, 44, 65.

- [16] Li Y., Boone E., El-Sayed M.A., Size effects of PVP-Pd nanoparticles on the catalytic Suzuki reactions in aqueous solution, *Langmuir*, 2002, 18, 4921.
- [17] Laruelle S., Dewaele G.S., Vidal D.A., Torcheux L., The curing reaction study of the active material in the lead-acid battery, *Journal of Power Sources*, 1999, 77, 83.
- [18] Higa Z.O., Rogero O.S., Machado D.B.L., Mathor B.M., Lugao B.A., Biocompatibility study for PVP wound dressing obtained in different conditions, *Radiation Physics and Chemistry*, 1999, 55, 705.
- [19] Lopes M.A.C., Felisberti I.M., Mechanical behaviour and biocompatibility of poly(1-vinyl-2-pyrrolidinone)-gelatin IPN hydrogels, *Biomaterials* 2003, 24, 1279.
- [20] Devine D.M., Higginbotham C.L., Synthesis and characterisation of chemically crosslinked N-vinylpyrrolidone (NVP) based hydrogels, *European Polymer Journal*, 2005, 41, 1272.

Preparation of methyl ester of L-serine

*Agnieszka Sebai¹, Agnieszka Gadomska-Gajadur¹, Paweł Ruśkowski¹, Małgorzata Konopka¹, Ludwik Synoradzki¹

¹Laboratory of Technological Processes, Faculty of Chemistry, Warsaw University of Technology, Warsaw, POLAND

e-mail: asebai@ch.pw.edu.pl

Keywords: *serine, amino acid ester, DOE*

ABSTRACT

It was decided to prepare the product – a methyl ester of L-serine through esterification reaction using thionyl chloride and then deprotection of amine group of obtained salt. The first reaction was completed with a satisfying yield. The second step was more challenging. Small size of side-product made it incredibly difficult to purify. The best results were obtained using triethylamine. The product has a form of yellow, adhesive wax and is a substrate for further purposes, which is to modify materials for polymeric scaffolds. The deprotection reaction was optimized using design of experiments (DOE).

INTRODUCTION

Amino acids are essential for human life. They are the building blocks for proteins and play an important role in biochemistry. All amino acids are optically active (except for glycine) and naturally occur only as L-stereoisomers. Serine (**1**) is an amino acid containing hydroxyl group in side chain, which, if included, increases the hydrophilicity of materials and bioavailability of drugs. It is also crucial for catalytic properties of numerous enzymes. It is a precursor of other amino acids (like glycine, cysteine, tryptophan) and many other metabolites in bacteria [1]. Esters in general are more reactive in condensation reactions than corresponding carboxylic acids, thus we decided to synthesize methyl ester of serine (**3**). It is also a common method of protection of carboxylic group in amino acids [2]. Amino acids normally occur in form of zwitterions, due to having both acidic side (C-end, carboxylic group) and basic one (N-end, amine group). Protection group destabilizes zwitterion equilibrium and as a result the unprotected end is more reactive.

Serine is an amino acid bearing a free hydroxyl group in the side chain. It makes it a very attractive substrate for further synthesis. One of the potential applications is the synthesis of new functional materials, such as biomaterials for tissue engineering, polydepsipeptides or polypeptides with controlled sequence [3].

MATERIALS AND METHODS

Commercially available solvents and reagents were used without previous purification. DOE calculation were performed with the use of *Microsoft Excel* program. IR spectra were collected on ALPHA spectrometer (Bruker) in FTIR-ATR methodology. ^1H NMR spectra were collected on Varian Mercury-400BB: frequency 400 MHz; TMS standard; CD_3OD , CDCl_3 solvents.

GC-FID analyses were performed on HP 6980 apparatus with nonpolar column HP1, 30 m length, 0.32 mm, stationary phase thickness 0.25 μm ; propellant gas flow (helium) 1 mL/min; temperature of the chamber 250°C; temperature of the oven 100°C with 10°C/min growth.

GC-MS analyses were performed on 6890N chromatograph (Agilent Technology) with nonpolar column HP 1MS, 30 m length, 0.25 mm, stationary phase thickness 0.25 μm ; propellant gas flow (helium) 1 mL/min; temperature of the chamber 250°C; temperature of the oven 100°C with 10°C/min growth; the detector: mass spectrometer MS 5973 Network (Agilent Technology) with quadrupole mass analyst.

RESULTS

Methyl ester of L-serine (**3**) was prepared in two-step method (Fig. 8). The first step was esterification of L-serine (**1**) that yielded hydrochloride salt (**2**) using reaction with thionyl chloride in methanol. It is well known method of obtaining methyl esters. The second step was deprotection of amine group. Three main methods of amine group deprotection were found in literature. Those methods utilized sodium bicarbonate, zinc powder or triethylamine. All of the abovementioned methods, modified by authors, were employed in order to determine the most efficient one.

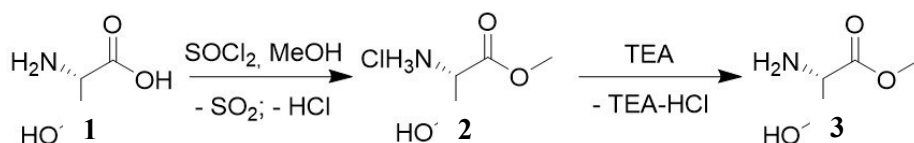


Fig. 8. Preparation of methyl ester of L-serine (**3**).

Synthesis of (L)-serine methyl ester hydrochloride (**2**)

The synthesis was conducted twice. The first time was encouraged by literature [4]. Thionyl chloride was added dropwise into cooled (0°C) methanol and then serine (**1**) was added in one portion. The mixture was refluxed for 12 hours. Product was crystallized from methanol. The IR spectrum did not confirmed the presence of methyl ester hydrochloride of serine (**2**).

Second time thionyl chloride was added dropwise into cooled methanol, but the temperature was controlled and did not exceed 10°C. **1** was added in small portions. After that the flask was spontaneously warmed to room temperature, then the temperature was increased until the mixture clarified (reflux temperature, ca.

65°C). The reaction was stirred at these conditions until all gas by-products (HCl, SO₂) were gone (about 0.5 hour). Obtained product (**2**) was crystallized from methanol. It has a form of white crystals.

The IR spectrum was prepared (Fig. 1). A new band of ester C=O stretching vibrations (1745 cm⁻¹) occurs. At the same time a carboxyl acid C=O (1577 cm⁻¹) was significantly less intense. The spectra proved that the reaction was completed and the product (**2**) was obtained with 71.9% yield.

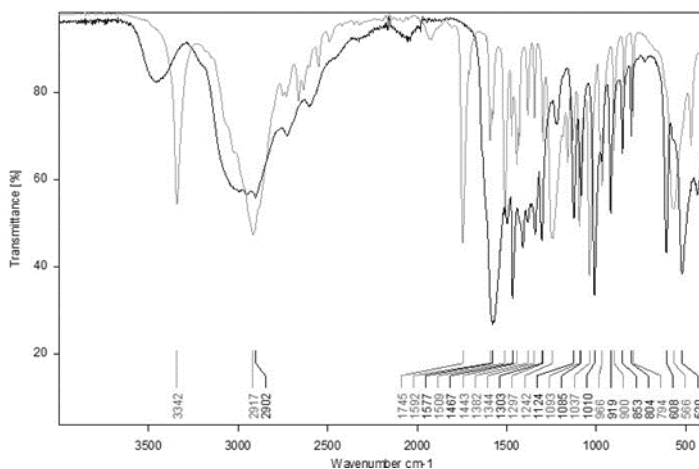


Fig.1 . IR spectra of L-serine (**1**, black) and its methyl ester hydrochloride (**2**, grey).

¹H NMR spectrum was also made (Fig. 2.). The signal at 3.85 ppm, from methyl group of ester proves further that the product was obtained. The broad signal at 4.91 ppm comes from the residual water (there was no need to use dry methanol).

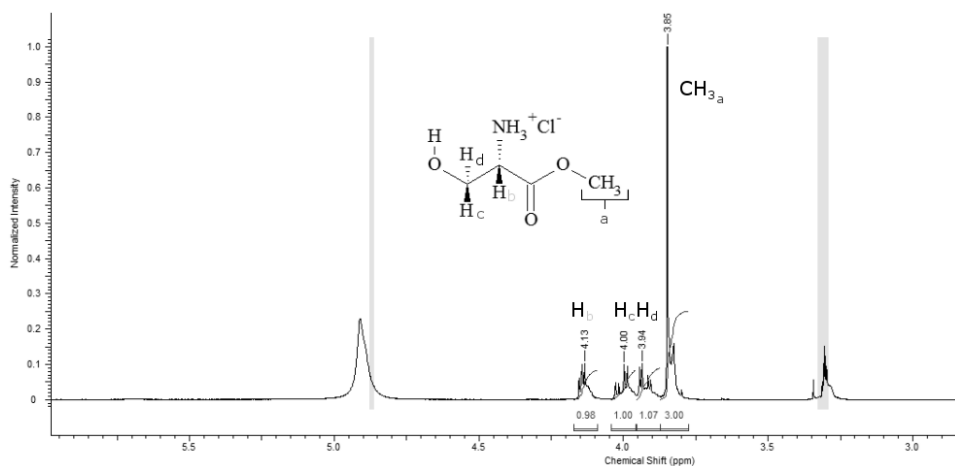


Fig.2. ¹H NMR spectrum of reagent **2**; dark area is the solvent – CD₃OD.

Synthesis of (L)-serine methyl ester (3) with zinc powder

The zinc powder deprotection method has many advantages. Those include mild conditions and short reaction times. The reaction was performed four times at different conditions (Tab. 1).

Tab. 1. The conditions of amine group deprotection using zinc powder.

Attempt	Time [min]	Temperature	Solvent	Purification
I	15	RT	THF	THF, MeOH
II	20	reflux, then RT	THF	THF, MeOH
III	15	RT	CH ₂ Cl ₂	-
IV	30	RT	THF	Et ₂ O, MeOH

The hydrochloride **2** was dispersed in tetrahydrofuran (THF), zinc powder was added and the mixture was stirred vigorously (600 rpm, magnetic stirrer). The substrate dissolved but the mixture was not clear due to the zinc residue and the by-product – zinc chloride. The residue was filtered out on Schott funnel under normal pressure. Then the filtrate was evaporated to half volume and precipitate was filtered out. This step were repeated a few times. As the last step methanol (MeOH) was added and remaining solids were filtered out. However, probably due to small particle size, some solids remained in the filtrate.

We decided to test whether the increase in temperature will solve the problem, but the results were not satisfying, so we changed the solvent according to literature procedure [5]. In this case the product (**3**), which is a yellow, adhesive wax did not dissolve in dichloromethane. Moreover it adhered to zinc chloride and unreacted zinc. As a result, pure product was not obtained.

Another purification method was tested, using precipitation of contaminants with diethyl ether (Et₂O). After filtration zinc chloride did not remain in the filtrate, but the IR spectrum showed that yield of the reaction was low. Anticipated bands from C=O in ester (about 1740 cm⁻¹) and N-H in primary amine (ok. 1650 cm⁻¹), usually strong, were hardly noticeable.

Synthesis of (L)-serine methyl ester (3) with NaHCO_{3(aq)}

Deprotection reaction using sodium bicarbonate was tested in two variants. First variant was motivated by literature [6]. The substrate **2** was dispersed in THF and then the aqueous solution of sodium bicarbonate was added. The mixture was stirred vigorously (600 rpm, magnetic stirrer) for 2 hours. Then the phases were separated with the addition of sodium chloride for better phase separation. Sodium chloride is also a by-product of the reaction. The organic phases were combined and dried using magnesium sulphate. MgSO₄ was filtered out and the filtrate was evaporated. The reaction yield was very low.

The other variant used dry sodium bicarbonate. The reaction conditions were similar, however the solvent was changed to a mixture of methanol and THF. Then

solids were filtered out and the solvent was evaporated. Product was contaminated by sodium chloride and unreacted sodium bicarbonate. Repetitive purification steps were conducted but crystals of sodium chloride still remained in the product.

Synthesis of (L)-serine methyl ester (**3**) with triethylamine

The third method of obtaining product **3** was using triethylamine (TEA). Triethylamine hydrochloride is the main by-product of this reaction.

Ester hydrochloride (**2**) was dispersed in acetonitrile. The mixture was cooled down to 0°C and triethylamine solution in acetonitrile was added dropwise. Then reaction mixture was stirred at RT for 2 hours. Subsequently, reaction mixture was kept at -18°C for two days. White, needle-like crystals of triethylamine hydrochloride were filtered out. The filtrate was evaporated and white crystals were filtered out. The process was repeated a few times but contaminant still occurred.

Another attempt was made, this time with dichloromethane and chloroform, because those solvents dissolve triethylamine hydrochloride but do not dissolve product **3**. Triethylamine was added dropwise to a cooled dispersion of **2** in dichloromethane. Then reaction was refluxed for 1.5 hour ($T=40^{\circ}\text{C}$). Unfortunately even after cooling down the product still did not precipitate. Solvents were evaporated and product was purified by precipitation in methanol. The product was still contaminated but IR spectrum showed that ester **3** was obtained (Fig. 3.). Strong band at 1654 cm^{-1} occurs, that is a band of N-H flexible oscillation in primary amines. It proved that amine group had been deprotected. The 1735 cm^{-1} strong band came from C=O stretching oscillation in ester. Broad band at about 3235 cm^{-1} originates from overlapped stretching oscillations of O-H and N-H bonds.

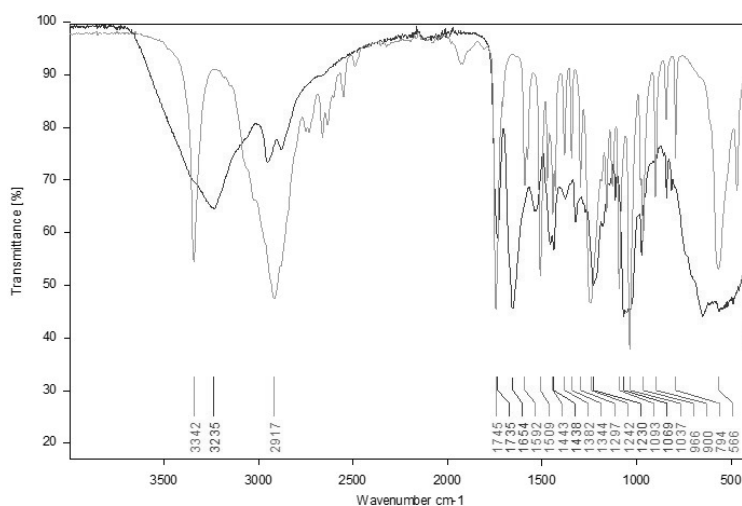
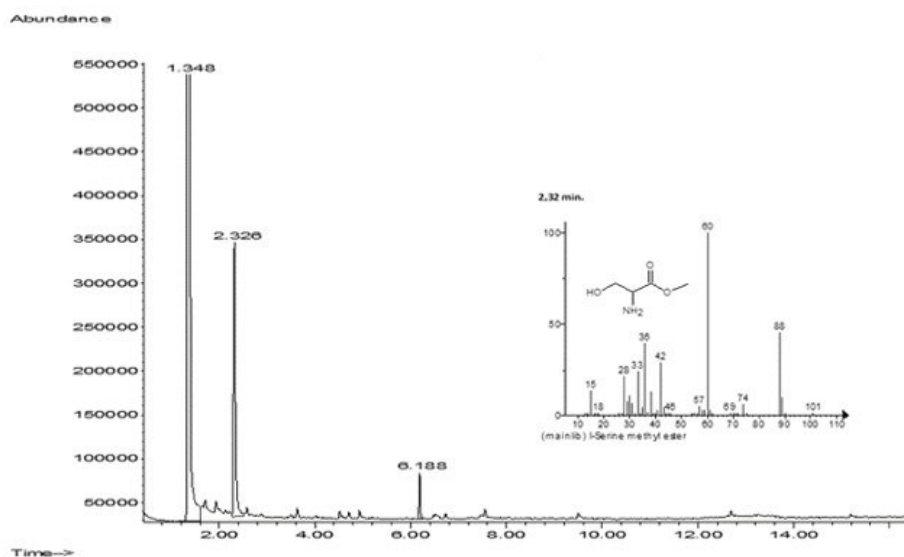


Fig. 3. IR spectra of methyl ester of L-serine (**3**, black) and its hydrochloride (**2**, grey).

To further prove that the product **3** was obtained the gas chromatography analysis was performed (GC). The GC method was coupled with mass spectrometer detector (GC-MS) and flame ionisation detector (GC-FID). The 2.326 min signal was assigned to L-serine methyl ester (Fig. 4.). The first peak was from the solvent – methanol. Rest of the signals might have come from triethylamine hydrochloride or product of reaction of **3** on the chromatography column. The GC-FID analysis shows that the sample contained 69.1% of product **3**.

Fig. 4. GC-MS chromatogram of the product **3** after triethylamine treatment.



^1H NMR analysis was attempted. Unfortunately there was problem with solubility. The best solvent – methanol – when changed to deuterated, no longer dissolved the product. The other available deuterated solvents caused only partial dissolution and obtained spectra were low quality, unsuitable for interpretation.

The isolation of pure product was troublesome and finding the best purification method was time-consuming. That way the main goal of optimisation process became to obtain the purest product, not the highest reaction yield. The triethylamine method allowed to meet that goal.

After successful deprotection in dichloromethane we decided to use chloroform based on the literature procedure [7]. Triethylamine was added dropwise to dispersion of **2** in chloroform at room temperature. Then reaction was refluxed for 5 hours ($T=60^\circ\text{C}$). After standard purification with tetrahydrofuran and methanol the product **3** was obtained, unfortunately with low yield and purity.

The temperature effect on the deprotection in dichloromethane was also tested. The reaction was kept at room temperature at all times (also during TEA addition), however the resulting reaction yield was still low.

The preparatory trials results are collected in Tab. 2. The best results were obtained for dichloromethane as a solvent and for adding triethylamine at 0°C .

Tab. 2. Preparatory trials for serine methyl ester hydrochloride deprotection using triethylamine.

Number of trial	Solvent	TEA added to cooled solution?	Reaction time [h]	Temperature [°C]	Yield (GC-FID) [%]
I	CH ₂ Cl ₂	Yes	2	reflux	69.1
II	CHCl ₃	No	5	reflux	45.7
III	CH ₂ Cl ₂	Yes	3	room	33.8

Optimisation through DOE

The process of deprotection of serine methyl ester hydrochloride using triethylamine was optimized through design of experiments (DOE) [8]. It allows to obtain a mathematical model that gives more information about the impact of the process' conditions. Those conditions were identified and illustrated as so called "black box" (Fig. 5.). The optimization's main criterion was to maximize the conversion.

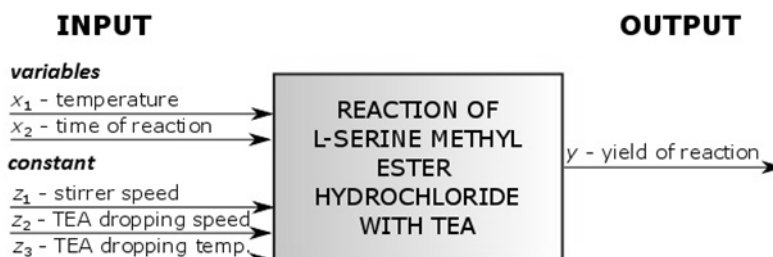


Fig. 5. Structure of the deprotection of methyl ester of serine hydrochloride process – “black box”.

Based on previous attempts for this method the range of the input variables was established (Tab. 3). The natural values of variables were coded into (-1;1) range. Codification allows further comparison of the influence on the output.

Tab. 3. The area of the experiments and codification of the input.

Natural variable		Codification		
		-1	0	+1
z_1	Temperature /°C	26	33	40
z_2	Time /h	1	2	3

The factorial 2² plan with three experiments in the centre was constructed (Tab. 4). Experiments were conducted from the same batch of substrates and in random order. The conversion was determined via GC-FID analysis.

Tab. 4. Factorial 2² plan with interactions and results of experiments, both obtained and calculated.

Signature	Coded variables				Results	
	x ₀	x ₁	x ₂	x ₁ *x ₂	obtained	calculated
					y ₁	ŷ ₁
%						
SEBKA020	1	-1	-1	1	41.5	41.5
SEBKA021	1	-1	1	-1	53.7	53.7
SEBKA022	1	1	-1	-1	36.4	36.4
SEBKA023	1	1	1	1	53.3	53.3
SEBKA024	1	0	0	0	67.7	46.2
SEBKA025	1	0	0	0	45.6	46.2
SEBKA026	1	0	0	0	51.5	46.2

Factorial plan assumes that the analysed process can be described by a linear equation:

$$y_1 = b_0x_0 + b_1x_1 + \dots + b_nx_n \quad (1)$$

If interactions between variables are considered then the equation is expanded with products of pair of variables x_i in all combinations.

Coefficients were calculated using the matrix method. *T*-Student significance test was performed. The value of repetitiveness variation was 87.05 and was calculated from the three experiments in the centre of the plan (in the same conditions). The aberration of the coefficients was 4.67. The t_{crit} for two freedom levels and 95% confidence interval is 4.30. *T* parameters for all coefficients (accept for the b_0 coefficient) were smaller than t_{crit} , thus they are insignificant.

The calculated output values (for equation with all coefficients with interactions) outside of the plan centre were similar to obtained. The equation is as follows:

$$y_1 = 46.24 - 1.38x_1 + 7.29x_2 + 1.17x_1x_2 \quad (2)$$

The adequacy statistical test (the *F* test) was taken. The residue variance is 488.49. The F_{crit} parameter for 2 and 4 freedom levels and 95% confidence interval is 199.50. The parameter for the equation is $F=5.61$, which is smaller than F_{crit} thus the equation is adequate.

The equation (2) shows that the reaction time has the most influence on the output, because the x_2 coefficient module has the biggest value. The longer the reaction time, the better is the result. Decreasing the reaction temperature is also beneficial. The interaction coefficient is positive. This means that the best results are obtained for long processes kept in high temperature or for shorter reaction times and low temperatures simultaneously. The area of response for all variables is shown in Fig. 6.

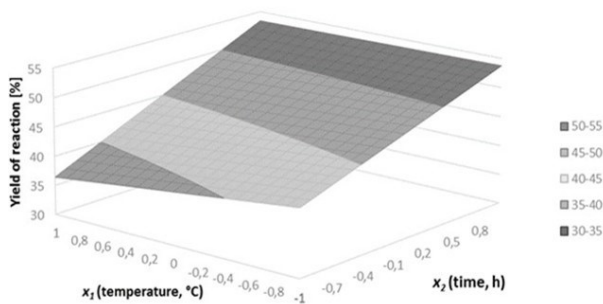


Fig. 6. The influence of time of the reaction (x_1) and the temperature (x_2) of the process on the conversion (y) – the area of response.

The insignificance of coefficients stems from wide divergence in the centre of the plan (about 20%, which determines high standard deviation). Better results should be obtained after repeating the experiment in those conditions few more times to exclude output errors. It is also possible that linear equation is not applicable in this situation. In that case the factorial plan should be stretched to rotatable plan. Then a few more experiments, so called star points, are required.

CONCLUSIONS

Amino acids are essential for human life. They are the building blocks for proteins and play an important role in biochemistry. Methyl ester of L-serine was synthesized through esterification using thionyl chloride and then deprotection of amine group of obtained salt. The first reaction was completed with a satisfying yield. The second step was more difficult, due to small side-product particle size and the form of the product – yellow, adhesive wax.

The best results were obtained using triethylamine in dichloromethane as a solvent. The influence of solvent and the temperature of the process were examined. The deprotection reaction was optimized using design of experiments (DOE) method. The factorial plan 2^2 was employed. Almost all coefficients turned out to be insignificant due to wide divergence in the center of the plan. Assuming that all coefficients are significant, the equation turned out to be adequate. Mathematical model shows that the best results are obtained for long processes in high temperatures or for shorter reaction times in low temperatures. Further optimisation experiments are necessary.

Serine methyl ester is a substrate for further purposes, which is to modify material for polymeric scaffolds.

ACKNOWLEDGEMENTS

This work was financially supported by Department of Chemistry, Warsaw University of Technology.

REFERENCES

- [1] Solomon E.P., Berg L.R., Martin D.W., *Biologia*, Wydawnictwo MULTICO, 2011.
- [2] Morrison R.T., Boyd R.N., *Chemia organiczna, t. 2*, Wydawnictwo Naukowe PWN, 1996
- [3] Sanda F., Endo T., Syntheses and functions of polymers based on amino acids, *Macromol. Chem. Phys.*, 1999, 200, 2651-2661, DOI: 10.1002/(SICI)1521-3935(19991201)200:12<2651::AID-MACP2651>3.0.CO;2-P
- [4] Gu K., Bi L., Zhao M., Wang C., Ju J., Peng S., Toward the development of chemoprevention agents. Part II: Chemo-enzymatic synthesis and anti-inflammatory activities of a new class of 5-amino-2-substitutedphenyl-1,3-dioxacycloalkanes, *Bioorg. Med. Chem.* 2007, 15, 6273–6290, DOI: 10.1016/j.bmc.2007.06.018
- [5] Ananda K., Suresh Babu V.V., Deprotonation of hydrochloride salts of amino acid esters and peptide esters using commercial zinc dust, *The Journal of Peptide Research*, 2001, 57, 223–226, DOI: 10.1111/j.1399-3011.2001.00790.x
- [6] Tarbell D.S., Yamamoto Y., Pope B.M., New Method to Prepare *N-t*-Butoxycarbonyl Derivatives and the Corresponding Sulfur Analogs from di-*t*-Butyl Bicarbonate or di-*t*-Butyl Dithiol Dicarbonates and Amino Acids, *P. Natl. Acad. Sci. USA*, 1972, 69, 3, 730-732
- [7] McKerrow J.D., Al-Rawi J.M.A., Brooks P., Use of Diphenyliodonium Bromide in the Synthesis of Some *N*-Phenyl α -Amino Acids, *Synthetic Commun.*, 2010, 40, 8, 1161-1179, DOI: 10.1080/00397910903051259
- [8] Jańczewski D., Różycki C., Synoradzki L., *Projektowanie procesów technologicznych. Matematyczne metody planowania eksperymentów*, Oficyna Wydawnicza PW, 2010

Determination of CMC values of the surfactant solutions

*Magdalena Szaniawska¹, Anna Taraba¹, Katarzyna Szymczyk¹

¹Faculty of Chemistry, Department of Interfacial Phenomena, Maria Curie-Skłodowska University, Lublin, POLAND

e-mail: magdalena.szaniawska@wp.pl

Keywords: *surfactant, critical micelle concentration, pyrene, I_1/I_3 parameter*

ABSTRACT

Surfactants (surface active agents) are extensive group of organic compounds, which is widely used in many industries and everyday life. Thanks to their specific structure surfactants have very high surface activity. Among the characteristics of surface active agents the chief position occupies micellization process. The micellization process is the most important one from properties, which surfactant have. This process is based on formation of colloidal aggregates. It begins in the aqueous surfactant solution, when the certain concentration called critical micelle concentration (CMC), is reached. One of the method, in which we can determine the CMC value is spectrofluorimetry. The aim of presented study was the determination of the critical micelle concentration of nonionic surfactant, Tween 20, at different temperatures, with use pyrene as a fluorescence probe.

INTRODUCTION

Surfactants are substances, which are composed of two parts in opposite behavior towards to water. This behavior makes the surfactants amphiphilic. They consist of hydrophilic “head” and hydrophobic “tail” [1]. The polar part of surfactant has an affinity to water, therefore it is responsible for the dissolution of the compounds in these medium. The most frequently hydrophilic groups are carboxylic, hydroxylic, sulfonic and quaternary nitrogen [2]. The hydrophobic part is responsible for the affinity of surface active agents for non-polar solvents, for example the oils. Hydrophobic groups are build of aliphatic chain, contain from 8 to 18 carbon atoms or an aromatic ring [3].

From the practical point of view surfactants are often classified according to their use. However, this is not very useful, because many surfactants have several applications. The most accepted classification of surfactants is based on their dissociation in water. We can divide them to two groups: ionic surfactants (including cationic, anionic, amphoteric and zwitterionic) and nonionic [4].

Nonionic surface active agents has polar „head” which consist of the group that do not dissociate in water. This surfactants have low sensitivity to the pH of environment in which they are used (excluding strongly acidic and strongly alkaline solutions). The exceptions of this rule are nonionic surfactants containing ester group in the molecule. Also nonionic surface active agents have a low sensitivity to the presence of electrolytes, which leads to a slightly changes of physicochemical

properties of these compounds. The solubility of nonionic surfactants is inversely proportional to the temperature [4].

There is a lot of classifications of nonionic surfactants. The most important are:

- based on their behaviour in water [5]:

- compounds soluble in water;
- compounds, which form dispersions in water that means they are soluble incompletely;
- compounds, which do not form dispersions and they are insoluble in water, but they can be soluble in fats.

- in terms of chemical structure and a method of obtaining [6]:

- nonionic surface active agents of natural origin – in this group we can distinguish mainly saponin, as well as glycolipids;
- condensation products of polyols with hydrophobic compounds - derivatives of substituted alcohols, glycols, glycerol, pentaerythritol and sugar alcohols. Of particular attention in this group compounds called Spans – this surfactants are obtained from D-sorbitol.
- block copolymers of alkylene oxides – in this group we are chiefly distinguish pluronics;
- products of polyoxyetylation hydrophobic compounds - prepared by condensation of compounds, which have active hydrogen with ethylene oxide or propylene oxide. Fatty alcohols, fats, alkyl phenol, amines and fatty amides, fatty acid esters of sucrose or sorbitolu are mostly used in the polyoxyetylation reaction.

In the group of nonionic surfactants, derivatives of D-sorbitol can be distinguished two subgroups - Spans and Tweens. Span is the trade name of the surfactants obtained by the dehydration of D-sorbitol, followed by esterification of the anhydro-fatty acids which was obtained. Thus obtained surfactants have good solubility in oils and a very weak solubility in water [4]. Tween is a general trade name of surfactants that can be obtained by ethoxylation compounds type Span. These are the mixtures of substituted ethylene oxide esters of sorbitol and its anhydrides – monocyclic sorbitan and bicyclic sorbide with fatty acid esters (lauryl, palmitic, stearic, and oleic). These compounds, unlike Spans, are well soluble in water [4].

Tween 20 (polyoxyethylenesorbitan monolaurate), T20, is a surface active agent, which is obtained during the polyoxyetylation of sorbitan monolaurate. This surfactant, because of its low toxicity, can be used as a detergent in many fields of industry, science, and pharmaceuticals. Tween 20 differs from the other Tweens in length of chain polyoxyethylene and the kind of fatty acid from which the ester group is made [7]. In the food industry Tween 20 is used as a wetting agent in the production of ice drops and also as an emulsifier in the production of ice cream and soft drink. Tween 20 as a food additive is identified in accordance with the international system INS (International Numbering System) as E432. Tween 20 is also used in the biological sciences as a cleaning agent in immunoassays, e.g. ELISA. It solubilized also membrane proteins and it helps stabilize the purified protein derivative (PPD)

during tuberculin test. In the pharmaceutical industry it is used to stabilize emulsions and suspension [8].

Critical Micelle Concentration

Asymmetric structure of the surfactants causes their high surface activity. They are able to lower the surface tension of aqueous solutions and the interfacial tension at the interface of two immiscible liquids [1]. The second important property of surfactants is their ability to form micelles (colloidal aggregates). In dilute solutions surfactants are present as monomers. With the increase of surfactant concentration in the solution, they start to "saturate" the interface. The micellization process begins, when the complete saturation of the interface happened, surfactant molecules are still present in the solution, and this occurs at a certain concentration value, called the critical micelle concentration (CMC). Aggregates of surfactants above the CMC value are thermodynamically stable and they remain in equilibrium relative to individual surfactant molecules [9,10].

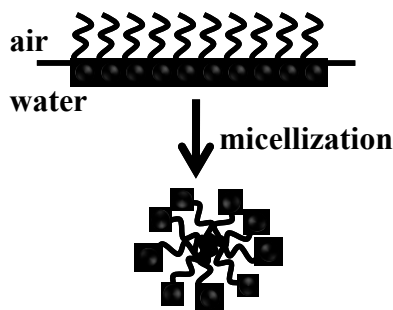


Fig. 1. Scheme of the micellization process in aqueous surfactant solution.

There are many methods of determining the CMC, they are based mostly on observation of certain properties, such as surface tension, conductivity, or osmotic pressure [11]. The fluorescence spectroscopy can be a good technique for determining the critical micelle concentration [12]. Unfortunately, in few molecules of the chemical compounds occur the groups which have the natural fluorescence, so the use of the fluorescence probes are important for the researchers [13]. Pyrene is very often used fluorescent probe in analysis of surface active agents. This substance is built from a system of four coupled aromatic rings. At room temperature pyrene is a crystalline colourless substance, which can be obtained by separation of the soot. It is a weakly toxic compound, but highly carcinogenic, especially dangerous for kidney and liver [14]. The emission spectra of pyrene can be observed a five characteristic peaks at 372, 379, 383, 388 and 393nm [15].

For the first time the possibility of applying pyrene to determine the critical micelle concentration proposed Thomas and Kalyanasundaram. They used in their work I_1/I_3 parameter, which is the ratio of intensity of the first peak to the third from the emission spectra of pyrene as a function of surfactant concentration [15]. Since

then, this method of determining the critical micelle concentration has become a valuable tool for many researchers.

Thus, the aim of presented study was to determine the critical micelle concentration of nonionic surfactant Tween 20 by fluorescence spectroscopy using pyrene, on the basis of I_1/I_3 parameter.

MATERIALS AND METHODS

A nonionic surfactant, Tween 20 and pyrene was used without previous purification (Sigma Aldrich). The aqueous solutions of Tween 20 ($C_{T20}=10^{-6}$ - 10^{-2} M) with the pyrene ($C_{pyrene}=6 \cdot 10^{-6}$ M) was prepared. The emission spectra of pyrene were recorded on Hitachi spectrofluorimeter FL-2700 (excitation wavelength $\lambda_{ex}=335$ nm) at the temperature range 293-318K. The solutions were thermostatted for 30 minutes in Lauda ECO Silver thermostate at each temperature. Then, by determining the parameter I_1/I_3 critical micelle concentration of Tween 20 in aqueous solutions was designated and the analyzed in the presented range of temperature.

RESULTS

Emission spectra of pyrene in aqueous solution of Tween 20 are shown in Fig. 2a-f. In the emission spectra of pyrene, as noted in the introduction, can be observed five characteristic peaks. The intensity of the pyrene's peaks increase with the increase of surfactant concentration in the solution. Simultaneously, the increase of temperature causes a decrease of the intensity of those peaks.

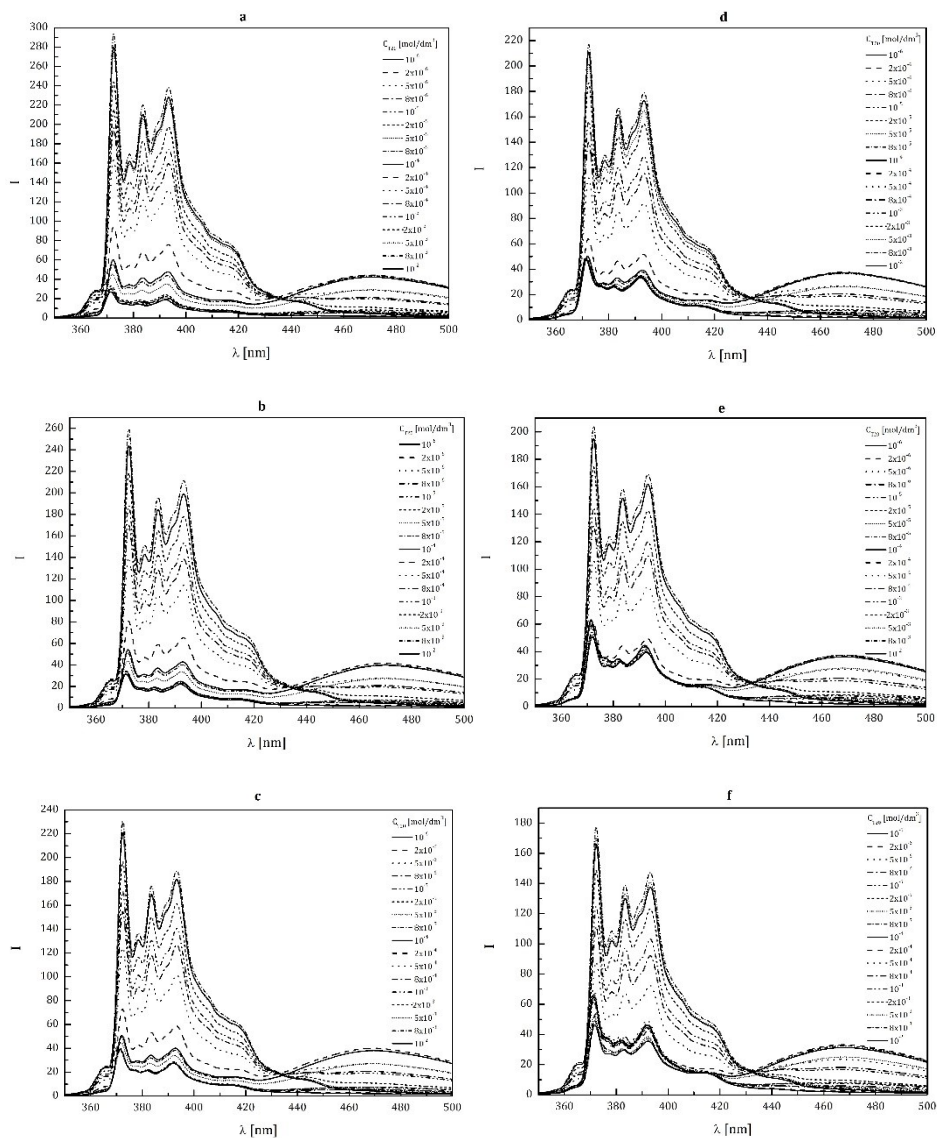


Fig. 2. Emission spectra of pyrene ($C_{\text{pyrene}}=6 \cdot 10^{-6}\text{M}$) in Tween 20 solutions ($C_{T20}=10^{-6}\text{M}-10^{-2}\text{M}$) solutions at different temperatures (a-293K, b-298K, c-303K, d-308K, e-313K, f-318K).

On the basis of the emission spectra at all temperatures the values of I_1/I_3 parameter were assigned. They are shown in the Fig. 3.

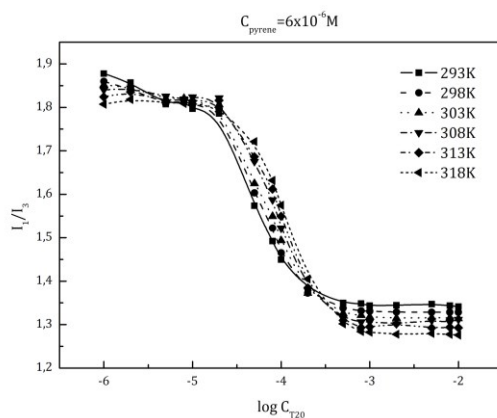


Fig. 3. A plot of the values of I_1/I_3 of aqueous solutions of Tween 20 versus the logarithm of the concentration of surfactant, $\log C_{T20}$.

In the analyzed aqueous solutions of surfactant Tween 20 with increase of its concentration the values of I_1/I_3 parameter decrease. It is interesting that the values of I_1/I_3 parameter increase in the range of 10^{-5} to 10^{-4} M concentration of Tween 20 with the increase of temperature. Above 10^{-4} M concentration the values of this parameter decrease until they reach almost constant value.

Based on I_1/I_3 parameter, which is presented in Fig. 3, the values of the critical micelle concentration of Tween 20 were determined and the results are shown in Tab. 1.

Tab. 1. The CMC values of Tween 20 at different temperatures (T).

T [K]	293	298	303	308	313	318
CMC [mol/dm ³]	$1,62 \cdot 10^{-4}$	$1,82 \cdot 10^{-4}$	$2,46 \cdot 10^{-4}$	$2,53 \cdot 10^{-4}$	$2,69 \cdot 10^{-4}$	$3,09 \cdot 10^{-4}$

Tab. 1. shows that with the increase of the temperature the CMC of the Tween 20 increases, based on I_1/I_3 parameter.

Effect of temperature on the CMC of surfactants solution depends on their chemical structure. The increase of the temperature causes the decrease of the degree of hydration for the surfactant hydrophilic group. This help in the process of micelles formation. Simultaneously, increase the temperature causes the destruction of the water structure around the hydrophobic group, which does not promote micellization. This two presented processes are opposite to each other, so the statement that the CMC increases or decreases depends on the temperature range and the structure of the surface active agent [1]. For most of the surfactants described in the literature CMC decreases with increase of the temperature [9,16].

The increase of the CMC of Tween 20 with the increase of the temperature may be result from the decreasing the interactions between the oxyethylene groups and the water molecules caused by changes in the conformation of polyoxyethylene chains, and thus a change of its hydration. Presented values of the CMC in (Tab. 1)

indicate of such phenomena, which probably occur in the examined solutions of surfactant.

CONCLUSIONS

The most important conclusion of the measurements is that the temperature will have an impact on values of the critical micelle concentration of the surfactants. The knowledge of the values of the surfactant CMC allows for suitable application of surfactant in the industry.

ACKNOWLEDGEMENTS

This work was supported by the National Science Centre, Poland, Project no. 2014/15/B/ST4/05086.

REFERENCES

- [1] Zieliński R., *Surfaktanty – budowa, właściwości, zastosowania*, Wydawnictwo Uniwersytetu Ekonomicznego w Poznaniu, 2009
- [2] Marzec A., *Chemia kosmetyków – surowce, półprodukty, preparatyka wyrobów*, Wydanie 3, Wydawnictwo „Dom Organizatora”, 2009
- [3] Molski M., *Chemia piękna*, Wydawnictwo Naukowe PWN, 2009
- [4] Zieliński R., *Surfaktanty – towaroznawcze i ekologiczne aspekty ich stosowania*, Wydawnictwo Akademii Ekonomicznej w Poznaniu, 2000
- [5] Anastasiu S., Jelescu E., *Środki powierzchniowo czynne*, Wydawnictwo Naukowo-Technologiczne, 1973
- [6] Kajl M., *Pollena – Tłuszcze, Środki Piorące, Kosmetyki*, 1972, 16, 3
- [7] Ayorinde F.O., Gelain S.V., Johnson J.H.Jr, Wan L.W., Analysis of some commercial polysorbate formulations using matrix-assisted laser desorption/ionization time-of-flight mass spectrometry, *Rapid Communication Mass Spectrometry*, 2000, 14, 2116-2124. DOI: 10.1002/1097-0231
- [8] Maqbool Q., Singh C., Paul A., Srivastava A., Uniform spheroidal nanoassemblies of magnetite using Tween surfactants: influence of surfactant structure on the morphology and electrochemical performance, *Journal of Material Chemistry C.*, 2015, 3, 1610-1618. DOI: 10.1039/C4TC02841D
- [9] Rosen J.M., *Surfactants and Interfacial Phenomena*, Wiley-Interscience, 2004.
- [10] Prochalska K., Bielska M., Dopierała K., *Wybrane fizykochemiczne aspekty filtracji membranowej, Membrany – teoria i praktyka*, 2009, 3, 80-109
- [11] Augiar J., Carpena P., Molina-Bolivar J.A., Carnero Ruiz C., On the determination of the critical micelle concentration by the pyrene 1:3 ratio method, *Journal of Colloid and Interface Science*, 2003, 258, 1, 116-122. DOI:10.1016/S0021-9797(02)00082-6
- [12] Shaw D. J., *Introduction to Colloid & Surface Chemistry*, Fourth Edition, Butterworth-Heinemann, 1992

- [13] Cooper A., *Chemia biofizyczna – Wprowadzenie do chemii fizycznej w badaniu makrocząsteczek*, Wydawnictwo Naukowe PWN, 2010.
- [14] Lakowicz J.R., *Principles of Fluorescence Spectroscopy*, 3rd Edition, Springer, 2006
- [15] Kalyanasundaram K., Thomas J.K., Environmental effects on vibronic band intensities in pyrene monomer fluorescence and their application in studies of micellar systems, *Journal of the American Chemical Society*, 1977, 99, 7, 2039-2044. DOI: 10.1021/ja00449a004

Polyphenols – description and preliminary study of alcohol extraction

*Anna Taraba¹, Magdalena Szaniawska¹

¹Faculty of Chemistry, Department of Interfacial Phenomena, Maria Curie-Skłodowska University, Lublin, POLAND

e-mail: anna.taraba@poczta.umcs.lublin.pl

Keywords: polyphenols, quercetin, ethanol, extraction

ABSTRACT

In the last years the polyphenols have reached the interest of researchers, because of their extremely interesting properties. These group of compounds has found the applications in medicine, pharmacy, and food supplementation. So the processes of obtaining polyphenols from plants is a necessity and very interesting for the topic of the research. The main focus of this paper is the characterization of polyphenols and one of the methods for obtaining these biologically active substances from plant origin (the object of interest are the polyphenols) – alcohol extraction. Also the ethanol and propanol extraction of biologically active plant based compound as quercetin will be shortly described.

INTRODUCTION

For the last ten years researchers have become interested in polyphenols and their applications. The main reason for this are the antioxidant properties of polyphenols, their probable anticancer properties and also great wealth in our diet. Moreover, polyphenols are found in medicinal plants, which are rich in active substances. This substances can modulate the activity of a wide range of enzymes and cell receptors. Till now the polyphenols are used in pharmacy as the dietary supplements. Unfortunately the natural polyphenols, mostly flavonoids, are poorly soluble in water, so in the pharmaceutical industries are using the synthetic ones. The researchers are looking for the new methods of obtaining the natural polyphenols from vegetables and fruits, which can be absorbed almost completely in human body [1].

The extraction is one of the basic methods of obtaining active substances from the plant material. It can be carried out under different conditions (hot, cold, with a variety of factors enabling i.e.: microwaves, ultrasound). This techniques are used to obtained polyphenols (particularly flavonoid). The simplest extraction, which can be used, is alcohol extraction. In this process the alcohol is used as solvent, in which the polyphenols are soluble [2]. So, the aim of presented article is to find the best concentration of ethanol and propanol, which can be used in alcohol extraction to obtain quercetin.

CHARACTERIZATION OF POLYPHENOLS

Structure and groups

Polyphenols are naturally occurring organic compounds, which can be found largely in plants. Polyphenols are secondary metabolites of plants and they are mostly responsible for the defense against ultraviolet radiation or pathogens. Polyphenols occur naturally in food and they may contribute to the color, bitterness, flavor, astringency, oxidative stability and odor [3,4].

Polyphenols contain at least two hydroxyl groups, which are attached to the aromatic ring. They can be divided into four main groups (Fig. 1), with the additional subgroups. On the basis of the number of the phenol rings, which they contain, and based on structural elements, which bind the rings to each other [3,4].

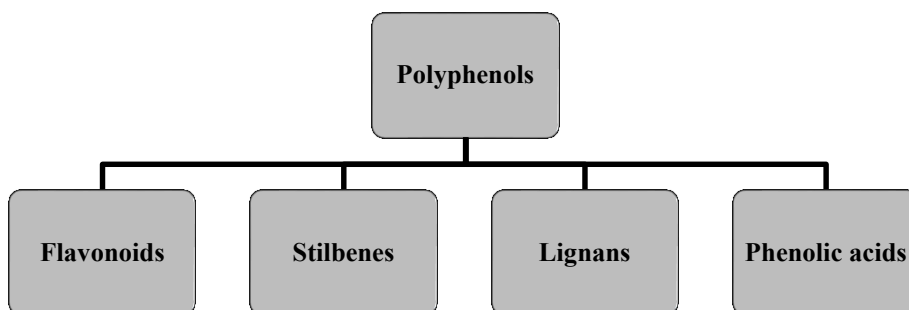


Fig. 1. Scheme of main groups of polyphenols [3,4].

Flavonoids

Favonoids represent the most studied group of polyphenols. The substances from this group have the basic structure, which consists of two aromatic rings bounded together by three carbon atoms that form an oxygenated heterocycle. For now there is known more than 4000 varieties of flavonoids, which have been identified. They are responsible mostly for colours of the flowers, vegetables and fruits, leaves. Flavonoids can be divided into six subclasses based on their variation in the type of heterocycle: flavonols, flavanones, flavones, flavanols, isoflavones and anthocyanins (Fig. 2). The difference in number and arrangement of the hydroxyl groups and also their extent of alkylation and/or glycosylation are the reasons of the individual differences between each subclass. The most common flavonoids are quercetin, rutin, myricetin, catechins etc [3,4].

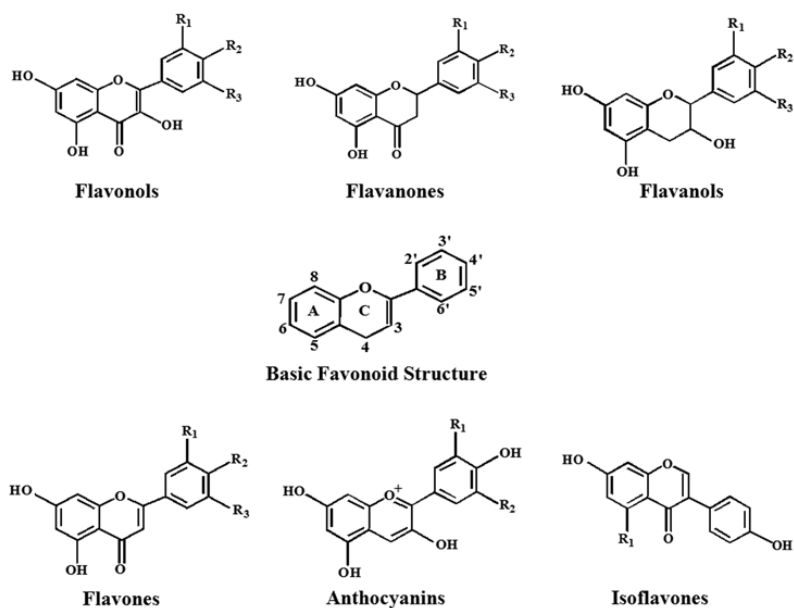


Fig. 2. The structure of the subclasses of flavonoids [3].

Stilbenes

Stilbenes are the substances, which contain two phenyl moieties. This moieties are connected by a two-carbon methylene bridge. Stilbenes naturally occur in plants and they act as antifungal phytoalexins, so they are synthesized only in response to infection or injury. In human diet the stilbenes occur in low quantities. One of the best studied stilbene, which occurs naturally is resveratrol (3,4',5-trihydroxystilbene), which can be found largely in grapes. A product of processing grapes, red wine also contains significant amount of resveratrol [3,4].

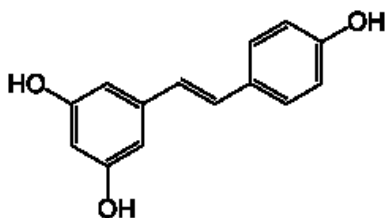


Fig. 3. The chemical structure of resveratrol from the stilbenes group [5].

Lignans

Lignans are the compounds, which are diphenolic and they contain a 2,3-dibenzylbutane structure. This structure is formed in the process of dimerization of two cinnamic acid residues. These substances are metabolized to enterodiol and enterolactone by the intestinal microflora. The dietary source, which is the richest in lignans is linseed. It contains secoisolariciresinol (up to 3.7 g/kg dry weight) and low quantities of matairesinol [3,4].

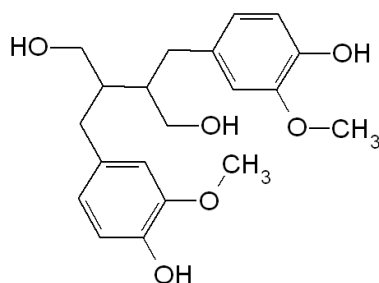


Fig. 4. The structure of secoisolariciresinol (group of lignans) [6].

Phenolic acids

Phenolic acids are the compounds, which can be found abundantly in foods. They can be divided into two classes: derivatives of cinnamic acid and derivatives of benzoic acid. The hydroxycinnamic acids consist mostly of p-coumaric, ferulic, caffeic and sinapic acids. Also they're more common than the hydroxybenzoic acids. The hydroxybenzoic acid occurs in plants, but they amount is low. The exceptions are certain red fruits, black radish and onions, This fruits and vegetables can have concentrations of the hydroxybenzoic acids about tens of milligrams per kilogram fresh weight of vegetable or fruit [3,4].

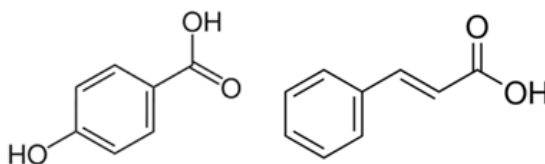


Fig. 5. The chemical structure of p- hydroxybenzoic acid and cinnamic acid [7,8].

HEALTH BENEFITS OF POLYPHENOLS

Researchers are evaluating more than 8000 different polyphenols, which have been identified. The completed studies will give the importance of these compounds in human diet. Epidemiological studies repeatedly shown that the diet rich in polyphenols prevents humans from chronic diseases [9]. The phenolic groups in the structure of polyphenols can accept an electron and then it can form relatively stable phenoxyl radicals. This processes can disrupt the chain oxidation reactions in cellular components [10]. The research shows that the food, which is rich in polyphenols, and beverages may increase the plasma antioxidant capacity. This increase of antioxidative capacity of plasma can be the result of either the presence of reducing polyphenols and their metabolites in plasma, also by effects of polyphenols on endogenous antioxidants. It can also be related with the effect of these compounds on the absorption of pro-oxidative food components (for example iron) [11]. Consumption of antioxidants makes the reduce of levels of oxidative damage to lymphocytic DNA. Researchers confirms that the antioxidants, polyphenols may

protect the cells from oxidation, later the damage of cells. So this group of compounds can protect humans from a wide range of diseases [4].

ALCOHOL EXTRACTION OF FLAVONOIDS

Recently the new methods of obtaining biologically active substances from plants are developing, because of the interest in obtaining the natural substances from plants. This natural ones have better absorption in human's body, so the researchers are looking for method in which they can obtain these substances. The polyphenols (mostly flavonoids) are these kind of substances, which occur in food, cosmetics, pharmaceuticals, or in aromatherapy. One of the easiest method of obtaining polyphenols from plants is alcohol extraction [12].

The antioxidant activity and the yield of the process of extraction mostly depends on the solvent polarity. It determines the qualitatively and quantitatively the extracted antioxidant compounds. The highest yields of the extraction process can be usually achieved with the short-chained alcohols such as ethanol and methanol or their mixtures with water. In the extraction of polyphenols from the plants there are also other solvents, which are widely used for example ethyl acetate or acetone. The reason why the water and ethanol are those most widely used is their low toxicity and high extraction yield. Also they give the advantage of modulating the polarity of the solvent by using the mixtures of ethanol and water [13].

MATERIALS AND METHODS

Quercetin belongs to a group of polyphenols, subgroup - flavonoids (3,5,7,3',4'-pentahydroxyflavonol) and it is one of the widely used pharmaceutical flavonoids compound. It is also a natural plant pigment. Quercetin can be found in plants and in food such as tea, juices, wine or honey. Moreover flavonoids, such as quercetin, have an antioxidant properties. So the quercetin also have many properties, which have positive effect on humans health. It can be used as strong antioxidant, because of its ability to scavenge free radicals and bind transition metal ions. It can also help to protect the vessels against heart disease and the tissues from cancer. Quercetin has anti-inflammatory and antihistamine properties, because it helps to stabilize the cells that release histamine in the body [14].

Two alcohols were chosen for the experiment, in which the quercetin was extracted. One of them is ethanol and the second one is propanol. This two alcohols are shorth-chain, and they have antibacterial properties, so they were used as the extraction solvent.

The alcohol-water solutions of:

- quercetin and ethanol ($C_{pEtOH}=0\% - 80\%$)
- quercetin and propanol ($C_{pPrOH}=0\% - 80\%$)

were prepared. Firstly the 0.004 mg portions of quercetin (Sigma-Aldrich) was weighted. Next the weighted amounts of quercetin were transferred into 100 ml flasks. And then the water, alcohol-water solutions were prepared by adding appropriate quantities of alcohol to obtain the desired solutions in the flasks. Then their absorption spectra were measured at 293K with the Helios γ spectrophotometer.

RESULTS AND DISCUSSION

Fig. 6. shows the absorption spectra of quercetin in ethanol solutions with different concentration at 293K. The maximum peak of the quercetin in the examined solutions is about $\lambda = 375$ nm. The lowest absorption is observed in quercetin solution in water (0% of ethanol). With the increase of ethanol concentration in the solution the absorbance increases. So the most appropriate concentration to extraction of quercetin is the 80% solution of ethanol (EtOH).

Fig. 7. also shows the absorption spectra of quercetin, but in the solvent, which is propanol (PrOH) at 293K. The maximum of the absorption of quercetin is about $\lambda = 375$ nm. The increases of the concentration of propanol in the solution causes the increase of the amount of the extracted quercetin, which is confirmed on the Fig. 7. So the most appropriate concentration of propanol to extraction of quercetin is 80%.

Next Fig. 8. shows the comparison of obtained results of maximum absorbance value of quercetin in two different solvents. In both solvents, in ethanol and propanol, the amount of extracted quercetin increases with the increase of the alcohol concentration in the solution.

Both alcohols, propanol and ethanol, used for the extraction allow to obtain extracts of the examined substance - quercetin. Moreover both of used alcohols are used in food production, so they can be widely used to extraction of quercetin.

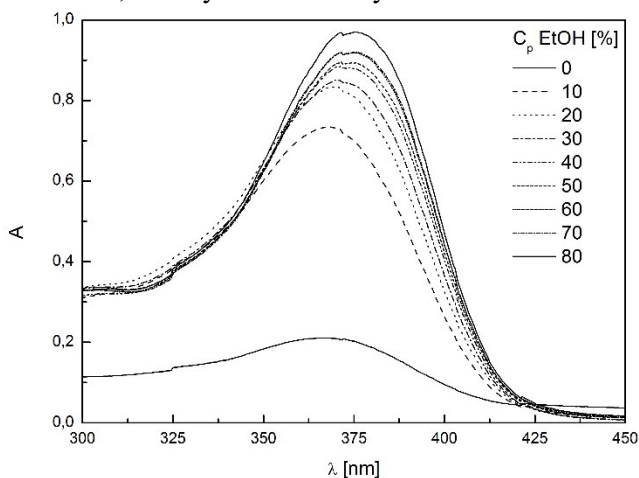


Fig. 6. Absorption spectra of quercetin in ethanol solutions (C_pEtOH= 0 - 80%).

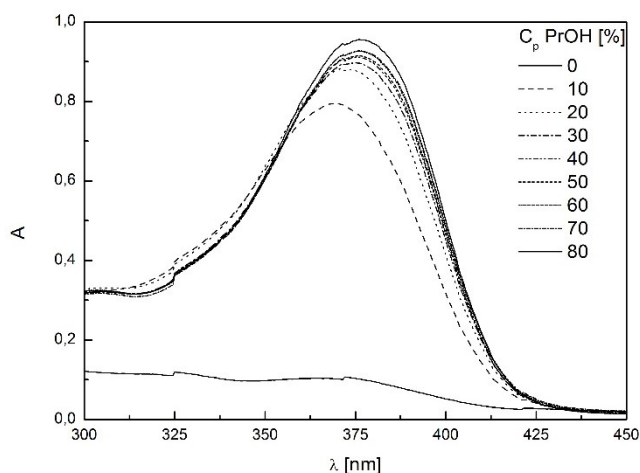


Fig. 7. Absorption spectra of quercetin in propanol solutions ($C_{p\text{PrOH}}= 0 - 80\%$).

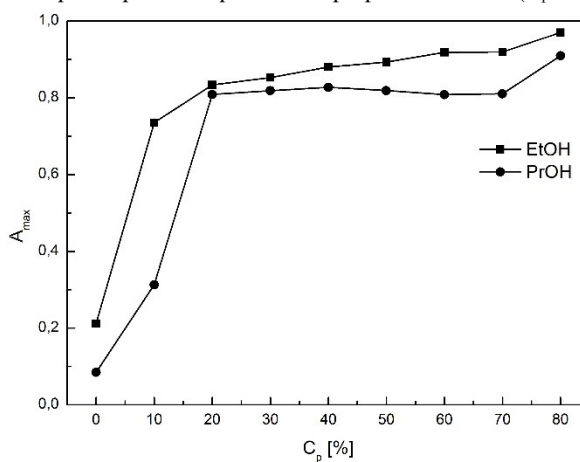


Fig. 8. A plot of maximum absorbance (A_{max}) of quercetin versus the concentration of alcohol solutions ($C_p= 0 - 80\%$).

SUMMARY

Polyphenols are the compounds, which has very interesting structures and properties. They found the application in wide range of industry sectors. Also they can be obtained from plants in the process of extraction.

The alcohol extraction techniques have many benefits, so it is used to obtain polyphenols, especially flavonoids, which are biologically active plant based compounds.

Ethanol and propanol are the alcohols, which can be successfully used in extraction of biologically active compounds (flavonoids). Quercetin can be extracted with the use of this both alcohols. The most appropriate concentration of ethanol and propanol to extraction of quercetin is 80%.

REFERENCES

- [1] Cacace J.E., Mazza G., Optimization of Extraction of Anthocyanins from Black Currants with Aqueous Ethanol, *Food Engineering and Physical Properties*, 2003, 68, 240-248
- [2] Handa S.S., Chapter in the book: Extraction Technologies for Medicinal and Aromatic Plants, *An Overview of Extraction Techniques for Medicinal and Aromatic Plants*, International Centre For Science And High Technology, 2008
- [3] Pandey K.B., Rizvi S.I., Plant polyphenols as dietary antioxidants in human health and disease, *Oxidative Medicine Cellular Longevity*, 2009, 2, 270-278
- [4] Manach C., Scalbert A., Morand C., Remesy C., Jimenez L., Polyphenols: food sources and bioavailability, *The American Journal of Clinical Nutrition*, 2004, 79, 727-747
- [5] <https://en.wikipedia.org/wiki/Resveratrol>
- [6] <https://commons.wikimedia.org/wiki/File:Secoisolariciresinol.PNG>
- [7].<http://fabricheminc.com/biochemicals-diagnostics-buffers/p-hydroxybenzoic-acid-phba/>
- [8].<http://www.sigmaaldrich.com/catalog/product/aldrich/c80857?lang=pl®ion=PL>
- [9] Graf B.A., Milbury P.E., Blumberg J.B., Flavonols, flavonones, flavanones and human health: Epidemiological evidence, *Journal of Medicinal Food*, 2005, 8, 281-290
- [10] Clifford M.N., Chlorogenic acids and other cinnamates. Nature, occurrence, dietary burden, absorption and metabolism, *Journal of the Science of Food and Agriculture*, 2000, 80, 1033-1043
- [11] Scalbert A., Manach C., Morand C., Remesy C., Dietary polyphenols and the prevention of diseases, *Critical Reviews in Food Science and Nutrition*, 2005, 45, 287-306
- [12] Cacace J.E., Mazza G., Optimization of Extraction of Anthocyanins from Black Currants with Aqueous Ethanol, *Food Engineering and Physical Properties*, 2003, 68, 240-248
- [13] Franco D., Sineiro J., Rubilar M., Sanchez M., Jerez M., Pinelo M., Costoya N., Nunez M.J., Polyphenols from plant materials: extraction and antioxidant power, *Electronic Journal of Environmental, Agricultural and Food Chemistry*, 2008, 7, 3210-3216
- [14] Boyle S. P., Dobson V. L., Duthie S.J., Hinselwood D. C., Kyle J. A. M., A. R. Collins A. R., Bioavailability and efficiency of rutin as an antioxidant: a human supplementation study, *European Journal of Clinical Nutrition*, 2000, 54, 774-782.

Carbon-based nanomaterials in chemistry

*Tomasz Wawer, J. Jonik, H. Grajek

Department of New Technologies and Chemistry, Military University of Technology,
Warsaw, POLAND

e-mail: tomasz.wawer@wat.edu.pl

keywords: carbon black, graphene, nanotubes, nanofibers

ABSTRACT

The applications of different carbon materials including carbon black, nanofibers, nanotubes and graphene have been reviewed and discussed. Carbon-based nanomaterials' properties strongly depend on the material structure despite its similar chemical composition as well as interactions with other materials. The particular attention has been paid to their applications in analytical chemistry. The unique chemical and electrical properties of carbon-based materials make them very interesting for developing new types of gas sensors or sorbents.

INTRODUCTION

In the last few years carbon-based nanomaterials (CBNs) found application in various areas. Due to their multifunctional nature CBNs are used in electrochemical sensors [1,2], biochemistry [2,3] and analytical chemistry [5-7]. The objective of this review is to provide a snapshot of applications in aforementioned areas.

STRUCTURE AND PROPERTIES OF CARBON MATERIALS

Carbon black

Carbon black is pure, more than 97% of elemental carbon, in the form of colloidal particles. It is produced in the process of incomplete combustion of hydrocarbons [8]. Carbon black is available in various forms, particle sizes and porosity [9]. It forms grape-like clusters of sizes lower than 50 nm, its surface area can be greater than $1500 \text{ m}^2 \cdot \text{g}^{-1}$, and density much lower than $2.25 \text{ g} \cdot \text{cm}^{-3}$, which is theoretical density of graphite [1,4].

Carbon nanofibers

Carbon nanofibers are nano-sized carbon fibers formed from hydrocarbon gases [10] or by carbonization of polymers [11-13]. Depending on the method of production they can be hollow or porous [1]. Many fiber grades are available with diameters from 40 to 400 nm and length of a few μm [5,13].

Carbon nanotubes

Carbon nanotubes (CNTs) are one-dimensionally extended fullerenes. Their ends may be capped. Their name is derived from their hollow structure limited by walls formed by rolled graphene sheets. CNTs are categorized as single-walled nanotubes and multi-walled nanotubes made of concentric tubes of rolled graphene. [1,6,14]

CNTs were observed for the first time by Iijima [15] during an arc discharge of graphite electrode. In the following years the new methods of CNTs synthesis were developed, such as laser ablation [16] or catalytic vapour-phase deposition [17].

Graphene

Graphene is the two-dimensional material made of single layer of carbon atoms arranged in honeycomb structure. Since Novoselov et al. [18] isolated graphene for the first time by mechanical exfoliation, many different methods to fabricate graphene have been reported. The most commonly used are chemical exfoliation [19], thermal decomposition of silica carbide [20], chemical vapour deposition [21].

APPLICATIONS OF CARBON MATERIALS

Gas sensors

The properties of carbon-based materials have been used to develop gas sensors employing different transduction principles, such as changes in electrical or optical properties [1]. Lewis et al. [22] developed commercially available carbon black with different polymers in 14 element array of sensors. The sensor was used for detection of components in mixture of 19 solvents vapors. It was possible to distinguish both similar (n-pentane and n-hexane) and differing in chemical properties (methanol and benzene) compounds of the mixture.

Due to the variety of preparation methods of carbon nanotubes there are many sensors for different gases. In sensor made by Lee et al. [23] carbon fibers were prepared in the process of electrospinning, thermal treatment, chemical activation using KOH solutions and addition of carbon black. That way of sensor material preparation led to increased electrical conductivity and sensitivity to carbon monoxide and nitrogen monoxide gases. Another sensor developed by Fong et al. [24], prepared by attachment of Pd nanoparticles to carbon nanofibers. This modification allowed detecting hydrogen due to its reduction reaction with Pd. Similarly to metals also metal oxides such as ZnO or SnO₂ [25] may be attached to carbon materials in order to lower the limit of detection to the level of 0.1 ppb.

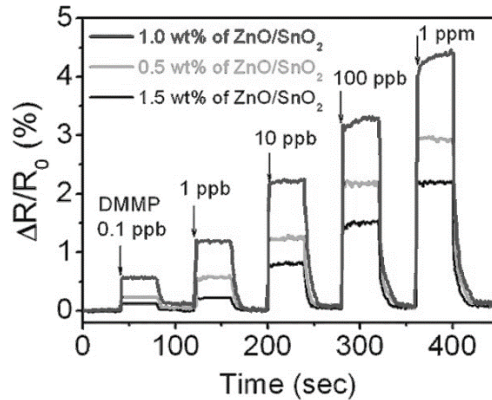


Fig. 1. Normalized resistance changes of ZnO/SnO₂/Carbon nanofibers gas sensor upon sequential exposure to various dimethyl methylphosphonate (DMMP) vapor concentration [25].

Next carbon material used in gas sensors are carbon nanotubes. Their first applications were announced seminally by groups led by Kong [26] and Collins [27]. There are many methods of gas detection using carbon nanotubes. The main ones are electrical resistance measurements [27], changes in photoemission spectra [28] and use of doped carbon nanotubes as semiconductors in transistors [26,29]. There were many studies shown that functionalization of carbon nanotubes can make them selective to certain analytes [30]. In some cases carbon nanotubes exhibit similar properties to carbon nanofibers for example Pd coated carbon nanotubes are sensitive to hydrogen [31].

Graphene properties for gas sensing were described for the first time by Schedin et al. [32]. The gas induced concentration dependent changes in resistivity had different magnitudes for different gases including the sign of changes whether the gas was electron acceptor or donor. By removing the contaminants in graphene by H₂/Ar mixture, responses to very small amount of gases can be measured [33]. However there is a need for graphene surface functionalization with B, N, Al or S in order to reach sub-ppb sensitivity [34]. Also the chemically modified graphenes are used as components of gas sensors [35,36].

Biochemistry and biomedical engineering

Due to capability of selective binding of target molecules or proteins electrochemical aptasensors (ECAS) are nowadays widely applied in biochemistry. Introduction of high specific surface area CBNs into ECASs increased their efficiency [2]. Some CBNs are sensitive only to certain molecular structures. This led to fabrication of aptasensor used for detection of single-stranded DNA in the mixture of single- and double-stranded DNA [37-39]. Xu et al. [40] developed graphene-based aptasensor for detection of Pb²⁺ and K⁺ with limits of detection of 2 μM for Pb²⁺ and 27 μM for K⁺, which were lower than previously reported methods. Carbon-based aptasensors are also widely used to thrombin detection. Besides

chemically modified graphenes [41] the composites of gold nanoparticles with CNTs [42], graphene [43,44] and reduced graphene oxide [45] are used for preparation of ECASs.

Unique optical properties of CNTs such as optical transitions in near-infrared (NIR) region make them useful in cell and tissue labeling and imaging. Combining the CNTs biomarkers with NIR fluorescent microscopy and optical coherence tomography results a higher quality images. High affinity of some proteins or DNA to CNTs make them considered as drug carriers [3,46,47]. The chemically modified graphenes are also considered as drug carriers. Dispersability in water solutions, hydrophilic functional groups and structural heterogeneity of graphene oxide are desirable features for applications in bioengineering. Thanks to ease of chemical modification of graphene oxide it found application as a drug carrier and cellular sensor [3,48,49].

Sample preparations

CBNs have found a wide range of applications in sample preparation techniques as adsorbents due to their strong interactions such as π - π stacking, electrostatic forces with organic molecules. However usage of some CBNs in flow-through methods is hampered by their tendency to aggregate, which causes pressure drop and deterioration of retention [5,7]. Materials with larger particle size, like carbon nanofibers, can overcome this problem. It make them possible to use in solid phase extraction (SPE) method of samples preparation of either organic or inorganic samples [50-52]. Despite the problem of pore clogging many types of CNTs are widely used in SPE for preconcentration of phenolic compounds, pesticides, pharmaceuticals, organometallic compounds and inorganic ions [53-57]. Another SPE sorbents is graphene and its oxide. To avoid their aggregation and escaping from cartridge graphenes were chemically bonded to aminosilica support [58,59]. Furthermore, CNTs may be placed on fibers and used in solid phase microextraction (SPME) [56,57,60]. Also graphene oxide, which may be modified with octadecylsilyl to lower its polarity, is used in SPME [61].

CONCLUSIONS

There is a big number of literature supporting the use of the CBNs. Their unique electronic properties give them a place between other nanomaterials in potential applications of electrical sensors. There is need for breakthrough in fabrication of cheap, high quality CBNs to introduce commercial production of CBN-based gas sensors and adsorbents. However, low quality CBNs like graphene oxide are also promising materials for gas sensing. [1,3]

Despite the use of nanotechnologies in analytical chemistry it is quite new approach many researchers around the world have recognized the utility of CBNs. Their use in the construction of ECASs can improve sensitivity to analytes with low limits of detections. Also, owing to their adsorption abilities, CBNs have found a wide

range of applications in sample preparations as sorbents. Their chemical and thermal stability are the advantages for application of some CBNs in the SPME technique as fiber coating materials. [2,5-7]

REFERENCES

- [1] E. Llobet, Gas sensors using carbon nanomaterials: A review, *Sensors and Actuators B: Chemical*, 2013, 179, 32-45
- [2] Z. Wang, J. Yu, R. Gui, H. Jin, Y. Xia, Carbon nanomaterials-based electrochemical aptasensors, *Biosensors and Bioelectronics*, 2016, 79, 136-149
- [3] C. Cha, S. R. Shin, N. Annabi, M. R. Dokmeci, A. Khademhosseini, Carbon-Based Nanomaterials: Multifunctional Materials for Biomedical Engineering, *ACS Nano*, 2013, 4, 7, 2891-2897
- [4] A. G. Pandolfo, A. F. Hollenkamp, Carbon properties and their role in supercapacitors, *Journal of Power Sources*, 2006, 157, 11-27
- [5] B. Zhang, X. Zheng, H. Li, J. Lin, Application of carbon-based nanomaterials in sample separation: A review, *Analytica Chimica Acta*, 2013, 784, 1-17
- [6] A. Speltini, D. Merli, A. Profumo, Analytical application of carbon nanotubes, fullerenes and nanodiamonds in nanomaterials-based chromatographic stationary phases: A review, *Analytica Chimica Acta*, 2013, 783, 1-16
- [7] K. Scida, P. W. Stege, G. Haby, G. A. Messina, C. D. García, Recent applications of carbon-based nanomaterials in analytical chemistry: Critical review, 2011, 691, 6-17
- [8] M. J. Wang, Encyclopedia of polymer science and technology, *John Wiley & Sons Inc, NJ USA*, 2003, 52-91.
- [9] M. Ciobanu, A. Lepadatu, S. Asaftei, Chemical and electrochemical studies of carbon black surface by treatment with ozone and nitrogen oxide, *Proceedings of the International Conference on Diamond and Carbon Materials*, 2016, 3S, S252-S257
- [10] G. G. Tibbets, Carbon fibers produced by pyrolysis of natural gas in stainless steel tubes, *Applied Physics Letters*, 1983, 42, 666-668
- [11] C. Lai, C. Lo, Preparation of Nanostructural Carbon Nanofibers and Their Electrochemical Performance for Supercapacitors, *Electrochimica Acta*, 2015, 183, 85-93
- [12] C. Liu, Y. Tan, Y. Liu, K. Shen, B. Peng, X. Niu, F. Ran, Microporous carbon nanofibers prepared by combining electrospinning and phase separation methods for supercapacitors, *Journal of Energy Chemistry*, 2016, 25, 587-593
- [13] C. Kim, Y. I. Jeong, B. T. N. Ngoc, K. S. Yang, M. Kojima, Y. A. Kim, M. Endo, J. W. Lee, Synthesis and characterization of porous carbon nanofibers with hollow cores through the thermal treatment of electrospun copolymeric nanofiber webs, 2007, 3, 91-95
- [14] S. Peng, K. Cho, Ab initio study of doped carbon nanotube sensors, *Nano Letters*, 2003, 3, 513-517
- [15] S. Iijima, Helical microtubules of graphitic carbon, *Nature*, 1991, 354, 56-58

- [16] T. Gou, P. Nikolaev, A. G. Rinzler, D. Tomanek, D. T. Colbert, R. E. Smalley, Self-assembly of tubular fullerenes, *Journal of Physical Chemistry*, 1995, 99, 10694-10697
- [17] M. José-Yacamán, M. Miki-Yoshida, L. Rendón, J. G. Santiesteban, Catalytic growth of carbon microtubules with fullerene structure, *Applied Physics Letters*, 1993, 62, 657-659
- [18] K. S. Novoselov, A. K. Geim, S. V. Morozov, D. Jiang, Y. Zhang, S. V. Dubonos, I. V. Grigorieva, A. A. Firsov, Electric Field Effect in Atomically Thin Carbon Films, *Science*, 2004, 306, 666-669
- [19] S. Park, R. S. Ruoff, Chemical methods for the production of the graphenes, *Nature Nanotechnology*, 2009, 4, 217-224
- [20] T. Seyller, A. Bostwick, K. V. Emtsev, K. Horn, L. Ley, J. L. McChesney, T. Ohta, J. D. Riley, E. Rotenberg, F. Speck, Epitaxial graphene. A new material, *Physica Status Solidi B*, 2008, 245, 1436-1446
- [21] K. S. Kim, Y. Zhao, H. Yang, S. Y. Lee, J. M. Kim, J. H. Ahn, P. Kim, J. Y. Chio, B. H. Hong, Large-scale pattern growth of graphene films for stretchable transparent electrode, *Nature*, 2009, 457, 706-710
- [22] B. J. Doleman, M. C. Lonergar, E. J. Severin, T. P. Vaid, N. S. Lewis, Quantitative Study of the Resolving Power of Arrays of Carbon Black-Polymer Composites in Various Vapor-Sensing Tasks, *Analytical Chemistry*, 1998, 70, 4177-4190
- [23] J. S. Im, S. C. Kang, S. H. Lee, Y. S. Lee, Improved gas sensing of electrospun carbon fibers based on pore structure, conductivity and surface modification, *Carbon*, 2010, 48, 2573-2581
- [24] L. Zhang, X. Wang, Y. Zhao, Z. Zhu, H. Fong, Electrospun carbon nano-felt surface-attached with Pd nanoparticles for hydrogen sensing applications, *Materials Letters*, 2012, 68, 133-136
- [25] J. S. Lee, O. S. Kwon, S. J. Park, E. Y. Park, S. A. You, H. Yoon, J. Jang, Fabrication of ultrafine metal-oxide-decorated carbon nanofibres for DMMP sensor applications, *ACS Nano*, 2011, 5, 7992-8001
- [26] J. Kong, N. R. Franklin, C. Zhou, M. G. Chapline, S. Peng, K. Cho, H. Dai, Nanotube molecular wires as chemical sensors, *Nature*, 2000, 287, 622-625
- [27] P. G. Collins, K. Bradley, M. Ishigami, A. Zettl, Extreme oxygen sensitivity of electronic properties of carbon nanotubes, *Nature*, 2000, 287, 1801-1804
- [28] A. Goldoni, R. Larciprete, L. Petaccia, S. Lizzit, Single-wall carbon nanotube interaction with gases: sample contaminants and environmental monitoring, *Journal of American Chemical Society*, 2003, 125, 11329-11333
- [29] S. Tan, A. Verschueren, C. Dekker, Room-temperature transistor based on a single carbon nanotube, *Nature*, 1998, 393, 49-51
- [30] P. Bondavalli, P. Legagneux, D. Pribat, Carbon nanotubes based transistors as gas sensors: state of the art and critical review, *Sensors and Actuators B: Chemical*, 2009, 140, 308-319

- [31] J. Kong, M. G. Chapline, H. Dai, Functionalized carbon nanotubes for molecular hydrogen sensors, *Advanced Materials*, 2001, 13, 1384-1386
- [32] F. Schedin, A. K. Geim, S. V. Morozov, E. W. Hill, P. Blake, M. I. Katsnelson, K. S. Novoselov, Detection of individual gas molecules adsorbed on graphene, *Nature Materials*, 2007, 6, 652-655
- [33] Y. Dan, Y. Lu, N. J. Kybert, Z. Luo, A. T. C. Johnson, Intrinsic response of graphene vapor sensors, *Nano Letters*, 2009, 9, 1472-1475
- [34] J. Dai, J. Yuan, P. Giazzoni, Gas adsorption on graphene doped with B, N, Al and S: a theoretical study, *Applied Physics Letters*, 2009, 95, 232105
- [35] W. Li, X. Geng, Y. Guo, J. Rong, Y. Gong, L. Wu, X. Zhang, P. Li, J. Xu, G. Cheng, M. Sun, L. Liu, Reduced graphene oxide electrically contacted graphene sensor for high sensitive nitric oxide detection, *ACS Nano*, 2011, 5, 6955-6961
- [36] J. T. Robinson, F. K. Perkins, E. S. Snow, Z. Wei, P. E. Sheehan, Reduced graphene oxide molecular sensors, *Nano Letters*, 2008, 8, 3137-3140
- [37] R. J. Chen, Y. Zhang, Controlled precipitation of solubilized carbon nanotubes by delamination of DNA, *Journal of Physical Chemistry B*, 2006, 110, 54-57
- [38] X. Zhao, J. K. Johnson, Simulation of adsorption of DNA on carbon nanotubes, *Journal of American Chemical Society*, 2007, 129, 10438-10445
- [39] K. Yang, C. Zhang, Simple detection of nucleic acids with a single-walled carbon-nanotube-based electrochemical biosensor, *Biosensors and Bioelectronics*, 2011, 28, 257-265
- [40] K. Xu, X. Meshik, B. M. Nichols, E. Zakar, M. Dutta, M. A. Stroschio, Graphene- and aptamer-based electrochemical biosensor, *Nanotechnology*, 2014, 25, 205501
- [41] G. Jin, L. Lu, X. Gao, M. Li, B. Qiu, Z. Lin, H. Yan, G. Chen, Magnetic graphene oxide-based electrochemiluminescent aptasensor for thrombin, *Electrochimica Acta*, 2013, 89, 13-17
- [42] L. Bai, R. Yuan, Y. Chai, Y. Zhuo, Y. Yuan, Y. Wang, Simultaneous electrochemical detection of multiple analytes based on dual signal amplification of single-walled carbon nanotubes and multi-layered graphene sheets, *Biomaterials*, 2012, 33, 1090-1096
- [43] Q. Xue, Z. Liu, Y. Guo, S. Guo, Cyclodextrin functionalized graphene-gold nanoparticle hybrids with strong molecular capability for electrochemical thrombin aptasensor, *Biosensors and Bioelectronics*, 2015, 68, 429-436
- [44] L. Bai, B. Yan, Y. Chai, R. Yuan, Y. Yuan, S. Xie, L. Jiang, Y. He, An electrochemical aptasensor for thrombin detection based on direct electrochemistry of glucose oxidase using a functionalized graphene hybrid for amplification, *Analyst*, 2013, 138, 6595-6599
- [45] Q. Wang, Z. Zhou, Y. Zhai, L. Zhang, W. Hong, Z. Zhang, S. Dong, Label-free aptamer biosensor for thrombin detection based on functionalized graphene nanocomposites, *Talanta*, 2015, 141, 247-252

- [46] B. S. Harrison, A. Atala, Carbon nanotube application for tissue engineering, *Biomaterials*, 2007, 28, 344-353
- [47] J. Wang, G. Liu, M. R. Jan, Ultrasensitive electrical biosensing of proteins and DNA: Carbon-nanotube derived amplifications of the recognition and transduction events, *Journal of American Chemical Society*, 2004, 126, 3010-3011
- [48] L. Zhang, J. Xia, Q. Zhao, L. Liu, Z. Zhang, Functional graphene oxide as a nanocarrier for controlled loading and targeted delivery of mixed anticancer drugs, *Small*, 2010, 6, 537-544
- [49] X. Sun, Z. Liu, K. Welscher, J. T. Robinson, A. Goodwin, S. Zaric, H. Dai, Nano-graphene oxide for cellular imaging and drug delivery, *Nano Research*, 2008, 1, 203-212
- [50] W. Boonjob, M. Miró, M. A. Segundo, V. Cedrà, Flow-through dispersed nanofiber-based microsolid-phase extraction coupled to liquid chromatography for automatic determination of trace levels of priority environmental pollutants, *Analytical Chemistry*, 2011, 83, 5237-5244
- [51] S. Chen, X. Zhan, D. Lu, C. Liu, L. Zhu, Speciation analysis of inorganic arsenic in natural water by carbon nanofibers separation and inductively coupled plasma mass spectrometry determination, *Analytica Chimica Acta*, 2009, 634, 192-196
- [52] S. Chen, M. Xiao, D. Lu, X. Zhan, Carbon nanofibers as solid-phase extraction adsorbent for the preconcentration of trace rare earth elements and their determination by inductively coupled plasma mass spectrometry, *Analytical Letters*, 2007, 40, 2105-2115
- [53] Y. Cai, G. Jiang, J. Liu, Q. Zhou, Multiwalled carbon nanotubes as a solid-phase extraction adsorbent for the determination of bisphenol A, 4-n-nonylphenol and 4-tert-octylphenol, *Analytical Chemistry*, 2003, 75, 2517-2521
- [54] H. Y. Niu, Y. Q. Cai, Y. L. Shi, F. S. Wei, J. M. Liu, G. B. Jiang, A new solid-phase extraction disk based on a sheet of single-walled carbon nanotubes, *Analytical and Bioanalytical Chemistry*, 2008, 392, 927-935
- [55] L. M. Ravelo-Pérez, A. V. Herrera-Herrera, J. Hernández-Borges, M. Á. Rodríguez-Delgado, Carbon nanotubes: Solid-phase extraction, *Journal of Chromatography A*, 2010, 1217, 2618-2641
- [56] A. V. Herrera-Herrera, M. Á. González-Curbelo, J. Hernández-Borges, M. Á. Rodríguez-Delgado, Carbon nanotubes applications in separation science: A review, *Analytica Chimica Acta*, 2012, 734, 1-30
- [57] K. Pyrzyńska, Carbon nanotubes as sorbents in the analysis of pesticides, *Chemosphere*, 2011, 83, 1407-1413
- [58] Q. Liu, J. Shi, J. Sun, T. Wang, L. Zeng, G. Jiang, Graphene and graphene oxide sheets supported on silica as versatile and high-performance, adsorbents for solid-phase extraction, *Angewandte Chemie*, 2011, 50, 5913-5917
- [59] Q. Liu, J. Shi, G. Jiang, Applications of graphene in analytical sample preparation, *Trends in Analytical Chemistry*, 2012, 37, 1-11

- [60] C. M. Hussain, S. Mitra, Micropreconcentration units based on carbon nanotubes (CNT), *Analytical and Bioanalytical Chemistry*, 2011, 399, 75-94
- [61] R. Sitko, B. Zawisza, E. Malicka, Graphene as a new sorbent in analytical chemistry, *Trends in Analytical Chemistry*, 2013, 51, 33-43

Recovery of zinc(II) from chloride solutions using hollow fibre contactor with pyridine derivates extractant

*Aleksandra Wojciechowska¹, M. Teresa A. Reis², M. Rosinda C. Ismael², Irmina Wojciechowska¹, Karolina Wieszczycka¹, Jorge M.R. Carvalho²

¹Poznan University of Technology, Institute of Chemical Technology and Engineering, Berdychowo St. 4, 60-965 Poznan, POLAND

²CERENA – Centre for Natural Resources and the Environment, Department of Chemical Engineering, Instituto Superior Técnico, Universidade de Lisboa, Av. Rovisco Pais, 1049-001 Lisboa, PORTUGAL

e-mail: aleksandra.w.wojciechowska@doctorate.put.poznan.pl

Keywords: *extraction, membrane process, zinc recovery, pseudo-emulsion hollow fiber strip dispersion (PEHFSD), pyridine derivates*

ABSTRACT

The extraction of zinc(II) ions from chloride solutions through pseudo-emulsion based membrane strip dispersion (PEHFSD) using pyridine derivates as the extractants was investigated. The metal ions transport was investigated as a function of various experimental variables: type of compound in the organic phase and the initial metal concentration in the feed phase. The overall mass transfer coefficient of permeation was calculated from the experimental data, the values being found in the range of 2.5×10^{-7} – 1.1×10^{-6} m/s. The recovery of Zn(II) in the stripping solution (H₂O or 5% Na₂SO₄) was around 70-80% for most conditions tested.

INTRODUCTION

Hollow fiber membranes (HF), originally was developed in the 1960s for reverse osmosis applications. They have been used in a variety of applications in the industry such as degasification of process solutions, separation of carbon dioxide, other gases from flue gas streams and waste water treatment [1]. Moreover the healthcare industry is still the biggest market of hollow fiber membranes for dialyzers for kidney failure [2]. A lot of researchers have studied the application (Tab. 1.) of hollow fiber membrane technology in various operations such as liquid-liquid extraction, gas separation by absorption and stripping, ozonation of water and removal of volatile components from water.

Tab. 1. Application of hollow fiber membranes [3].

Applications of membrane contactor technology
Removal of dissolved oxygen in the microelectronics industry
Removal of carbon dioxide to extend the life of ion exchange beds and improve performance of edi (electrodeionization) technology
Removal of bulk oxygen and nitrogen in the make-up system
Removal of oxygen in the polishing loop to <1ppb
Total gas control to enhance megasonic cleaning technologies
Removal of dissolved nitrogen from blanketed storage tanks
Accurate total control of dissolved gasses at point of use
Removal of voc's from liquids
Humidification of gasses
Degassing inks, developers, photo resists and other emulsions in imaging and photographic markets
Debubbling coating solutions used in paper manufacturing
Carbonation, decarbonation and nitrogenation in the beverage industry

Hollow fiber membrane modules are particularly useful because processes can be easily up-scaled from small volume R&D applications to full-scale production. The same filtration conditions used to optimize R&D experiments or lab scale filtration can be used in full-scale production when the length of the filtration flow path is maintained while filter's surface area is increased by adding more fibers to process large volumes [4,5].

The advantage of the Pseudo-Emulsion Hollow Fiber Strip Dispersion (PEHFSD) technique is connected to membrane extraction process, whereby a single membrane module is carried out simultaneously extraction and re-extraction, the consumption of the extractant is much smaller than in the classical extraction. Pseudoemulsion system is a very promising method for treatment of liquid waste streams with toxic or valuable metal ions [6-9].

In the experiments, as the feed stream is pumped through the membrane cartridge, retentate, including species excluded by the membrane pores, continues through the recirculation loop while the permeate, including solvent and solutes transported through the membrane pores, is collected on the shell side of the cartridge (Fig. 1.).

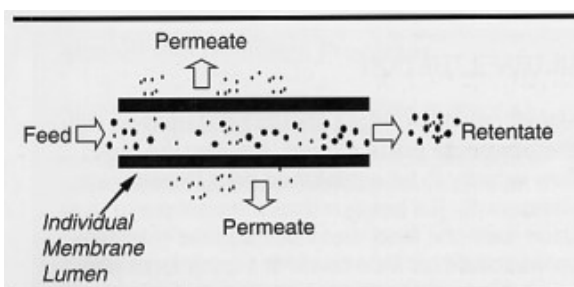


Fig. 1. Mechanism of hollow fiber process (HF).

A number of extractants which remove Zn(II) from chloride solutions have been studied, including pyridine derivatives. The hydrophobic pyridylketoximes have been proposed as a new type of ligands to the selective removal of metal using a liquid-liquid extraction technique [10-14] and as a ligand in membrane transportation of various metal ions [9]. The basic compound, hydrophobic 1-(3-pyridyl)undecan-1-one oxime has been proposed by Wieszczycka [19] as ligands for a selective removal of zinc(II) from multielemental hydrochloride feed solution in liquid-liquid extraction process and for the removal of zinc(II) from chloride solutions using pseudo-emulsion based hollow fiber strip dispersion (PEHFSD). The basic oxime (0.1 mol/L 1-(3-pyridyl)undecan-1-one oxime dissolved in toluene with 10% v/v decan-1-ol) gave better results for lower concentrations of zinc (to 1 g/L) and was more effective at a lower concentration than TBP (2.9 mol/L) [9]. Moreover, the quaternary pyridinium ketoximes were investigated like selective extractants of zinc ions from chloride solutions [15] and molybdenum(VI) from sulfate media [16].

The aim of this work was to study the possibility of using the novel extractants - pyridine derivatives for the recovery of Zn(II) from chloride medium using the PEHFSD technique.

MATERIALS AND METHODS

Reagents

1-(3-pyridyl)undecan-1-one oxime (3PC10), 3-[1-(hydroxyimine)undecyl]-1-propylpyridinium bromide (3PC10-PrBr) and 3-[1-(hydroxyimine)undecyl]-1-propylpyridinium chloride (3PC10-PrCl) (Fig. 2.) (they were used as the carriers for transport experiments) were synthesized according procedure described in previous papers [15-18]. Toluene (ACS reagent, Chem-Lab NV, Belgium) and decan-1-ol (Merck, Germany) were used as components of the organic phase. Sodium chloride (ACS reagent, Panreac, Spain), hydrochloric acid (35%) (AR reagent; VWR, USA); sodium sulfate (ACS reagent, AppliChem, Germany); zinc(II) chloride (anhydrous) (ACS reagent, Chem-Lab NV, Belgium) were used to compose the aqueous phase.

The organic phase used in the extraction studies contained the synthesized compounds (0.1 mol/L) and toluene as a diluent with a 10% (v/v) addition of decan-1-ol.

The aqueous solutions before and after tests were analyzed for zinc(II) concentration by AAS using a Perkin Elmer - AAnalyst 200 at 213 nm in the air-acetylene flame.

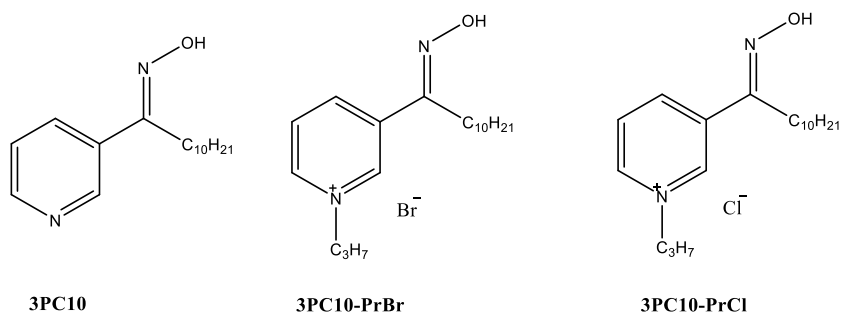


Fig. 2. The synthesized compounds: 1-(3-pyridyl)undecan-1-one oxime (3PC10), 3-[1-(hydroxyimine)undecyl]-1-propylpyridinium bromide (3PC10-PrBr) and 3-[1-(hydroxyimine)undecyl]-1-propylpyridinium chloride (3PC10-PrCl).

Pseudo-emulsion based membrane strip dispersion tests

The PEHFSD experiments were carried out in the Liqui-Cel® Extra-Flow commercial membrane modules (2.5×8 inch) produced by CELGARD (USA)[2]. Diagram of the experimental system is shown in Fig. 3. Further module (contactor G501) details are given in Tab. 2.

The aqueous strip solution was dispersed in the organic solution containing the synthesized extractant reagents, quaternary pyridinium salts. The pseudoemulsion was pumped into the membrane contactor flowing through the shell side of the fibres. While the aqueous feed solution containing zinc(II) ions flowed through inside of the polypropylene fibres. The organic phase wetted the membrane pores and low pressure differential between both phases guarantee the separation of both phases.

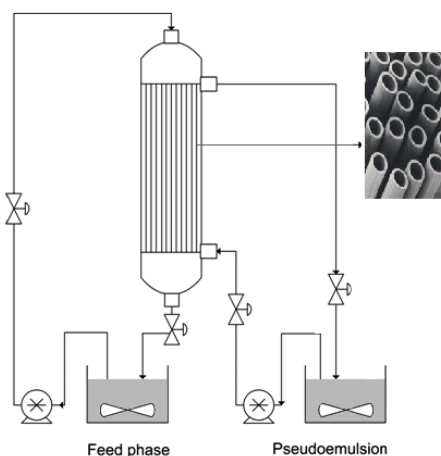


Fig. 3. PEHFSD experimental setup.

The volume of the pseudo-emulsion phase used in the experiments was 800 cm³, 400 cm³ of the organic solution (0.1 mol/L of synthesised compound dissolved in toluene with 10% v/v decan-1-ol) and 400 cm³ of strippant (5% Na₂SO₄ solution). The feed phase (800 cm³), was aqueous solution with appropriate concentration of

Zn(II) ions. All tests were carried out for around 3 h. The samples of feed phase and pseudo-emulsion phases were collected at regular time intervals, during the process. Each experiment was repeated in at least two times for verifying the repeatability of results. The overpressure on the tube side was in the range of 20–40 kPa. Both phases were pumped to the module by two pumps capable of variable flows; the flow rate of the feed phase was kept at ~300 mL/min, whereas the flow rate of the pseudo-emulsion phase was kept at ~260 mL/min. The experiments were conducted at room temperature (typically 22°C).

Table 2. Characteristics of hollow fiber membrane module [3].

Type of module : G501 (contactor)	
Module length (cm)	28
Module diameter (cm)	7.7
Case inner diameter (cm)	5.55
Centre tube diameter (cm)	2.22
Number of fibers	~10,800
Fiber	X50 – polypropylene
Effective fiber length (cm)	15.6
Inner diameter of the fibers (µm)	214
Outer diameter of the fibers (µm)	300
Pore size (µm)	0.03
Porosity (%)	40
Tortuosity	2.6
Inner interfacial area (m ²)	1.13
Area per unit volume (cm ² /cm ³)	28

RESULTS AND DISCUSSION

The same extractants have been also studied on the recovery of Zn(II) in classical liquid-liquid extraction [15,18].

The extraction of the zinc(II) with (3PC10), (3PC10-PrBr) and (3PC10-PrCl) are carried out according to an ion exchange mechanism, where the quaternary pyridinium salts can form ion-pair (anionic chloro-complexes) complexes with ZnCl₃⁻ or ZnCl₄²⁻.

Fig. 4. illustrates the zinc(II) ions concentration profiles in the feed and stripping phases along the permeation. All reagents exhibited similar effects. The removal of the target metal from the solution containing 1 g/L Zn(II) was about 96%, while the recovery yielded around 70%. The extraction rate of zinc(II) was observed to be slightly higher for the 3PC10.

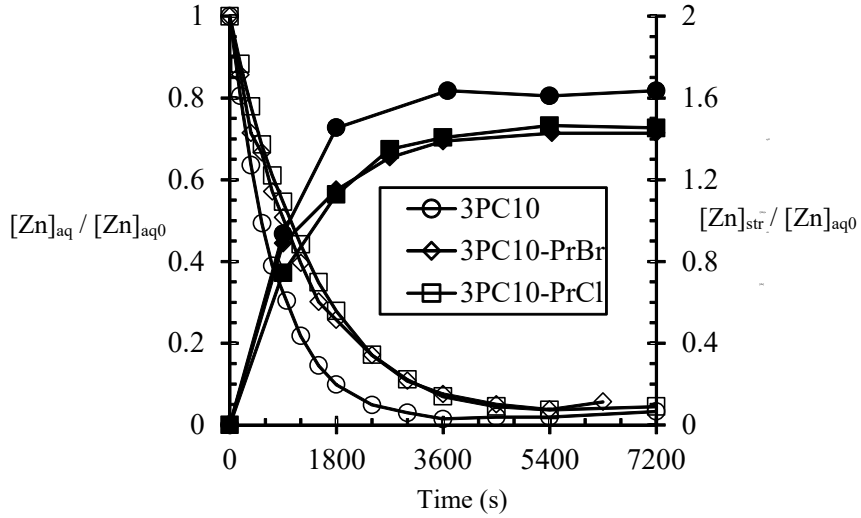


Fig. 4. Zinc(II) concentration profiles in the feed phase (primary axis, $[Zn]_{aq}$) and stripping phase (secondary axis, $[Zn]_{str}$) along the permeation for the 3PC10, 3PC10-PrBr and 3PC10-PrCl extractants (0.1M). Feed phase: 1 g/L Zn(II), 1 mol/L HCl, 1 mol/L NaCl and stripping agent: 5% (m/v) Na_2SO_4 .

Experiments were conducted to check the operation of PEHFSD in different conditions on changing type of extractant, initial concentration of zinc(II) and the contents of NaCl and HCl in the feed solution.

The analysis of the results was made on the basis of the overall mass transfer coefficient of Zn(II) permeation K_p .

The overall mass transfer coefficient of Zn(II) permeation, K_p , was estimated from the experimental data according to the model for the transport in PEHFSD operating in the recycling mode presented elsewhere [9, 19] being given as:

$$K_p = -\frac{u_{aq} r_i}{2L} \ln \left[1 - \left(\frac{S}{Q_{aq}} \right) \right] \quad (1)$$

where the subscript aq refers to the aqueous feed phase, u is the linear velocity, Q is the flow rate, r_i is the inner radius of the fiber, L is the fiber length and S is the slope of the linear relationship obtained from the concentration of zinc in the feed reservoir against time t as follows:

$$V_{aq} \ln \frac{[Zn]_{aq,0}}{[Zn]_{aq}} = St \quad (2)$$

where V is the volume of the phase and 0 refers to the initial value.

Based on the assumption of instantaneous extraction and stripping reactions, the reciprocal of K_p can be related to the resistance in the feed boundary layer (R_{aq})

and to the resistance in the membrane (R_m) by following the resistance in series approach:

$$\frac{1}{K_P} = \frac{1}{k_i} + \frac{r_1}{m k_m r_{lm}} = R_{aq} + R_m \quad (3)$$

where k_i and k_m are the local mass transfer coefficients for the boundary layer in the tube side and the membrane, respectively, r_{lm} is the hollow fiber log-mean radius, and m is the distribution ratio ($[Zn]_{org}/[Zn]_{aq}$).

The plotting of $\ln \frac{[Zn]_{aq,0}}{[Zn]_{aq}}$ against time is shown in Fig. 5., which also displays the

K_P values for the various experiments.

The error associated with the parameter K_P was calculated from errors propagation and data analysis of the linear regression, with a confidence level of 95%. For these experiments, the relative error of K_P was found not to exceed 10%.

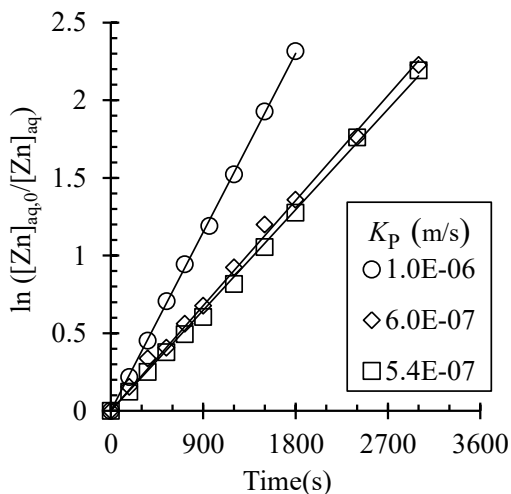


Fig.5. Effect of the initial zinc(II) concentration in the aqueous feed phase on the overall mass transfer coefficient K_P (\circ – 3PC10; \diamond – 3PC10-PrBr; \square – 3PC10-PrCl), Feed phase: 0.3–1 g/L Zn(II), 1 mol/L HCl, 1 mol/L NaCl and stripping agent: 5% (m/v) Na_2SO_4 .

Considering only quaternary salts and comparing them, found that they were slightly worse extractants than 3PC10. The values of the K_P coefficient were found within $5.4\text{--}6.5 \times 10^{-7}$ m/s for 0.3–1 g/L of zinc and decreased significantly to 2.5×10^{-7} m/s, when the initial concentration of zinc was 5 g/L (Fig. 6.). Therefore, the overall mass transfer resistance ought to be increased due to the increase in the membrane resistance because of the significant reduction in the distribution ratio for the highest concentration of zinc and/or the chemical reaction might well contribute to the overall resistance. Even though the K_P values were found quite similar for both extractants, under 0.3 – 1 g/L of zinc in the feed phase, a trend of better results

achieved with the bromide salt was observed. Actually, the equilibrium (data not shown) was favored in the presence of 3PC10-PrBr instead of 3PC10-PrCl. Also, the pseudo-emulsion formed with that extractant showed to be very easily separated after stopping mixing. In fact, the separation time of the phases (0.8 L) was in the range of 50 s – 2 min for around 3 h of continuous agitation.

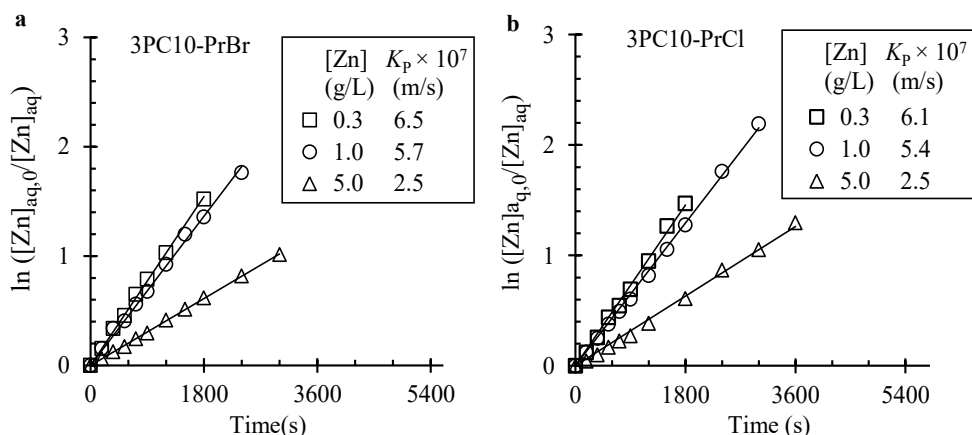


Fig.6. Effect of the initial zinc(II) concentration in the aqueous feed phase on the overall mass transfer coefficient K_p a) for 3PC10-PrBr; b) 3PC10-PrCl. Feed phase: 0.3–1 g/L Zn(II), 1 mol/L HCl and 1 mol/L NaCl.

CONCLUSION

The removal and recovery of metals using the pseudo-emulsion hollow fiber strip dispersion (PEHFSD) technique is a promising alternative to conventional solvent extraction, particularly in the case of dilute solutions. The use of hollow fiber membrane system provide to a lot of information about the effectiveness of the new extractants and their usefulness in the treatment of liquid waste streams with toxic or valuable metal ions. The synthesized extractants: 1-(3-pyridyl)undecan-1-one oxime and its quaternary salts, 3-[1-(hydroxyimine)undecyl]-1-propylpyridinium chloride and 3-[1-(hydroxyimine)undecyl]-1-propylpyridinium bromide showed to be potential carriers of zinc(II) ions from chloride medium by using the pseudo-emulsion hollow fiber strip dispersion technique. The results showed that the selected reagents can recover zinc(II) with the yield above 70%, this result depends on the metal content of the feed phase.

ACKNOWLEDGEMENTS

This work was financed within the Polish National Centre of Science funds according to decision No. DEC-2015/17/N/ST8/00285. Financial support through the project UID/ECI/04028/2013 from the “Fundação para a Ciência e a Tecnologia” (FCT, Portugal) is also acknowledged.

REFERENCES

- [1] Encyclopedia of Life Support Systems (Eolss): v.1 : *Desalination and Water Resources (Desware): Membrane Processes*. Oxford: EOLSS Publishers Co Ltd. 2010
- [2] Zhang Q., Lu X., Liu J., Zhao L., Preparation and Preliminary Dialysis Performance Research of Polyvinylidene Fluoride Hollow Fiber Membranes. *Membranes*. 2015, 5, 120–135. DOI: 10.3390/membranes5010120
- [3] <http://www.liquicel.com>; *Design & Operating Guidelines; 2.5 x 8 EXTRA-FLOW PRODUCT DATA SHEET*
- [4] Wang L., Chen J., Hung Y., Shammas N., *Membrane and Desalination Technologies*. Springer Science & Business Media
- [5] Prasad R., Sirkar K.K., Membrane-based solvent extraction, in: W.S.W. Ho, K.K. Sirkar (Eds.), *Membrane Handbook*, Van Nostrand Reinhold, New York, 1992, 727–763
- [6] Gonzalez R., Cerpa A., Alguacil F.J., Nickel(II) removal by mixtures of Acorga M5640 and DP8R in pseudo-emulsion based hollow fiber with strip dispersion technology, *Chemosphere*. 2010, 81,1164–1169; DOI: 10.1016/j.chemosphere.2010.08.054
- [7] Bey S., Criscuoli A., Figoli A., Leopold A., Simone S., Benamor M., Drioli E., Removal of As(V) by PVDF hollow fibers membrane contactors using Aliquat-336 as extractant, *Desalination*. 2010, 264, 193–200. DOI: 10.1016/j.desal.2010.09.027
- [8] Roy S.C., Sonawane J.V., Rathore N.S., Pabby A.K., Janardan P., Changrani R.D., Dey P.K., Bharadwaj S.R., Pseudo-emulsion based hollow fiber strip dispersion technique (PEHFSD): optimization, modelling and application of PEHFSD for recovery of U(VI) from process effluent, *Separation and Purification Technology*. 2008,43, 3305–3332. DOI: 10.1080/01496390802064141
- [9] Wieszczycka K., Regel-Rosocka M., Staszak K., Wojciechowska A., Reis M.T.A., Ismael M.R.C., Gameiro M.L.F., Carvalho J.M.R., Recovery of zinc(II) from chloride solutions using pseudo-emulsion based hollow fiber strip dispersion (PEHFSD) with 1-(3-pyridyl)undecan-1-one oxime or tributylphosphate, *Separation and Purification Technology*. 2015,154, 204–210 DOI: 10.1016/j.seppur.2015.09.017
- [10] Klonowska-Wieszczycka K., Olszanowski A., Parus A., Zydorcak B., Removal of copper(II) from chloride solutions using hydrophobic pyridyl ketone oximes, *Solvent Extraction and Ion Exchange*. 2009, 27, 50–62, DOI: 10.1080/07366290802544593
- [11] Parus A., Wieszczycka K., Olszanowski A., Zinc(II) ions removal from chloride solutions by hydrophobic alkyl-pyridyl ketoximes, *Separation Science and Technology*. 2012, 48, 319–327, DOI: 10.1080/01496395.2012.688784

- [12] Parus A., Wieszczycka K., Olszanowski A., Cadmium(II) extraction from chloride solutions by hydrophobic pyridyl ketoximes, *Hydrometallurgy* 105 (2011) 284–289, <http://dx.doi.org/10.1016/j.hydromet.2010.10.007>
- [13] Parus A., Wieszczycka K., Olszanowski A., Solvent extraction of iron(III) from chloride solutions in the presence of copper(II) and zinc(II) using hydrophobic pyridyl ketoximes, *Separation Science and Technology*. 2011, 46, 87–93, DOI: 10.1080/01496395.2010.498802
- [14] Wieszczycka K., Wojciechowska A., Krupa M., Equilibrium and mechanism of cobalt(II) extraction from chloride solution by hydrophobic 2-pyridineketoxime, *Separation and Purification Technology*. 2015, 142, 129–136, DOI: 10.1016/j.seppur.2014.12.034
- [15] Wieszczycka K., Wojciechowska A., Krupa M., Kordala-Markiewicz R., Quaternary Pyridinium Ketoximes as Zinc Extractants from Chloride Solutions, *Journal of Chemical & Engineering Data*. 2013, 58, 3207–3215 DOI: 10.1021/je400646z
- [16] Wejman-Gibas K., Wieszczycka K., Wojciechowska A., Ochromowicz K., Pohl P., Extraction of molybdenum(VI) from sulfate media by 3-pyridineketoxime and its quaternary salts, *Separation and Purification Technology*. 2016, 158, 71–79 DOI: 10.1016/j.seppur.2015.11.037
- [17] Wojciechowska A., Wieszczycka K., Wojciechowska I., Olszanowski A., Lead(II) extraction from aqueous solutions by pyridine extractants, *Separation and Purification Technology*. 177 (2017) 239–248; DOI: 10.1016/j.seppur.2016.12.036
- [18] Wieszczycka K., Recovery of Zn(II) from multielemental acidic chloride solution with hydrophobic 3-pyridineketoxime. *Separation and Purification Technology*. 2013, 114, 17–23; DOI: 10.1016/j.seppur.2013.04.002
- [19] Agarwal S., Reis M.T.A., Ismael M.R.C., Carvalho J.M.R., Zinc extraction with Ionquest 801 using pseudo-emulsion based hollow fibre strip dispersion technique, *Separation and Purification Technology*. 2014, 127, 149–56; DOI: 10.1016/j.seppur.2014.02.039

Recovery of iron(III) from chloride solutions

*Aleksandra Wojciechowska, Irmina Wojciechowska, Katarzyna Staszak, Karolina Wieszczycka

Poznan University of Technology, Institute of Chemical Technology and Engineering, Berdychowo St. 4, 60-965 Poznan, POLAND

e-mail: aleksandra.w.wojciechowska@doctorate.put.poznan.pl

Keywords: *liquid-liquid extraction, iron recovery, surface properties, pyridine derivatives, ionic liquids*

ABSTRACT

In this study, the Fe(III) extraction from chloride and chloride/nitrate solution with novel hydrophobic extractants: 1-(3-pyridyl)undecan-1-one oxime and its pyridinium salts: 3-[1-(hydroxyimine)undecyl]-1-propylpyridinium bromide and 3-[1-(hydroxyimine)undecyl]-1-propylpyridinium chloride) were discussed. In this work various factors affecting iron(III) extraction, such as concentration of chloride, mineral acid and metal ions in the aqueous feed solution, as well as the structure and concentration of the extractant were analysed. The surface properties of the various aqueous/organic systems were also determined.

INTRODUCTION

The solvent extraction is one of the most important techniques for the separation and recovery of metals in the industry. The undoubted advantage is the low power consumption and the ability to re-use extractants. This method is attractive from economic and environmental point of view.

The recovery of iron(III) from aqueous solutions is usually carried out by precipitation as jarosite, goethite or hematite. Although the iron removal is mainly achieved by precipitation techniques. The solvent extraction technique also allows the iron(III) removal from acidic aqueous solutions.

The presence of iron in acidic leach of liquor is a common problem in most of the hydrometallurgical processing. Removal of iron from the acidic leach liquors is usually carried out by precipitation and solvent extraction methods[1].

There is a variety of commercial extractants such as Alamine 336 [2-3], Cyanex 272 [4], Cyanex 301 [5], Cyanex 302 [6], Cyanex 923 [7], D2EHPA [4,8], PC88A [3-4], MIBK [3], TBP [9], TOPO [10], TOA [11] and LIX 860 [12] and they potential applications in Fe(III) recovery. From novel extractants, such as pyridine derivatives, 1-(2-pyridyl)tridecane-1-one oxime and 1-(4-pyridyl)tridecane-1-one oxime were also proposed as selective extractants for iron(III) [13]. Although many extractants are known and used in industry, the research of finding new extractants is still very important. The researchers are looking for a new cheaper and more selective extractans, which can be used repeatedly. Pyridineketoximes could be the interesting group of a new extractant agent.

The aim of this work was the synthesis of oxime 1-(3-pyridyl)undecane-1-one and its quaternary pyridinium salts (3-[1-(hydroxyimine)-undecyl]-1-propylpyridinium chloride and 3-[1-(hydroxyimine)-undecyl]-1-propylpyridinium bromide) to determine they they selectivities towards iron(III). Furthermore the surface properties of the various aqueous/organic systems and mass transfer resistances were determined by the Du Noüy ring method with a K12 KRÜSS tensiometer.

MATERIAL AND METHODS

Reagents

The synthesized extractants: 1-(3-pyridyl)undecan-1-one oxime, 3-[1-(hydroxyimine)undecyl]-1-propylpyridinium bromide and chloride (Fig. 1.) were synthesized in several stages reaction and described in a previous papers [14-17].

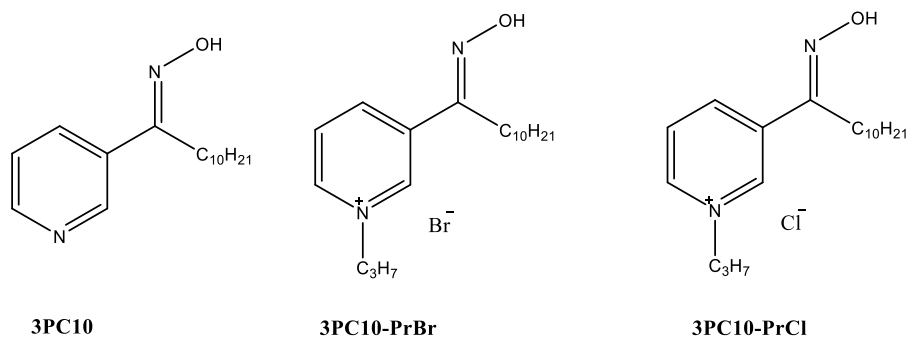


Fig. 1. Structure of studied reagents: 1-(3-pyridyl)undecan-1-one oxime (3PC10), 3-[1-(hydroxyimine)undecyl]-1-propylpyridinium bromide (3PC10-PrBr) and chloride (3PC10-PrCl).

All reagents used in this study were of high purity analytical grade. Toluene (ACS reagent, Chem-Lab NV, Belgium) and decan-1-ol (Merck, Germany) were used as components of the organic phase (toluene: decan-1-ol 9:1). 1-(3-pyridyl)undecan-1-one oxime, 3-[1-(hydroxyimine)undecyl]-1-propylpyridinium bromide (3PC10-PrBr) and 3-[1-(hydroxyimine)undecyl]-1-propylpyridinium chloride (3PC10-PrCl) synthesized with purities 99-99.5% [15,16] and used as the carriers for the transport experiments. Sodium chloride (ACS reagent, Panreac, Spain), hydrochloric acid (35%) (AR reagent; VWR, USA); sodium sulfate (ACS reagent, AppliChem, Germany); zinc(II) chloride (anhydrous) (ACS reagent, Chem-Lab NV, Belgium) were used to compose the aqueous phase. The aqueous solutions were analyzed for iron(III) concentration by AAS using a Hitachi Z 8200 in the air-acetylene flame.

The interfacial tension was measured by the Du Noüy ring method with a K12 KRÜSS tensiometer, with resolution 0.01 mN/m, at a constant temperature 21°C. The deviation between replicate measurements (five times) was in the range 0.03 to 0.18 mN/m. Measurements were made for the aqueous solution/organic phase system at the initial concentration of extractants equal 0.2 M, other solutions were obtained by serial dilution method. Toluene with 10% (v/v) of decan-1-ol was used as

the organic phase, while the aqueous phase was water or the aqueous solutions of 1M HCl with 1M NaCl or 5% Na₂SO₄.

Extraction procedure

Extraction studies were carried out in a test tube using organic to aqueous volume ratio (O/W) equal to 1. Both phases were shaking for 30 minutes at room temperature (21-23°C) using bio-mix BWR04 shaker. Aqueous feed solutions were prepared by dissolving the appropriate amounts of chloride salt of iron(III), chloride or nitrate salts of sodium and lithium in ultrapure water. The research was carried out at a constant chloride ion concentration (4 mol/L) and various hydrochloric acid or sodium chloride concentrations (from 0 to 4 mol/L), at constant concentration of mineral acid (0.5 mol/L HNO₃), $\omega=0.835$. The ionic strength of the aqueous solutions was constant at 4 mol/L and adjusted by an appropriate addition LiNO₃ and NaNO₃. In the experiments the chloride ions concentration was constant at 4M. The concentration of the extractant in the organic phase was 0.1 mol/L, but in experiments in which the influence of the extractant concentration on the iron(III) ions distribution ratio was examined the concentration of ligand was changed from 0.025 to 0.2 mol/L. The stripping of Fe(III) was carried out with 1-10% hydrochloric acid.

Calculations

The Fe(III) content in the organic phase was determined by a mass balance between the concentrations of the metal in the aqueous phases before and after the extraction. Distribution coefficient (D), percentage extractions (%E) and separation factor (β) were calculated from equations:

$$D = \frac{[M]_{org}}{[M]_{aq}} \quad (1)$$

$$\%E = \frac{[M]_{aq}}{[M]_{o,aq}} \quad (2)$$

$$\beta_{Fe/M} = \frac{D_{Fe}}{D_M} \quad (3)$$

Where $[M]_{o,aq}$ represents the initial concentration of metal ions, $[M]_{aq}$ and $[M]_{org}$ are the metal concentration after the extraction in the aqueous and organic phases respectively.

RESULTS AND DISCUSSION

Effect of shaking time

The extraction studies of Fe(III) ions extraction were carried out by equilibrating the aqueous feed containing 0.01 mol/L FeCl₃, 4 mol/L HCl with 0.1 mol/L of extractants (3PC10/ 3PC10-PrBr/ 3PC10-PrCl) dissolved in toluene with 10%(v/v) addition of decan-1-ol. The tests time range was between 5 and 60 minutes. As shown in Fig. 2. the maximum iron(III) extraction with 3PC10-PrBr was around 70%. The optimal time for the process is 30 minutes. It was also noted, that the organic and aqueous phases separation after extraction was very fast and emulsion was not observed.

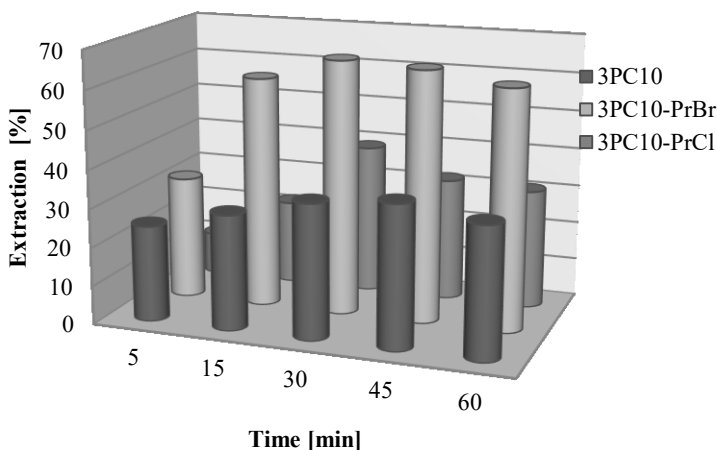


Fig. 2. Effect of contact time on Fe(III) ions extraction, [Fe³⁺] = 0.01 mol/L; [HCl] = 4 mol/L; [L] = 0.1 mol/L.

The effect of the metal ions concentration on the extraction was studied using the aqueous solutions containing constant concentration of HCl (4 mol/L) and different in the range of Fe(III) concentration, ranged in 0.001-0.2 mol/L and 4 mol/L HCl with 0.1 mol/L of ionic liquids dissolved in toluene with 10%(v/v) addition of decan-1-ol. It was observed that (Fig. 3.) for all studied extractants the recovery extraction of Fe(III) decreases with increasing metal concentration from 36 to 25% (3PC10), from 64 to 27% (3PC10-PrBr) and from 42 to 24 (3PC10-PrCl).

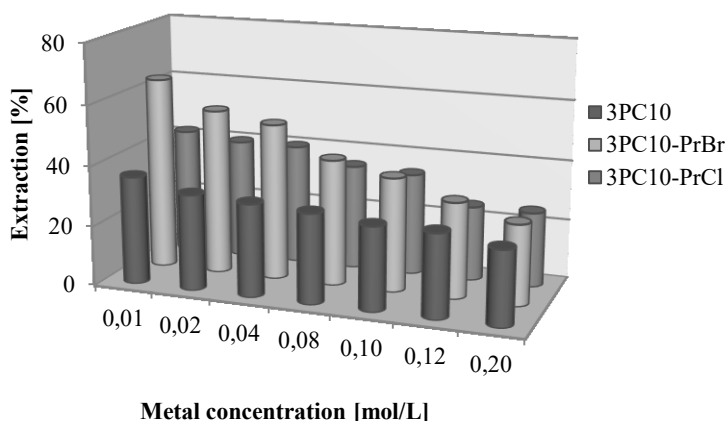


Fig. 3. Influence of metal concentration on extraction process, $[Fe^{3+}] = 0.01 - 0.2 \text{ mol/L}$; $[HCl] = 4 \text{ mol/L}$; $[L] = 0.1 \text{ mol/L}$.

The effect of the extractant concentration on the extraction was studied in the range of 0.025-0.2 mol/L using as the aqueous phase the solution containing 0.01 mol/L Fe(III) and 4 mol/L HCl. Fig. 4. shows that initially extractant concentration ranging between 0.025 and 0.05 mol/L resulted in 10% extraction. Further increase of the extractant concentration increases that parameter and at 0.1 mol/L the extraction was already 40% (3PC10), 70% (3PC10-PrBr) and 55% (3PC10-PrCl).

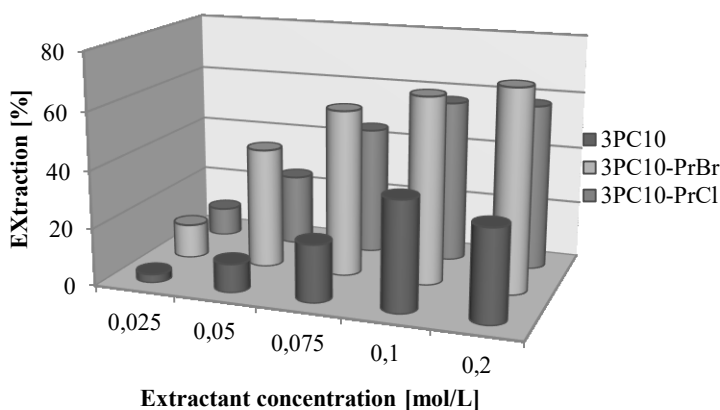


Fig. 4. Influence of extractant concentration on extraction of Fe(III), $[Fe^{3+}] = 0,01 \text{ mol/L}$; $[HCl] = 4 \text{ mol/L}$; $[L] = 0,025 - 0,1 \text{ mol/L}$.

The influence of HCl concentration on the Fe(III) extraction was presented in Fig. 5. It was observed, that the recovery of iron(III) is maintained at a constant level throughout the range of HCl concentrations ($c_{HCl} = 0 - 2 \text{ mol/L}$), extraction efficiency was lower than 10%. Above 3 mol/L concentration of HCl present of extraction increases reaching the maximum at 4 mol/L HCl.

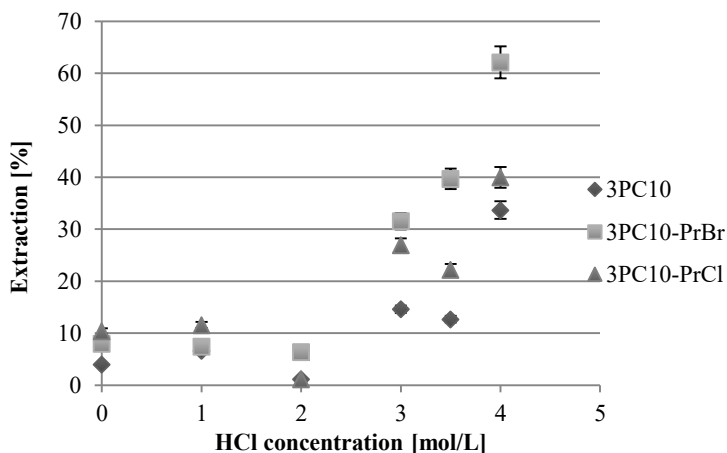


Fig.5. Effect of HCl concentrations on Fe(III) extraction.

The effect of chloride ions concentration on the extraction of iron(III) at a constant water activity of 0.835 and a constant concentration of nitric acid (0.5 M HNO₃) was also studied (Fig. 6.). Using synthesized extractants the extraction is maintained at a constant level throughout the range of chloride concentrations (c_{Cl^-} = 0-2 mol/L), E%=0-20%. The maximum of recovery of Fe(III) ions is observed for the quaternary salt with bromide anion, for which E = 40%.

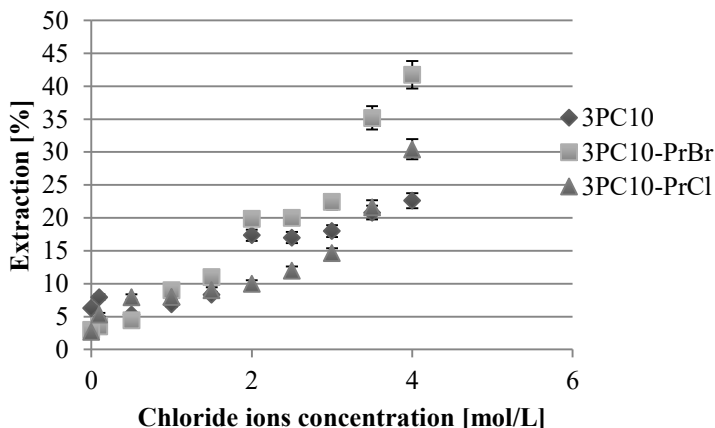


Fig. 6. Influence of chloride ions concentration on Fe(III) extraction ($[Fe^{3+}]$ =0.01 mol/L; $[HNO_3]$ =0.5 mol/L; a_w = 0.835 and $[HL]$ =0.1 mol/L.

Surface properties of extractants

As the extraction reaction in many cases occurs at the interface, the properties of the interface can dramatically influence the equilibrium of the extraction. In the analyzed systems, studied reagents dissolved in toluene with addition 10% (v/v) of decan-1-ol was used as the organic phase, while water, mixture of HCl (1M) and NaCl (1M) and 5% solution of Na₂SO₄ were used as the models aqueous feed and stripping solutions. The results presented in Fig. 7. show that 3PC10 and its chloride (3PC10-PrCl) and bromide (3PC10-PrBr) salts adsorb at the liquid/liquid interface

and reduce the interfacial tension of all considered systems. However, the obtained results showed a lower interfacial activity of 3PC10 compared with its salts.

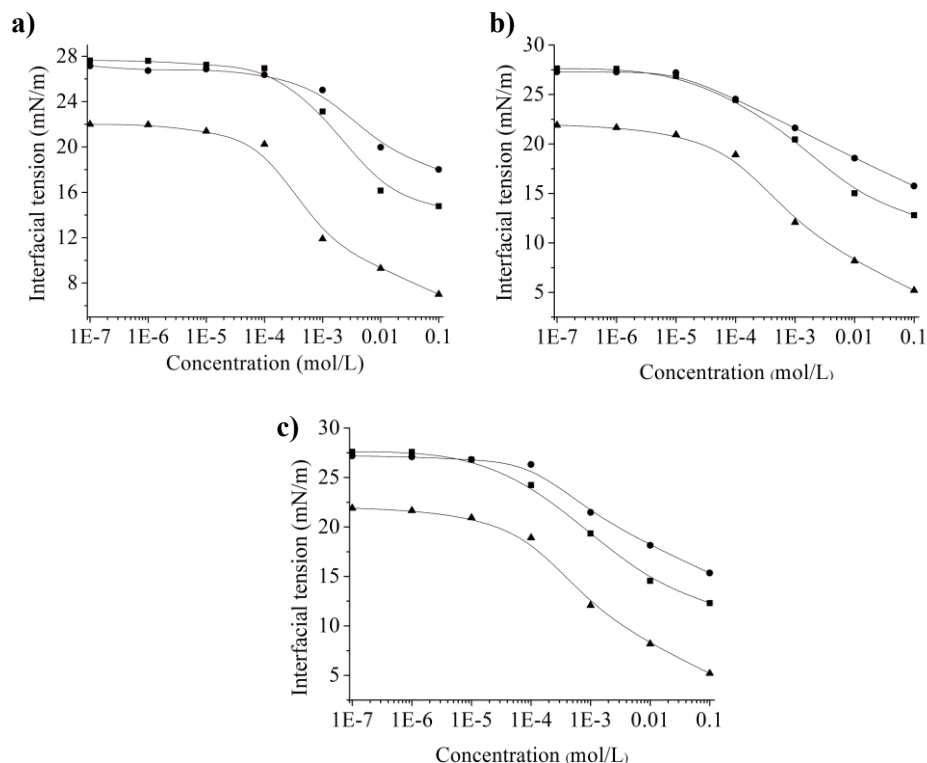


Fig. 7. Interfacial isotherms for 3PC10 (a), 3PC10-PrCl (b), and 3PC10-PrBr (c), in systems with
 • - water, ■ - 5% Na₂SO₄, ▲ - 1 M HCl + 1 M NaCl as aqueous phase.

CONCLUSION

The obtained results showed that extraction of Fe(III) strongly depended on the composition of the aqueous feed solutions. Especially, in the case of the aqueous solutions containing 4 mol/L HCl, 4 mol/L NaCl and 0.5 mol/L HNO₃ the extraction of Fe(III) was the most efficient. The interfacial isotherms for the studied extractants are also presented, but the presented results did not explain why the 3PC10-PrBr is much more efficient extractant than other considered reagents.

ACKNOWLEDGEMENTS

This work was financed within the Polish National Centre of Science funds according to decision No. DEC-2015/17/N/ST8/00285. Financial support through the 03/32/DS-PB/0701 grant was also acknowledged.

REFERENCES

- [1] Ritcey G.M., Solvent Extraction in Hydrometallurgy: Present and Future, *Tsinghua Science and Technology*, 2006,137-152
- [2] Mishra R.K., Rout P.C., Sarangi K., Nathsarma K.C., Solvent extraction of Fe(III) from the chloride leach liquor of low grade iron ore tailings using Aliquat 336, *Hydrometallurgy*, 2011, 108, 93–99 DOI: 10.1016/j.hydromet.2011.03.003
- [3] Lee M.S., LeeK.J., Separation of iron and nickel a spent FeCl₃ etching solution by solvent extraction, *Hydrometallurgy*, 2005, 80, 163-169 DOI: 10.1016/j.hydromet.2005.06.010
- [4] Sandhibigraha, A., Sarma, P.V.R.B., Chakravorty, V., Solvent extraction of iron(III) from aqueous hydrochloric acid solutions using D2EHPA, PC 88A and Cyanex 272 and their mixtures, *Scandinavian Journal of Metallurgy*, 1996, 25,135–140
- [5] Ocio A., Elizalde M.P., Iron(III) Extraction from Phosphoric Acid Solutions by Cyanex 301, *Solvent Extraction and Ion Exchange*, 2011, 29, 337-362 DOI: 10.1080/07366299.2011.573431
- [6] Biswas R.K., Ali R., Karmakar A.K, Asadujjaman M., Extraction by Cyanex 302 and Spectrophotometric Estimation of Fe(III), *Journal of Applied Spectroscopy*, 2014, 80, 983–990 DOI: 10.1007/s10812-014-9876-y
- [7] Saji J.,Prasada Rao T., Iyer C.S.P., Reddy M.L.P., Extraction of iron(III) from acidic chloride solutions by Cyanex 923, *Hydrometallurgy*, 1998, 49, 289–296 DOI: 10.1016/S0304-386X(98)00030-9
- [8] Singh D.K., Kartikey K. Yadav, Singh H., Extraction and Stripping Behavior of Iron (III) from Phosphoric Acid Medium by D2EHPA Alone and Its Mixtures with TBP/TOPO, *Separation Science and Technology*, 2013, 48, 1556-1564 DOI: 10.1080/01496395.2012.753084
- [9] Azizitorghabeh A., Rashchi F., Babakhani A., Noori M., Synergistic extraction and separation of Fe(III) and Zn(II) using TBP and D2EHPA, *Separation Science and Technology*, 2017, 52, 476-486, DOI: 10.1080/01496395.2016.1250778
- [10] Hariharan A.V.L.N.S.H., Sudhakar C., Srinivasanaidu A., Solvent Extraction of Iron(III) by Tri-n-Octyl Phosphine Oxide, *Journal of Chemical and Pharmaceutical Research*, 2011, 3, 945-950
- [11] Južnič K., To the Extraction of Fe (III) from Hydrochloride Media with TOA in Benzene, *Radiochimica Acta*, 1971, 16, 51-53 DOI: 10.1524/ract.1971.16.1.51
- [12] Simpson J., Navarro P., Alguacil F. J., Iron(III) extraction by LIX 860 and its influence on copper(II) extraction from sulphuric solutions, *Hydrometallurgy*, 1996, 42, 13-20, DOI: 10.1016/0304-386X(95)00078-U
- [13] Parus A., Wieszczycka K., Olszanowski A., Solvent Extraction of Iron(III) From Chloride Solutions in the Presence of Copper(II) and Zinc(II) Using Hydrophobic Pyridyl Ketoximes, *Separation Science and Technology*, 2010, 46 87–93 DOI: 10.1080/01496395.2010.498802

- [14] Wieszczycka K., Regel-Rosocka M., Staszak K., Wojciechowska A., Reis M.T.A., Ismael M.R.C., Gameiro M.L.F., Carvalho J.M.R., Recovery of zinc(II) from chloride solutions using pseudo-emulsion based hollow fiber strip dispersion (PEHFSD) with 1-(3-pyridyl)undecan-1-one oxime or tributylphosphate, *Separation and Purification Technology*. 2015, 154, 204–210
DOI: 10.1016/j.seppur.2015.09.017
- [15] Wieszczycka K., Wojciechowska A., Krupa M., Kordala-Markiewicz R., Quaternary Pyridinium Ketoximes as Zinc Extractants from Chloride Solutions, *Journal of Chemical & Engineering Data*. 2013, 58, 3207–3215
DOI: 10.1021/je400646z
- [16] Wojciechowska A., Wieszczycka K., Wojciechowska I., Olszanowski A., Lead(II) extraction from aqueous solutions by pyridine extractants, *Separation and Purification Technology*. 177 (2017) 239–248; DOI: 10.1016/j.seppur.2016.12.036
- [17] Wejman-Gibas K., Wieszczycka K., Wojciechowska A., Ochrowicz K., Pohl P., Extraction of molybdenum(VI) from sulfate media by 3-pyridineketoxime and its quaternary salts, *Separation and Purification Technology*. 2016, 158, 71–79 DOI: 10.1016/j.seppur.2015.11.037

Tapered long- period fiber gratings made by filament heating

*Renata Wonko¹, Leszek R. Jaroszewicz¹

¹Institute of Applied Physic, Military University of Technology, 2 St. Kaliskiego, 01-476 Warsaw, POLAND

e-mail: renata.wonko@wat.edu.pl

Keywords: Long- period fiber gratings, LPFG, filament heating, resonant peak, point-by-point method

ABSTRACT

In the recent years, the long- period fiber gratings are the object of research in the field of fiber optic sensors based on different configurations. Such structures give possibility to detect temperature, banding, stress or surrounding refractive index change by observing variation in the LPFG transmittance characteristic. In this paper we propose tapered LPFGs fabrication on two types of single-mode fibers: SMF28 and Nufern 1550B-HP-80. The LPFGs were made by filament heating using point-by-point method. The parameters which have been changed was: period, number of periods and technical parameters of filament. The analysis of attenuation bands was carried out by observing transmission spectrum.

INTRODUCTION

The long- period fiber gratings (LPFGs) are the few centimeters of the optical fiber in which the core is subjected of the periodical modulation of the refractive index. The refractive modulation facilitates the coupling of fundamental mode which propagates in the core of fiber to different higher order modes propagating in the cladding of the fiber. Such phenomena results of series of attenuation dips in the transmission spectrum at discreet wavelength what is well described as coupled- mode theory (CMT) [1-4]. LPFGs are related to fiber Bragg gratings, however in terms of LPFGs the period of refractive index modulation should be in the range from 100 μm to 1000 μm . The study of the transmission spectrum of LPFG and behavior of attenuation peaks with change in various physical parameters broadened the optical fiber field both in communication, as well as sensing [5-7].

Generally, the main method to obtain such structures is to expose bare fiber to high - energetic UV laser, where introduces stress in material creates periodical perturbation of refractive index. However, laser implementation requires the using of photosensitive types of optical fibers. Rewarding alternative is to use non-UV laser technique or make series of tapers which lead to obtain LPFG structures [8]. The arc - induce technique of LPFGs has been already reported [9]. This method bases on stress relaxation enabled by the using of optical splicer, where microbends are introduced into the fiber structure. The use of commercially available splicer requires an additional set - up with build - in motors.

In this paper we demonstrate tapered LPFGs fabrication using filament heating, where a particular feature is the homogenous heating of the cylindrical optical fiber. We have studied an influence of the technical parameters of the filament heating for the shape of the transmission spectrum. We have also compared a spectral characteristic of two different types of fiber.

METHODS

The experimental set- up

The series of the adiabatic tapers were made on the experimental set - up of tapered LPFGs, which is shown in the Fig. 1a. We have employed a glass processing platform GPX-3400 (Vytran), which has built-in graphite filament as an resistive heat source. The range of the fiber holding blocks movement is ± 90 mm and this enables to precision shifting of the fiber to manufacture the another biconical tapers. The proposed configuration eliminated concerns of the introductions of unexpected stresses. The processed fiber was illuminated by the broadband light source (SuperK EXTREME - NKT Photonic). To control transmission characteristics, we have used optical spectrum analyzer OSA (YOKOGAWA AQ6376) with the span 1200 nm - 2400 nm and resolution 0.1 nm.

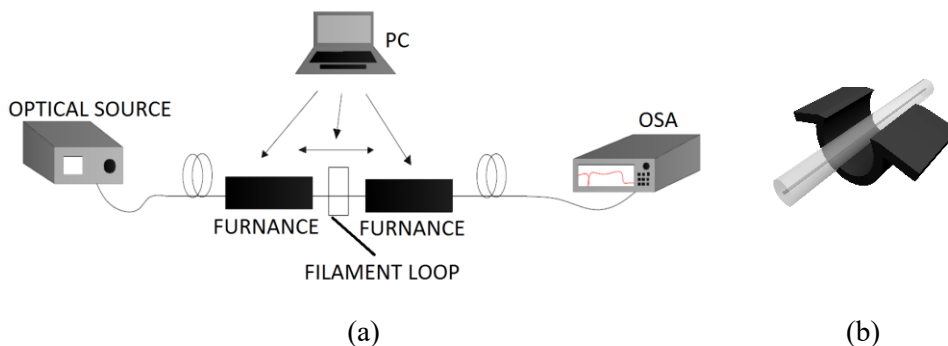


Fig. 1. The set- up for tapered LPFGs fabrication (a) and the “Omega”- shaped filament (b).

In the first step of the LPFG fabrication the fiber was placed on the fiber holder blocks (FHB), while the bare part of fiber was exposed on the filament. In order to achieve the symmetric tapers we used the “Omega”- shaped filament (Fig. 1b). After a single drawing of fiber, the furnaces was displacement by a predetermined value which is identified with the period (Λ) of LPFG. Although after each drawing of the tapers, fiber was abandoned for several second to cooled down. The whole process took place under the cover of argon and we have set gas flow rate of 0.35 l/min. The method describe above is named point-by-point method and is commonly use in arc - technique LPFGs.

The theoretical background

The result of LPFG fabrication is the attenuation peaks, which the position is strictly depended of the change of refractive index in the place of the taper. A technically approach of the refractive index change is explained by the thermal diffusion of the silica dopant. Therefore, coupling between fundamental mode and higher order modes occurs at specific resonant wavelength which satisfies phase matching condition according to the following equation:

$$\lambda_{res} = (n_{cor} - n_{clad})\Lambda \quad (1)$$

where the n_{cor} and n_{clad} are respectively the effective refractive index of the core mode the coupled cladding mode and Λ is period of LPFG.

The coupled - mode theory claims that the resonant peaks are determined by the coupling coefficient, which is a function of index change and modal overlap between the guided mode and cladding modes in the fiber [10]. Taking into account our case, where change of refractive index is obtain by the local release of the mechanical stress, the modulation of refractive index can be express as:

$$\Delta\lambda = \Delta n_{residue} + \Delta n_{taper} \quad (2)$$

where, $n_{residue}$ and Δn_{taper} are respectively the initial refractive index perturbation induced by the residual stress relaxation as a result of the high local temperature and the refractive index perturbation caused by the periodic tapers on the fiber. If the technical parameters of tapers drawing are manipulated (i.e. velocity of taper drawing, power of filament, time of heating), the $\Delta n_{residue}$ and Δn_{taper} can be control.

RESULT AND DISCUSSION

In this experiment we studied the influence of the taper amounts on the depth of the resonant peaks for two types of optical fibers: single-mode SMF28 and single-mode Nufern 1550B-HP-80. We have also determined the impact of the velocity to the transmittance profile of the LPFG.

The geometry of tapers for the both studied types of fiber was established 0.2x0.3x0.2, where 0.2 respectively is transition region and 0.3 is taper waist. The diameter of tapers was 100 μm for SMF28 and 70 μm for 1550B-HP-80. We have conducted several experiments with another diameters, however adoption of smaller diameter resulted in homogenize of the tapers. On the other hand, bigger dimension of taper caused insufficient change in refractive index. We have established the power of filament of 50 W for SMF28 and 95 W for 1550B-HP-80.

In the Fig. 2 we have demonstrated the transmission spectrum of the LPFG made on SMF28 with the diameter of cladding equal to 125 μm . The following spectrums correspond to different velocity of the taper drawing. In each cases number of periods of the LPFGs was equal to 18.

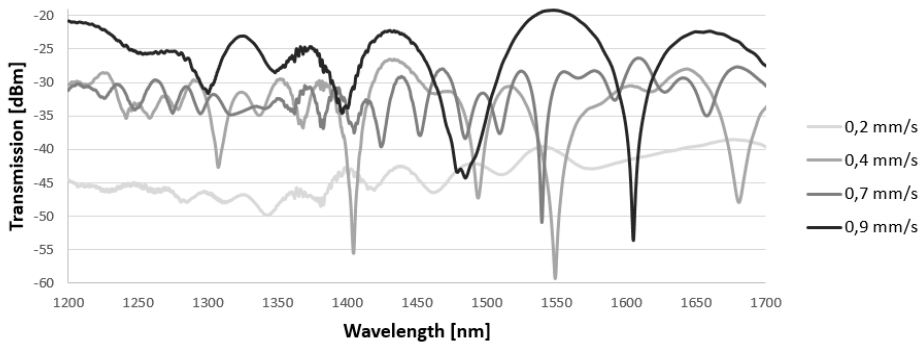


Fig. 2. Transmission spectrum profiles for the different velocity of the tapers of the LPFG based on single-mode fiber SMF28.

It can be noticed that for lower velocity of the taper drawing resonance effect is distributed. This may be due to impaired process of the dopant diffusion. The spectrum transmissions for higher than 0.9 mm/s velocity of furnaces movement have not been shown because of the destruction of the grating structures. The optimum taper drawing was established as 0.9 mm/s. This value was used in the following part of the work.

A section of the LPFG with different number of periodic tapers is shown in Fig. 3. The fabricated LPFGs were characterized by the period amount to $400 \pm 5 \mu\text{m}$.

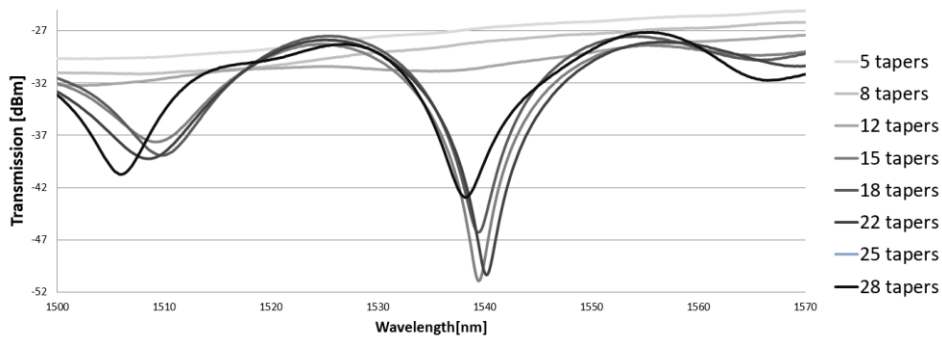


Fig. 3. Transmission spectrum profiles of the LPFG based on single-mode fiber SMF28.

The attenuation of main peak amounts to -22.8 dBm at resonant wavelength of 1540.2 nm and the optimum number of periods equilibrated with 18 tapers. Appearance of resonant peak shifting can be induced by the characteristics recording in the different temperature. It was mentioned above that LPFGs are sensitive to the temperature changes.

The conducted research on single-mode fiber with diameter of cladding of 80 μm are shown on Fig. 4. We have produced LPFG with period amounts to $400 \pm 5 \mu\text{m}$.

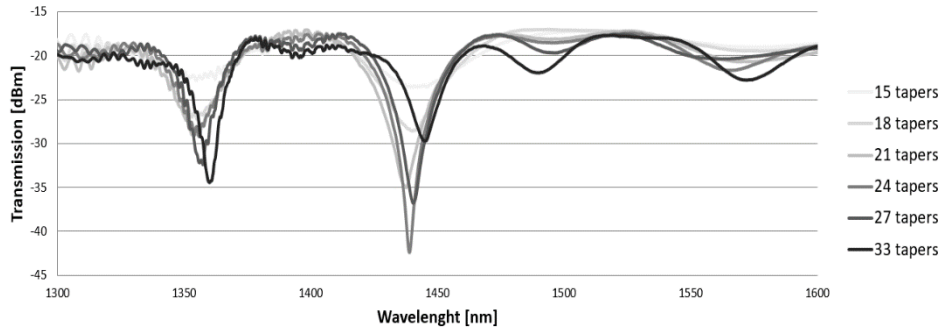


Fig. 4. Transmission spectrum profiles of the LPFG based on single-mode fiber 1550B-HP-80.

The attenuation depth of main resonant peak amounts to -24.5 dBm at resonant wavelength of 1438.8 nm, wherein the optimum number of tapers was determined on 24 periods. In this case, resonant peak shifts toward longer wavelength with increasing number of periods. Other peaks seen on spectrum profile correspond to coupling of fundamental mode with lower cladding modes.

CONCLUSION

It has been demonstrated that fabrication of LPFGs using resistive filament heating can be the satisfactory alternative for the UV- laser or the arc- induced technique. Within the confines of this work we have established the technological parameter for both single-mode fibers, especially the velocity of the tapers drawing as 0.9 mm/s. The benefits of the obtain fiber structures are short length, as well as large attenuation peak. The main resonant peak for the LPFG made on 1550B-HP-80 fiber is shifting toward shorter wavelength in contrast to conventional SMF28. This phenomenon is profitable for the further sensing applications. The high integrated platform to the fiber processing enables to produce the desire LPFG. The LPFG devices are applied as an optical sensor, where change of temperature, stress or surrounding refractive index caused shifting of resonant peak.

ACKNOWLEDGEMENTS

This work was supported by the Ministry of Science and Higher Education as a statutory activity PBS - 654.

REFERENCES

- [1] Raikar U. S., Lalasangi A. S., Akki J. F., Raikar P., Manohar K. G., Srinivas T., Badiger N. M., Radhakrishnan P., Cd concentration sensor based on fiber grating technology, *Sensors and Actuators B*, 2012, 161, 818-823; DOI: 10.1016/j.snb.2011.11.039

- [2] Erdogan T., Cladding-mode resonances in short- and long-period fiber grating filters, *J. Optical Society of America A*, 1997, 14, 8, 1760-1773; DOI: 10.1364/JOSAA.14.001760
- [3] Akki J. F., Lalasangi A. S., Raikar P. U., Srinivas T., Laxmeshwar L. S., Raikar U. S., Core-cladding mode resonances of long period fiber grating in concentration sensor, *IOSR Journal of Applied Physics*, 2013, 4, 3, 41-46; DOI: 10.9790/4861-0434146
- [4] MacDougall T. W., Pilevar S., Haggans C. W., Jackson M. A., Generalized expression for the growth of long period gratings, *IEEE Photon Technol Lett*, 1998, 10, 10, 1449-1551, DOI: 10.1109/68.720290
- [5] Bhatia V., Applications of long-period gratings to single and multi-parameter sensing, *Optics Express*, 1999, 4, 11, 457-466, DOI: 10.1364/OE.4.000457
- [6] Kashyap R., Fiber Bragg Gratings Optics and Photonics Series, *Elsevier Science*, 2009
- [7] Mizunami T., Ishida Y., Yoshikura Sh., Long-Period Fiber-Grating Temperature Sensors in Ge-B-Codoped Fibers with Temperature/Strain Discrimination, *Japanese Journal of Applied Physics*, 2008, 47, 8S1, 6833-6837
DOI: 10.1143/JJAP.47.6833
- [8] G. Xijia, M. Waleed, Q. Li, P. W. E. Smith, All-Fiber Laser Beam Shaping Using a Long-period Grating, *IEEE Photonics Technology Letters*, 2008, 20, 13, 1130 – 1132, DOI: 10.1109/LPT.2008.924640
- [9] S-Y. Tan, Y-Th. Yong, Sh-Ch., Fa. Abd-Rahman Lee, Review on an arc-induced long-period fiber grating and its sensor applications, *Journal of Electromagnetic Waves and Applications*, 2015, 29, 6, 703-726
DOI: 10.1080/09205071.2015.1021019
- [10] Zhu Y., Shum P., Chong J.-H., Rao M. K., Lu C., Deep-notch, ultracompact long-period grating in a largemode-area photonic crystal fiber, *Optic Letters*, 2003, 28, 24, 2467-2469 , DOI: 10.1364/OL.28.002467

Abstracts

Building a Mobile Liquid Nitrogen Generator

*Paweł Antkowiak, Patryk Baran, Michał Fedoryk, Radosław Krzosa, Michał Wojtalik

Scientific Supervisors: Anna Jackiewicz PhD, Piotr Machniewski PhD
Faculty of Chemical and Process Engineering, Warsaw University of Technology,
Warsaw, POLAND

Scientific Club of Chemical and Process Engineering, Faculty of Chemical and
Process Engineering, Warsaw University of Technology, Warsaw, POLAND

e-mail: pawel.antkowiak.pw@gmail.com

Keywords: *liquid nitrogen, Linde cycle,*

Building miniaturized installations to liquefy gases using Linde method can be an alternative method to currently available liquefiers with Stirling engines. Their construction is simpler and cheaper than precisely made Stirling coolers while ensuring high efficiency of liquefaction. This installation is scientific and research object but with vacuum isolation and more effective compressor it can be successfully utilize in medicine and industry.

The research was focused on technical and process aspects of running the installation. The major identified difficulties were separating compressor oil from liquefied gas, separating nitrogen from the air to desired purity and proper insulation of the system, as well as reducing its heat capacity. Additional research was conducted in order to verify a possibility of using unidimensional numerical simulations for analyzing operational parameters of countercurrent heat exchanger. Possible technical solutions improving condensate separation and construction of a countercurrent heat exchanger were also indicated.

Miniaturized installations utilizing Linde cycle can be successfully used for liquefying gases with relatively low cost. However, installation is more difficult to operate and more demanding than available solutions based on a Stirling engine. Moreover, frequent and regular maintenance of the device is necessary (the gas purification system and a high pressure compressor were found to be the most problematic).

Sorption properties of mesoporous ZSM-5 and BEA zeolites

*Kamila Brylewska^{1,2}, Magdalena Król¹, Kamil Kornaus¹, Tomasz Bajda³, Włodzimierz Mozgawa¹

¹Faculty of Materials Science and Ceramics, AGH University of Science and Technology, Krakow, POLAND

²Faculty of Chemistry, Jagiellonian University, Krakow, POLAND

³Faculty of Geology, Geophysics and Environmental Protection, AGH University of Science and Technology, Krakow, POLAND

e-mail: kamilaaa@agh.edu.pl

Keywords: *zeolites, sorption, heavy metals, mesoporosity, IR spectroscopy*

Zeolites are widely used in industry and environmental protection. This kind of materials plays a special role in environment protection, as sorbents of heavy metals. Zeolites are microporous crystalline aluminosilicates which structure consists of [SiO₄] and [AlO₄] tetrahedrons. Their structure is often modified to obtain mesoporous and macroporous structure. The first are usually obtained by post-synthesis modification: desilication in the presence of bases or dealumination in the presence of acids. That allows to obtain better diffusion of the reagents and improvement the sorption properties of materials. For this reason, the aim of the research was to investigate the influence of generated system of mesopores on the sorption properties of zeolites.

In the studies ZSM-5 and BEA zeolites were used. Zeolites were treated with NaOH&TBAOH mixture and NaOH solution. On this materials, the sorption of Pb²⁺, Cd²⁺ and Cr³⁺ ions was carried out. The following methods were used: XRF (chemical composition), XRD (phase composition), AAS method (the concentrations of analyzed ions in aqueous solutions before and after sorption), IR and Raman spectroscopy (structural studies), BET (surface area).

Studies have shown that it is possible to generate a system of mesopores during proposed method. The effective cation exchange capacity and the domination of one of the mechanisms of sorption depends on the type of zeolite structure, Si/Al ratio or concentration of cations in the insert solution. Sorption of cations resulted in the changes in the IR spectrum. A slight change in the intensity of the bands caused by the introduction of heavy metal cations was connected with ring bands. Depending on the type of cation and zeolite, changes also the intensity and the location.

Studies have shown that zeolites can have potential use as sorbents for heavy metals.

Acknowledgement

This work was financed by Grant No. 2016/21/N/ST8/01332 from the National Science Centre, Poland.

Polymer nanospheres with isoniazid preparation and antituberculosis activity studies

*Monika Budnicka¹, Agnieszka Gadomska-Gajadur¹, Paweł Ruśowski¹

¹Technological Processes Laboratory, Faculty of Chemistry, Warsaw University of Technology, Warsaw, POLAND

e-mail: mbudnicka@ch.pw.edu.pl

Keywords: *nanospheres, emulsion solvent evaporation method, drug delivery system, isoniazid, tuberculosis*

Tuberculosis again poses a threat to society, not only in third world countries, but also in developed countries of Europe and North America. Tuberculosis treatment requires high doses of antitubercular drugs and in many cases is ineffective. The development of a cost-effective, short-term, safe and comfortable therapy is desired. In response to the needs in many research centres, extensive studies on drug delivery systems (DDS) containing substances already used for the treatment of tuberculosis, have started. Nanocarriers of active substances - one of DDS forms are of great interest. Polymer nanospheres are promising form. Due to the small size they can be administered intravenously without the risk of blood clots, easily penetrate the smallest capillaries, tissues and cells.

The aims of this study were to obtain a polymer nanospheres containing isoniazid (INH), to determine the effect of input variables on the process of encapsulation, then to determine INH antitubercular activity in the polymer matrix. A method of nanospheres preparation emulsion solvent evaporation was selected, due to its simplicity, lack of sophisticated equipment and the possibility of obtaining spheres of relatively small size.

Poly (L-lactide), poly (DL-lactide), lactide and ϵ -caprolactone block copolymer and polycaprolactone were used as polymer nanospheres matrix. Isoniazid was used as active pharmaceutical ingredient (API), evenly incorporated in polymeric matrix. The impact of agitation rate and the tacticity of the polylactide on obtained nanospheres size was examined. Activity assays of polymer nanospheres using *M. tuberculosis* bacteria were performed.

Poly(L-lactide), poly (DL-lactide), a lactide and ϵ -caprolactone block copolymer, polycaprolactone nanospheres with INH were received. A sphere diameter did not exceeded 270 nm in all cases. The greater agitation rate, the bigger size of obtained nanospheres. It was noted that the more D entities content in polylactide, the larger size of the obtained spheres. The resulting polymer nanospheres have antitubercular activity.

Synthesis of nanohydroxyapatite using microwave energy

*Agnieszka Chodara¹, Sylwia Kuśnieruk¹, Tadeusz Chudoba¹, Jacek Wojnarowicz¹, Witold Łojkowski^{1,2}

¹Laboratory of Nanostructures, Institute of High Pressure Physics, Polish Academy of Sciences, Sokolowska Street 29/37, 01-142 Warsaw, Poland

²Białystok University of Technology, Faculty of Management, Białystok, Poland
e-mail: chodara.agnieszka@gmail.com

Keywords: *hydroxyapatite, nanopowder, microwaves*

Hydroxyapatite (HAp) is a calcium phosphate compound having a chemical formula $\text{Ca}_{10}(\text{PO}_4)_6(\text{OH})_2$. It is an inorganic component of hard tissues such as bones and teeth. Hydroxyapatite is mostly responsible for its strength and stiffness. It has been used extensively for biomedical applications, because of osteoconductive property and biocompatibility with human body. Hydroxyapatite is using in regenerative medicine e.g. bone implants for regeneration of bone defects.

Nanohydroxyapatite were synthesised by using precipitation method in room temperature and hydrothermal synthesis using microwave reactor MSS2 (Microwave Solvothermal Synthesis). Thanks to the microwave energy we can easily control the grain size of nanoparticles. Obtained nanoparticles were in the range of 8-45 nm grain size. Phase purity was measured using X-ray diffraction. Thanks to scanning electron microscopy (SEM) the morphology of produced nanohydroxyapatite was characterized. The density and specific surface area was determined using helium pycnometry and Brunauer–Emmett–Teller (BET) method.

During research six types of hydroxyapatite with different crystallinity degree and grain size was obtained. Crystallinity is higher with increasing grain size. Wide variety of GoHAPTM can be used in many applications (e.g. implants, scaffold layers).

The Laboratory of Nanostructures is able to synthesize innovative HAp nanoparticles. Thanks to a wide variety of hydroxyapatite grain size crystallinity it can be used in different application depending on desired resorption time of hydroxyapatite. GoHAPTM could be a perfect component of the medical implants thanks to good similarity to the natural apatite.

The effect of substrate temperature on the properties of tungsten boride layers deposited by radio frequency magnetron sputtering and pulsed laser deposition

*Justyna Chrzanowska¹, Dariusz Garbiec², Łukasz Kurpaska³, Piotr Denis¹, Jacek Hoffman¹, Tomasz Mościcki¹, Zygmunt Szymański¹

¹Institute of Fundamental Technological Research, Polish Academy of Sciences, Pawińskiego 5B, 02-106 Warsaw, Poland

²Metal Forming Institute, Jana Pawła II 14, 61-139 Poznan, Poland

³National Centre for Nuclear Research, A. Soltana 7, 05-400 Otwock, Poland

e-mail: jchrzan@ippt.pan.pl

Keywords: RF magnetron sputtering, hard materials, PLD, tungsten boride

Tungsten borides (W-B) with a hardness exceeding 40 GPa belong to the group of superhard materials. Moreover, it has been confirmed that (W-B) layers are about twice harder than the equivalent bulk material. Hence, W-B layers are presently under great interest. In this paper we present the effect of substrate heating on the properties of W-B layers deposited by laser pulse and magnetron.

All layers were deposited from the same target with the boron to tungsten ratio of 4.5. During the deposition the Si substrate was in room temperature or was heated up to 320°C or 540°C. In the pulsed laser deposition (PLD) process the Nd: YAG laser ($\lambda = 355$ nm, $\tau = 10$ ns, fluence = $4.8 \text{ J}\cdot\text{cm}^{-2}$, $f = 10$ Hz) has been used and the deposition process was occurred in vacuum. In the magnetron sputtering (MS) process the power supply to the magnetron cathode was 60 W and process occurred in argon pressure of $9.8 \cdot 10^{-3}$ mbar (gas flow of argon was 19.2 mL/min).

Layers deposited on unheated substrates were amorphous and had low adhesion. In SEM images many cracks and delamination have been observed. After heating the substrate up to 320°C both types of layers had better adhesion but their structures were different: MS layer was amorphous and PLD layer was partially crystalline (about 8%) where the crystal phase (CrPh) has been identified as WB_3 (cell parameters $a = 5.204 \text{ \AA}$, $c = 6.300 \text{ \AA}$). Further increase of the substrate temperature up to 540°C resulted in adhesion increase. The CrPh of PLD layer remained WB_3 and the CrPh content was 17%. MS layer was fully crystalline and the CrPh has been identified as WB ($a = 3.128 \text{ \AA}$, $c = 16.559 \text{ \AA}$).

Presented results indicate that to ensure good adhesion of W-B layers is required to heat the substrate at least up to 320°C. Moreover, the elemental composition of deposited layers is strongly dependent on the deposition method.

Acknowledgements

This work was supported by the NCN (National Science Centre) Research Project: UMO-2015/19/N/ST8/03928

The influence of irydoids content on effectiveness of cosmetic formulations

*Marta Dąbrowska, Izabela Nowak

Adam Mickiewicz University in Poznań, Faculty of Chemistry, Poznań, POLAND

e-mail: marta.dabrowska@amu.edu.pl

Keywords: *irydoids, application tests, skin topography, skin hydration, skin macro relief*

Irydoids influence the acceleration of the wound healing process through the synergistic anti-inflammatory and antioxidative action. Moreover, they have a beneficial effect on the induction of differentiation of skin keratinocytes. The properties of irydoids predispose them to use as effective cosmetic ingredients in anti-aging formulations.

The research started with the preparation of different types of cosmetic formulations containing consecutively 0.5 wt.% of aucubin and 0.5 wt.% of catalpol. Application tests lasted six weeks and they were conducted to evaluate the effectiveness of irydoids in cosmetic formulations containing these compounds. The biophysical skin parameters such as skin hydration and transepidermal water loss (TEWL) were measured using *Courage+Khazaka* apparatus (Corneometer CM825 and Tewameter TM300). Visioscan® VC 98 USB enabled to estimate the skin topography and due to the analysis of the distribution of gray on the skin image to define a number of skin parameters, such as smoothness, roughness and skin density. Visioline® VL 650 was used to analyse the deeper wrinkles and assess the skin macro relief. The measurement was based on skin replica and oblique lighting. The replica was illuminated at an angle of 35° and the mountains representing the wrinkles of the skin produced measurable shadows. That allowed for determination of length, depth and area of the wrinkles.

The results of application tests showed that irydoids have an influence on effectiveness and anti-wrinkle properties of cosmetic formulations containing them. The epidermal barrier function (TEWL values, skin hydration level) and parameters associated with dimension of skin wrinkles were improved.

Stability testing of cosmetic bases for skin care products using multiple light scattering method

Marta Dąbrowska, Izabela Nowak

Adam Mickiewicz University in Poznań, Faculty of Chemistry, Poznań, POLAND

e-mail: marta.dabrowska@amu.edu.pl

Keywords: *stability, cosmetic base, multiple light scattering*

Cosmetic formulations are composed of two immiscible phases (oil and water), in which one is dispersed in the form of small droplets in the other one. Due to the fact that they are thermodynamically unstable systems, the determination of the tendency of their particles to agglomerate is essential.

The commonly used tests include: (i) measurement of the voltage potential changes over time at different temperatures; (ii) Beiersdorf's rheological swing test comparing G' (storage modulus) and G'' (loss modulus) using a cone plate rheometer; (iii) tracking particle size over time by laser diffraction technique and (iv) observation of changes in light back scattering across a sample from top to bottom. Typically, if an emulsion has less than 5% increase in particle size over the first 2 weeks of storage, it will remain stable for at least a year. Stability tests can be carried out by multiple light scattering method using Turbiscan Lab Expert apparatus. This technique is based on measuring the intensity of the transmitted and/or backscattered light from the sample and provides information about the different types of emulsions instabilities such as creaming, sedimentation, flocculation and coalescence.

In this study three types of cosmetic bases for skin care products were obtained. They were stored at different storage conditions (at 4°C, 25°C and 40°C) during six months in order to examine their stability using multiple light scattering method. The results showed that storage temperature had influence on the value of Turbiscan Stability Index (TSI). The difference was particularly evident in the case of cosmetic bases stored at 4°C when TSI value underwent smaller fluctuations than in the other storage conditions. Moreover, the type of cosmetic base also influenced TSI. One of tested samples showed inappreciable increase in particle size over time and thus it is considered as the most stable cosmetic base which can be successfully used in skin care products.

The degradation tests of ceramic-polymer composites with hydroxyapatite for orthopedic implants

*Sylvia Dąbrowska^{1,2}, Elżbieta Pietrzykowska^{1,2}, Roman Mukhovskiy¹, Agnieszka Chodara^{1,2}, Tadeusz Chudoba¹, Janis Locs⁴, Witold Łojkowski^{1,3}

¹Institute of High Pressure Physics, Sokolowska 29/37, 01-142 Warsaw, Poland

²Warsaw University of Technology, Faculty of Materials Science and Engineering, Warsaw, Poland.

³Bialystok University of Technology, Faculty of Management, Bialystok, Poland.

⁴Riga Technical University, Riga, Latvia.

e-mail: s.dabrowska.unipress@gmail.com

Keywords: *hydroxyapatite, polylactic acid, biomaterials, degradation*

Nowadays more and more bioactive materials are used in orthopedic and dental applications, which can support bone ingrowth and osseointegration. Bioactive hydroxyapatite (HAP) is one of the inorganic component of hard tissues, which is manufactured in The Institute of High Pressure Physics of the Polish Academy of Sciences (IHPP PAS) and it is called GoHAPTM. The morphology, grain size and specific surface area of the nanopowder can be controlled by the microwave reactor and the high pressure consolidation technology. To get better mechanical properties in our laboratory combination of GoHAPTM and biocompatible polymers like polylactic acid (PLA) was used. The aim of the GoIMPLANT project was to develop resorbable, tough, strong and biocompatible hybrid composite implants in according to patient's needs.

Isostatic pressing and uniaxial pressing to form our hybrid composite in form of cylinder or wedge were used. Biodegradable composites can be decomposed naturally after a certain period of implantation. Mechanical and biological performance of composites for implantation depends on the degradation rate, used degradation medium, its pH and temperature. The study was performed according to the ISO standards of medical devices, using Phosphate-buffered saline (PBS) and Simulated Body Fluid (SBF) solutions. Testing the changes of Ca²⁺ concentration, the conductivity and pH under equilibrium conditions at 37°C buffer was checked once in a week. After test changes of dimensions, porosity, and structure shown in the SEM microscopy was measured. The hybrid composite changed the properties of immersing medium, so the degradation process was perceived from the first week.

Acknowledgements

Research was realized by the "GoIMPLANT" Project and it is founded by M-Era Net program of The National Centre for Research and Development, co-financed from the European Union, Regional Development.

Synthesis and characterization of palladium catalysts supported on SBA-16 materials

*Paulina Dębek, Agnieszka Feliczak-Guzik, Izabela Nowak

Adam Mickiewicz University in Poznań, Faculty of Chemistry, Poznań, POLAND

e-mail: paulina.debek@amu.edu.pl

Keywords: mesoporous materials, SBA-16, palladium, synthesis procedure

Since the first publication on the mesoporous silica of M41S family, mesoporous materials have attracted much attention. SBA-type (Santa Barbara Amorphous) ordered mesoporous materials have a great scientific and commercial interests due to their unique morphology. One of them is SBA-16 - a siliceous mesoporous material, which possesses cubic mesoporous structure with three-dimensional ordered network of interconnected pores and large surface area. Because of such exceptional properties, these nanostructured materials have been considered as a promising support of heterogeneous catalysts in many reactions.

Therefore, our studies were focused on the obtaining of palladium-modified ordered mesoporous silicas of SBA-16 type, with varying amounts of metal on the surface.

A series of mesostructured SBA-16 materials with different quantities of palladium atoms (0.5-3.0 wt.%) was prepared by templating method using triblock copolymer Pluronic F127 (EO₁₀₆PO₇₀EO₁₀₆) as a surfactant and tetraethyl orthosilicate (TEOS) as a silicon source. Template removal was based on the calcination procedure. Palladium was incorporated into the siliceous matrix using impregnation technique with palladium chloride(II) as a metal source and followed by hydrogen reduction to obtain pure metallic species.

Structure and surface properties of the obtained materials were evaluated by several techniques, namely: X-ray diffraction (XRD), low-temperature N₂ adsorption/desorption measurements, transmission and scanning electron microscopies (TEM, SEM) and Fourier transform infrared spectroscopy (FTIR).

Based on the obtained results, it can be concluded that synthesized materials are characterized by very good morphology (surface area ca. 700 m²/g and total pore volume ca. 0.45 cm³/g) therefore they can be used as support in many catalytic reactions.

Acknowledgements

National Science Centre is kindly acknowledged for the financial support (project no: DEC-2013/10/M/ST5/00652).

Hydrodeoxygenation of anisole as bio-oil model compound over Ru/MCM-41 catalysts

*Paulina Dębek, Agnieszka Feliczak-Guzik, Izabela Nowak

Adam Mickiewicz University in Poznań, Faculty of Chemistry, Poznań, POLAND

e-mail: paulina.debek@amu.edu.pl

Keywords: *MCM-41, ruthenium catalyst, hydrodeoxygenation, anisole, biofuels*

MCM-41 is a mesoporous silica with unique properties of highly ordered mesoporous materials, namely high surface area and pore volume. Such properties make them promising catalysts in many reactions. The walls of the silica matrix can be modified, e.g. with transition metal atoms, and such systems as catalyst in hydrodeoxygenation (HDO) reaction can be used.

HDO is one of the chemical routes to convert the bio-oil feedstock (produced by pyrolysis) obtained from lignocellulosic biomass into biofuels under elevated temperature and hydrogen pressure. Laboratory tests are carried out on model compounds – most commonly with the use of anisole. Our research focuses on the synthesis of MCM-41 materials modified with ruthenium species and their use as catalysts in HDO process of anisole.

Syntheses of MCM-41 matrices were performed via typical hydrothermal method by using tetraethyl orthosilicate (TEOS) as a silica source and hexadecyltrimethylammonium bromide (CTABr) as a structure-directing agent. Ruthenium atoms were introduced into the surface of the silica by wet impregnation of ruthenium chloride(III) and followed by hydrogen reduction.

To determine the physicochemical properties of obtained materials several techniques were used, namely: XRD, N₂ adsorption/desorption, TEM, XPS, ICP-OES. HDO of anisole was performed in a high-pressure reactor varying two different reaction factors: temperature (90-130°C) and hydrogen pressure (25-60 bar).

Cyclohexane, cyclohexene, toluene (main product), benzene, 1-methoxycyclohexene, 1,1'-dimethoxycyclohexane, cyclohexanone and cyclohexanol were identified as reaction products by GC. The catalytic activity of examined catalysts increased with increasing reaction temperature and hydrogen pressure. For the reaction carried out at a temperature of 130°C and a pressure of hydrogen at 60 bar, 70% conversion of anisole was obtained.

Acknowledgements

National Science Centre is kindly acknowledged for the financial support (project no: DEC-2013/10/M/ST5/00652).

Heterogeneous degradation of xenobiotics by sunlight radiation

*Emilia Drozdek¹, Magdalena Foszańczyk¹, Marta Gmurek¹

¹Department of Bioprocess Engineering, Faculty of Process and Environmental Engineering, Lodz University of Technology, Lodz, POLAND

e-mail: 801055@edu.p.lodz.pl

Keywords: *sunlight radiation, xenobiotics, photodegradation, photosensitized oxidation, heterogenic system*

Nowadays there is a growing problem with micro-pollutants present in our environment, including drinking water. This problem is caused by increasing the amount of produced chemicals such as fertilizers, pesticides, preservatives or pharmaceuticals. Anthropogenic origin of all these compounds caused that they are under the common name of xenobiotics. Many of them cause cancer and mutations of different kinds. Some of xenobiotics have exhibiting hormonal activity called to as Endocrine Disruptors (EDs).

The current methods of removing contaminants are based on mechanical and biological treatment with chemical support. Hardly degradable contaminants can be removed from water by Fenton processes or Advanced Oxidation Processes (AOPs). The high costs of use of these processes and their limited application cause that they are not widely used. An interesting alternative to AOPs seems to be photosensitising oxidation process. This process occurs via photochemical oxidation especially using molecular oxygen. The advantages of photosensitising oxidation process is that the singlet oxygen can be generated from air oxygen by solar radiation.

The results of an investigation of photodegradation of the mixture parabens and mixture of chlorophenols under photosensitized oxidation with visible light in aerated aqueous solutions are presented herein. The study was conducted in a semi-continuous system in reactors of the volume 0.6 dm³. Reactor was positioned on solar radiation. The reaction mixtures were prepared in different kind of water. The reaction mixtures were agitated by air stream. Phthalocyanine (AlPcS₄) were used as sensitizer. Phthalocyanine was immobilized on chitosan beads.

Degradation of examined xenobiotic in the aqueous solution by photosensitized oxidation in heterogeneous system under solar radiation is effective. The efficiency of the photodegradation strongly depends on light intensity but is still quite effective in cloudy day.

Acknowledgements

This research was supported by the National Science Centre (NCN) in Poland within research project 2012/07/B/ST8/03787.

Analysis of IR spectra of three ring liquid crystalline chiral esters

*Anna Drzewicz¹, Marzena Tykarska¹, Magdalena Żurowska¹

¹Faculty of Advanced Technologies and Chemistry, Military University of Technology, Warsaw, POLAND

e-mail: anna.drzewicz@wat.edu.pl

Keywords: *liquid crystal, antiferroelectric smectic phase, ferroelectric smectic phase, infrared spectroscopy*

The infrared (IR) spectroscopy covers the range of the electromagnetic spectrum between 0.78 and 1000 μm . The most useful region is called *middle* IR and lies between 2.5-50 μm (4000-200 cm^{-1}). This type of spectroscopy measures the vibrations of atoms and based on this it is possible to determine the functional groups. Vibrations are divided on the two main categories: stretching (change in inter-atomic distance along bond axis) and bending (change in angle between two bonds). There are also four types of bend: in-plane rocking and scissoring, out-of-plane wagging and twisting.

The aim of this study was the analysis of infrared spectra for three ring liquid crystalline chiral esters. These esters have antiferroelectric and ferroelectric smectic phases. The influence of the length of alkyl chain and the presence of fluorine atoms in the benzene ring on their character has been examined. The most interesting for this kind of compounds is the range of absorption of carbonyl groups (1700-1750 cm^{-1}). The shift and the diversity of amount signals in the respective compounds for two bands: about 1740 cm^{-1} from carbonyl group located between the benzene rings and about 1720 cm^{-1} from carbonyl group located between the benzene ring and aliphatic chain has been observed. The measurements were made by Nicolet iS10 Spectrometer Thermo Scientific by Attenuated Total Reflectance Fourier Transform Infrared Spectroscopy (ATR-FTIR) method on the diamond crystal.

IR spectra as well as their interpretation of region corresponding to stretching vibrations of ester and phenyl groups will give the information about changes of conformers structure. The presence of fluorine atom next to the ester group in a rigid core causes hindering of rotation of carbonyl group and formation of two conformers.

Helical pitch of bicomponent systems of 3FnXPhY series

*Anna Drzewicz¹, Marzena Tykarska¹, Magdalena Żurowska¹

¹Faculty of Advanced Technologies and Chemistry, Military University of Technology, Warsaw, POLAND

e-mail: anna.drzewicz@wat.edu.pl

Keywords: *liquid crystal, antiferroelectric smectic phase, helical pitch, helical twist sense inversion*

Still new antiferroelectric compounds are synthesized to improve parameters of mixtures possible to use in display applications. One of such parameter is helical pitch which should be long for better unwinding of the macroscopic helical structure in liquid crystals cells.

Recently synthesized three ring antiferroelectric liquid crystals used in this work form macroscopic helical structure of the opposite twist sense despite they have the same chiral center. Bicomponent systems prepared from such compounds show very high helical pitch and even unwind helix.

The aim of this study was the analysis of helical pitch for three ring liquid crystalline chiral esters of 3FnXPhY series and their mixtures (where n is number of methyl groups, X and Y are H or F atom respectively). The measurements of phase transition temperatures were made by the polarizing optical microscope Olympus. The spectrophotometer Shimadzu UV-Vis-NIR in the range of 360-3000 nm was used to measure the light transmission and to determine the helical pitch. The tested compounds were placed on a glass plate with an aligning layer. The temperature controller MLW U7 with a Peltier element was used for changing the temperature. The temperature range of measurement was 2-110°C.

The results show independence of phase miscibility and helical pitch changes. Regardless of the chiral center structure the complete miscibility of ferroelectric smectic phase can be obtained. In antiferroelectric smectic phase the increasing values of helical pitch with increasing the temperature and right-handed helicoidal structure for most of compounds is observed. The inversion of helical pitch occurs for other compounds with longer alkyl chain (n=7) and also for compounds of 3F5HPhF type.

Investigations of Fe thin films deposited on Si substrates by XRR, RBS, AFM and HSEM

*Aneta Duda, Magdalena Krupska, Sylwia Sowa, Hoa Kim Ngan Nhu-Tarnawska
Nanostructure Laboratory, Institute of Physics, Pedagogical University,
Podchorazych 2, 30-084 Krakow, POLAND
e-mail: anetaduda@up.krakow.pl

Keywords: *Thin films, RBS, AFM, annealing, ion beam irradiation*

Recently with large interest examines a thin layer because of the needs to improves the quality of materials. Examination of thin layers of Fe and Pd can give the opportunity to use them in the future new generation magnetic recording media or Bit Patterned Media technology due to its strong perpendicular magnetic anisotropy. In our group we are interest on characterizing the stability of Fe, Pd thin films on an amorphous substrates, especially post-annealing and after being irradiated conditions. Here we present the results obtained for 10 nm- and 50 nm-thick Fe films prepared by the thermal evaporation method on Si(001) and Si(111) substrate.

We have investigated the films in three different states: as-grown state, after annealing and upon high-energy ion beam irradiation by means of X-ray reflectometry (XRR), Rutherford backscattering spectrometry (RBS), Atomic Force Microscopy (AFM) and high-resolution scanning Electron Microscopy (HSEM). The simulation code SIMNRA was used for RBS data analysis.

A good agreement was obtained between XRR and RBS results revealing that the film surface in the as-grown state was oxidized and a thin Fe-oxidized layer was present. No Fe or Si interdiffusion was observed and thus a sharp borderline (without interface) was found between Fe film and the Si substrate. The rapid annealing at 600°C for 90s has induced changes in the surface morphology. The microstructure studied by AFM and HSEM revealed a granular film with a nonuniform grain size of 30-50 nm. Irradiation by 1MeV Kr⁺ ion beam implied a strong Fe-Si mixing revealed by a large non-zero background between the Fe peak and the Si edge in the RBS spectra.

A new method to compare micromixedness results obtained in iodide-iodate method using different reactant concentrations

*Michał Fedoryk, Manfred Kraut

Institute for Micro Process Engineering, Karlsruhe Institute of Technology, Karlsruhe, GERMANY

e-mail: michal.fedoryk@partner.kit.edu

Keywords: *Villiermaux-Dushman, micromixedness ratio, cyclone type micro mixers*

Micromixing investigations are conducted using different experimental methods. One of them is iodide-iodate reaction method, so-called Villiermaux-Dushman method. Due to reaction kinetics, which is not fully known, usually one 'standard set' of reactants concentrations is applied. Subsequently, optical densities of obtained mixtures are compared.

The proposed approach is based on experimental results of optical densities of mixtures generated by the cyclone type micro mixer. Mixing was investigated using different concentration sets at the same hydrodynamic conditions. Molar ratios of reactants were maintained. Obtained results allowed calculating values of micromixedness ratio. Application of higher concentrations of reactants ended up in lower apparent micromixedness ratio.

This paper presents the new protocol to compare micromixedness ratios obtained using different concentrations of reactants. The presented method is applicable for continuous-flow systems in microdevices where different reactants concentrations have been used. It was found that calculated micromixedness ratio is a function of the concentration ratio to the power of -3.73 .

Thanks to the presented protocol it is possible to broaden the range of investigated hydrodynamic conditions: higher reactants concentrations at higher flows as well as lower ones when mixing is less intensive can be applied and still calculated micromixedness ratios are comparable. The method allows the calculation of exit iodine concentrations, without the explicit knowledge of the actual kinetic data.

Membrane assisted continuous-flow reactions

*Tamás Földi^{1,2}, Christos Didaskalou¹, József Kupai², György Tibor Balogh^{2,3}, Péter Huszthy², Gyorgy Szekely¹,

¹School of Chemical Engineering & Analytical Science, The University of Manchester, Manchester, United Kingdom

²Faculty of Chemical Technology and Biotechnology, Budapest University of Technology and Economics, Budapest, Hungary

³Chemical Works of Gedeon Richter Plc., Budapest, Hungary

e-mail: fodi.tamas@mail.bme.hu

Keywords: *flow chemistry, supported base, nanofiltration.*

Continuous-flow processes showing promising opportunities toward sustainable fine chemical production. Due to the excellent parameter control of these setups reproducibility, scalability, safety, efficiency and productivity could be much better compare to batchwise production.

In our work *Michael* addition of nitromethane to *trans*-chalcone was chosen as a model reaction. Numerous bases were investigated to enhance the reaction rate in batch conditions. The most promising catalysts were tested in a continuous-flow packed-bed reactor applying a solid base containing column. The reactor was able to produce the desired *Michael* adduct with short residence time with almost quantitative yield, when a polymer supported trialkylamine base were applied.

In order to reduce solvent consumption nanofiltration membrane unit was connected to a continuous-flow reactor. Where the membrane unit was used to concentrate the retentate flow and to get lower concentration permeate flow, which could be reused in the process. In order to reach acceptable flux as $0.2 \text{ mL}\cdot\text{min}^{-1}$ through the membrane it was necessary to apply high pressure between 20-40 bar in case of isopropanol solvent. With the application of a polybenzimidazole (PBI) membrane it was possible to reach 23% rejection for the reaction product. The membrane unit performance remained constant during the period of three days operation.

This model system represents a green approach for fine chemical production as it applies an effective heterogeneous catalyst and solvent recycling.

Acknowledgements

Financial support of the Hungarian Scientific Research Fund/National Research, Development and Innovation Office (OTKA/NKFIH No. K 112289).

1-alkyl-4-(dimethylamino) pyridinium bis(trifluoromethylsulfonyl)imides as electrolytes for supercapacitors

*Agnieszka Gabryelczyk¹, Małgorzata Graś¹, Grzegorz Lota¹, Monika Stasiewicz²

¹Institute of Chemistry and Technical Electrochemistry, Poznan University of Technology, Poznań, POLAND

²Institute of Chemical Technology and Engineering, Poznan University of Technology, Poznań, POLAND

e-mail: agnieszka.a.gabryelczyk@doctorate.put.poznan.pl

Keywords: supercapacitor, ionic liquid, electrolyte

Ionic liquids are a very large group of compounds, which brings out a great interest of researchers in modern chemistry. Their melting point is under 100°C or sometimes even around the room temperature. Some of 1-alkyl-4-(dimethylamino) pyridinium bis(trifluoromethylsulfonyl)imides belong to room temperature ionic liquids (RTIL). They show low viscosity, high thermal stability and negligible solubility in water. Besides, they can be synthesized during quite simple process. These properties make them good candidates for organic electrolytes in electrochemical capacitors. Supercapacitors are devices for efficient energy storage, which release charge very quickly. Organic electrolyte can enhance their voltage significantly to the values unreachable for water-based electrolyte.

The main target of presented work was to examine mentioned ionic liquids with various substituent length as electrolytes for supercapacitors. Cyclic voltammetry and galvanostatic charge/discharge measurements were carried out to test their properties.

Ionic liquids used in the study were synthesized in two step reaction according to the following equation:



Electrochemical tests were conducted in two-electrode system in the Swagelok® cell.

Obtained results showed that ionic liquids with shorter side branches has higher conductivity. Capacitance of supercapacitors with such substance as an electrolyte increases.

Acknowledgements

The studies were conducted under the project No. 03/31/DSPB/0337 funded by the Ministry of Science and Higher Education.

The influence of ionic liquids structure on corrosion parameters in lead-acid battery

*Agnieszka Gabryelczyk¹, Grzegorz Lota¹, Marek Baraniak¹, Kacper Kopczyński¹, Juliusz Pernak², Ewa Jankowska³, Waldemar Rzeszutek⁴

¹Institute of Chemistry and Technical Electrochemistry, Poznan University of Technology, Poznań, POLAND

²Institute of Chemical Technology and Engineering, Poznan University of Technology, Poznań, POLAND

³Institute of Non-Ferrous Metals Division in Poznań Central Laboratory of Batteries and Cells, Poznań, POLAND

⁴PPUH Autopart Jacek Bąk Sp. z o.o., Mielec, POLAND
e-mail: agnieszka.a.gabryelczyk@doctorate.put.poznan.pl

Keywords: *corrosion inhibitor, ionic liquid, lead-acid battery*

Since years lead-acid battery (LAB) has been considered a very useful device for energy conversion. Its applicability for motor vehicles or uninterruptible power supplies as well as simple recycling technology makes them one of the most popular secondary batteries. Nonetheless, it has a few drawbacks. Among them quite severe is corrosion of positive plate. To suppress the rate of corrosion in LAB, countermeasures like corrosion inhibitors can be used.

Nowadays, ionic liquids (IL), a very promising group of compounds, are considered substances, which can inhibit corrosion rate of alloys. They play a role of green solvents in organic synthesis and electrolyte in electrochemistry. Moreover, their properties and applications can be design by various cations and anions in the molecule and by controlling the length of the side branches.

The aim of presented work was to correlate the influence of the IL cation structure with the rate of corrosion of LAB positive current collector. Corrosion parameters such as corrosion potential and current were measured by means of linear sweep voltammetry and corrosimetry.

Lead-calcium-tin alloy utilized in industry for manufacturing current collectors was used as the working electrode. Electrolyte (37 wt.% sulfuric acid solution) was modified by addition of four IL with different cations.

Obtained results showed that IL additive can affect corrosion rate of LAB plates. Their influence depends on the structure of the cation in their molecule.

Acknowledgements

This work was supported by the National Centre for Research and Development of Poland, grant No PBS3/A5/43/2016.

Study of series of antiferroelectric smectic mixtures composed with smectogens exhibiting synclinic and anticlinic phases

*Katarzyna Gaładyk¹, Magdalena Żurowska², Maciej Chronik¹, Wiktor Piecek¹, Przemysław Kula²

¹ Institute of Applied Physics, Faculty of Advanced Technologies and Chemistry, Military University of Technology, Warsaw, POLAND

²Institute of Chemistry, Faculty of Advanced Technologies and Chemistry, Military University of Technology, Warsaw, POLAND
e-mail: katarzyna.galadyk@wat.edu.pl

Keywords: *antiferroelectric liquid crystal (AFLC), tilt angle θ , spontaneous polarization P_s , switching times τ_{10-90} , rotational viscosity γ_ϕ*

The orthoconic antiferroelectric liquid crystals (OAFLC) are interesting due to properties such as tilt angle θ close to 45° . Such property generates an optically isotropic medium at the surface stabilized structure providing near perfect dark state hence a maximum contrast. In search for a working OAFLC mixture was investigated an influence of doping of such a mixture with homostructural dopants exhibiting synclinic smectic phase only.

The target of work was to improve properties (tilt angle θ , switching times τ_{10-90} , spontaneous polarization P_s , rotational viscosity γ_ϕ) of a parent near OAFLC denoted W_1000, which shows a tilt angle $\theta \sim 43^\circ$. There was prepared a testing, synclinic only, W_355 mixture, which added to parent OAFLC W_1000 affecting its properties. W_355 lowers the optical tilt angle θ and the spontaneous polarization P_s . Most significant result of such a doping, was pronounced decreasing of the rotational viscosity γ_ϕ .

In this work there are presented a new AFLCs which were prepared with different weight ratio of mixtures W_1000 and W_355. In this work we discuss influence of the molecular structure of mixtures W_1000 and W_355 on physical and electrooptical properties new AFLC mixtures. The special attentions was payed for the influence of polar properties of the compounds forming W_355 mixture on the performance of a final anticlinic one.

Acknowledgements

The project has been supported with the MUT grant PBS 23-652.

Surface properties of the layers based on cerium doped black glass on austenitic stainless steel substrate

*Magdalena Gawęda, Elżbieta Długoń, Maciej Sitarz

Faculty of Materials Science and Ceramics, AGH University of Science and Technology, Krakow, POLAND

e-mail: mgaweda@agh.edu.pl

Keywords: *black glasses, cerium, protective layers, atomic force microscopy, scanning electron microscopy*

Black glass is the amorphous material based on silicon oxycarbide. The structure of this material lies in between amorphous silica ($v\text{-SiO}_2$) and silicon carbide (SiC). In comparison with it has denser and stiffer network. This is due to the difference in the oxygen and carbon valence. This causes the improvement of mechanical properties, chemical and corrosive resistibility of the material. The obtainment of black glasses by classical melting of mineral raw materials is impossible due to oxidation, decomposition and crystallization processes. It is possible to obtain black glasses with the use of sol-gel method, which enables to transpose the critical silicon-carbon bond from the precursor to the final material. Before the ceramization, the sol might be deposited on various kinds of substrates by the dip-coating method.

The parameters of the material might be improved by doping with elements such as cerium. Implementation of this element to the black glass layer may give it new features, i.e. self-healing, antibacterial, anti-fungal properties. The use of these properties requires great quality of the surface of the layer. The roughness and the contact angle are only two of plenty of the important parameters.

In this work the study of the surface properties are presented. The results of atomic force microscopy (AFM), scanning electron microscopy (SEM) and laser confocal microscopy analyses are presented. The results indicate that continuous, hermetic layers were obtained with the morphology characteristic for the layers based on the sol-gel method and deposited with the use of dip-coating. Cerium doped black glasses coatings are rough and hydrophilic, the double phase structure is visible.

Acknowledgments

This work was supported by the NCN project “Functional layers of black glasses based on ladder-like silsesquioxanes 2014/15/B/ST8/02827”.

Cerium doped amorphous materials based on silicon oxycarbide and their possible applications

*Magdalena Gawęda, Elżbieta Długoń, Maciej Sitarz

Faculty of Materials Science and Ceramics, AGH University of Science and Technology, Krakow, POLAND

e-mail: mgaweda@agh.edu.pl

Keywords: *silicon oxycarbide, black glasses, cerium, protective layers, spectroscopy*

For many applications, aggressive environment requires very specific functional properties of the used materials. These are primarily resistance to the high temperatures and corrosion, suitable hardness, Young's modulus, flexible and plastic energy. In many cases, the materials of proper mechanical parameters do not meet requirements of the widely understood durability. The example of such material is steel. It is possible to improve the materials by applying the protective layers which will isolate the basal material from the working environment. Such layers might be deposited on the surface by various methods, i.e. chemical vapour deposition, physical vapour deposition, electrophoretic deposition, dip-coating.

In this work, the protective amorphous layers based on silicon oxycarbide modified by cerium ions were proposed. The structure of so-called black glasses might be compared to the amorphous silica with part of oxygen ions replaced by carbon ions in 2:1 ratio. It causes stiffening and densification of the silica network. The material possesses high mechanical properties, chemical and thermal resistance.

The obtained layers were examined with the use of X-ray diffractometry, middle infrared, Raman, X-ray photoelectron spectroscopy, thermal analysis. The research enables authors to determine the structure and chemical characteristics of the cerium doped materials based on silicon oxycarbide. The obtained by sol-gel method precursors, oligo- and polysilsesquioxanes, had the desired ladder-like structure. Their usage was the efficient path of transferring silicon-carbon band to the structure of the final ceramic amorphous material after pyrolysis. Moreover, it was shown that cerium ions had the significant influence on the structure of both precursors and black glass. It was clearly proven based on the spectroscopic analyses.

Acknowledgments

This work was supported by the NCN project "Functional layers of black glasses based on ladder-like silsesquioxanes 2014/15/B/ST8/02827".

The determination of benzophenanthridine and protopine derivatives in biological fluids

*Aleksandra Glówka¹, Matylda Resztak², Izabela Nowak¹

¹ Adam Mickiewicz University in Poznan, Faculty of Chemistry, Poznan, POLAND

² Poznan University of Medical Sciences, Department of Physical Pharmacy and Pharmacokinetics, Poznan, POLAND

e-mail: aleksandra.glowka@amu.edu.pl

Keywords: *Chelidonium majus*, biological activity, alkaloids, biological fluids

The world of plants is one of the main sources of raw materials used in many areas of our lives. To a large extent, this is due to the abundance that it represents. In nature, there are currently about 2,000 plant species considered as medicinal, which can be a potential source of raw materials for the pharmaceutical industry [S.M.K. Rates, Plants as source of drugs, *Toxicol* 39 (2001) 603–613]. *Chelidonium majus* L., also known as a greater celandine, is a member of the family *Papaveraceae*, naturally occurring in Europe, Asia and South America, which has been known as a medicinal herb for the centuries. The biological activity is determined mainly by alkaloids contained in *Chelidonium majus*. More than 30 alkaloids present in that plant e.g.: benzophenanthridine (chelidonine, chelerythrine, sanguinarine), protoberberine (coptisine, berberine), porphine (magnoflorine) and protopine type (protopine) compound were identified [Council of Europe. Committee of Experts on Cosmetic Products, Active Ingredients Used in Cosmetics: Safety Survey, 2008]. This plant possesses a wide spectrum of pharmacological activities including potent cytotoxic, anticancer, antimicrobial, antifungal, antispasmodic, anti-inflammatory effects and many others.

The most important alkaloids in greater celandine are: chelidonine, sanguinarine, chelerythrine, protopine and its derivative - allocryptopine. Pharmacokinetic study of these alkaloids is helpful to better understand the pharmacological actions of *Chelidonium majus*.

In this study, the HPLC method was conducted for the determination of chelidonine, allocryptopine, sanguinarine chloride and chelerythrine chloride in biological fluids. In this research UV-vis detector was used. The analytical method suitable for quantitative determination of discussed alkaloids in biological fluids was developed.

Antioxidant activity of *Chelidonium majus* L. plant extract

*Aleksandra Glówka¹, Izabela Nowak¹

¹ Adam Mickiewicz University in Poznan, Faculty of Chemistry, Poznan, POLAND
e-mail: aleksandra.glowka@amu.edu.pl

Keywords: *Chelidonium majus*, antioxidant activity, DPPH, alkaloids

Free radicals are highly reactive and hazardous particles, to which recently a key role in the pathogenesis of so-called lifestyle diseases was assigned. Their omnipresence means that we live in a chronic oxidative stress, which is the cause of the failure and inefficiency of the natural defense systems of organisms. Secondary plant metabolites present in the diet and extracts from medicinal plants often have strong antioxidant properties. There are a number of methods for measuring this activity. The most common is the use of in vitro methods (e.g. 2,2-diphenyl-1-picrylhydrazyl – DPPH, 2,2-azinobis-3-ethylbenzothiazoline-6-sulfonic acid – ABTS, *N,N*-dimethyl-*p*-phenylendiamine – DMPD) scavenging activity) [Aurelia Magdalena Pisoschi, Gheorghe Petre Negulescu, Methods for Total Antioxidant Activity Determination: A Review, Biochemistry & Analytical Biochemistry (2011) 1:106. doi: 10.4172/2161-1009.1000106].

DPPH is a free radical of relatively high stability and therefore can be easily prepared for testing. Alcoholic solutions of DPPH are the most commonly used. They are purple with a maximum absorbance at a wavelength of 515 nm. During the reduction reaction color of the solution is changing to yellow. Method using DPPH reagent is widely used for measurements of antioxidant capacity of natural ingredients e.g. herbal extracts.

Chelidonium majus L., also known as a greater celandine, belong to the Papaveraceae family and it grows in many regions of the world. The biologically active compounds from greater celandine can be found especially in roots, but also in leaves and flowers, and belong to the benzophenanthridine and isoquinoline alkaloids. The main alkaloids from *C. majus* are chelerythrine, sanguinarine, chelidonine, coptisine, homochelidonine, protopine, allocryptopine.

In this study, the antioxidant activity of extract from *Chelidonium majus* by using the DPPH method was tested. The alcoholic solutions were used. The absolute antioxidant capacity of individual compounds and extract was determined only when reactions have reached a steady state condition.

Anode material for direct borohydride fuel cell

Małgorzata Graś¹, Agnieszka Sierczyńska², Katarzyna Lota², Ilona Acznik²,
*Grzegorz Lota^{1,2}

¹Institute of Chemistry and Technical Electrochemistry, Poznan University of Technology, Berdychowo 4, 60-965 Poznan, Poland

²Institute of Non-Ferrous Metals Division in Poznan Central Laboratory of Batteries and Cells, Forteczna 12, 61-362 Poznan, Poland

e-mail: Grzegorz.Lota@put.poznan.pl

Keywords: *direct borohydride fuel cell, AB₅ alloy, borohydride electrooxidation reaction, anode composition, alkaline electrolyte*

Fuel cells are quiet, efficient and environmentally safe energy devices that directly convert chemical energy into electricity. Borohydride as a solid fuel (DBFC) is more convenient to store and transport than hydrogen, moreover it is chemically stable and non-flammable. This type of power source is technically more simple than traditional fuel cells, because it does not require any hydrogen container and noble metals. Theoretically, borohydrides are able to release 8 e⁻ from one molecule. Hydrogen evolution during hydrolysis can be inhibited by modification of anode materials.

In order to prepare the working electrode, the commercial AB₅ – type alloy of formula LaMnNi_{3.55}Al_{0.30}Mn_{0.40}Co_{0.75} was used. The alloy was mixed with nickel carbonyl and carbon nanotubes or graphite or silicon powder. Then, the composite material was blended with a 3 wt.% poly(vinyl alcohol) solution as a binder. This resulting mixture (250 mg) was coated into a 1 cm x 1 cm nickel foam (porosity >95%). A three-electrode measurement system was built of the working electrode, the counter electrode made of the nickel foam and the Hg/HgO electrode as the reference one, immersed in fuel solution.

Two types of electrolytes and compositions of anode material for direct borohydride fuel cell are compared. The greatest stability of polarization potential for the anode consisted of hydrogen storage alloy with nickel carbonyl was obtained for 0.5 M NaBH₄ + 6 M KOH electrolyte, therefore it was chosen for further measurements. Graphite proved to be the best additive to the anode material. This type of carbon material improved the conductivity of anode composites as well as extended stability of DBFC.

Acknowledgements

The authors acknowledge the financial support from the European Fund of Regional Development within the framework of the operating program "Innovative Economy 2007–2013" under Project No. POIG.01.03.01-00-086/09.

The effect of electrode modification on the electrochemical capacitor performance

Małgorzata Graś¹, Jarosław Wojciechowski¹, *Grzegorz Lota^{1,2},
Łukasz Kolanowski¹, Karol Szubert³

¹Institute of Chemistry and Technical Electrochemistry, Poznan University of Technology, Berdychowo 4, 60-965 Poznan, Poland

²Institute of Non-Ferrous Metals Division in Poznan Central Laboratory of Batteries and Cells, Forteczna 12, 61-362 Poznan, Poland

³Faculty of Chemistry, Adam Mickiewicz University in Poznan, Poznan, Poland
e-mail: Grzegorz.Lota@put.poznan.pl

Keywords: *supercapacitors, activated carbons, electrode modification, corrosion protection, organosilicon coatings*

Electrochemical capacitors are interesting energy storage systems. Most frequently used electrode material in electrochemical capacitor is activated carbon. Various modification treatment can be distinguished. The electrodes are composed of active electrode material which is applied on the metal or steel current collector surface. Current collectors are exposed to corrosive electrolytes. On its surface there is a formation of oxidation reaction products layer. This phenomenon changes working parameters of the electrochemical capacitors, including self-discharge, capacitance, diffusion/charge transfer resistance. Promising candidates are organofunctional silanes, which contain in its structure silicone atom.

In this study we present a new approach to silane coatings deposited on the surface of stainless steel and aluminum current collectors subsequently used in electrochemical capacitors. The deposition was performed from two different sol-gel solutions with a variety of pH values. The electrodes were assembled in a Swagelok® type cell to perform two- and three-electrode electrochemical measurements by means of the following techniques: cyclic voltammetry, galvanostatic charge/discharge and electrochemical impedance spectroscopy.

On the basis of the obtained results it is concluded that corrosion potentials and evolution of oxygen potentials of samples treated with silane solutions were shifted toward more positive (more noble) values. Moreover, in case of electrochemical capacitor measurements, this phenomenon provides change of operating cell voltage, resulting in enhancement of specific capacitance values.

Acknowledgements

This work was supported by funds from the National Science Centre (Poland) granted on the basis of decisions number DEC-2013/10/E/ST5/00719.

The application of coalescing plate for separating water and oil in water treatment plant in the petroleum industry by utilizing CFD simulation

*Sorani S. Ibrahim¹, Sedat Yayla², Ali B. Olcay³, Ahmed E. Hemedmin⁴

¹The ministry of municipality in water surrounding Erbil-Iraq

²The yuzuncu yil university Van-Turkey

³Yeditepe university Istanbul-Turkey

⁴The ministry of agriculture and water resources Erbil-Iraq

e-mail: soran_1982@yahoo.com

Keywords: *CFD, Coalescing plate, Laminar, Oil-water separation efficiency, flow. Two-phase flow*

Petroleum fabrication generates an immense amount of oily polluted water which may have damaging effects on environment. At the same time, produced water is the biggest waste stream produced in the petroleum industry. In the past decades, produced water treatment was the point of attention. Coalescing plates which are a wavy plate pack are widely applied in the separation efficiency.

In order to investigate the effect of parameters such as space between plates, orifice diameter and velocity on separation efficiency in coalescing plates which are used to separate oil-water mixture, the computational fluid dynamics (CFD) two dimensions 2D was utilized in this research. Different spacing between plates 8, 12, 16, 20 and 24 mm with orifice diameters of coalescing plate 10, 15 and 20 mm were examined. In addition various shape such as cylindrical, rectangular and ellipse and four different velocities 0.020, 0.030, 0.040, and 0.050 m/sec have been focused on to discover the effect of each diameters on the separation efficiency.

The investigation revealed that the increase in the distance between plates is inversely proportional to the separation efficiency and the increase in the velocity of the mixture or mass flow rate inlet is inversely proportional to the separation efficiency. It is also found that the best separation efficiency was obtained for cylindrical shape of plates with a hole diameter equal to 15 mm. The efficiency outcome was varied between 24 % to 99.25 % depending on the use of different velocities and distance between plates.

In conclusion, it can be stated that the space between plates and orifice diameter highly impact the separation efficiency. Furthermore the velocity has a great role in the separation process.

Research on structural properties of antimony-silicate glasses doped with thulium ions

J. Zmojda¹, M. Kochanowicz¹, P. Miluski¹, *R. Jadach², P. Jeleń², M. Sitarz², D. Dorosz²

¹Bialystok University of Technology, Faculty of Electrical Engineering, Wiejska 45D, 15-351 Bialystok, Poland

²University of Science and Technology in Krakow, Faculty of Materials Science and Ceramics al. Mickiewicza 30, 30-059 Kraków, Poland

e-mail: rjadach@agh.edu.pl

Keywords: *antimony-silicate glasses, luminescence, structure, spectroscopy.*

Photonic materials technology characterize of dynamic development. Follow this fact new optical glasses doped with rare earth ions are sought. Glasses of high thermal stability, good mechanical properties and low phonon energy are perfect candidate for efficient luminescence sources. Silicate glasses posses properties (high phonon energy equals 1100 cm^{-1}) which prevent to obtain strong emission in the near infrared (NIR) range. To change that properties of silicate glasses those are mixed with components with different vibrational energies to lower phonon energy of whole system. Emission in the range of $1.5\text{-}1.9\text{ }\mu\text{m}$ can occur in mentioned glasses doped with thulium ions.

The investigated glassy system: $\text{SiO}_2\text{-Sb}_2\text{O}_3\text{-Al}_2\text{O}_3\text{-Na}_2\text{O}$ was doped with Tm_2O_3 (0.2-1 mol%). High-purity oxides were used to prepare samples by melting at the range from 1350 to 1550°C for 60 min and then poured into a brass mold and annealed at 450°C for 12hrs. Transparent glasses with none effect of crystallization were obtained. Following properties of prepared glasses' samples were investigated: thermal properties (SETARAM Labsys thermal analyzer), FTIR spectra (Bruker Company Vertex 70v spectrometer and Horriba Yvon Jobin LabRAM HR micro-Raman spectrometer), spectral absorbance (Acton Spectra Pro 2300i monochromator with InGaAs detector in the range of $0.35\text{-}2.3\text{ }\mu\text{m}$) and luminescence spectra (Acton Spectra Pro 2300i monochromator in the range of $1350\text{-}2300\text{ nm}$ and laser diode $\lambda_{\text{exc}}=795\text{ nm}$).

The increase of Sb_2O_3 molar content cause shift of transformation temperature of glasses in lower temperatures. According FTIR spectra antimony turned out to be ion co-forming the network in the presented glasses. Intensity of absorption band at 615 cm^{-1} is associated with vibration of Si-O-Sb bridges. As a result of optical excitation of investigated glasses two strong luminescent bands ($1460\text{ nm }^3\text{H}_4\rightarrow^3\text{F}_4$ and $1800\text{ nm }^3\text{F}_4\rightarrow^3\text{H}_6$) were observed. Emission spectra analysis presents that the greater separation of active centers (increase of antimony ions) cause depopulation of the $^3\text{F}_4$ level.

Structural and luminescence properties of germanate glasses modified by aluminium oxide

*R. Jadach¹, M. Kochanowicz², J. Zmojda², P. Miluski², M. Sitarz¹, D. Dorosz¹

¹ University of Science and Technology in Krakow, Faculty of Materials Science and Ceramics al. Mickiewicza 30, 30-059 Kraków, POLAND

²Bialystok University of Technology, Faculty of Electrical Engineering Wiejska, 45D, 15-351 Bialystok, POLAND

e-mail: rjadach@agh.edu.pl

Keywords: *germanate glasses, luminescence, structure, spectroscopy*

In recent decade mid-infrared luminescence materials emitting at around 2µm increasing interest. It results from many applications in such fields as: medicine, material processing and remote sensing. A lot of types of glasses were studied (Fluoride, Tellurite, Germanate, Chalcogenide) but Germanate Glass turn out to be the best of the respondents. Germanate glasses are widely used as host material thanks to their good thermal stability, phonon energy (900 cm⁻¹), excellent mechanical properties and good rare earth ions solubility.

In this paper research on the influence of type and amount of modifier on luminescence efficiency of germanate glasses were executed. Additionally it was tried to investigate correlation between structure and luminescence properties of received glasses.

The investigated glassy system GeO₂-Ga₂O₃-BaO-xAl₂O₃ (x=5, 10, 15, 20 and 25 mol%) was doped with Yb, Tm and Ho ions. Transparent glasses with none effect of crystallization were obtained. Following properties of prepared glasses' samples were investigated: thermal properties (SETARAM Labsys thermal analyzer), FTIR spectra (Bruker Company Vertex 70v spectrometer and Horriba Yvon Jobin LabRAM HR micro-Raman spectrometer), luminescence spectra (Acton Spectra Pro 2300i monochromator in the range of 1350-2300 nm and laser diode λ_{exc}=976 nm).

Aluminum oxide which is modifier causes bonds breaking inside the glass structure which affect luminescence properties of doped Germanate Glasses. It can be conclude that environment of dopants in the glass systems structure was modified and additional absorption process or changes in energy transfer occurred.

Esterification reactions conducted in the presence of sulfonated mesoporous silica

*Sylvia Jarmolińska, Agata Wawrzyńczak, Izabela Nowak

Adam Mickiewicz University in Poznań, Faculty of Chemistry, Poznań, POLAND

e-mail: sylvia.jarmolinska@amu.edu.pl

Keywords: *esterification reaction, myristic acid, MCM-41, KIT-6, MSU*

Different acid-catalyzed reactions, among others esterification, can be effectively promoted by solid acid catalysts, like sulfonic-functionalized mesoporous silica. Therefore, the aim of the presented study was to investigate catalytic properties of mesoporous silica modified with functional groups containing sulfur atoms. In order to examine catalytic activity of this type of materials, esterification reactions of fatty acid were applied.

To carry out an esterification reaction several mesoporous materials based on silica were used, namely: MCM-41 with a hexagonal pore ordering, KIT-6 with a regular structure and MSU with a worm-like arrangement of channels. These pristine materials were synthesized with tetraethyl orthosilicate (TEOS) as a silicon source and various surfactants as templates. Physical and chemical properties of the obtained mesoporous materials were modified by incorporation of sulfur-containing organic groups. Functionalization process was performed by grafting procedure, in which 3-mercaptopropyltrimetoxysilane was used as a source of thiol groups. In the next step thiol-modified materials were oxidized by H_2O_2 in order to obtain sulfonic-functionalized mesoporous materials.

Physicochemical properties of the synthesized mesoporous materials were characterized by different techniques, viz.: X-ray diffraction, transmission electron microscopy and low-temperature N_2 sorption measurements. The resulting materials were also tested for their catalytic activity in the esterification of myristic acid with *n*-butanol, *n*-propanol or isopropanol. Performed tests showed, that synthesized sulfonic-modified mesoporous materials: MCM-41, KIT-6 and MSU, may be applied as efficient solid acid catalysts in the above mentioned reactions, resulting in a significant conversion of myristic acid and a high selectivity to the desired product – myristate.

Acknowledgements

National Science Centre is kindly acknowledged for the financial support (project no: DEC-2013/10/M/ST5/00652).

Platinum supported on mesoporous silica of MCM-41 type – synthesis and characterization procedures

*Sylwia Jarmolińska, Agata Wawrzyńczak, Izabela Nowak

Adam Mickiewicz University in Poznań, Faculty of Chemistry, Poznań, POLAND

e-mail: sylwia.jarmolinska@amu.edu.pl

Keywords: *platinum, MCM-41, co-condensation, impregnation*

MCM-41 mesoporous silica can be applied as a support for various catalytically active species, due to its high specific surface area, ordered mesoporous structure and large pore volume, which increase functionalization potential of this type of materials. Transition metals may be incorporated into the siliceous framework or supported onto the surface of mesopores, leading to a high dispersion of active species and lack of diffusion limitations. Thus, the aim of our studies was the development of synthesis procedures for obtaining MCM-41 mesoporous silica modified with platinum species.

MCM-41 materials were synthesized with tetraethyl orthosilicate (TEOS) and cetyltrimethylammonium bromide (CTABr) as a silicon source and template, respectively. Moreover, hexachloroplatinic(IV) acid solution ($\text{H}_2\text{PtCl}_6 \cdot 6\text{H}_2\text{O}$) was applied as a metal precursor. Platinum species were incorporated into the siliceous matrix using “one-pot” and impregnation techniques. Prepared samples had various metal loadings, i.e. 1% wt. or 3% wt. of Pt. Two different methodologies were employed in order to transform the metal precursor into metallic form, namely: chemical reduction with NaBH_4 solution and reduction under a constant H_2 flow.

Obtained Pt-MCM-41 samples were characterized using several techniques, specifically: X-ray diffraction (XRD), transmission electron microscopy (TEM), X-ray photoelectron spectroscopy (XPS), low temperature N_2 adsorption-desorption measurements, and elemental analysis. Results obtained from different characterization techniques demonstrated that the transition metal species were quite well dispersed onto the mesoporous silica matrix. Furthermore, catalytically active crystallites of Pt(0) were also observed on the silica surface.

Acknowledgements

National Science Centre is kindly acknowledged for the financial support (project no: DEC-2013/10/M/ST5/00652).

Application of galinstan film electrode for determination of thallium (I) traces using anodic stripping voltammetry

*Katarzyna Jedlińska, Bogusław Baś, Krystian Węgiel

Faculty of Materials Science and Ceramics, AGH University of Science and Technology, Krakow, POLAND

e-mail: kat.jedlinska@gmail.com

Keywords: *anodic stripping voltammetry; thallium; trace electroanalysis; galinstan.*

The monovalent thallium is known as an extremely toxic and carcinogenic element which, like other heavy metals, may cause polymorphism in some genes. In biogeochemical reactions it has tendency to substitute potassium ions, thus it might disrupt the vital potassium-dependent processes. Since the concentration of thallium in environment is very low, therefore, a sufficiently sensitive method is required for its determination.

This work describes a procedure of determination of Tl(I) on trace level by home-made electrochemical sensor via differential pulse anodic stripping voltammetry (DP ASV). A prototype construction of renewable metallic electrode consists of silver wire coated by thin film of galinstan – eutectic alloy of gallium, indium and tin which is liquid at room temperature. The analysis was performed with a conventional three-electrode system. A galinstan electrode was employed as a working electrode with Ag/AgCl/3 M KCl and platinum wire as the reference and counter electrodes, respectively. All solutions used for analyses were purged with argon. The optimisation of experimental conditions included selection of the appropriate supporting electrolyte solution, potential and time of preconcentration, and DP mode parameters.

As a result of optimization process, quantitative measurements were performed in the supporting electrolyte containing 0.002 M KCl, 0.001 M KNO₃ in presence of HNO₃. The obtained DP ASV calibration curves for an accumulation time of 40 s was linear from 50 ng·L⁻¹ to over 350 ng·L⁻¹.

The study showed that galinstan film electrode might be used as an electrode material in electroanalysis. Voltammetric determination of Tl(I) at trace level proves, that in some cases galinstan may be a substitute for mercury. Therefore the idea of fabrication of this working electrodes is promising and we continue to develop this type of electrode.

Acknowledgements

This work was supported by the Polish National Science Centre (Project No. 2015/19/B/ST5/01380).

The renewable galinstan film metal based electrode for voltammetry

*Katarzyna Jedlińska, Bogusław Baś, Krystian Węgiel

Faculty of Materials Science and Ceramics, AGH University of Science and Technology, Krakow, POLAND

e-mail: kat.jedlinska@gmail.com

Keywords: *stripping voltammetry; renewable sensor; mercury-free electroanalysis; galinstan.*

Voltammetry is one of the most sensitive electrochemical methods for trace analysis. Mercury is considered as the best electrode material for voltammetric measurements due to its excellent properties. Among them there is a fact that it is liquid at standard conditions, therefore it can create drops or films with a smooth and uncontaminated surface, which does not need to be cleaned or polished like a solid electrode. However high toxicity of mercury has led to a growing interest in search for new electrode materials.

In the present work it was demonstrated a novel type of film electrode, where liquid mercury is replaced by the galinstan – the eutectic mixture of gallium, indium and tin which is liquid at room temperature (m.p. -19°C). The construction of the electrode consists of cylindrical outer casing ended with special latex gasket. On top of the gasket a drop of galinstan and solution which prevent this alloy from oxidation were placed. Inside of the outer casing, a high purity metal wire connected with slider from the stainless steel were bested. The procedure of refreshing of the electrode is based on movement (up and down) of the slider with the metal wire, alongside the outer casing. The metal wire is coated with thin film of galinstan while it goes through the drop of this alloy. Afterwards, the wire pass through the tiny hole in gasket, which prevent galinstan and internal solution from leaking and removes of excess of galinstan.

Numerous experiments were performed for optimization of this construction. The usefulness of several metallic materials, as well as composition of internal solution were tested. To evaluate the device and the method a lead determination by anodic stripping voltammetry was carried out. The results indicate that silver and copper wire are the best materials for galinstan film electrode.

Presented construction is a promising alternative to the commonly used mercury film electrodes and will be developed in future.

Acknowledgements

This work was supported by the Polish National Science Centre (Project No. 2015/19/B/ST5/01380).

The thermodynamic properties of the liquid crystal stationary phase

*Justyna Jonik, Marcin Purchała, Tomasz Wawer, Henryk Grajek

Faculty of New Technologies and Chemistry, Military University of Technology,
Warsaw, POLAND

e-mail: justyna.jonik@wp.pl

Keywords: liquid crystal stationary phase, inverse gas chromatography

Liquid crystals are known as materials with the intermediate properties between solids and liquids. There are many types of liquid crystals, which are widely used in industry, for example in displays, mass memories for computers, optoelectronics (optical fibers), production non-mercury thermometers and as additives for paints and emulsions changing color under the influence of temperature.

Nowadays, liquid crystals are also used in analytical chromatography as stationary phases. Therefore, it has been decided to test usefulness of [4-(4-trans-butylcyclohexanecarbonyloxyphenyl)4-(4-trans-pentylcyclohexyl)benzoate as stationary phase for gas chromatography.

The aim of this work was determination of the physicochemical and separation properties of the liquid crystal stationary phase by use inverse gas chromatography. The basic values of retention, i.e. retention time, net and specific retention volumes, and also the basic values of the thermodynamic (values of enthalpy, entropy and free energy of adsorption) were determined during the research. The basic thermodynamic values were used to determine the interactions (intermolecular forces) occurring between the studied liquid crystal stationary phase and the injected substances. It was found that there were stronger interactions between liquid crystal stationary phase and the injected substances with higher molecular mass (n-undecane and butyl acetate).

Next step of research was the separation of four mixtures. The first mixture was composed of n-heptane, n-octane, n-nonane, n-decane and n-undecane. The second mixture was composed of xylene's isomers. The third mixture was composed of ethyl acetate, propyl acetate and butyl acetate. The latter mixture was composed of all of the previously mentioned compounds.

During research was found that the tested liquid crystal stationary phase show weak separation properties against three mixtures (the second, the third and the fourth mixture). Separation properties against mixture, which was composed of n-alkanes was satisfying. At the chromatogram there was observed five completely separated peaks. Received results show that tested crystal stationary phase might be used for separation some mixtures, therefore other mixtures will be tested in future research.

The Raman spectroscopy and X-ray photoelectron spectroscopy as the methods of graphene analysis

*Justyna Jonik, Łukasz Farczak, Tomasz Wawer, Marcin Purchała, Henryk Grajek
Faculty of New Technologies and Chemistry, Military University of Technology,
Warsaw, POLAND
e-mail: justyna.jonik@wp.pl

Keywords: *X-ray photoelectron spectroscopy, Raman spectroscopy, graphene oxide, reduced graphene oxide*

The analytical analysis X-ray photoelectron spectroscopy (XPS) is used to determine the binding energy of electrons in the atomic cores of the sample. The sample of graphene is exposed to a beam of X-rays with well-defined energy. The incident radiation of quanta excites the atoms of the sample, there by causing transitions of electrons from the specified electron shell. Some of them goes through the focusing lens to the electron analyzer, and then are acquired by the detector. The analyzer determines the amount of photoelectrons as a function of their kinetic energy. Thus, the binding energy of the electron in the atomic core is determined which allows for qualitative analysis. While the intensity of the signal corresponding to given kinetic energy, allows the quantitative analysis of an atoms in the sample, in this particular case, in graphene sample.

The Raman spectroscopy is a method used to observe vibrational, rotational, and other low-frequency modes in a given system. Therefore, Raman spectroscopy is commonly used in chemistry, since vibrational information is specific to the chemical bonds and symmetry of molecules. Thus, it provides a fingerprint on the basis of which the molecule can be identified. It is one of the basic spectroscopic technique used to characterize the derived graphene. Analyzing the Raman's spectra it is possible to specify whether the obtained graphene sample consists of multiple layers or a single layer, and whether it contains any defects. What is more, Raman spectroscopy is a fast method, not destroying the test sample and there is no necessity of special preparation of the test sample for analysis.

The aim of this study is to characterize graphene oxide and reduced graphene oxide using the afore-mentioned methods. The results of Raman's analysis and changes in Raman's spectra are presented, which depend on the cooling rate of graphene or the presence of defects in the structure of graphene. Moreover, qualitative and quantitative composition of graphene obtained by X-ray photoelectron spectroscopy is presented.

Laser additive manufacturing of composites based on tungsten carbide

*Magdalena Karpowicz¹, Marek Polański¹, Magdalena Łazińska¹

¹Faculty of Advanced Technologies and Chemistry, Military University of Technology, Warsaw, POLAND

e-mail: magdalena.karpowicz@wat.edu.pl

Keywords: *additive technologies, tungsten carbide, metal – ceramic composites, laser engineered net shaping*

The last two decades of the twentieth century, characterized by a very rapid development, as well as the steadily increasing demand for new and more durable materials used in mining, construction and to production of wear-resistant tools and machine parts. This is due to large progress in the field of new technologies, creating more and better materials, equipment and machinery. Composites based on tungsten carbide are the answer to the constantly increasing demand for materials with improved chemical, physical, mechanical, useful and operating properties. Therefore in this study will be presented manufacturing methods of metal-ceramic composite with metal matrix (Inconel 625) and reinforcement in form of ceramic particles (tungsten carbide - WC) and its characteristics.

Metal-ceramic composites based on WC are combination of good properties of both metal and ceramics. They have greater mechanical strength than ceramics and better thermal resistance than metal. Tools made of these composite quickly found application in many industries because they are materials with improved performance, which led to the replacement of steel tools by cermets.

Currently cermets are mainly produced using powder metallurgy, however equally important and increasingly used are the laser additive technologies. This is certainly due to the increasing desire to speed up the manufacturing process and the possibility of regeneration of worn tools and machine parts. The most popular technologies are SLM (Selective Laser Melting), DMLS (Direct Metal Laser Sintering), SLS (Selective Laser Sintering), and LENS (Laser Engineered Net Shaping).

In this work composites were manufactured using LENS technology. This technique allowed to receive composite containing 30, 40, 50, 60, 80 and 90 percent by weight of WC in a matrix of Inconel 625. The resulting sample has a much higher hardness than the matrix material. Manufactured samples are characterized by structural discontinuities (cracks and splinters), but in the volume are consistent.

Size enlargement and recovery of some cinchona-based organocatalysts applying organic solvent nanofiltration

*Péter Kisszékelyi¹, Petra Kozma¹, Bálint Zeller¹, György Székely², Péter Huszthy¹, József Kupai¹

¹ Faculty of Chemical Technology and Biotechnology, Budapest University of Technology and Economics, Budapest, Hungary

² School of Chemical Engineering & Analytical Science, The University of Manchester, Manchester, United Kingdom

e-mail: pkisszekelyi@mail.bme.hu

Keywords: *asymmetric synthesis, organocatalyst, organic solvent nanofiltration*

As a result of the increasing demand for optically pure products, asymmetric organocatalysis is of great interest for organic chemists, specifically in the pharmaceutical industry. However, the relatively high cost and low commercial availability of chiral organocatalysts, in addition to the high catalytic loading required in some cases (typically 1–30 mol%), pose a general challenge to the industrial development of economical and sustainable asymmetric organocatalytic processes.

The recycling of the organocatalyst may provide a suitable solution for this challenge. The application of organic solvent nanofiltration (OSN) was studied for some cinchona-based organocatalyst. OSN is capable of distinguishing molecules with size from 50 to 2500 Da, by only applying a pressure gradient. One possible way to enhance the catalyst rejection towards the membranes is to increase the molecular weight of the catalyst.

In this study, the so-called “hub approach” for the catalyst enlargement was used, where a trifunctional unit connects three catalyst molecules. Starting from 1,3,5-triethynylbenzene and 2-azidoethanol a click reaction was carried out resulting in the benzene *tris*(triazole)triethanol derivative. This skeleton was modified with three moles of cinchona squaramide catalysts.

As a second method, a β -cyclodextrin-based cinchona-thiourea catalyst was prepared in a reaction between a permethylated cyclodextrin isothiocyanate and the amino derivative of hydroquinine. These potential OSN organocatalysts can be applied in asymmetric *Michael* reactions (pentane-2,4-dione addition to β -nitrostyrene) and *Friedel–Crafts* reactions (indole addition to β -nitrostyrene).

Acknowledgements

Financial support of the Hungarian Scientific Research Fund/National Research, Development and Innovation Office (OTKA/NKFIH No. PD108462 and K 112289).

Ionic liquids additives for nickel electroplating

*Łukasz Kolanowski¹, Jarosław Wojciechowski¹, Marek Baraniak¹,
Juliusz Pernak², Grzegorz Lota¹

¹Institute of Chemistry and Technical Electrochemistry, Poznan University of
Technology, Poznan, POLAND

²Institute of Chemical Technology and Engineering, Poznan University of
Technology, Poznan, POLAND

e-mail: lukasz.m.kolanowski@doctorate.put.poznan.pl

Keywords: *nickel electroplating, ionic liquids, corrosion protection*

Nickel electroplating is a technique of deposition of thin layer of nickel on the metal surface. The nickel coatings exhibit protective as well as decorative properties. The nickel electrodeposition can be conducted using a few different types of baths. The most popular are Watts-type bath. This kind of electrolyte contain nickel sulfate, nickel chloride, boric acid and other organic additives that affect the kinetics of nickel reduction as well as mechanical/decorative properties of obtained coatings.

The aim of the presented study was to determine the effect of additions of sulfate ionic liquid precursors on the protective properties of nickel coatings electrodeposited from Watts-type baths.

The nickel coatings were deposited on the AISI 1018 steel. The steel was cleaned mechanically using abrasive paper, degreased chemically and rinsed with distilled water. Then, the chemical etching process in HCl solution was conducted. After that the nickel electroplating were performed in the Watts-type bath at the following composition: 250 g dm⁻³ NiSO₄·7H₂O, 30 g dm⁻³ NiCl₂·6H₂O and 40 g dm⁻³ H₃BO₃. The addition of ionic liquid precursor was 500 mg in 1 dm³ of the bath.

The samples were subjected to electrochemical testing in the three-electrode system. Platinum was used as an counter electrode and a saturated calomel electrode as a reference electrode. The all measurements were performed at ambient temperature in 3.5% NaCl solutions as an electrolyte. Electrochemical tests were conducted using the potentiostat/galvanostat VMP3 Biologic, France.

The conducted electrochemical measurements indicated a significant impact of the used ionic liquid precursors on the corrosive inhibition of the obtained coatings.

Acknowledgements

This work was supported by the Ministry of Science and Higher Education, project no. 03/31/DSPB/0337

Heteroatom-doped carbons for electrochemical applications

*Łukasz Kolanowski¹, Małgorzata Graś¹, Grzegorz Lota¹

¹Institute of Chemistry and Technical Electrochemistry, Poznan University of Technology, Poznan, POLAND

e-mail: lukasz.m.kolanowski@doctorate.put.poznan.pl

Keywords: *carbon materials, electrochemical capacitor,*

Carbon materials such as activated carbons due to good conductivity, high surface area and microporosity are desirable as electrodes in energy storage and conversion. The chemical and electrochemical properties of carbon materials depend on the microstructure as well as the presence of functional groups. This kind of materials could be used for the electrode preparation of an electrochemical capacitors. These devices accumulate electric charge by charging an electric double layer which is an electrostatic attraction of ions at an electrode/electrolyte interface. The increase in capacitance can be realized by additional quick faradaic reactions, commonly known as pseudocapacitive effects. This phenomenon can be reached by exploitation of transition metal oxides, conducting polymers as well as by incorporation of heteroatoms, such as: oxygen or nitrogen into carbon structure.

The purpose of the presented study was to determine the correlation between chemical structure/composition of modified (by incorporation of heteroatoms) and unmodified carbon materials and phenomena occurring at the electrode/electrolyte interface.

A scanning electron microscope was used to investigate the structure of the materials. The BET specific surface area was determined from N₂ adsorption/desorption at 77 K. Functional groups presented on the carbon surface were determine by means of infrared spectroscopy.

All prepared materials (modified and unmodified) were used as the active electrode material for electrochemical capacitors. In order to estimate the performance of the electrochemical capacitor, all measurements were carried out with two- and three-electrode cells assembled in a Swagelok[®] system. The capacitance (expressed per mass of a single electrode) were examined by galvanostatic charge/discharge, cyclic voltammetry and electrochemical impedance spectroscopy.

All obtained results indicate that the modification of carbon materials is crucial to construct an electroactive material that could be used for energy storage and conversion.

Acknowledgements

This work was supported by the National Science Centre of Poland, grant No DEC-2013/10/E/ST5/00719

Removal of organic contaminants from water systems by using hybrid process

*Kacper Kopczyński¹, Daria Pęziak-Kowalska¹, Florence Fourcade², Michał Niemczak³, Abdeltif Amrane², Łukasz Chrzanowski³, Grzegorz Lota¹

¹Institute of Chemistry and Technical Electrochemistry, Poznan University of Technology, Poznań, POLAND

²Université Rennes 1/Ecole Nationale Supérieure de Chimie de Rennes, Rennes, FRANCE

³Institute of Chemical Technology and Engineering, Poznan University of Technology, Poznań, POLAND

e-mail: kacper.kopczynski@put.poznan.pl

Keywords: *herbicidal ionic liquids, electro-Fenton, biodegradation*

Herbicidal ionic liquids (HILs) are a new group of compounds. They combine simplicity of physicochemical properties designing (taken from ionic liquids) with herbicidal properties. Generally higher efficiency of those compounds allow to reduce herbicidal field dose. However, since they still are introduced to the environment, it is necessary to find appropriate method for its removal to avoid possible contamination.

The new approaches to removal of organic contamination like pesticides, herbicides etc. from water system are Electrochemical Advanced Oxidation Processes combined with biological methods, named hybrid processes. The electrochemical processes: electrochemical oxidation or electro-Fenton are used as pretreatment, which initially degrade the pollutions and in consequence improved the efficiency of later biodegradation.

In this study didecyldimethylammonium(4-chloro-2-methylphenoxy) acetate was selected to evaluate the efficiency of a hybrid treatment method. Electro-Fenton was considered as a pretreatment step, whereas biodegradation was selected as the secondary treatment method. The efficiency of degradation, oxidation and mineralization was evaluated during 6 h of electrochemical process. This process decreased the total organic carbon and chemical oxygen demand (COD) values and increased biochemical oxygen demand (BOD₅) on the COD ratio to a value close to 0.4, showing that the electrolyzed solutions can be considered as “readily biodegradable”.

Acknowledgements

The authors acknowledge the financial support from the Ministry of Science and Education (Poland)- Grant no 03/31/DSPB/0337.

Ionic liquids as additives for lead-acid battery

*Kacper Kopczyński¹, Grzegorz Lota¹, Marek Baraniak¹, Juliusz Pernak², Włodzimierz Majchrzycki³, Henryk Przybyło⁴

¹Institute of Chemistry and Technical Electrochemistry, Poznan University of Technology, Poznań, POLAND

²Institute of Chemical Technology and Engineering, Poznan University of Technology, Poznań, POLAND

³Institute of Non-Ferrous Metals Division in Poznań Central Laboratory of Batteries and Cells, Poznań, POLAND

⁴PPUH Autopart Jacek Bąk Sp.z.o.o., Mielec, POLAND

e-mail: kacper.kopczynski@put.poznan.pl

Keywords: *ionic liquid, lead- acid battery, electrochemistry*

Lead - acid battery, due to its unique parameters, such as low price of production, simplicity of recycling (aqueous solution of sulfuric acid (VI), lead and its compounds, polypropylene, polyethylene and small amounts of additives) and good electrical properties (high discharge rates and low self-discharge) result in high utilization of those devices in many aspects of everyday life, for example in vehicles or backup power systems. Construction of this kind of cell is constantly developed to enhance electrochemical properties of it. Better exploitation of active mass as well as improved electrical characteristic will lead to more environmentally friendly production and higher durability of lead - acid cell.

Due to exceptional properties of ionic liquid like: high conductivity, thermal and chemical stability, low volatility and low toxicity they found many applications including electrochemistry industry. The most important feature of this kind of compounds is its ability to change chemical and physical properties by changing cation structure or anion.

Influence of ionic liquids addition on working parameters of lead/ lead(IV) oxide cells were presented. Electrochemical parameters were tested by means of linear sweep voltammetry, galvanostatic charge/discharge and electrochemical impedance spectroscopy. It was proven that ionic liquid increase electrochemical stability of electrolyte, reduce resistance of electroactive mass and increase of discharge capacitance of lead acid cell.

Acknowledgements

The authors acknowledge the financial support from the National Centre for Research and Development (Poland)- Grant no PBS3/A5/43/2015.

Analysis of the effect of shaping the plate of plate heat exchanger on the effectiveness of its work

*Marcin Kos

Faculty of Mechanical Engineering, Opole University of Technology, Opole, POLAND

e-mail: kos.marcin.91@gmail.com

Key words: *plate heat exchanger, flow simulation, shape of plate, efficiency of the heat exchange, CFD*

This paper presents the results of numerical analysis of the phenomena of heat-flow in the inner space of the plate heat exchanger. The main objective of the work was to determine the shape of the plate on the efficiency of heat exchange. Numerical simulations were carried out for the representative for the whole volume of the heat exchanger. Which consisting of three adjacent plates and a fluid contained there between. The analysis consisted of 9 types of discs and 3 different flow condition. All the boards were formed using a V-ribbed and geometrical differences include the opening angle of the arms and the profile ribbing embossments (triangular and semi-circular) and the number of rows.

As mediums of heat transfer adopted the most popular gas - air. For all types of plates being studied under the same conditions of co-current and countercurrent flow of gas. As the initial conditions assumed constant streams of mass and temperature of the gases. The use of an adiabatic wall of the outer allowed to eliminate effects of the environment on the transfer of the heat exchanger.

The results of numerical calculations made it possible to assess the impact on the shape of the plate heat exchanger on the working him. This evaluation was based on analysis of the intensity of heat exchange and the power required to pump fluids. Power determined based on the calculated pressure drop. As a criterion for assessing the efficiency of the heat exchanger was adopted three commonly used for this purpose indicators - efficiency η , the number of transfer units NTU and pumping power P. A detailed analysis of the simulation results showed that none of these indicators are not uniquely identify the best geometrical shape of the plate. For this reason, it is considered that as a criterion for evaluating the heat exchanger should be considered a product of the indicators $\varphi = \varepsilon \cdot NTU \cdot P$. Given the value of the index φ it can be considered that the highest efficiency of heat exchange plates provide a semicircular profile ribbing and the angle of the arms transfusion of at 70°. This is related primarily to the favorable relationship for these boards intensity of heat transfer and pressure loss of fluids. There was no apparent effect while the positioning of ribbing on the surface of the disc on efficiency heat exchangers.

Investigation of the integrated reactive adsorption process

*Tomasz Kotkowski¹, Michał Lewak¹ and Eugeniusz Molga¹

¹Faculty of Chemical and Process Engineering, Warsaw University of Technology, Warsaw, POLAND

e-mail: tomkot93@gazeta.pl

Keywords: *process intensification, process integration, reactive adsorption*

Reactive adsorption is an example of process integration. In this approach the chemical reaction is carried out simultaneously with adsorption of one of the reaction product. This kind of integration is particularly effective for reversible reaction, as it helps to remove one product from the reaction zone, so to shift the reaction equilibrium towards the total conversion of reactants. Additionally, there is no need to separate the products after reaction completion and the non-adsorbed product is relatively pure.

In these investigations the reactive adsorption process was carried out in the stirred tank reactor. Two series of experiments have been carried out: first carrying out the reaction without of the adsorbent, then at the presence of the sorbent. The experiments have been carried out with use of the testing reversible esterification reaction. The molecular sieves 3A has been employed as a sorbent of the water produced during the reaction progress. Due to removal of water from the reaction zone, the chemical equilibrium of the reaction is shifted towards the ester production, so even complete conversion of alcohol and acid is possible. The influence of the temperature, the reactant concentrations, a presence of the catalyst as well as a presence of the sorbent on the reaction progress has been investigated.

The mathematical model of the process have been formulated, which includes the reaction kinetics and thermodynamics as well as the sorption of the product. Predictions obtained with the elaborated model have been compared to the experimental results.

The obtained results indicate that the addition of sorbet into the reaction mixture helps to increase productivity of the reaction (practically total conversion of substrates can be obtained), so the post-reaction mixture contains almost pure product (ester). The process variables, as well as amount of sorbent, to carry out the process effectively has been indicated.

Synthesis and application of cinchona-squaramide organocatalyst supported on polybenzimidazole membrane

*Petra Kozma¹, Péter Kisszékelyi¹, György Székely², Péter Huszthy¹, József Kupai¹

¹ Faculty of Chemical Technology and Biotechnology, Budapest University of Technology and Economics, Budapest, Hungary

² School of Chemical Engineering & Analytical Science, The University of Manchester, Manchester, United Kingdom

e-mail: jkupai@mail.bme.hu

Keywords: immobilization, membrane, asymmetric synthesis, organocatalyst

Cinchona-based bifunctional catalysts have been extensively employed in the field of organocatalysis due to the incorporation of both hydrogen-bonding acceptors (quinuclidine) and hydrogen-bonding donors (e.g., alcohol, amide, (thio)urea and squaramide) in the molecule, which can simultaneously activate nucleophiles and electrophiles, respectively. Among them, cinchona-derived (thio)urea and squaramide catalysts have shown remarkable application potential by using their bifurcated hydrogen bonding donors in activating electrophilic carbonyls and imines.

Polymer-supported chiral organocatalysts have emerged as a rapidly expanding field of research in recent years, in part due to the traditionally emphasized advantages of polymeric immobilization (facilitated separation and recovery procedures, recycling etc.). We present a simple strategy to prepare cinchona modified polybenzimidazole (PBI) membrane.

While hydroquinine is available directly, its amino derivative was prepared from it, via azide, in a two-step sequence by using the *Bose–Mitsunobu* reaction followed by *Staudinger* reduction. The amino group was converted to squaramide by reacting with the appropriate half-squaramide derivative. This organocatalyst was immobilized to a propargyl modified PBI membrane after a functionalization with azidoethylene group and a click reaction.

Applying our immobilized cinchona-derived squaramide organocatalysts in *Michael* additions and aldol reactions we achieved excellent enantioselectivities, allowed for unprecedented practical applications in the synthesis of valuable bioactive synthons.

Acknowledgements

Financial support of the Hungarian Scientific Research Fund/National Research, Development and Innovation Office (OTKA/NKFIH No. PD108462).

Potential toxic effects of selected nanoparticles on pulmonary surfactant system

*Katarzyna Kramek-Romanowska¹, Tomasz R. Sosnowski¹

¹Faculty of Chemical and Process Engineering, Warsaw University of Technology, Warsaw, POLAND

e-mail: k.kramek@ichip.pw.edu.pl

Keywords: *nanoparticles, pulmonary surfactant, adverse health effects*

Pulmonary surfactant (PS) system is a structure defining the behaviour of the most important surface of interaction between the body and the environment, whose biological function and performance in health and disease are directly determined by its composition, structure and mechanical properties. Scientific interest in interactions between inhaled nanoparticles (NPs) and pulmonary surfactant system has grown immensely over the past few years, as interactions of NPs with different PS components may alter the structure and composition of PS, with a potential impact on its physiological performance.

The goal of this work is to present a short review on the current knowledge regarding NPs-PS interactions studied by physicochemical methods. Up till now, different studies have focused on the biophysical effects of benzopyrene and diesel NPs, as well as polymeric, metallic and mineral ones, which constitute a crucial characterization both for optimization of pulmonary drug delivery and determination of their potential toxicity. So far it has been established that NPs can affect the lung surfactant functions mainly by interfering with the adsorption of surface active molecules at the interface and, thus, preventing the formation of a fully functional interfacial film. In addition, NPs could induce pulmonary inflammation, oxidative stress and lipid peroxidation, which indirectly might lead to the impairment of PS system. The possibility of coating NPs with polyethylene glycol (PEG) has been also evaluated, showing that it minimises the detrimental NPs interactions, and it could be an alternative strategy for the development of pulmonary surfactant-compatible inhalable drug nanocarriers.

Although certain investigations have already been performed in this field, further studies are still needed not only for better understanding, potentially hazardous, interactions of environmental NPs with respiratory system, but also for the development of safer biomedical applications and the optimisation of novel drug delivery strategies through the pulmonary surfactant.

Acknowledgments

Work supported by NCN project no. 2014/13/B/ST8/00808.

New, simple method of determining necessary conditions of dead zone formation in catalyst pellet

*Grzegorz Król¹, Mirosław Szukiewicz¹

¹Department of Chemical and Process Engineering, Faculty of Chemistry, Rzeszow University of Technology, Rzeszow, POLAND

e-mail: ich_gk@prz.edu.pl

Keywords: *dead zone in catalyst pellet, necessary conditions of dead zone formation in catalyst pellet*

In a heterogeneous reaction systems, mass transfer of reactants first takes place from the bulk fluid to the external surface of the pellet. The reactants then diffuse from the external surface into and through the pores within the pellet, with reaction taking place only on the catalytic surface of the pores. So that both diffusion of the reactants into a catalyst pellet and reaction rate have an influence on a rate of processes running on solid-state catalyst. If diffusion is much slower than reaction rate, concentration of reactants inside pellet decreases rapidly. For sufficiently strong diffusional limitations, concentration of a reagent in a pellet center drops down to zero – in a pellet center appears zone without reaction (so called 'dead zone'). In consequence, efficiency of catalyst process decreases.

Determination of conditions of dead zone formation is quite hard task, for this reason they have not been fully formulated. Most frequently only necessary conditions have been presented. They must be satisfied, otherwise the concentration inside a catalyst pellet always will be greater than zero and the dead zone will not appear. But fulfilling of necessary condition not guarantees that dead zone appears. However knowledge of necessary conditions is very important from practical point of view. It enables to exclude the cases for which dead zone cannot be formed. One of researchers presented general method of determining necessary conditions of dead zone formation and applied them to few well know reaction systems. The method seems to be a bit complex. For this reason, new, simple method was developed. It is based on elementary mathematical knowledge. The method was tested on for the same reaction systems as presented earlier in literature. The results obtained were the same as those presented, with one exception. Application of our algorithm for multicomponent systems allowed to obtain more precise relationships. Moreover, the necessary conditions for others reaction schemes were developed.

Acknowledgements

This work was supported by grant no. 2015/17/B/ST8/03369 of the National Science Centre, Poland.

The influence of classic pore precursors on a morphology and mechanical properties of polyesters membranes for tissue engineering

*Aleksandra Kruk¹, Agnieszka Gadomska-Gajadur¹, Paweł Ruśkowski¹, Urszula Stodulska¹, Karolina Łojek¹, Ludwik Synoradzki¹

¹Faculty of Chemistry, Warsaw University of Technology, Warsaw, POLAND

e-mail: akruk@ch.pw.edu.pl

Keywords: *tissue engineering, scaffolds, polylacide, poly-ε-caprolactone, biodegradable polymers, cell cultures*

Recently, has been the rapid development of tissue engineering as a modern science. It is a new, interdisciplinary branch of regenerative medicine, which is combination of the biological sciences and modern technologies of biomaterials. The main and the latest issue of this science are scaffolds. There are microporous structures characterized by a highly developed, three-dimensional spatial structure. One of the form of scaffolds are semi-permeable membranes.

For the preparation of scaffolds mainly are used polymers - natural and synthetic. Recently, in tissue engineering very popular are polyesters e.g. polylactide, poly-ε-caprolactone. This polymers differ in degradation time. This time increases with the length of carbon chain. This feature has influence on the degradation time of the whole scaffold and mechanical properties. For this reason, depending on the type of tissue to be regenerated it is necessary to select a proper polymer.

Experimental results of the preparation of semi-permeable membranes for cell cultures were presented. Membranes were obtained from poly-L-lactide and poly-ε-caprolactone by inversion phase method. Morphology of the membranes was analyzed using Scanning Electron Microscopy. Mechanical properties were examined in tests of tensile strength.

The effect of classic pore precursors on the morphology and mechanical properties of the membranes was studied. The results shown that membranes depending on used polymers differ in morphology and mechanical properties. Additionally, depending on used pore precursors for each polyesters, different changes in the internal structure and mechanical properties of the membranes occur.

Characterization and modification of FePd thin films deposited on SiO₂/Si(001)

*Magdalena Krupska, Hoa Kim Ngan Nhu-Tarnawska, Aneta Duda, Sylwia Sowa, Nanostructure Laboratory, Institute of Physics, Pedagogical University, Podchorazych 2, 30-084 Cracow, Poland
e-mail: krupska.@up.krakow.pl

Keywords: *FePd alloys, RBS, Ar⁺ and Kr⁺ ion irradiation*

Recently, a great attention has been paid to the FePd, FePt and CoPt alloys with L1₀ structure by cause of the fact that they are considered as promising candidates for future ultra-high density magnetic recording applications [1] T. Schied et al., J. Appl. Phys. 108 (2010) 033902, 2) J.R. Skuza, C. Clavero, K. Yang, B. Wincheski, R.A. Lukaszew, IEEE Trans. Magn. 46 (2010) 1886]. In our work we concentrate in characterizing the stability of such type of thin films against high-energy ion bombardments.

The [Fe(0,9nm)/Pd(1,1nm)]x5 film deposited on 100 nm-thick SiO₂ layer grown on Si(001) substrate has been prepared by a thermal evaporation method, similar to the procedure described in [3] M. Perzanowski et al., Appl. Surf. Sci. 302 (2014) 129–133, A. Polit, D. Makarov, C. Brombacher, M. Krupinski, 4) M. Perzanowski, Y. Zabala, M. Albrecht, M. Marszałek, J. Magn. Mater. 381 (2015) 316–321]. We have performed the investigations on the film in three different states: 1) as-deposited state (as-grown film), 2) irradiation by 1MeV Kr⁺ beam (Kr⁺-irradiated film) and 3) after irradiation by 1MeV Ar⁺ beam (Ar⁺-irradiated film).

Rutherford Backscattering Spectroscopy (RBS, 2MeV He⁺ ion beam, scattering angle of 171°) and the X-ray reflectivity (XRR) have been employed to determine the chemical composition and the layer thickness (for as-grown film as well as for film after modification by ion irradiation). For the data evaluation, the computer code SIMNRA was employed.

The obtained results shows that both Kr⁺ and Ar⁺ ion irradiation causes a decrease of the Fe and Pd peak intensity. Moreover a strong mixing has been seen, indicated by a non- zero background between the Fe peak and the Si edge.

Acknowledgements

The authors express their thank to the group of prof. Marta Marszałek for film preparations with required thickness suitable for our RBS and IBMM experiments.

Ion beam mixing and interdiffusion in magnetite thin films after Ar⁺ ion irradiation

*Magdalena Krupska¹, Hoa Kim Ngan Nhu- Tarnawska¹, Sylwia Sowa¹, Ladislav Havela², Petr Malinsky³, Anna Mackova³,

¹Nanostructure Laboratory, Institute of Physics, Pedagogical University, Podchorazych 2, 30-084 Cracow, Poland

²Faculty of Mathematics and Physics, Charles University, Ke Karlovu 5, 12116 Prague, Czech Republic

³Department of Neutron Physics, Nuclear Physics Institute, Czech Academy of Sciences (ASCR), CZ-25068 Řež, Czech Republic

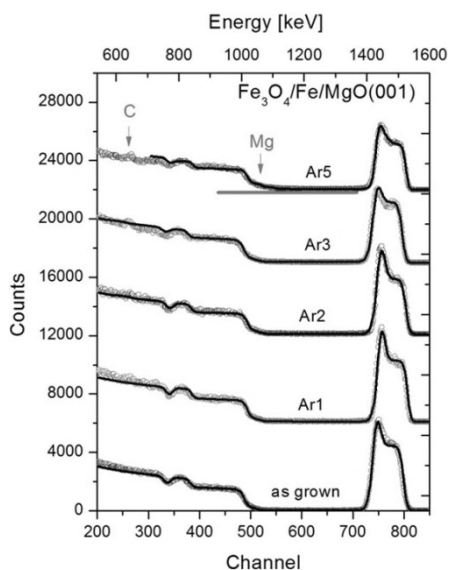
e-mail: krupska.@up.krakow.pl

Keywords: magnetite, ion beam mixing, interdiffusion

The objective of this work is investigations of the structure and physical properties of the magnetite thin film systems with single- and bi-layer structure, and with different layer thicknesses.

Fe₃O₄/MgO(001) and Fe₃O₄/Fe/MgO(001) magnetite films with a total layer thickness ranging from 25 to 200 nm have been prepared by a Molecular Beam Epitaxy Technique. The film chemical composition, layer thicknesses and structure in the as grown state and after being modified by 1MeV Ar⁺ ion beam have been investigated by means of Rutherford back-scattering (RBS), RBS- channeling (RBS-C) and X-ray reflectometry (XRR). For the data evaluation, the computer code SIMNRA was employed.

As an example we show in the picture RBS spectra of the Fe₃O₄/Fe/MgO(001) film irradiated by 1MeV Ar⁺ ion beam with four different ion fluences (Ar1=1.67·10¹⁶Ar⁺/cm², Ar2=5.77·10¹⁶ Ar⁺/cm², Ar3=15.41·10¹⁶ Ar⁺/cm², Ar4=25.71·10¹⁶ Ar⁺/cm²). The Ar⁺ ion irradiation produces Fe-Mg ion mixing which is revealed by a non-zero background between the Fe peak and the Mg edge. A large change can be also observed in the slope of the iron peak. It corresponds to a change in the composition of Fe and O in the Fe₃O₄-Fe interface.



Preparation of synthetic metalloporphyrins and their application in biomimetic oxidations of drugs in flow systems

*József Kupai¹, Tamás Földi¹, Gergő Ignác¹, Péter Huszthy¹, György Tibor Balogh²

¹ Faculty of Chemical Technology and Biotechnology, Budapest University of Technology and Economics, Budapest, Hungary

² Chemical Works of Gedeon Richter Plc., Budapest, Hungary

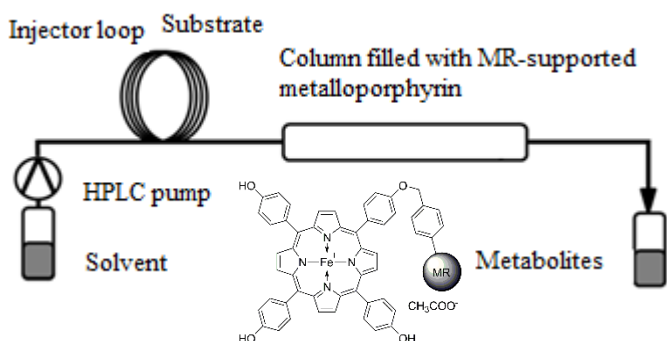
e-mail: jkupai@mail.bme.hu

Keywords: *flow technique, metalloporphyrins, drug metabolites, biomimetic oxidation*

The oxidation of organic substrates catalyzed by metalloporphyrins constitutes a major class of biomimetic oxidation reactions used in modern synthetic chemistry. Iron and ruthenium porphyrins are among the most extensively studied metalloporphyrin oxidation catalysts.

However, due to the complexity of these systems, they were not often used in the pharmaceutical industry. We developed a process allowing main biological oxidations occurring in Phase I metabolism. This process allows for rapid and efficient production of milligram quantities of metabolites.

A metalloporphyrin derivative was immobilized to *Merrifield* resin, and a screening of numerous drugs was performed with different oxidating agents in different solvents. After a selection of the drugs featuring the best metabolite profile, a flow system was developed to achieve higher productivity. The setup presented here is suitable for the preparation of drug metabolites with biomimetic oxidations in continuous-flow.



Acknowledgements

Financial support of the Hungarian Scientific Research Fund/National Research, Development and Innovation Office (OTKA/NKFIH No. PD108462).

Interferometric fibre sensor for rotational seismology application

*Anna Kurzych¹, Leszek R. Jaroszewicz¹, Zbigniew Krajewski¹, Jerzy K. Kowalski²

¹Institute of Technical Physics, Military University of Technology, Warsaw, POLAND

²m-Soft Ltd., Warsaw, POLAND

e-mail: anna.kurzych@wat.edu.pl

Keywords: *torsional effects, interferometer, sensor, engineering construction, rotation*

Rotational seismology is relatively young field of study all aspects of rotational movements induced by earthquakes, explosions or existing in engineering constructions. Its development is conditioned by application of appropriate sensors which ought to fulfil a series of technical requirements. Rotational sensors should be characterized by wide range of detected amplitude signal (10^{-11} - 10^0 rad/s) and wide detection frequency band (10^{-3} - 10^2 Hz). Moreover, they have to possess additional following features: immunity to environmental influences, low cost (for widely usage) as well as portability.

This paper presents laboratory investigation of an innovative rotational sensor - Fibre Optic System for Rotational Events & Phenomena Monitoring (FOSREM) which fulfilled technical requirements for rotational seismology. Its construction bases on the Sagnac effect which allows to measure rotation directly. The main parameter of FOSREM is its wide range of measurements: a signal amplitude from 10^{-8} rad/s to 10 rad/s and frequency from 0 Hz to the upper frequency between 2.56 Hz to 328.12 Hz. FOSREM is equipped with communication module which allows to its control remotely.

In order to confirm the unique parameters of FOSREM the series of laboratory investigation have been carried out. First of all the measurements on the special rotational table. Then we measured the Earth's rotation in various frequency detection bandpass. Moreover, the thermal stability of FOSREM has been checked.

Laboratory investigations confirmed FOSREM's wide range of measurements both in signal amplitude as well as frequency. Moreover, the measurements in climatic chamber pointed out that FOSREM is stable in temperature range from 0°C to 50°C. In conclusion, the laboratory investigation has confirmed that FOSREM is totally appropriate device for receiving significant data regarding rotational seismology. This system can be used in seismic monitoring in observatories, buildings, mines and even on glaciers and in their vicinity.

The four-channel polarimeter to examining the selected optical elements

*Marlena Kwiatkowska, Leszek R. Jaroszewicz

Institute of Technical Physics, Faculty of New Technologies and Chemistry, Military University of Technology, Warsaw, POLAND

e-mail: marlena.kwiatkowska@wat.edu.pl

Keywords: *polarymetry, polarimeter, Stokes vector, Mueller matrix*

Polarimetry is ancient science from range of optics, however today it is possible to meet, many new areas of for her applying. In this range, should take note of the development of the system allowing for effective and reliable, polarizing characterizing chosen optical elements.

Four-channel polarimeter, allows for the measurement of parameters of optical different medium and optical elements using the four photodetectors for it. The most important feature of the system is possibility of registering the state and degree of polarization of the light passing through the examined element in a moment of time what is not possible in many used measuring devices. This optical system is predicted for checking static and dynamic properties of liquid crystal cells, which are very significant from the point of view of future applications. An essential element of verification of the quality of effects of this system is its proper calibration and comparative studies with the reference system. Will be presented calibration measurement of built system with commercially available polarimeter from Thorlabs company, acting based upon the quarter-rotating. The main difference of these systems is that the four-channel polarimeter measures the Stokes vector in a moment of time, while the commercially available system allows the measurement of 33 samples per second.

During conducted surveys Mueller Matrix of following samples was compared: polarizers, quarter-wave plate, half-wave plate, non-polarizing beam splitter and specially prepared for this purpose liquid crystal cell. Results achieved from the four-channel polarimeter was compared with the reference polarimeter and was stated their very great unanimity. In the next step of the testing dynamically measurement of select liquid crystal materials will be carried out. This will allow for evaluation of the optical properties of these materials in the time domain. Examinations of optical elements of this type so far were not presented in world literature.

Hydrodynamic studies of magnetically assisted external loop air-lift

*Joanna Lechowska^{1,2}

¹West Pomeranian University of Technology in Szczecin, Faculty of Chemical Technology and Engineering, POLAND

²Students' Scientific Association of the Institute of Chemical Engineering and Environmental Protection Processes, Faculty of Chemical Technology and Engineering, West Pomeranian University of Technology in Szczecin, Szczecin, POLAND

e-mail: lechowska.joanna@zut.edu.pl

Keywords: *airlift reactor, hydrodynamic, rotating magnetic field*

The air-lift reactors are classified as one of the important group of bubble devices. These apparatus are commonly applied for gas-liquid processes, such as production of organic acids, manufacturing pharmaceuticals, antibiotics and enzymes or water purification. The air-lift reactor has a wide range of application in the fields of both chemical engineering and biotechnology because it offers simple and effective mixing in two-phase processes involving gases and liquids. The air-lift reactor offers advantages of no moving parts, low shear power consumption and good mixing quality.

Typically, the air-lift reactor consists of two vertical regions: the riser, equipped with gas distributor, and the unaerated zone called the downcomer. These regions are connected with a gas-liquid disengagement section and a horizontal bottom section. In the case of this reactor, the liquid circulation is the result of the difference of the hydrostatic pressures between the aerated and unaerated sections. Thus far, several studies have suggested that the magnetic field influenced on the hydrodynamics in air-lift reactors.

Therefore, an experimental study on the behavior of the novel type of air-lift has been performed. Special attention has been paid on the rotating magnetic field effect on the hydrodynamic characteristics in the tested apparatus. The mixing time and the liquid velocity were determined by the tracer impulse method. The mixing time were measured as the time necessary to achieve 99% homogeneity and the liquid circulation velocity were calculated as a quotient of the distance between two conductivity probes and the time period between two parallel peaks of these probes. Simple data correlations are created and discussed.

Summarizing, the use of the RMF-assisted air-lift reactor described in the current study allows to significantly increase the liquid circulation velocities. Another significant observation is the positive effect of RMF on the hydrodynamic condition in the tested reactor, confirmed by the mixing time.

The effect of addition of various Ti powders on the zirconia matrix composite

*Paula Maria Łada, Aleksandra Miazga, Katarzyna Konopka

Faculty of Material Science and Engineering, Warsaw University of Technology, Warsaw, POLAND

e-mail: paula.lada@inmat.pw.edu.pl

Keywords: *zirconium oxide (ZrO₂), titanium particles, XRD, SEM*

Partially stabilized zirconia is a popular ceramic material because of the combination of properties like low thermal conductivity, biocompatibility and high fracture toughness which allows the use in many applications. Titanium is the metal which is characterized by excellent corrosion resistance, high strength-to-weight ratio and high melting point (1667°C). A combination of both materials: zirconium oxide and titanium gives a possibility to create new, interesting composite with wide possibility of application.

In this work the samples were prepared from the nano-size ZrO₂ powder stabilized by 3 mol% Y₂O₃ with the addition of titanium powders: titanium (I) (MercChemicals) with the grain size ~15 μm and density 4.4 g/cm³ and titanium (II) (Alfa Aesar) with the grain size ~11 μm and density 4.5 g/cm³. The samples were formed by slip casting method and sintering at 1450°C in argon atmosphere. The physical properties of prepared samples were measured by Archimedes method. The phase composition and microstructure of the zirconia-titanium composites were characterized by X-Ray diffraction. The SEM and TEM observations was conducted for the verification of distribution of metal particles in the matrix and the titanium/zirconia interface.

The relative density of the green bodies and the sinters were higher for the samples prepared with titanium (II) powder. The distribution of titanium particles in the ceramic matrix were homogeneous in the both samples series with various kind of titanium. The microstructure with titanium (I) powder was characterized by zirconia grains growth on the Ti particle – ceramic matrix interface. The changes of zirconia grains size were not observed in the samples with addition of titanium (II) powder.

Acknowledgements

The work was done in frame of the project financed by National Center of Science (NCN), project DEC-2013/11/B/ ST8/00309.

Effect of modification of carbon paste electrodes pasted on the quality of the analytical signal

*Agnieszka Grzybowska, Łukasz Magda, Władysław W. Kubiak

Faculty of Materials Science and Ceramics, Department Analytical Chemistry, AGH University of Science and Technology, al. Mickiewicz 30, 30-059 Krakow, POLAND
e-mail: Lukas.magda1989@gmail.com

Keywords: *carbon paste electrodes, modification, cyclic voltammetry, dopamine*

Modification of the electrode has to improve its metrological properties or obtain new functionality. Most often it seeks to improve parameters such as sensitivity, detection limit. The spectrum of substances used for modification is very wide. In recent years, nanomaterials and, in particular, nano-carbon and metal have gained much popularity.

Carbon paste electrodes (CPE) has been created with the thoroughly mixed graphite powder and paraffin oil. The enormous popularity of carbon paste electrodes due to the ease of preparation and use, a convenient range of potentials allowing determination of both analytes of organic and inorganic. However, the main advantage is the possibility of modifying the electrode by weight of the paste, achieved by a straight admixing a modifier into the graphite paste.

Modification of carbon paste electrode nanopowders type xNi-3YSZ. Used nanopowder modifier was zirconia stabilized with yttria in an amount of 3 mol% (abbreviated by hereinafter as YSZ), which was doped with varying amounts of nickel. The aim of this study was to investigate the effect of the addition nanopowder xNi-3YSZ type on pasting properties of graphite electrodes in the test compared with the unmodified electrode and the electrode modified by nickel (Ni) nanopowders. The electrode was modified by the addition of a nanopowder with different nickel content (12.1% and 45%) in an amount of 10% based on the weight of the graphite paste. The cyclic voltammetry was used to define the relationship of current peaks on the rate of the polarization, and to assess the impact of interferent (ascorbic acid) on the analytical signal and settings the analytical parameters.

Results of studies have shown that, for the determination of dopamine, the modification of electrode with 45% Ni-3YSZ nanopowders provides the improvement in analytical parameters.

Acknowledgements

This study was carried out within the AGH – University of Science and Technology (Kraków), grant number 15.11.160.017.

Dopamine detection used to glassy carbon electrode modified by conductive polymer with nanopowders of TiO₂

*Łukasz Magda, Agnieszka Grzybowska, Władysław W. Kubiak

Faculty of Materials Science and Ceramics, Department Analytical Chemistry, AGH University of Science and Technology, al. Mickiewicza 30, 30-059 Krakow, POLAND

e-mail: Lukas.magda1989@gmail.com

Keywords: *polymers, nanopowders, electrochemical methods, glassy carbon electrodes, parameters*

Electrochemical sensors using conductive polymers such as Poli(3,4-etyleno-1,4-dioksytylofen) or PIROL as modifiers are increasingly applied. They are characterized by good durability membranes, high density and small size of the electrode. Conductive polymers can also be used as a template to introduce a modifier such as nanoparticles. With this application, the most important criterion is appropriately selected immobilization method of the nanoparticles in the polymer matrix.

Electrochemical methods play an important role in the study of pharmaceutical formulations and environmental samples. This is due to the high sensitivity and selectivity of these methods, and also not very high cost of analysis and time saving as compared to other analytical methods. After appropriate preparation of the sample matrix typically does not interfere analytical signal and can easily dissolve the analyte in a suitably selected solvent.

Preliminary measurements suggest that the modification based on a polymer with a ceramic nanopowders affects the quality of the analytical signal of the determined substance. Work is being done on the improvement of parameters such as sensitivity, detection limit or durability of the resulting layer. Introducing nanoparticles into the polymer matrix is designed to increase the contact surface area of the electrode with the analyte. This modification is to increase the sensitivity of the electrode to enable detection of lower concentration of test substances which is very important in the analysis of pharmaceuticals and environmental samples.

Acknowledgements

This study was carried out within the AGH – University of Science and Technology (Kraków), grant number 15.11.160.017.

New application of gassy carbon electrode modified by material composed of ceramic nanopowder and conductive polymers

*Łukasz Magda, Agnieszka Grzybowska, Władysław W. Kubiak

Faculty of Materials Science and Ceramics, Department Analytical Chemistry, AGH University of Science and Technology, al. Mickiewicz 30, 30-059 Krakow, POLAND
e-mail: Lukas.magda1989@gmail.com

Keywords: *polymers, nanoparticles, cyclic voltammetry, glassy carbon electrodes*

The purpose of this work is to show the possibility of modifying the voltammetric electrode using ceramic nanopowders such as titanium dioxide (TiO₂) and zirconia stabilized with yttria (3YSZ). The measurements were carried out on glassy carbon electrode and glassy carbon electrode modified with composite material ceramic nanopowder – mixed with conductive polymers.

The conductive layer was prepared using electropolymerization of the nanopowder suspension in conductive polymers. The glassy carbon electrode was polished on the polishing cloth with nanopowders Al₂O₃ and washed with deionized water. The solution before electropolymerization had been mixed using a magnetic stirrer.

For received layers there were taken pictures of scanning electron microscope (SEM) and energy dispersive spectroscopy (EDS), then analysed in order to illustrate their structure. These images show nanopowders into polymer layer which was the aim of this modification.

Preliminary measurements suggest that additional amount of nanopowder in the structure of the polymer influence on increase the number of active centers on the surface of the electrode which resulted in improvement of measurements parameters such as sensitivity or detection limit. Increase of the slope of calibration curves the electrodes modified in respect to the electrode unmodified, shows that the sensitivity of the method is increasing and we can expect a reduction in the limit of detection. Application of nanoparticles as a possibility of further modification of the measurement electrodes in order to improve their operational parameters were confirmed.

Acknowledgements

This study was carried out within the AGH – University of Science and Technology (Kraków), grant number 15.11.160.017.

Investigating the possibility of manufacturing the composite from nanocrystalline hydroxyapatite and silk fibers and study of its selected properties

*Maria Małyśa^{1,2}, Tadeusz Chudoba¹, Elżbieta Pietrzykowska^{1,2}, Sylwia Dąbrowska^{1,2}, Agnieszka Omiotek^{1,2}, Roman Mukhovskiy¹, Witold Łojkowski^{1,3}

¹Laboratory of Nanostructures, Institute of High Pressure Physics PAS, Sokołowska 29/37, 01-142 Warsaw, POLAND

²Faculty of Materials Engineering, Warsaw University of Technology, Warsaw, POLAND

³Faculty of Management, Białystok University of Technology, Białystok, POLAND
e-mail: m.malysa@labnano.pl

Keywords: *hydroxyapatite, silk fibers, composite, biomaterial, bone implant*

Nowadays technologies of the regenerative medicine are developing at an increasing rate. Therefore, the demand for the new, biocompatible and bioactive materials with particular mechanical properties is rapidly growing. Because of the need for the specific properties, composite materials which include two or more components with unique features are under great consideration. The solution is needed for a proper material for bone implant. This kind of material should be biocompatible and should have high mechanical properties. Its morphology, chemical composition and strength should be similar to those characteristic for the bone. It is often crucial that the material is bioactive and biodegradable.

The results of testing of the composite materials for bone implants made of nanocrystalline hydroxyapatite and silk fibers are shown in the following study. Few types of the composite materials were made. Hydroxyapatite was used as a matrix and as a reinforcement 5% or 15% wt. silk fibers were added. The composites were made using cryomilling and then uniaxial pressing under the pressure of 1 GPa. Bending strength, compressive strength and Young modulus were characterized. Samples with the highest mechanical properties were degraded in water and in the physiological saline solution. After degradation the mechanical properties were tested again.

Highest mechanical properties were reached for the samples made from 15% wt. silk fibers and 85% wt. nanocrystalline hydroxyapatite pressed in 80°C. Compressive strength was 276,3±39,7 MPa, Young modulus was 8,4±0,9 GPa and bending strength was 82,3±39,7 MPa, which met the set requirements. The first results of degradation tests were satisfying.

Further development is required for the material to be used in real life applications.

Investigating the possibility of manufacturing the composite from nanocrystalline hydroxyapatite and silk fibers and study of its selected properties

*Maria Małyśa^{1,2}, Tadeusz Chudoba¹, Elżbieta Pietrzykowska^{1,2}, Sylwia Dąbrowska^{1,2}, Agnieszka Omiotek^{1,2}, Roman Mukhovskiy¹, Witold Łojkowski^{1,3}

¹Laboratory of Nanostructures, Institute of High Pressure Physics PAS, Sokołowska 29/37, 01-142 Warsaw, POLAND

²Faculty of Materials Engineering, Warsaw University of Technology, Warsaw, POLAND

³Faculty of Management, Białystok University of Technology, Białystok, POLAND
e-mail: m.malysa@labnano.pl

Keywords: *hydroxyapatite, silk fibers, composite, biomaterial, bone implant*

Nowadays technologies of the regenerative medicine are developing at an increasing rate. Therefore, the demand for the new, biocompatible and bioactive materials with particular mechanical properties is rapidly growing. Because of the need for the specific properties, composite materials which include two or more components with unique features are under great consideration. The solution is needed for a proper material for bone implant. This kind of material should be biocompatible and should have high mechanical properties. Its morphology, chemical composition and strength should be similar to those characteristic for the bone. It is often crucial that the material is bioactive and biodegradable.

The results of testing of the composite materials for bone implants made of nanocrystalline hydroxyapatite and silk fibers are shown in the following study. Few types of the composite materials were made. Hydroxyapatite was used as a matrix and as a reinforcement 5% or 15% wt. silk fibers were added. The composites were made using cryomilling and then uniaxial pressing under the pressure of 1 GPa. Bending strength, compressive strength and Young modulus were characterized. Samples with the highest mechanical properties were degraded in water and in the physiological saline solution. After degradation the mechanical properties were tested again.

Highest mechanical properties were reached for the samples made from 15% wt. silk fibers and 85% wt. nanocrystalline hydroxyapatite pressed in 80°C. Compressive strength was 276,3±39,7 MPa, Young modulus was 8,4±0,9 GPa and bending strength was 82,3±39,7 MPa, which met the set requirements. The first results of degradation tests were satisfying.

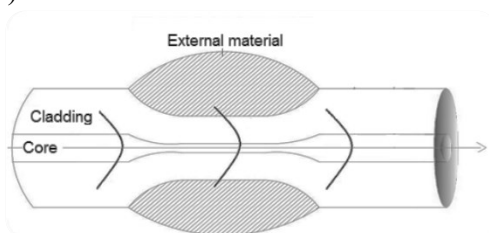
Further development is required for the material to be used in real life applications.

Influence of different materials on light propagation in tapered optical fiber

*Joanna Moś, Karol Stasiewicz, Magdalena Karpowicz, Leszek R. Jaroszewicz
Faculty of New Technology and Chemistry, Military University of Technology,
Warsaw, POLAND
e-mail: joanna.musial@wat.edu.pl

Keywords: *taper technology, optical sensor, optical fiber taper*

Optical fiber taper can be obtained as a result of heat to melting temperature of glass and elongation optical fiber to a certain length of the fiber. A taper can be divided on three region: untapered, transition and waist. Tapered waist region is very important in respect of application in optical sensors. Possibility to affect by external factors on propagating light beam in the optical fiber taper is connected with change of boundary conditions. Light is not propagate on surface core/cladding, like in a standard optical fibers, but on surface modify core/environment (air).



Structure an optical fiber taper and extra material.

In tapered optical fibers, when conditions of environment are changed, also a light beam propagation in optical fiber was changed. Combination of an optical fiber taper with an extra material like liquid crystal, metal etc. caused increasing sensitivity for some parameters like a temperature, electric field etc. Combination a tapered optical fibers with material can cause different, interesting effects (for example surface plasmon resonance). That structure can be basic for construction an optical sensors.

Tapered optical fiber was obtained used FOTET (Fiber Optic Taper Element Technology). Tapered optical fiber characterized parameters: 0.2 dB loss, 20-30 mm elongation, and diameter of taper waist 10-20 μm . Measurement was obtained by used laser 1550 nm ThorLabs, Laser Supercontinuum 420-2000 nm, Power Meter ThorLabs and Optical Spectrum Analyzer. As a result connected tapered optical fibers and liquid crystals will be filter in wavelength 500-700 nm dependent on the electric field 0-160V. Combination with metals (Gold, Titanium) showed effect surface plasmon resonance dependent of the thickness of metal layer 25-100 nm.

Aluminosilicates as an effective filler for epoxy resin composites

*Jolanta Nieroda^{1,2}, Andrzej Rybak², Maciej Sitarz¹

¹Faculty of Materials Science and Ceramics, AGH University of Science and Technology, Krakow, POLAND

²ABB Corporate Research Center, Krakow, POLAND

e-mail: jolsroka@agh.edu.pl

Keywords: *aluminosilicate, thermal conductivity, dielectric properties, mechanical parameters*

Low thermal conductivity is one of the main problem for electrical insulation material like the epoxy resin. Heat transferring can be improved by filler incorporation, however it must be remembered that the electrical insulation properties of composite must be maintained at the same time. Mineral fillers as a natural insulators are preferred candidates and one of the most commonly used is the silica flour. This type of filler allows to obtain epoxy resin composite with five time greater thermal conductivity and excellent mechanical properties in relation to pure epoxy. Both this parameters are strongly dependent on amount of the added filler.

In the presented work the different types of commercial aluminosilicate fillers covered with silane coupling agents were tested. Thermal conductivity, dielectric properties and three types of mechanical parameters, namely: tensile strength, Young Modulus and fracture toughness were studied in order to examine the influence of amount of the filler and type of silanization.

The obtained results were compared with values of standard composite filled with silica flour. Composites filled with auminosilicates exhibit much better mechanical properties with up to 61% relative increase of fracture toughness as well as enhanced insulating properties with 61% relative increase of thermal conductivity. It makes aluminosilicates a very attractive fillers for composites with insulating properties.

The preliminary characterization of amorphous metal surface for power industry application

*Jolanta Nieroda^{1,2}, Andrzej Rybak², Grzegorz Kmita², Maciej Sitarz¹

¹Faculty of Materials Science and Ceramics, AGH University of Science and Technology, Krakow, POLAND

²ABB Corporate Research Center, Krakow, POLAND

e-mail: jolsroka@agh.edu.pl

Keywords: *metallic glass, x-ray photoelectron spectroscopy, surface energy*

Metallic glass is a metallic material which exhibit long-range disorder in its structure. It is mostly three or more component alloy, where some of them are magnetic metals. The amorphous metal is technical glass, however it is much tougher and less brittle than regular oxide glasses and ceramics. Additionally, unlike regular glass which is used in electrical insulators on power lines, amorphous metals characterize with high electrical conductivity. At the same time, they exhibit very good magnetic properties (e.g. low-magnetization loss). The above mentioned properties are very useful in electrical engineering industry and this material is more and more popular as a substance for high-efficiency transformer core production. Transformers with cores made of amorphous metals present lower losses while they working in relation to the regular one. However, production technology of amorphous metal core is still evolving, and thus even higher efficiency of transformers is expected. A raw material must be carefully investigated and characterized before the main production process is started.

Presented work contain results of complementary examination of amorphous metal material. X-ray fluorescence and scanning electron microscopy with energy dispersive spectroscopy were selected for sample characterization in the whole volume. Two more methods, namely x-ray photoelectron spectroscopy and Raman spectroscopy were used in order to get information about outside layer of studied material. Additionally, surface cleaning process was optimized with surface free energy measurement by means of Drop Shape Analyzer as a control method.

Used methods allow to fully investigate the amorphous metal samples. Information about surface character and appropriate cleaning pretreatment were received and let to apply the best parameters in further experiments.

ZnS nanowires as a new acceptor material for the photovoltaic cells

*Elżbieta M. Nowak¹, Adam Żaba¹, Svitlana Sovinska¹, Jerzy Sanetra², Katarzyna Matras-Postołek¹

¹Faculty of Chemical Engineering and Technology, Cracow University of Technology, Cracow, POLAND

²Institute of Physics, Cracow University of Technology, Cracow, POLAND

e-mail: nowak.elzbieta@student.pk.edu.pl

Keywords: *solar cells, ZnS nanowires, poly(3-hexylthiophene)*

Photovoltaic (PV) effect is the process of the direct conversion of light energy to electricity. Solar radiation is a never-ending source of green energy, which exploitation by mankind is still incipient and being limited by several hurdles like the low PV efficiency, fabrication complexity and a high price. The latter two challenges could be successfully solved through introduction of multilayered “soft” PV architectures instead of hard silicon-technology. Such new solar cells don’t require expensive fabrication equipment and are scalable.

For the energy conversion processes the first main step is to absorb sun light in the so called “active layer” of the PV cell. For the high efficiency of the light absorption it is important to choose the right donor material with high extinction coefficient covering most of the sun spectrum. After the photon is absorbed, the exciton – the bounded pair of an electron and a hole - is created. This exciton gets separated on the potential difference which is created by the acceptor material.

This work presents the investigation of the donor-acceptor devices where conductive polymer (poly(3-hexylthiophene)) plays the role of the donor material and ZnS nanowires play the role of the acceptor material. Additionally, to block electrons from migrating to the anode (tin-doped indium oxide, ITO) a layer of polystyrenesulfonate-doped poly(3,4-ethylenedioxythiophene) (PEDOT:PSS) was used. The cathodes were made of the aluminium (Al). The influence of composition and preparation parameters, such as content of the ZnS nanowires, thicknesses of the active layers and the temperature of drying on the resulting PV parameters of the cell was studied. Through optimization of the parameters the PV efficiency of 0.57% was obtained. To the best of our knowledge, this is the first time when ZnS in the form of nanowires was used as an acceptor material for the nanocomposite-based bulk heterojunction hybrid solar cells.

Acknowledgements

This work was supported in part by the project from National Center for Research and Development (grant no. LIDER/009/185/L-5/13/NCBR/2014) and Foundation for Polish Science (grant no. HOMING PLUS /2012-6/5).

Preparation of poly(vinyl alcohol)/graphene composites

*Maksymilian Nowak, Marta Mazurkiewicz-Pawlicka, Leszek Stobiński

Faculty of Chemical and Process Engineering, Warsaw University of Technology,
Warsaw, POLAND

e-mail: msf.nowak@gmail.com

Keywords: *graphene, polymer composites, poly(vinyl alcohol)*

Graphene is a very interesting material due to its extraordinary characteristics, such as high electrical and thermal conductivity, excellent mechanical properties and the ability of shielding electromagnetic radiation. These properties make graphene a perfect filler for polymer composites. For this purpose, reduced graphene oxide obtained by oxidation and reduction of graphite powder is a good candidate. Poly(vinyl alcohol), as opposed to many other polymers, does not degrade in UV-light and because of that is used as a coating resin in textile, paper and packaging industry. Addition of graphene to this polymer can enhance its electromagnetic radiation shielding properties, expanding its applications as a protective coating material.

Reduced graphene oxide (rGO) was prepared from graphite powder using the Hummers' method and further reduction using hydrazine. Poly(vinyl alcohol) (PVA) of molecular mass 72000 and degree of hydrolysis 85-89% was dissolved in water. The PVA/rGO dispersions were prepared using a rotor-stator homogeniser, ultrasonic homogeniser, three roll mill or a ball mill. The solid content of rGO was set as either 0.1 wt% or 1 wt% compared with PVA. Two main approaches were used for the mixing procedure: a) rGO powder without modifications was mixed with the dissolved polymer and b) rGO powder was first dispersed in water and next mixed with the polymer. In order to increase the dispersion in water a chemical modification of rGO powder with terephthalic acid was used. Obtained dispersions were poured into a silicone mold and dried in room temperature. The samples were then examined using an optical microscope to determine the degree of dispersion of rGO in PVA. Chemical composition was studied using Fourier transform infrared spectroscopy (FT-IR).

In the samples acquired using both homogenisers there were clearly visible aggregates. Earlier dispersion and the chemical modification of rGO in water both resulted in a better distribution of flakes in composite films. The best dispersion was achieved in the samples mixed in the ball mill for 30 minutes at 400 rpm.

The performed research allowed to develop an effective preparation method of PVA/rGO composites.

The influence of the addition of ZrO₂ on the surface parameters of a porcelain glazes

*Katarzyna Pasiut¹, Janusz Partyka¹

¹Faculty of Ceramic and Refractory Materials, AGH University of Science and Technology, Kraków, Poland

e-mail: kpasiut@agh.edu.pl

Keywords: *glaze, porcelain, zirconium oxide, whiteness, gloss, roughness*

The production of ceramic porcelain glazes is strongly dependent on the chemical composition of the glaze. In production process it is very important to obtain an appropriate surface parameters. Addition of some oxides can significantly change the parameters.

This researches were carried on the influence of adding the zirconium oxides on the surface parameters, for firing temperature 1230°C. The examined glazes had a constant of molar ratio of SiO₂/Al₂O₃=4 and Na₂O/K₂O=1 and variable of a molar ratio of CaO/MgO and amount of added of zirconium oxide (1,5%, 3% and 6%).

During this research some parameters such as: whiteness in CIE L*a*b* in system, gloss by glossmeter, and roughness of the surface by the confocal microscope, were measured. In addition, studies of chemical durability were made.

The obtained results show that the addition of zirconium oxide and variable of molar ratio of the alkaline earth oxides in an interesting way affects on the appearance and parameters of the surface of glaze.

The influence of the addition of ZrO₂ on the technological parameters of a porcelain glazes

*Katarzyna Pasiut¹, Janusz Partyka¹

¹Faculty of Ceramic and Refractory Materials, AGH University of Science and Technology, Kraków, Poland

e-mail: kpasiut@agh.edu.pl

Keywords: *glaze, porcelain, zirconium oxide, HSM*

Ceramic glazes are coatings which are applied to a ceramic body to improve its parameters. The proper modification of glazes with use some oxides or chemical compounds causes the changes of technological parameters of glazes. One of the oxides which are added to glazes is zirconium oxide.

The research focused on the influence of addition of zirconium oxide on some technological parameters of porcelain ceramic glazes, which were created to fire in temperature 1230°C. The examined glazes had a constant molar ratio of SiO₂/Al₂O₃ =4 and Na₂O/K₂O=1. The variables were a molar ratio of CaO/MgO and amount of added of zirconium oxide (1.5%, 3% and 6%).

As the result of examination some parameters were obtained such as: characteristic temperatures obtained by HSM and dilatometric measurements by mechanical dilatometer, coefficient of thermal expansion by dilatometric method and the viscosity of glaze as a function of temperature, using *Vogel – Fulcher – Tammann models*.

The obtained results indicate on a lot of important dependences, which were caused by the changing molar ratio of the alkaline earth oxides and the addition of zirconium oxides to the glazes.

Study of selected aspects in microalgae *Chlorella vulgaris* cultivation in laboratory conditions

*Agnieszka Patyna, Stanisław Witczak

Department of Process Engineering, Faculty of Mechanical Engineering, Opole University of Technology, Opole, POLAND

e-mail: patyna.a@gmail.com

Keywords: *Chlorella vulgaris*, photobioreactor, algal cultivation, biomass productivity

Algae biomass is increasingly regarded as a potential resource that could be used to produce biofuels, electricity and heat. Due to high prices of crude oil and increase of environmental pollution, more extensive research are undertaken to verify the possibility of use of algal biomass as a source of alternative energy. Algae contain a lot of nutrients, so they can be used as food for humans and livestock. Algae cultivation does not demand large areas of land to expose cells to sunlight, so their production rate is higher than vascular plants. Moreover algae cultivation lets to achieve high biomass concentration. Important cultivation factors are: illumination (light intensity is an important factor because it drives photosynthesis), CO₂ supply, culture medium and mixing.

The experimental research was conducted using *Chlorella vulgaris* BA 002 strain. For the cultivation of algae was used a standard cultivation medium prepared according to the original recipe. The aim of this study was to determine the effectiveness of biomass growth in laboratory condition. Cultures were cultivate in 50 ml Erlenmeyer flask and were mixed by using flask-shaker which was turned on regularly with the same timing. The cultivation time lasted 70 hours. A source of artificial light and its intensity was consistent during the experiment.

Algal growth was determined by measuring the amount of dry mass and optical density. After 70 hours dry mass of microalgae increased from 200 mg/dm³ to almost 500 mg/dm³. A productivity calculated according to the dry mass was decrease within the experiment. In was caused, by depletion of cultivation medium. The average productivity reached 8 mg/(dm³·h). The optical density was measured by optical 560 nm densitometer. The initial dimensionless density was 0.5 and after 70 hours it reached value 1.3.

A comparison of experimental data with literature data made it possible to specify favorable culture conditions for the tested strain of microalgae. Continuation of research in this area finally will permit to determine operating parameters of photobioreactor for algal cultivation in a large scale.

Monitoring of domestic sewage treatment plant

*Monika Pawlita-Posmyk¹, Małgorzata Wzorek²

¹ Department of Process Engineering, Faculty of Mechanical Engineering, Opole University of Technology, Opole, POLAND

² Department of Process Engineering, Faculty of Mechanical Engineering, Opole University of Technology, Opole, POLAND

e-mail: mpawlita@wp.pl

Keywords: *sewage, domestic sewage treatment plant, monitoring*

In areas with scattered low population density, where it is unprofitable to build extensive sewer networks wastewater infrastructure is insufficiently developed. In these areas some residents use domestic sewage systems i.e. septic tanks and domestic sewage treatment plants. In recent years, domestic sewage treatment plants have become one of the most popular method of sanitation in rural areas. In the case of a properly operating treatment plant the treated sewage should contain minimum concentration of harmful substances. However levels of these substances may be significantly higher for systems overloaded or operating in an incorrect way. In order to evaluate the operation parameters of a domestic biological sewage treatment plant, an analysis of selected physicochemical parameters (such as pH, BOD₅, suspended solids, chlorides, sulphates, heavy metals, etc.) was tested. Sewage was collected at different stages of treatment e.g. from a settling tank and two aerobic zones with biological system. Samples were taken in the spring and autumn of 2016.

The conducted study showed that the values of the examined treated sewage indicators do not exceed the permissible values contained in the Regulation of the Minister of the Environment on the conditions to be met when putting sewage in water or ground or on substances especially harmful to the aquatic environment.

Based on the obtained results it can be stated that the tested domestic sewage treatment plant works properly, treated sewage was characterized by the parameters specified by the manufacturer and therefore this solution is safe for the environment.

Encapsulation of linalool in solid lipid nanoparticles

Irina Pereira^{1,2}, *Aleksandra Zielińska^{1,3}, Francisco J. Veiga^{1,4}, Amélia M. Silva², Ana C. Santos^{1,5}, Izabela Nowak³, Eliana B. Souto^{1,4}

¹Department of Pharmaceutical Technology, Faculty of Pharmacy, University of Coimbra, PORTUGAL, ² Department of Biology and Environment, University of Trás-os-Montes and Alto Douro, PORTUGAL, ³ Faculty of Chemistry, Adam Mickiewicz University in Poznań, Poznań, POLAND, ⁴ REQUIMTE/LAQV, Group of Pharmaceutical Technology, Faculty of Pharmacy, University of Coimbra, PORTUGAL, ⁵ Institute for Innovation and Health Research, Institute for Molecular and Cell Biology, Porto, PORTUGAL

e-mail: ola.zielinska@amu.edu.pl

Keywords: *high pressure homogenization, hydrophilic drugs, linalool, monoterpenes, solid lipid nanoparticles*

Linalool (3,7-dimethyl-1,6-octadien-3-ol) is an acyclic monoterpene tertiary alcohol. Linalool is a volatile compound present in the flower scent of different plant families. According to recent reports, linalool has a wide range of biological effects which makes it suitable to be encapsulated in drug delivery nanocarriers. Furthermore, it becomes a challenge to encapsulate linalool in lipid nanocarriers due to its hydrophilic structure. The aim of this study was to optimize the encapsulation of linalool in solid lipid nanoparticles (SLN).

SLN formulations were produced by hot homogenization using high pressure homogenization (HPH). Thereupon production of linalool-loaded SLN a qualitative analysis was performed using dynamic light scattering (DLS).

Firstly, an optimization process to find the correct proportions of each ingredient has been carried out, as well as the production parameters that resulted in formulations with a small particle size and polydispersity index (PDI) below 0.5. Two formulations, SLN-linalool no. 1 (with 1 wt. % linalool; 4 wt. % solid lipid and 1.25 wt. % surfactant) and no. 3 (with 1 wt. % linalool; 4 wt. % solid lipid and 2.5 wt. % surfactant) showed satisfactory results.

Subsequently, linalool-loaded SLN dispersions were storage at different temperatures: 4, 25 and 40°C for a period of 1 month. At 4°C both linalool-loaded SLN dispersions (no. 1 and 3) showed a high mean particle size (Approximately 2533 nm). In contrast, at 40°C particles displayed the smallest mean particle size, particularly SLN-linalool no. 3 showed the lowest particle size (84.2 nm). The best storage temperature to obtain smaller and stable linalool-loaded SLN dispersions was at 40 °C.

In summary, linalool-loaded SLN no. 3 was the most stable formulation resulting from the optimization process since it showed the smallest mean particle size and PDI values, both at 25 and 40 °C.

Improving of nitrate sensors parameters by applying graphene-based intermediate layers

*Magdalena Pięk, Joanna Smajdor, Robert Piech, Beata Paczosa-Bator

Faculty of Materials Science and Ceramics, AGH-UST University of Science and Technology, Cracow, POLAND

e-mail: mras@agh.edu.pl

Keywords: *graphene, tetrathiafulvalene, high capacitance, ion-selective electrode*

Ion-selective electrodes have been well established analytical tools in environmental monitoring, clinical diagnostics or process control for many years. The potential stability of all-solid-state ion-selective electrodes can be improved by introduction of intermediate layer between the ion-selective membrane and the substrate electrode. Such solid contact layer should show redox and ion-exchange properties and suitable materials are still sought and examined. Moreover, interlayer should be characterized by large surface area, high hydrophobicity and insensitivity to oxygen or light.

Graphene is one of the carbon nanomaterials which exhibits not only a high surface area, but also distinctive electrical conductivity and chemical stability. Whereas tetrathiafulvalene (TTF) is organic conductive compound frequently used as a redox mediator.

Nitrate-selective electrodes were modified with TTF and its nitrate salt (TTF(NO₃)) and graphene nanocomposite. Solid contact layers were investigated by scanning electron microscopy and electrochemical methods. Electrical and analytical parameters of sensors were determined using chronopotentiometric, electrochemical impedance spectroscopy and potentiometric measurements.

Studied electrodes present improved functional properties in comparison to sensors where graphene or tetrathiafulvalene were applied separately. A Nernstian response and low detection limit were observed. The mixing and simultaneous usage of materials which shows electronic and ionic conductivity has a positive impact on the electrical and analytical parameters of electrodes. The high surface area of graphene is responsible for forming a high double layer capacitance at the solid contact and the nitrate-selective membrane interface. Such solution improves the potential stability of developed sensors.

Acknowledgments

The financial support from AGH project 11.11.160.799 is gratefully acknowledged.

Comparison of influence of used nanomaterials on Na⁺-ISEs parameters

*Magdalena Pięć

Faculty of Materials Science and Ceramics, AGH-UST University of Science and Technology, Cracow, POLAND

e-mail: mras@agh.edu.pl

Keywords: *carbon nanomaterials, 7,7,8,8-tetracyanoquinodimethane, potentiometric sensors, potential stability*

Carbon nanomaterials such as graphene, carbon black, single-walled carbon nanotubes, multi-walled carbon nanotubes, and ordered mesoporous carbon are characterized by hydrophobic properties, large surface area and high conductivity. It would seem that the properties of these nanomaterials will be similar due to the same composition. However, some differences between them can be observed and may be associated with their structure, surface chemistry and conductivity.

Each of these carbon nanomaterials were mixed with 7,7,8,8-tetracyanoquinodimethane (TCNQ) and its sodium salt (NaTCNQ) and used as solid contact layers in all-solid-state sodium-selective electrodes. Such interlayers were characterized by a high capacity of carbon nanomaterials and contained a redox couple TCNQ/TCNQ⁻. The morphologies of solid contact layers were investigated using a scanning electron microscope. Proposed sensors were examined during potentiometric and chronopotentiometric measurements in order to compare their parameters and to assess the impact of the type of nanomaterials applied on electrode performance.

Studied interlayers are very stable and mark by good adherence. Type of carbon nanomaterial used in solid contact layer affects in various ways on the analytical and electrical parameters of developed sensors. Carbon black-contacted electrodes show the highest capacitance value obtained so far for sodium sensors and perfect potential stability. Moreover, these electrodes also have the best sensitivity. The lowest capacitance was determined for electrodes with multi-walled carbon nanotubes solid contact. On the other hand, graphene-modified sensors exhibit the most reproducible standard potential value.

Acknowledgements

This work was supported by AGH University of Science and Technology grant (Project No. 11.11.160.799).

The environmental impact of installations for depolymerization of plastic waste

*Paulina Pięta¹, Daria Polek¹, Marta Wołosiewicz-Głąb¹, Łukasz Grabowski¹

¹AGH - University of Science and Technology, Faculty of Mining and Geoengineering, Department of Environmental Engineering and Mineral Processing, 30 A. Mickiewicz Ave., 30-059 Cracow, POLAND

e-mail: ppieta@agh.edu.pl

Keywords: *plastic waste, polyolefins, impact of depolymerization technology on the environment, energy recovery*

Plastic waste is a challenge to society, regardless of their awareness of sustainable development and technological progress. In this paper the depolymerization technology of plastic waste and their impact on the environment will be presented. Particular emphasis will be devoted to the waste produced from the waste of polyolefin compounds, which is a great percentage of disposable products used in everyday life. Depolymerization of plastic waste will help to clean up the environment and will allow to recover and use the energy contained in the waste of mixed plastics.

Polyolefins (polyethylene PE and polypropylene PP) are a major group of synthetic plastics. Due to the distinctive uniform chemical composition and high availability, they are interesting raw material for further processing and, consequently, to reduce the amount of waste.

The paper presents and characterized polyolefins. The treatment and management of this type of waste have been shown. Describes the process of obtaining a pure synthetic oil in distilleries. The possibilities to use thermocatalytic polyolefin processing system.

Outlines the prospects for using this type of technology. Their analysis was carried out taking into account the various stages of the recovery process, economics and environmental impact.

Thanks to its diverse and unique chemical and physical properties, and any possibility of modifying them using a variety of additives plastics have almost unlimited possibilities of use. Such diversity complicates the process of waste management and the ways of reuse of plastics.

Electrooptic properties of nematic liquid crystal mixtures doped with gold nanoparticles

*Natalia Przybysz^{1,2}, *Agnieszka Mackiewicz¹, Paweł Marć¹, Noureddine Bennis¹, Przemysław Kula¹, Emilia Tomaszewska², Jarosław Grobelny², Leszek R. Jaroszewicz¹

¹Institute of Applied Physics, Faculty of Advanced Technologies and Chemistry, Military University of Technology, 2 Kaliskiego St., 00-908 Warsaw, Poland

²Department of Materials Technology and Chemistry, Faculty of Chemistry, University of Lodz, 163 Pomorska St, 90-236 Lodz, Poland

e-mail: natalia.przybysz@wat.edu.pl

Keywords: *Au NPs, gold nanoparticles, nematic liquid crystal doped with gold nanoparticles, electrooptic properties of nematic liquid crystal*

Implementation of the gold nanoparticles (Au NPs) to the structures of nematic liquid crystal (LC) mixtures change its functioning.

Au NPs colloids and LC mixtures have specific physicochemical properties which allowed for the effective transfer of Au NPs from an organic solvent to a LC mixture. From that moment, the LC mixture becomes a new environment for the Au NPs molecule. In this respect, the organic colloids of Au NPs and the LC mixtures must be modified to allow for Au NPs dispersion in the new environment.

Stable nematic liquid crystal mixtures doped with gold nanoparticles were prepared with the use of various size of molecules and concentrations of NPs in the colloids in a wavelength range of visible light and thereby in an area of surface plasmon resonance. As a result, in liquid crystal cells (thickness of 5 μm) filled with the prepared mixture, with increasing temperature changes of refractive indices and optical birefringence was observed, therefore absorption of electromagnetic wave was not registered.

Moreover, changes in the transmission in the LC-NPs system in liquid crystal cells, were measured with increase of the temperature from 30 to 55°C. Measurements of Mueller matrix, ellipsometric, UV/ViS spectrometry, surface plasmon resonance and changes in the phase of light will be made at our earliest convenience.

Effective methods of selective filling of the air holes in the polarization-maintaining photonic crystal fiber

*Natalia Przybysz¹, *Angelika Molska¹, Paweł Marć¹, Leszek R. Jaroszewicz¹

¹Institute of Applied Physics, Faculty of Advanced Technologies and Chemistry, Military University of Technology, 2 Kaliskiego St., 00-908 Warsaw, Poland

e-mail: natalia.przybysz@wat.edu.pl

Keywords: *polarization-maintaining photonic crystal fiber, filling photonic crystal fibers, higher alkanes*

Optical fiber sensors' technology has evolved rapidly during last decades. This type of sensors are often used in industry, medicine and military applications because they provide important advantages e.g. low insertion loss, low weight and dimensions, high reliability and electro-magnetic immunity.

The most important part of the sensor is an optical fiber. In a proposed work a single mode polarization-maintaining photonic crystal fiber PM 1550 (NKT Photonics) have been chosen for designing a special sensor transducer based on a selective filling the air holes. This photonic crystal fiber (PCF) cross-section consists of five rings of the air holes in a honey comb structure with diameter around 2.2 μm and two main holes with diameters equal to 4.4 μm symmetrically placed around the core region of it. The main idea of the transducers manufacturing was selective filling of these main air holes. It was done by several steps. First, the fusion splicer FSU 975 (Ericsson) was used to collapse smaller air holes. Then, the main air holes were filled with selected mixture of polymers at the length less than 4 cm and the photopolymerization was performed by a laser emitted at 532nm wavelengths. Next, the fiber was cleaved to open small air holes. Those holes were filled with a polymer and the photopolymerization process was carried out. Then, the fiber was cleaved to open main air holes. In the last step of the process it is possible to fill the PCF with material which has proper physical properties. The electron microscope images were used to control the states of the air holes of the PCF at each step of described above process.

To summarize the technology procedure of selective air holes filling of the PM – 1550 PCF allows to design optical fiber transducers for temperature threshold sensors in which we will use n-alkanes and nanoparticles doped n-alkanes as a filling material.

Synthetic pathways of novel high fluorinated C4-C4 dialkylphenyltolanes

*Marta Pytlarczyk, Jakub Herman, Piotr Harmata, Przemysław Kula

Institute of Chemistry, Faculty of Advanced Technologies and Chemistry, Military University of Technology, Warsaw, POLAND

e-mail: marta.pytlarczyk@wat.edu.pl

Keywords: *phenyltolanes, birefringence, liquid crystal, nematic, cross-coupling*

Rod-like molecules, based on phenyltolane core are important class of high-birefringence nematic liquid crystals. Unsubstituted dialkylphenyltolanes have high melting and clearing point (respectively above 160°C and above 220°C) and only nematic phase. When fluorine or more bulky substituents are placed at the middle ring of the core or at a proximal position to polar group, lower melting points are obtained and smectic phase can be stabilized. Few examples of higher fluorinated analogues of C4-C4 phenyltolanes are known from the literature. These liquid crystals are promising as medium birefringent, low viscous materials.

In synthesis of phenyltolane core two important reactions were used: Suzuki-Miyaura coupling and Sonogashira-Hagihara coupling. Those approaches require suitable functional groups in key intermediates such as terminal acetylenes, boronic acids and aryl halides. In most cases Directed Ortho Lithation Metallation was used to obtain aryl iodides. In our synthesis of fluorinated dialkylphenyltolanes we can distinguish three groups of important intermediates (based on tolane core, biphenyl core and single benzene ring) used directly in finishing synthesis of target molecules.

The purity and structures of the final products and intermediates were confirmed by spectral methods: gas chromatography GC-MS, GC-FID and nuclear magnetic resonance. The phase transition temperatures, phase situation and enthalpy data were determined by polarizing optical microscopy (POM) and differential scanning calorimeter.

To sum up, novel fluorinated liquid crystals based on 4-butyl-4'-[2-(4-butylphenyl)ethynyl]-1,1'-biphenyls core were synthesised. All of the received compounds have clearing point below 160°C. Five compounds have a very wide nematic phase. Only for one compound we observed smectic phase. Temperatures and enthalpies prove that these compounds are very promising as medium birefringent LC.

New nematic liquid crystals with long conjugated π electronic system

*Marta Pytlarczyk, Przemysław Kula

Institute of Chemistry, Faculty of Advanced Technologies and Chemistry, Military University of Technology, Warsaw, POLAND

e-mail: marta.pytlarczyk@wat.edu.pl

Keywords: *terphenyl, birefringence, liquid crystal, nematic, terminal acetylene*

Liquid crystalline materials are widely used in displays and photonic devices. Some applications of LC materials require high values of birefringence (Δn). This parameter is related to the maximal modulation of light by the LC medium reoriented in certain geometry. In the case of rod-like LC molecules, designing molecules with long conjugated π electronic systems can generate higher values of Δn .

One of the molecular design approaches is based on lateral fluorinated p-terphenyl core with terminal acetylene bridge ($C\equiv C$) as a coupler with alkyl chain of molecule. In the case of 1,4-bis[4-(alkyl-1-yn-1-yl)phenyl]-2,3-difluorobenzene with longer alkyl part (longer than four atoms of carbon) we used commercial available terminal alkynes. In Sonogashira reaction of terminal alkynes with 1-bromo-4-iodobenzene we obtained terminal parts of 4-(alkyl-1-yn-1-yl)-phenyl-4-yl. This synthons can be used directly in further reactions to synthesis of final molecules. The situation becomes more complicated for shorter homologues of 1,4-bis[4-(alkyl-1-yn-1-yl)phenyl]-2,3-difluorobenzene. This approach cannot be employed because terminal alkynes (shorter than five atoms of carbon) are gases at normal conditions. In this case necessary was synthesis of 1-bromo-4-ethynylbenzene and in next step deprotonation- alkylation of terminal acetylene group $-C\equiv C-H$.

In this work we developed synthesis of 1,4-bis[4-(alkyl-1-yn-1-yl)phenyl]-2,3-difluorobenzenes with alkyl chain $R = -C\equiv C-C_3H_5$ and $R = -C\equiv C-C_4H_9$. In the case of shorter homologues synthesis of intermediates and synthetic problems of this work will be presented. The purity and structures of the final products and intermediates were confirmed by spectral methods: gas chromatography GC-MS, GC-FID and nuclear magnetic resonance. The phase transition temperatures, phase situation and enthalpy data were determined by polarizing optical microscopy (POM) and differential scanning calorimeter.

Microstructural changes of cast nickel alloys induced by laser beam

*Łukasz Rakoczy¹, Anna Zielińska-Lipiec¹, Lechosław Tuz¹, Krzysztof Pańcikiewicz¹

¹ Faculty of Metals Engineering and Industrial Computer Science, Department of Physical Metallurgy and Powder Metallurgy, AGH University of Science and Technology, Cracow, Poland

e-mail: lrakoczy@agh.edu.pl

Keywords: *superalloys, cracking, laser beam*

Precipitation hardened nickel based alloys are the most complex and used for the hottest parts in gas turbines in the largest scale and to many materials engineers more interesting than iron based and cobalt based superalloys. In aircraft structure they are used mainly in the cast form (equiaxed, directionally solidified and monocrystal) which allow to extend service temperature to the highest homologous values of any common alloy system. The main characteristics of superalloys are the high phase stability of the face centered cubic structure, excellent mechanical properties and resistance to hot corrosion in operating temperature often near melting point. Alloys have an austenitic γ - matrix and include a variety of secondary phases. The most common are intermetallic phase γ' and metal carbides. Gamma prime phase is an ordered $L1_2$ structure that has good crystallographic matching with matrix. Weldability of superalloys, although being an important case, has been subject of much less investigation than that of steels and aluminum alloys.

In this study precipitation hardened alloys with commercial name MAR-M247, Rene 77 and Inconel 713C were used. Surface of samples was modified by a low pulsed Nd-YAG laser machine under shielding with pure argon. In order to observe microstructural changes light microscopy and scanning electron microscopy equipped with Energy Dispersive X-ray Spectroscopy detector was carried out. The materials in fully heat treatment condition (solutioning and aging) consist of high volume fraction of coherent γ' particles, the main strengthening phase.

The high content of refractory elements and elemental segregation during solidification cause the formation of carbides and eutectic island (γ - γ') in the interdendritic spaces. Microstructural investigation of welded specimen revealed hot cracking both in fusion zone and heat affected. However cracking in fusion zone is not as great welding problem as that of HAZ liquation cracking along grain boundaries. Heat affected zone liquation is known to occur by non-equilibrium melting below solidus temperature.

Optimization of instrumental parameters for voltammetric determination of 4-chloro-3-methylphenol using Bi-CCE

*Justyna Robak, Barbara Burnat, Sławomira Skrzypek

Faculty of Chemistry, University of Lodz, Lodz, POLAND

e-mail: justynarobak@poczta.fm

Keywords: carbon ceramic electrode, amplitude, frequency, step potential, square wave voltammetry

Square wave voltammetry (SWV) is one of the most popular and sensitive electrochemical method for biologically active compounds determination. Very important step in electroanalytical measurements is optimization of kind and pH value of supporting electrolyte and instrumental parameters. In presented research the parameters such as: amplitude, frequency, pulse width and step potential for determination of 4-chloro-3-methylphenol (PCMC) were optimized. PCMC is a soluble in water biocide from the group of phenols. It is a model example of chlorophenolic pollutant frequently found in wastewater treatment plants and industrial landfill leachates.

The analytical procedure was performed using three-electrodes system, where the counter electrode was platinum wire, reference electrode was silver-silver chloride electrode and working electrode was modified carbon ceramic electrode (CCE). The working electrode was obtained using sol-gel method by mixing in suitable proportions alcohol solvent, silica precursor and acid catalyst. Typically to the silicon matrix the graphite powder was introduced. In this case to the silicon matrix the mixture of bismuth oxide nanoparticles and graphite powder was added.

The application of proposed method for analytical determination of PCMC at Bi-CCE was tested as a relationship between peak current intensity and increasing PCMC concentration. The linear dynamic range determined for proposed electrode was equal for concentration from $9.0 \times 10^{-8} \text{ mol L}^{-1}$ to $4.4 \times 10^{-5} \text{ mol L}^{-1}$. Based on obtained calibration curve, the values of limit of detection (LOD) and limit of quantification (LOQ) were also calculated. The estimated values of LOD and LOQ were relatively low and were amounted to $8.8 \times 10^{-8} \text{ mol L}^{-1}$ and $2.7 \times 10^{-7} \text{ mol L}^{-1}$ respectively.

The performed research shown that the addition of the bismuth nanoparticles improve the electroanalytical properties of carbon ceramic electrode. Additionally, the electrode with Bi_2O_3 exhibited a better stability in time.

The influence of bismuth oxide nanoparticles on electrochemical properties of carbon ceramic electrode

*Justyna Robak, Barbara Burnat, Sławomira Skrzypek

Faculty of Chemistry, University of Lodz, Lodz, POLAND

e-mail: justynarobak@poczta.fm

Keywords: *carbon ceramic electrode, cyclic voltammetry, bismuth oxide nanoparticles, graphite powder, syringic acid*

The literature data shows that the unmodified carbon ceramic electrode (CCE) do not have satisfactory electroanalytical properties. For this reason, various kind of modification of CCE are performed. The most popular modification is surface modification. Generally, the surface modifications allow to obtain sensitive sensors, giving high and well-shaped analytical signals, but possess one significance disadvantage. The layer of the modifier can be damaged very easily and it is needed to clean the surface of the electrode and deposit a new layer. That problem can be solved by constructing electrodes modified in the entire volume. Electrode materials modified in whole volume are more stable and obtained results are more repetitive.

In the presented work the entire volume modified electrode using bismuth oxide nanoparticles was obtained. The electrochemical properties of fabricated sensor were analyzed by cyclic voltammetry in 1 mM ferrocyanide solution as a model probe. The parameter such as peak potential separation and the cathodic and anodic peak ratio were estimated. For the determination of influence of bismuth for the electrochemical properties reference electrode without modification also was fabricated.

The positive influence of bismuth oxide nanoparticles on the electrochemical properties of proposed sensor was found. The electrode with bismuth was more stable and exhibited higher sensitiveness compared with reference electrode. Additionally, in case of estimation an analytical properties of proposed material, the determination of syringic acid was performed and very good results was achieved.

Entire volume modification of carbon ceramic electrode using zeolite

*Justyna Robak, Barbara Burnat, Sławomira Skrzypek

Faculty of Chemistry, University of Lodz, Lodz, POLAND

e-mail: justynarobak@poczta.fm

Keywords: *carbon ceramic electrode, entire volume modification, ferrierite*

Carbon ceramic electrode (CCE) are produced using sol–gel technology based on hydrolysis and condensation reactions. Typically, to the ceramic matrix the graphite powder (GP) is introduced. The combination of large surface area of the sol–gel ceramic matrix and conductivity of the carbon materials enables the construction of a renewable surface electrode similar to the carbon paste electrode (CPE). The preparation of CCEs is very easy and cheap. Furthermore, construction of mentioned material, causes that it can be modified in entire volume in quick and simply way.

In the presented work, the CCE was modified using zeolite – ferrierite. For investigation of influence of ferrierite on analytical performance the bare and modified electrode were produced. The first step, was optimization of measurement medium and measurements parameters of differential pulse voltammetry such as: amplitude, step potential and pulse width. Next, the calibration curves for both electrode were obtained. The peak current was proportional to the concentration of estradiol in the range from 4 to 32 $\mu\text{mol L}^{-1}$ and from 0.5 to 16 $\mu\text{mol L}^{-1}$ for GP–CCE and FER–CCE, respectively. Using the calibration curves the limit of detection (LOD) and the limit of quantitation (LOQ) were calculated.

The proposed DPV procedure was successfully applied for determination of estradiol in pharmaceutical samples (Estrofem tablet) with good precision and accuracy.

Acknowledgements

This work was supported from the University of Lodz, Poland (Grant No. B1611100001291.02).

Ultrasonic coating as a method of medical implants surface modification with bioactive nanoparticles

*Julia Rogowska-Tylman^{1,2}, Bartosz Woźniak¹, Sylwia Kuśnieruk¹, Barbara Ostrowska², Wojciech Świążkowski², Witold Łojkowski¹

¹Institute of High Pressure Physics Polish Academy of Sciences, Warsaw, POLAND

²Warsaw University of Technology, Faculty of Materials Science and Engineering, Warsaw, POLAND

e-mail: rogowskatylmanjulia@gmail.com

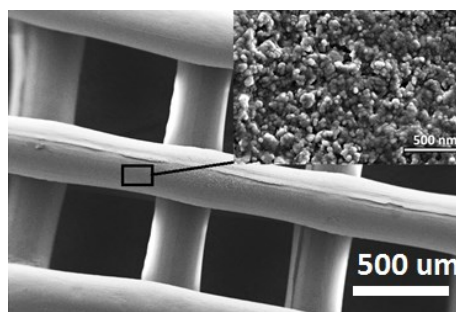
Keywords: *implants, nanoparticles, ultrasonic cavitation, surface modification*

Implantable medical devices are placed into the body for various reasons including orthopedic applications (e.g., hip replacement, spinal procedures, knee replacement, bone fracture repair, etc). In view of the structural integrity required by such devices, materials of fabrication are limited and generally consist of metal, plastic and composites. The benefits derived from these devices are often offset by infection, which in some cases can lead to sepsis and death.

Ultrasonic coating method of various materials dedicated for implantology can overcome these problems by increasing surface wettability and limit bacteria adhesion typical for most of hydrophobic surfaces. This type of surface modification is based on cavitation phenomenon occurring in liquid medium under ultrasonic wave of high frequency. Cavitation is a process of formation and violent collapse of steam voids. Particles present in vicinity of the collapsing bubble jet are naturally speed up to the coated surface direction, which result in uniform coverage of the surface with nanoparticles layer of 200-350 nm thickness.

We used highly biocompatible hydroxyapatite ceramic nanoparticles of 10-50 nm size for implant coating in present study. It was proved by authors that application of ceramic nanoparticles of high specific area can significantly increase water contact angle and cellular activity on polymeric scaffolds as well as new bone tissue formation when implanted *in vivo*.

New Zealand rabbit animal test have shown more than 30% of new bone tissue formation in comparison to unmodified scaffold surfaces.



Solidification of hazardous solid waste incineration bottom ash

*Piotr Rożek, Magdalena Król, Włodzimierz Mozgawa

Faculty of Materials Science and Ceramics, AGH University of Science and Technology, Cracow, POLAND

Al. Mickiewicza 30, 30-059 Kraków

e-mail: prozek@agh.edu.pl

Keywords: *bottom ash, solidification, heavy metals, immobilization*

Due to many disadvantages of waste landfilling, incineration is the method which is gaining popularity. But about 300 kg of residues are generated from every ton of incinerated solid wastes. Bottom ash comprises 75–80% of incinerator residues. A problem with bottom ash disposal is related to the presence of heavy metals, which can be released during landfilling and pollute the environment. Solidification of bottom ash, e.g. with cement, allows to prevent heavy metals from leaching. The presented work is aimed to investigate bottom ash and the possibility of its solidification in three different ways in order to obtain materials with significant durability and heavy metals immobilization.

The content of heavy metals in two bottom ashes (classified as hazardous waste) from incineration plants located in Poland was determined by X-ray fluorescence (XRF) method. Solidification of ground bottom ashes was prepared with two types of binder: Portland cement and granulated blast furnace slag. The last one was alkali-activated by using sodium hydroxide solution. Binder to bottom ash mass ratio was 7:3. Third method of bottom ashes solidification was hydrothermal treatment (autoclaving) process. Compressive strength, FT-IR spectra and X-ray diffraction patterns (XRD) of prepared materials were examined. Scanning electron microscope was used to observe the microstructure of samples. Heavy metals leaching test was performed and their content in eluates was measured by atomic absorption spectroscopy (AAS).

The studies revealed calcium silicate hydrate gel (C-S-H) as the main hydration phase product in prepared materials. The highest compressive strength was observed for hydrothermally treated materials (ca. 18 MPa and 32 MPa). The results of AAS showed that the degree of heavy metals cations immobilization is the best also for autoclaved materials (exceeding 99%).

In case of both bottom ashes the most satisfactory results of immobilization and compressive strength were obtained for autoclaved materials. Therefore, the hydrothermal treatment process can be considered as most effective and sustainable method of bottom ash solidification.

Acknowledgements

Financial support: 15.11.160.015

Stability of water silica suspension with polymer addition

*Diana Rymuszka¹, Salvador Perez Huertas¹, Konrad Terpiłowski¹, Marta Tomczyńska-Mleko²

¹Department of Physical Chemistry, Interfacial Phenomena, Faculty of Chemistry, Maria Curie-Skłodowska University, Lublin, POLAND

²Institute of Plant Genetics, Breeding and Biotechnology, University of Life Sciences, Lublin, POLAND

email: d_rymuszka@vp.pl

Keywords: *polyvinylpyrrolidone (PVP), silica, stability*

The polyvinylpyrrolidone (PVP) is a vinyl nonionic polymer soluble in water which can be obtained from monomer N-vinylpyrrolidone by free radical polymerization of vinyl monomers. It finds application, both, as flocculant and stabilizer of colloidal systems. Furthermore, PVP can be used as an ingredient in pharmaceuticals (especially tablets) and as a filler or binder in cosmetics and hygiene products: shampoos, hair conditioners, tooth pastes. Because of the protective effect on the epithelium of the cornea and conjunctiva, it can be also used in ophthalmology. On the other hand, silica is a very good material, which because of its valuable properties like very low chemical reactivity or durability enhancement of products is widely used in pharmaceutical, paint and cosmetic industry.

The influence of the adsorption of the polyvinylpyrrolidone (PVP) (55 kDa) on the silica surface was studied. The studies were carried out in different range of silica concentration in the absence and presence of PVP and the same dilution. The following experimental techniques were applied for investigations of stability: turbidimetry method and zeta potential measurements.

The obtained results indicate that suspensions without polymer were characterized by the smallest stability. The turbidimetric data and the calculated values of turbiscan stability indexes (TSI) show that the addition of PVP causes improvement of silica stability. The most stable system was obtained for the lowest solid content in the suspension and the highest PVP concentration. The mechanism of stabilization is steric and polymeric adsorption layer covering silica particles assures their effective repulsion.

Preparation of methyl ester of L-serine

*Agnieszka Sebai¹, Agnieszka Gadowska-Gajadur¹, Paweł Ruśkowski¹, Małgorzata Konopka¹, Ludwik Synoradzki¹,

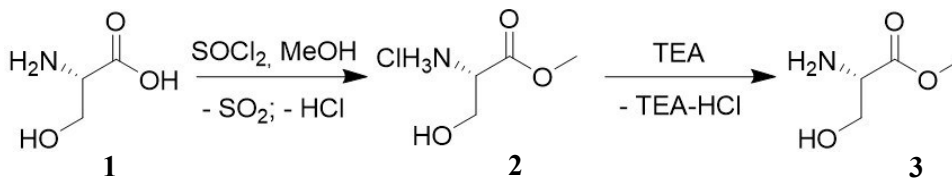
¹Laboratory of Technological Processes, Faculty of Chemistry, Warsaw University of Technology, Warsaw, POLAND

e-mail: asebai@ch.pw.edu.pl

Keywords: *L-serine, deprotection of amine group, esters of amino acids, DOE*

Amino acids are essential for human life. They are the building blocks for proteins and play an important role in biochemistry. All amino acids are optically active (except for glycine) and naturally occur only as L-stereoisomer. Serine (**1**) is an amino acid containing hydroxyl group in side chain, which increase hydrophilicity of materials and bioavailability of drugs. It is also crucial for catalytic properties of many enzymes. It is a precursor of other amino acids (like glycine, cysteine, tryptophan) and many other metabolites in bacteria. Esters in general are more reactive in condensation reactions than corresponding carboxylic acids, so it was chosen to synthesize methyl ester of serine (**3**).

It was decided to prepare product **3** through esterification using thionyl chloride and then deprotection of amine group of obtained salt (**2**). The first reaction was accomplished with a satisfying yield. The second step was more challenging. Small size of side-product made it incredibly difficult to purify. The best results were obtained using triethylamine. The deprotection reaction was optimized using design of experiments (DOE).



In summary, methyl ester of L-serine was obtained. The process of deprotection following esterification was optimized using DOE. The product has a form of yellow, adhesive wax and is a substrate to further purposes, which is to modify material for polymeric scaffolds.

Future of Flywheels Technology in Transportation

*Albasher Shareif¹

¹Institute of Mathematics, Pedagogical University of Cracow, Krakow, POLAND

e-mail: shareif@up.krakow.pl

Keywords: *flywheels, Energy storage, rotating kinetic energy, kinetic energy recovery systems, hybrid vehicles*

Energy storage systems highly support energy saving and security ways, and generally based on energy conversion between different kinds of energy. All energy systems in transportation depend on storing energy in chemical, electrical or mechanical energy. One of the efficient ways for storing energy in transportation is the rotating kinetic energy storage in flywheels (which is form of mechanical energy storage). Flywheels provide high energy density and efficiency compared to other storage systems, especially when the flywheels are made from perfect materials. Currently there are different types for flywheel applications in transportation. It can be used for operating trams, trains, buses and cars. Many of modern hybrid vehicles use flywheels to decrease the wastage of energy.

This presentation is about an analysis overview of flywheel energy storage systems in transportation. The presentation covers overview and technical description of flywheel energy storage applications. With using the machines learning, different case studies had been investigated to be presented in order to understand the flywheel's operation and behavior under different conditions and the future of flywheels technologies.

Potential of remote sensing data for detection of hydrographic features of lowland river: meandering and oxbow lakes shape changes and water quality. The Biebrza River case study

*Małgorzata Słapińska¹, Tomasz Berezowski¹, Magdalena Frąk², Jarosław Chormański¹

¹Department of Hydraulic Engineering, Warsaw University of Life Sciences, Warsaw, POLAND

²Department of Environmental Improvement, Warsaw, POLAND

e-mail: m.slapińska@levis.sggw.pl

Keywords: *oxbow lakes, remote sensing, meandering, water quality, model*

The study is focused on analyzing two hydrographical aspects of lowland natural river valley, namely first, monitor meanders shape changes over time in river channel and second, water quality in oxbow lakes. The research area is located in the Biebrza River valley. Biebrza meanders are undergoing almost natural processes, there is no urbanization in the catchment, so analysis can tell us a lot about natural river erosion processes.

The timescale of the analysis were years 1927-2015. Archive topographic maps, satellite and airborne remote sensed data were used. Changes in oxbow lakes types were analysed (according to their connection with the river), dynamics of their cutoff and degradation as well as the sinuosity changes in the river itself. Another part of this study was retrieving empirical formulas for water quality with the use of hyperspectral HySpex airborne imaging spectrometer (data from 01-02.07.2015) and the ground measurements campaign (conducted 03-04.07.2015). Hyperspectral HySpex camera which covers the range of 400-2500 nm. The ground measurements consisted of two parts. First part included spectral reflectance sampling with spectroradiometer ASD FieldSpec 3, which covered the wavelength range of 350-2500 nm at ~1 nm intervals. *In situ* data were collected both for water and for specific objects within the area. Second part of the campaign included water parameters such as Secchi disc depth (SDD), electric conductivity (EC), pH, temperature and phytoplankton.

Biebrza river is very dynamic, oxbow lakes are undergoing constant changes. The period of 88 years is long enough to observe and describe meandering processes. The empirical formulas for water parameters were retrieved based on the reflectance data. This study confirmed applicability of remote sensing data to retrieve water quality even for small water bodies like oxbow lakes.

This research present the river evolution over time. It is especially interesting topic, because Biebrza River was never analysed on meandering and sinuosity changes. Also there were no detailed remote sensed researches on oxbow lakes in Poland.

Carbon black as a modification layer for high sensitive melatonin determination

*Joanna Smajdor, Magdalena Pięk, Martyna Ławrywianiec, Robert Piech, Beata Paczosa-Bator

Faculty of Materials Science and Ceramics, AGH UST University of Science and Technology, Kraków, POLAND

e-mail: smajdorj@agh.edu.pl

Keywords: *Voltammetry, nanomaterials, melatonin, carbon black*

Melatonin, known as a sleep hormone, is synthesized mainly in the pineal gland, as a product of tryptophan biotransformation. It is primarily responsible for maintaining circadian rhythm of organisms and its secretion is highly regulated by exposition to light. Melatonin is often used for treating insomnia and to reduce jet lag effects. It also manifest major effects on immune system and as an anti-inflammatory and an antioxidant agent. It is known that melatonin influences course of mental disorders and supports treatment of breast cancer.

In this work, the new method of melatonin detection has been proposed, using stripping voltammetry and glassy carbon electrode modified by layer of carbon black as the working electrode. The simple preparation of carbon black glassy carbon modified electrode allows to apply method to any conditions and provides stable melatonin signal. Instrumental parameters of DPAdSV method, such as pulse of amplitude, potential step, preconcentration time and composition of supporting electrolyte were optimized. Repeatability of measurements was determined as RSD (%).

The new procedure was examined and successfully applied for determination of low melatonin concentration in tablet samples with good recovery, which confirms the usefulness of the method for routine pharmaceutical product analysis or quality control.

Acknowledgments

The work was supported by Ministry of Education and Science (AGH University Project No. 11.11.160.799).

Use of the renewable mercury film electrode for sensitive determination of selected hormones

*Joanna Smajdor, Magdalena Pięk, Martyna Ławrywianiec, Beata Paczosa-Bator, Robert Piech

Faculty of Materials Science and Ceramics, AGH UST University of Science and Technology, Kraków, POLAND

e-mail: smajdorj@agh.edu.pl

Keywords: *Voltammetry, hormones determination, film electrode*

Considering numerous of endocrine illnesses nowadays, requiring long time drug administration, new sensitive methods of quantitative analysis of active substances are highly desired. One of the methods that ensures high sensitivity and selectivity of measurements along with low costs and quick time of analysis is voltammetry.

In this work new method of prednisolone, (PR) hydrocortisone (HK) and sodium levothyroxine (LS) are presented. As the working electrode, silver based mercury film electrode has been proposed, in order to ensure high sensitivity of measurements. Instrumental parameters, such as electrode surface or supporting electrolyte composition has been investigated.

Linear range of method, recovery and limit of detection has been calculated. Surface of renewable mercury film electrode was different for each analyte, in the range from 10.2 mm² to 15.9 mm². According to the obtained results, the lowest amount of hormones possible to analyse was equal to $1 \cdot 10^{-8}$ (PR), $0.48 \cdot 10^{-8}$ (HK) and $1.8 \cdot 10^{-8}$ (LS).

Proposed procedures have been successfully applied for hormones determination in available pharmaceutical products. Possible reaction mechanisms were proposed for each analysed substance. Renewable mercury film electrode was applied for the first time as the working electrode in hormones and steroids detection procedures. Wide range of linearity and lack of matrix interferences led to the conclusion that proposed methods could be brought to the quality control systems in pharmaceutical companies.

Acknowledgments

The work was supported by Ministry of Education and Science (AGH University Project No. 11.11.160.799).

Modification layers used in voltammetric measurements

*Joanna Smajdor

Faculty of Materials Science and Ceramics, AGH UST University of Science and Technology, Kraków, POLAND

e-mail: smajdorj@agh.edu.pl

Keywords: *Voltammetry, nanomaterials, conducting polymers, carbon black*

A modern denouement used in voltammetry in order to improve sensitivity of measurements is applying modification layers on the electrode surface. Their role is to strengthen the signal of redox reaction overlapping in the voltammetric cell. Two main types of applying layer procedure could be distinguished: mechanical placement of the drop on the electrode surface or electrochemical deposition from the solution. The most recent methods allow to maintain the precise control of morphology and thickness of the obtained layer. Especially carbon nanomaterials, such as carbon nanotubes, graphene and carbon black are particularly interesting in the electrochemistry field, along with conducting polymers mixtures and metal nanoparticles.

Use of the nanomaterial modifications in voltammetry cause in the reinforcement of signals obtained in the consequence of the electrochemical reaction at the electrode surface. The reason of that is increase in the active surface of the electrode, caused by materials such as nanotubes or carbon black. The higher the surface is, the more active centres are available for electrochemical reaction.

In this work, different types of nanomaterials are presented as a modification layers of the working electrode. Morphology of the layers as well as the results of measurements performed on modified electrodes are shown. Due to usage of the modification layers, new methods of hormonal and steroid drugs determination has been elaborated using stripping voltammetric techniques with preconcentration step. Lower detection limits could be possible to obtain as a consequence of the electrode modification.

Acknowledgments

The work was supported by Ministry of Education and Science (AGH University Project No. 11.11.160.799).

Is chemometrics and voltammetry a great couple for food profiling and authenticity?

*Wanda Sordoń, Łukasz Górski, Małgorzata Jakubowska

Department of Analytical Chemistry, Faculty of Material Science and Ceramics, AGH University of Science and Technology, Krakow, POLAND

e-mail: wsordon@agh.edu.pl

Keywords: *voltammograms, chemometrics, multivariate analysis, food quality*

Food science and authentication are of particular importance both consumers and scientist. The consumer need of food quality guarantee is the reason of the continuous scientific work to search more and more effective tools to investigate food chemistry. In this point “food quality” should be explained – in means nutritional value and safety of use, but also absences of adulteration or alteration. However to obtain good results the corporation of analytical chemistry methods and chemometrics must be used.

This study will be divided into two parts. First one will be the presentation of a review of quality control methods and applications of multivariate statistical techniques on the verification of agricultural products. The considered food products will be vegetables, fruits, juices, as well as wines, oils, tea, coffee, honey.

Next to theoretical considerations the obtained results of study with alcoholic beverages (such as Polish ciders and absinthe from different countries) will be presented. Voltammetric techniques and registered voltammograms were used as a part of analytical chemistry. Chemometric approach was realized by the multivariate analysis. Preliminary data mining was performed using clustering methods and principal components analysis (PCA). The perspective of multivariate statistics as a promising tool to authenticate and classify these food products according to their variety will be demonstrated.

This study will show that the combination of modern analytical techniques with chemometric pattern recognition provides a powerful approach to quality assurance in the food sector.

Voltammetric determination of antioxidants

*Wanda Sordoń, Łukasz Górski, Małgorzata Jakubowska

Department of Analytical Chemistry, Faculty of Material Science and Ceramics, AGH
University of Science and Technology, Krakow, POLAND

e-mail: wsordon@agh.edu.pl

Keywords: *voltammetry, phenolic acids, DPV technique, working electrode, free radicals*

Fruits and vegetables are known to contain beneficial compounds called phenolic acids, that are strong antioxidants. These substances can reduce the effect of harmful formations in the body called reactive oxygen species (ROS). ROS are commonly known as free radicals. Free radicals can cause cell damage in the human body. Omitting the process of rapid aging as a result of free radicals activity, these substances can eventually leads more dangerous diseases such as cancer, neurodegenerative disorders or atherosclerotic changes. Consumption of food products rich in antioxidants minimizes the negative impact of free radicals.

Voltammetry as electroanalytical method is increasingly used in the process of determination organic compounds. It is repeatedly used in the study of antioxidative compounds such flavonoids. However this study will focus on the determination of above-mentioned antioxidants – phenolic acids (for example ferulic acid).

The study will utilize electrochemical methods called cyclic and differential pulse voltammetry in the determination of selected phenolic acids. What is more, the best working electrode will be selected as well as supporting electrolyte. The choice of the best measurement parameters of voltammetric techniques will allow to get the best result in the process of determination. Both the electrode of the older generation containing mercury and the quite new boron-doped diamond (BDD) electrode will be used in this investigation. The last step of this study will be determination of antioxidants in model liquids such as synthetic wine solution (of 12% (v/v) ethanol, 0.033 M tataric acid).

The obtained result will allow to have complete procedure of the voltammetric determination of antioxidative organic compound's.

Determination of CMC values of the surfactant solutions

*Magdalena Szaniawska¹, Anna Taraba¹, Katarzyna Szymczyk¹

¹Faculty of Chemistry, Department of Interfacial Phenomena, Maria Curie-Skłodowska University, Lublin, POLAND

e-mail: magdalena.szaniawska@wp.pl

Keywords: *surfactant, micelles, critical micelle concentration*

Surfactants (Surface Active Agents) are substances that lower the surface tension of a liquid, allowing easier spreading, and can lower the interfacial tension between two liquids. They are usually organic compounds and they are amphiphilic. Surfactants are built of hydrophilic (“tail”) and hydrophobic (“head”) groups. These compounds are soluble in both organic solvents and water. In aqueous solution surfactants can aggregate and they form micelles. Micellar aggregates are formed, when the concentration of the surfactant in the solution reaches a given concentration called Critical Micelle Concentration (CMC). There is a lot of methods of determining CMC. One of them is fluorescence spectroscopy, in which are used fluorescent probes. Pyrene is very often used as fluorescent probe in analysis of surface active agents. In emission spectra of pyrene can be observed five characteristic peaks. One way of determining the CMC of the surfactant is drawing the dependence of I_1/I_3 (intensity of first peak to third peak) of pyrene in the function of surfactant concentration in the solution. The aim of presented studies was the determination of CMC values of aqueous solutions of Tween 20 by the spectroscopic methods.

The aqueous solutions of nonionic surfactant, Tween 20 ($C_{T20}=10^{-6}$ - 10^{-2} M) with the pyrene ($C_{\text{pyrene}}=6 \cdot 10^{-6}$ M) was prepared. The emission spectra of pyrene were recorded on Hitachi FL-2700 spectrofluorimeter at the temperature range 293-318K. By determining the parameter I_1/I_3 critical micelle concentration of Tween 20 in aqueous solutions was designated in the presented range of temperature.

The most important conclusion of the measurements is that the temperature has an impact on values of the critical micelle concentration of the surfactants. For Tween 20, with the increase of temperature, the increase of CMC is observed.

Acknowledgements

This work was supported by the National Science Centre, Poland, Project no. 2014/15/B/ST4/05086.

Influence of solid concentration on rheological properties of the suspensions

*Adriana Szydłowska¹

¹Faculty of Mechanical Engineering, Opole University of Technology, Opole, POLAND

e-mail: a.szydłowska@doktorant.po.edu.pl

Keywords: *rheology, thixotropy, non-Newtonian, suspension, viscosity*

Suspensions are fluids which properties are complex. The solid particles, which are included in the suspensions, change their viscosity as well as they impact on rheological behaviour of whole system because they form other structures in liquid phase. Both, the command of rheological properties of fluids employed in the technological process and ability to predict changes of these properties influence on process conditions and they are required to correctly design the process. Therefore, it is essential to these fluids to be researched in terms of their rheological properties with emphasis on the rheological stability.

Results of measurements of rheological properties suspensions are included in this work. These suspensions were composed of vegetal solid (shells walnuts) with different volume fractions suspended in aqueous solutions of the polymer of three different concentrations. Such mixtures are applied e.g. in polymer industry for manufacturing biodegradable products. The measurements were done by rotational rheometer type CR with coaxial cylinders. The research was conducted with increasing and subsequently decreasing shear rate, what permitted to determine the rheological stability of the samples.

On the base of received results the curves of shear stress versus shear rate were prepared. The analysis of obtained curves indicate on clear difference between viscosity values of each of the suspensions as a result of different solid concentrations. Based on these curves researched suspensions were determined as thixotropic, hence their viscosity depends also on duration of deforming. The thixotropy of these suspensions intensifies along with increasing solid fraction up to certain concentration, whereupon this phenomenon begins to weaken and at certain amount of solid (different for each of liquid phase and relatively non-high) the suspensions lose capability for flowing.

Presence of solid in pseudoplastic continuous liquid phase causes change of rheological behaviour of all two-phase systems. Additionally, researched suspensions, which solid fraction was equal 20% – 25% vol. lose capability for flowing after exceeding shear rate approximately equal to 10 s^{-1} . At the current status of knowledge determining suspensions viscosity in non-Newtonian continuous phase is possible only by experiments.

External mass transfer limitation of heterogeneous processes for various types of hydrodynamics

*Jakub Szyman, Dominika Boroń¹

¹ Chair of Chemical and Process Engineering, Faculty of Chemical Engineering and Technology, Cracow University of Technology

e-mail: jszyman@chemia.pk.edu.pl

Keywords: *mass transfer, reactors, catalysis, hydrodynamics*

The superficial model may be used to describe some kind of catalytic processes with immobilized catalysts. It is possible to describe photocatalytic dyes decomposition or biological processes this way. The external mass transfer may have strong influence on the overall reactor effectiveness. It seems to be possible that it may also be related with reactor hydrodynamics. Evaluation the threshold of mass transfer limitation may be applied in reactor hydrodynamics optimization. Thus allows design reactors that have higher effectiveness. For that reason it is important to find the threshold of mass transfer limitation.

Numerical simulations were presented in this reseach. They shows, that for some process parameters the mass transfer limitation no longer affects the overall effectiveness. Mathematical model was obtained in case of processes operated in a couple of liquid stream flow types: laminar flow, plug flow and swirl flow. It was assumed that reaction occurs only on the surface, where the catalyst is immobilized. A new procedure to examine the mass transfer limitation threshold has been evaluated. Furthermore this procedure was used to exam the threshold of mass transfer limitation of overall process rate. In calculation specialist software in engineering Matlab and Matlab's tool for solving partial differential equations PDEToolbox was used. Numerical simulations were based on dimensionless Peclet and Damköhler number. It makes possible to analyze the external mass transfer limitation for numerous kinetics types.

Simulations let to create maps of errors of assumption about neglected external mass transfer in evaluating the overall reaction rate for different dimensionless numbers. Comparison of these maps, created for different flow regime shows which is the most effective from the point of view of mass transfer.

Comparison of micellar and alcohol extraction of flavonoid

*Anna Taraba¹, Magdalena Szaniawska¹, Katarzyna Szymczyk¹

¹Faculty of Chemistry, Department of Interfacial Phenomena, Maria Curie-Skłodowska University, Lublin, POLAND

e-mail: annataraba@gmail.com

Keywords: *flavonoids, quercetin, extraction, surfactant, alcohol*

Flavonoids are a group of plant metabolites thought to provide health benefits through cell signaling pathways and antioxidant effects. These molecules are found in a variety of fruits and vegetables. They have the general structure of a 15-carbon skeleton, which consists of two phenyl rings and heterocyclic ring.

Flavonoids are important antioxidants, and promote several health effects. Aside from antioxidant activity, these molecules provide the following beneficial effects: anti-viral, anti-cancer, anti-inflammatory, anti-allergic. Quercetin is one of the flavonoids and it can help to alleviate eczema, sinusitis, asthma, and hay fever. Some studies have shown that flavonoid intake is inversely related to heart disease, with these molecules inhibiting the oxidation of low-density lipoproteins and therefore reducing the risk of atherosclerosis developing.

One of the latest methods to obtain the flavonoids from plant is the use of micellar solution of surfactants for the extraction. So, the purpose of the presented studies was to determine the interactions between the non-ionic surfactant, Tween 80 micelles and quercetin by the spectroscopic methods and their comparison to the alcohol extraction of flavonoid – quercetin.

The solutions of quercetin ($C_{\text{qe}}=10^{-4}\text{M}$) and Tween 80 ($C_{\text{TW80}}=10^{-6}\text{M} - 10^{-3}\text{M}$) were prepared in 100 ml flasks. Next their absorption spectra were measured at 293 and 303K with the Helios γ spectrophotometer. Also the solution of quercetin ($C_{\text{qe}}=10^{-4}\text{M}$) and propanol ($C_{\text{PrOH}}= 0\text{-}80\%$) were prepared in 100 ml flasks. And their absorption spectra were measured at 293 and 303K with the Helios γ spectrophotometer.

In the absorption spectra of quercetin exist the characteristics peak located at about 375 nm, which comes from this substance. The differences in absorbance values of quercetin in two examined series are expected to show that micellar extraction is more effective than alcohol one.

Influence of hot dip galvanizing on the microstructure and hardness of heat-treated construction steel

Lechosław Tuz¹, Krzysztof Pańcikiewicz¹, Łukasz Rakoczy¹, Zbigniew Żurek¹

¹ Faculty of Metals Engineering and Industrial Computer Science, Department of Physical Metallurgy and Powder Metallurgy, AGH University of Science and Technology, Cracow, Poland

e-mail: ltuz@agh.edu.pl

Keywords: *galvanizing, zinc, coating*

Hot dip galvanizing in accordance with EN ISO 1461, is the performance of a coating of zinc or a zinc-iron alloy on the surface of steel. Process is carried out by dipping of properly prepared steel in the liquid zinc. Overall content of other chemical elements in the molten zinc, with the exception of iron and tin, there should not exceed 1.5% by weight fraction. The nominal density of zinc coating is 7.2 g/cm³ and is slightly lighter than the density of steel (7.85 g/cm³). Applying a protective zinc coating to steel is carried out in order to prevent rusting. High quality coating allow to reduce formation of iron oxides on the surface. In the case of small scratches on surface zinc acts as a cathodic protection preventing the development of corrosion. It is effective method of protection of low and high strength construction carbon steels. Increase of mechanical properties in high strength steels is achieved by controlled rolling and heat treatment (thermomechanical rolling) not only by change of chemical composition. Galvanizing is carried out in substantially high temperature and so microstructure and properties can be changed.

This work presents the results of the characterization of microstructure and hardness survey of high strength steel after galvanizing at 450°C. Investigation revealed decrease of hardness which indicated on loss of mechanical properties.

Characterization of sol-gel derived glasses from binary system SiO₂-CaO containing cerium ions

*Aleksandra Wajda, Maciej Sitarz

Faculty of Materials Science and Ceramics, AGH University of Science and Technology, Krakow, POLAND

e-mail: olawajda@agh.edu.pl

Keywords: *bioactivity, silico-phosphate glasses, antibacterial properties, glass structure and microstructure, FTIR spectroscopy*

So-called bioactive glasses promote bone-tissue formation at their surface and bond to surrounding living tissue when implanted in the living body. Controlled release of ionic dissolution products, in particular, concentrations of soluble silica (Si⁴⁺) and calcium (Ca²⁺) are known to be essential to the bioactive process. This has led to investigators to synthesize novel bioactive glasses to improve bioactivity and/or antibacterial properties. The choice of cerium was related to its low toxicity associated with bacteriostatic properties.

Cerium-doped bioactive glasses could be useful when implantation concerns local infected areas. Addition of antibacterial ions into bioactive materials can reduce microbial numbers on implants surface and kill bacteria or inhibit their growth.

The subject of this paper is cerium-doped glasses from binary SiO₂-CaO system. Several compositions of glasses were synthesized by sol-gel method, to obtain bioactive glass ceramics in a simpler system than those at present. X-ray, IR and Raman spectroscopy measurements were performed to characterize amorphous state and the structure of the samples. Morphology of the glasses was defined by scanning electron microscopy equipped with energy dispersive analyser. The glasses were soaked in a simulated body fluid (SBF) at 37°C for 30 days to test their bioactivity and ICP measurements were carried out for ion concentration determination. Moreover thermal analysis (DTA) was carried out to check if the crystallization of the glass is possible.

Acknowledgements

This work was supported by NCN project “Bioactive silico-phosphate glassy and glass-crystalline materials containing antibacterial ions 2016/20/T/ST8/00204”.

Synthesis and analysis of oxidised graphite

*Tomasz Wawer, J. Jonik, M. Purchała, H. Grajek

Department of New Technologies and Chemistry, Military University of Technology,
Warsaw, POLAND

e-mail: tomasz.wawer@wat.edu.pl

Keywords: *graphite oxide, X-ray diffraction, X-ray photoelectron spectroscopy*

The results of graphite oxidation by original and modified method of Hummers and Offeman have been presented and discussed. Due to berthollidic nature of the obtained products a need of verifying their chemical composition has arisen. This has been performed by X-ray photoelectron spectroscopy (XPS) and energy dispersive X-ray spectroscopy (EDS). The Raman spectroscopy and X-ray diffraction (XRD) analysis have been employed for the structural analysis of the graphite oxidation products being the second essential problem tested during research.

The obtained results of aforementioned analysis allowed to predict the structure and determine the chemical composition of the products. The chemical composition of the product was characterized by the C:O ratio. That ratio, based on EDS results, was 2.061 ± 0.250 and for XPS it was 2.316 ± 0.056 . The spacing between subsequent layers in the product was 862 pm. The results have been compared with the values of commercial products such as graphite oxide and multi-layered graphene oxide. Both, the elemental composition and structural parameters correspond with the literature data relating to aforementioned materials.

Taking into consideration all the obtained results, was concluded that product of graphite oxidation is multilayered carbon material composed mainly of carbon and oxygen atoms. Oxygen atoms are chemically bonded to the carbon structure causing an increase in the distance between graphene sheets in the structure. However, some part of the substrate has been probably intercalated.

Elimination of environmental sample matrix interferences by using XAD-7 resin in voltammetric determination of Mo(VI)

*Krystian Węgiel¹, Małgorzata Grabarczyk², Bogusław Baś¹

¹Faculty of Material Science and Ceramics, AGH University of Science and Technology, Kraków, POLAND

²Faculty of Chemistry, Maria Curie-Skłodowska University, 20-031 Lublin, POLAND

e-mail: krystweg@agh.edu.pl

Keywords: *stripping voltammetry, environmental analysis, organic matrix interferences, molybdenum trace analysis,*

The main components of real water samples which can interfere during adsorptive voltammetric measurement are foreign ions and organic substances, particularly surface-active substances such as typical industrial pollutants. In the case of surface-active substances, they tend to adsorb on the working electrode, thus inhibiting the deposition step and/or stripping processes, causing a decrease or total decay of the analytical signal.

In this work, to elimination of environmental sample organic matrix interferences the XAD-7 resin was used. This materials it has been used for removal of organic pollutants from aqueous wastes, ground water and vapor streams. Amberlite XAD-7 resin was obtained from Sigma-Aldrich and it was washed four times with triple-distilled water and dried up at temperature of 50°C.

To study the influence of surface-active substances on Mo(VI) signals, a nonionic surfactant Triton X-100 was used. The voltammetric signal of Mo(VI) is very sensitive to the presence of the nonionic surfactant. The addition of Triton X-100 at concentration 0.5 mg L⁻¹ causes decrease of the stripping peak current up to 30%. Addition of 1 mg L⁻¹ of Triton X-100 causes complete loss of the signal. Mixing of the analysed sample with Amberlite XAD-7 resin drastically eliminates the unwanted negative influence of the nonionic surfactant on Mo(VI) stripping peak current. In the presence of 8 mg L⁻¹ of Triton X-100 after mixing of 5 mL of sample with 0.25 g XAD-7 of resin the relative signal of Mo(VI) decrease by 45%.

Conditioning of bismuth bulk electrode for the characterization of clothianidin and its determination in selected samples by DPV

*Krzysztof Węgiel, Bogusław Baś

Faculty of Material Science and Ceramics, AGH University of Science and Technology, Kraków, POLAND

e-mail: krystweg@agh.edu.pl

Keywords: *bismuth bulk electrode, clothianidin, environmental analysis, mercury-free electroanalysis*

In the last several years, neonicotinoids have represented one of the most important classes of insecticides on the market. As potent agonists, they act on the nicotinic acetylcholine receptors of insects. Their widespread use however, results in their frequent appearance in the environment and foods. Because of that, there is a growing need for the development of fast and simple methods for the characterization and determination of neonicotinoids.

Clothianidin (Clo) is a representative of a third generation of neonicotinoids insecticides, belonging to the nitroguanidine and thiazole subclasses. It was discovered by the former Agro Division, Takeda Chemical Industries, Co., Ltd.

In our work, we present a new method to determination of trace clothianidin by differential pulse voltammetry (DPV). As an alternative to mercury electrodes, the environmentally friendly bismuth bulk electrode (BiABE) electrochemically activated prior to each measurement was used. The proposed method is based on registration of the current reduction of the nitro group ($-\text{NO}_2$) at the potential of -0.91 V. The measurements were carried out in a supporting electrolyte consist of 0.02 mol L^{-1} solution of Britton-Robinson buffer (pH 9.0). Bismuth is hydrolysed in a basic solution, hence electrochemical activation and cleaning of the electrode surface is necessary. Finally, the BiABE was used to determination of clothianidin in tap water and river water samples; the latter were collected at two different sites on the outskirts of Kraków (Poland).

The main advantages of the developed sensor is the minimal toxicity of metallic bismuth relative to the mercury electrodes, higher sensitivity and precision and quick way of regenerating the surface of the Bi electrode before each measurement cycle.

Electrochemical properties of riboflavin at a metallic annular band electrodes

*Krystian Węgiel, Bogusław Baś

Faculty of Material Science and Ceramics, AGH University of Science and Technology, Kraków, POLAND

e-mail: krystweg@agh.edu.pl

Keywords: *metallic bulk electrode, riboflavin, mercury-free electroanalysis*

Riboflavin, called vitamin B2 is a water-soluble vitamin which is present in a wide variety of foods. It plays an important role as cofactor in enzymes and catalyzes a diverse of biochemical reaction. At present, there are many analytical methods of riboflavin determination, the main are chromatography and spectrometry. Recommended by the Association of Official Analytical Chemist is standard – fluorometric – method for determination of riboflavin in foods. These methods characterized by high sensitivity but in comparison with electrochemical techniques are expensive, complicated and time consuming.

The aim of the present work was application of a friendly use and mercury free electrochemical sensor with the bismuth (BiABE), gold (AuABE) and silver (AgABE) bulk annular band electrodes for determination of riboflavin and compare their electrochemical properties. The voltammetric behaviour of riboflavin has been investigated using cyclic voltammetry (CV) and differential pulse voltammetry (DPV) on the above mentioned electrodes. The effect of several parameters such as pH, kind and concentration of the supporting electrolyte was investigated.

Optimum conditions for DPV determination of riboflavin have been found in 0.02 mol L⁻¹ acetate buffer of pH 4.5. The results show that the anodic peak current is higher than cathodic for bismuth electrode. Moreover, it is possible to preconcentration analyte on the surface electrode with different accumulation time. In the case of gold and silver electrodes the cathodic peak current was higher, but the preconcentration was not possible.

Finally, selected metallic bulk annular band electrodes was applied to determination of riboflavin in fruit juices and pharmaceutical products.

Voltammetric determination of Mo(VI) at the in situ regenerated BiABE electrode

*Krystian Węgiel¹, Małgorzata Grabarczyk², Bogusław Baś¹

¹Faculty of Material Science and Ceramics, AGH University of Science and Technology, Kraków, POLAND

²Faculty of Chemistry, Maria Curie-Skłodowska University, 20-031 Lublin, POLAND

e-mail: krystweg@agh.edu.pl

Keywords: *bismuth bulk electrode, stripping voltammetry, molybdenum, mercury-free electroanalysis*

Molybdenum is a naturally occurring in the environment metal and can be found in small amounts in groundwater, soil and rock, it is also found in leafy vegetables, grains, legumes, cauliflower and sunflower seeds. Molybdenum is also an essential trace element for animals, including humans, as it is crucial in enzymatic redox reactions. Although small amounts of molybdenum are essential to human health, large amounts can be toxic. The World Health Organization has established guidelines for drinking water quality, defined its permitted concentration equal to 70 $\mu\text{g L}^{-1}$. The evaluation of molybdenum content in the environmental samples is needful and highly recommended. The viable alternative to spectrometry techniques are electrochemical methods, especially adsorptive stripping voltammetry (AdSV), which provides very low detection limit and good selectivity.

In this work, for the first time, the bismuth bulk annular band electrode (BiABE) was used as an alternative to mercury or bismuth film electrodes for molybdenum(VI) determination by means of the DP AdSV method. The proposed procedure is based on simple and fast regeneration of the BiABE surface in the presence of testing solution, by application of the activation potential equal to -1.8 V for a 5 s. The next, Mo(VI) ions are complexation by chloranilic acid (CAA) and preconcentration at -0.5 V (vs. Ag/AgCl/3 mol L⁻¹ KCl) on the electrode surface in 0.02 mol L⁻¹ acetate buffer (pH 4.0). The dependence of the Mo(VI) peak current on the concentration was found to be linear in the range from 1.0×10^{-9} to 7.3×10^{-8} mol L⁻¹, with $r = 0.9994$, for accumulation time of 20 s. The detection limit was $2.1 \cdot 10^{-10}$ mol L⁻¹ (at S/N = 3).

Finally, the proposed method was successfully applied to determine Mo(VI) in the certified reference waters, Humber river sediment and tap water samples.

Investigation of the rate of oxygen absorption in a wave-type agitated single-use bioreactor

*Kamil Wierzchowski, Paweł Sobieszuk, Maciej Pilarek

Faculty of Chemical and Process Engineering, Warsaw University of Technology,
Warsaw, POLAND

e-mail: kwierzchowski0@gmail.com

Keywords: *wave-type agitation, single-use bioreactor, oxygen absorption*

Wave-type agitated single-use bioreactors are commonly applied for scale-up of *in vitro* cultures of animal cells. The oscillating movement of the bioreactor's tray induces waves in the two-phase culture system (i.e. gas phase and liquid culture medium) what allows to intensify the mass transfer effects inside the single-use polymer-based bags substituting classical culture vessels known from typical glass or stainless steel bioreactors. During the wave-induced agitation, the interfacial area between gas phase and culture medium is continuously renewed and bubble-free surface aeration of the culture broth is accomplished. Simultaneously, wave-type agitation significantly limits the level of shear forces observed in the culture system, as well as the shear stress effects negatively influencing the fragile biomass, i.e. isolated animal cells.

The ReadyToProcess WAVE™25 single-use bioreactor system (WAVE 25; GE Healthcare Bio-Sciences AB, Sweden), equipped with 2 dm³ polymer-based culture bag, has been used for studying the oxygen absorption rate in the wave-induced agitation system. WAVE 25 lets to develop the bioprocess in the volume of milliliters, i.e. from 0.1 dm³ to 1 dm³. The rate of oxygen absorption from N₂/O₂ mixture into distilled water has been measured and the values of the volumetric mass transfer coefficient (k_{La}) has been investigated.

The influence of the hydrodynamic conditions (frequency and angle of oscillations), the oxygen concentration in gas mixture, as well as the flow rate of gas mixture dosed to the single-use culture vessel in WAVE 25, on the mass transfer rate has been discussed. Oscillations frequency, as well as oscillation angle mostly influenced on the value of k_{La} coefficient. The flow rate of the gas flowing through the single-use bioreactor has rather minor effect.

The range of measured k_{La} values are consistent with previously published literature data. The results of the studies confirmed the applicability of the wave-induced agitation bioreactor system as the right platform for proceeding the submerged culture of animal cells.

Acknowledgements

This work has been supported by the budget sources for The National Centre for Science, Poland, Grant no. DEC-2015/17/B/ST8/00631.

Adsorption of benzo[a]pyrene on natural and synthetic materials

*Katarzyna Wilkosz, Anna Niebieszczańska, Ewa Niewiara

AGH University of Science and Technology, Faculty of Material Science and Ceramics, Department of Analytical Chemistry, Cracow, POLAND

e-mail: katwilkosz@gmail.com

Keywords: *adsorption, benzo[a]pyrene, zirconium dioxide, titanium dioxide, montmorillonite*

Nowadays, water pollution is a world class problem. This fact enforces the development of the water treatment systems with additional processes. The adsorption shows the great efficiency in the processes of water treatment which combined with nanotechnology provides promising results and opens up a possibility of its widespread use.

Natural and synthetic materials were tested to investigate their adsorption efficiency of benzo[a]pyrene in aqueous solutions. Zirconium dioxide, titanium dioxide (P90) and montmorillonite were tested. Additionally, the influence of humic acids, heavy metals and polycyclic aromatic hydrocarbons (PAHs) on adsorption of benzo[a]pyrene were examined. The adsorption process was carried out in acidic, alkaline, and in an environment at pH corresponding to the isoelectric point for the individual nanoparticles.

Adsorption efficiency for montmorillonite was 89.06% but heavy metals intensified adsorption from 46.1 to 61.49%. Modification of zirconium dioxide nanopowders improved sorption properties from 88.72% to 99.9%. In presence of heavy metals adsorption efficiency decreased even by 60%. For titanium dioxide (P90) adsorption efficiency was 56.42% and it was lower than for zirconium dioxide and montmorillonite. Humic acids intensified adsorption efficiency even by 35% for zirconium dioxide. For all zirconium nanopowders increase of adsorption efficiency in presence of humic acids was observed. In presence of polycyclic aromatic hydrocarbons increase of adsorption efficiency was observed. In pH corresponding to the isoelectric point the best efficiency was in presence of PAHs for all nanopowders based on zirconium dioxide.

Based on received results there is a possibility to apply tested nanopowders based on zirconium dioxide as sorbent for benzo[a]pyrene particles in aqueous solutions.

Recovery of zinc(II) from chloride solutions using hollow fibre contactor with pyridine derivates extractant

*Aleksandra Wojciechowska¹, M. Teresa A. Reis², M. Rosinda C. Ismael², Irmina Wojciechowska¹, Karolina Wieszczycka¹, Jorge M.R. Carvalho²

¹ Poznan University of Technology, Institute of Chemical Technology and Engineering, Berdychowo St. 4, 60-965 Poznan, Poland.

² CERENA – Centre for Natural Resources and the Environment, Department of Chemical Engineering, Instituto Superior Técnico, Universidade de Lisboa, Av. Rovisco Pais, 1049-001 Lisboa, Portugal.

e-mail: aleksandra.w.wojciechowska@doctorate.put.poznan.pl

Keywords: *extraction, membrane process, zinc recovery, pseudo-emulsion hollow fiber strip dispersion (PEHFSD), pyridine derivates*

Hollow fiber membranes have been used in a variety of applications in the industry such as degasification of process solutions, separation of carbon dioxide and other gases from flue gas streams and waste water treatment. A lot of researchers have studied the application of hollow fiber membrane technology in various operations such as liquid-liquid extraction, gas separation by absorption and stripping, ozonation of water and removal of volatile components from water.

The advantage of the Pseudo-Emulsion Hollow Fiber Strip Dispersion (PEHFSD) technique is connected to either membrane extraction process, whereby a single membrane module is carried out simultaneously extraction and re-extraction, the extractant and the consumption it is much smaller than in the classical extraction. Pseudoemulsion system is a very promising method for treatment of liquid waste streams with toxic or valuable metal ions.

The aim of this work was to study the possibility of using the novel extractants - pyridine derivatives for the recovery of Zn(II) from chloride medium using the PEHFSD technique.

The transport of zinc(II) ions was investigated as a function of various experimental variables: type of compounds in the organic phase and the initial metal concentration in the feed phase. The overall mass transfer coefficient of permeation was calculated from the experimental data, the values being found in the range of 2.5×10^{-7} – 1.1×10^{-6} m/s. The recovery of Zn(II) in the stripping solution (H₂O or 5% Na₂SO₄) was around 70-80% for most conditions tested.

Acknowledgements

This work was financed within the Polish National Centre of Science funds according to decision No. DEC-2015/17/N/ST8/00285. Financial support through the project UID/ECI/04028/2013 from the “Fundação para a Ciência e a Tecnologia” (FCT, Portugal) is also acknowledged.

Recovery of iron(III) from chloride solutions

*Aleksandra Wojciechowska, Irmina Wojciechowska, Katarzyna Staszak, Karolina Wieszczycka

Poznan University of Technology, Institute of Chemical Technology and Engineering, Berdychowo St. 4, 60-965 Poznan, Poland.

e-mail: aleksandra.w.wojciechowska@doctorate.put.poznan.pl

Key words: *liquid-liquid extraction, iron recovery, surface properties*

The solvent extraction is one of the most important techniques for the separation and recovery of metals in many industrial fields. The undoubted advantage is the low power consumption and the ability to re-use extractants. This method is attractive from economic and environmental point of view.

The recovery of iron(III) from aqueous solutions is usually carried out by precipitation as jarosite, goethite or hematite. Although the iron removal is mainly achieved by precipitation techniques, the use of solvent extraction also allows the iron(III) removal from acidic aqueous solutions.

The aim of the work was the synthesis of oxime 1-(3-pyridine)undecane-1-one and its quaternary pyridinium salts (3-[1-(hydroxyimine)-undecyl]-1-propylpyridinium chloride and 3-[1-(hydroxyimine)-undecyl]-1-propylpyridinium bromide) and determine their properties in relation to the extraction of iron(III) ions. The extraction of iron(III) chloride was carried out by constant water activity $a_w=0.835$ (constant total concentration of ions and molecules dissolved in aqueous solution $\sigma=4$ M). NaCl, LiNO₃ and NaNO₃ were used to adjust the activity of water. The studies were carried out by constant iron (III) concentration equal to 0.01 M. The concentration of extractant in the organic phase was changed from 0.01 to 0.2 M. Toulon with 10% addition of decan-1-ol was used as the diluent. Furthermore the surface properties of the various aqueous/organic systems and mass transfer resistances were determined by the Du Noüy ring method with a K12 KRÜSS tensiometer.

The study showed that the synthesized compounds may be a potential extractants of Fe(III) ions from chloride and chloride-nitrate solutions.

Acknowledgements

This work was financed within the Polish National Centre of Science funds according to decision No. DEC-2015/17/N/ST8/00285. Financial support through the 03/32/DS-PB/0601 grant was also acknowledged.

Microwave solvothermal synthesis and characterization of ZnO nanoparticles co-doped with Co²⁺ and Mn²⁺ ions

*Jacek Wojnarowicz¹, Myroslava Omelchenko², Jarosław Rybusiński², Jacek Szczytko², Tadeusz Chudoba¹, Witold Lojkowski¹

¹Laboratory of Nanostructures, Institute of High Pressure Physics, Polish Academy of Sciences, Warsaw, Poland

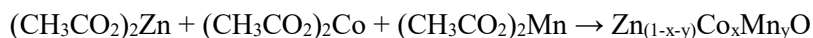
²Institute of Experimental Physics, Faculty of Physics, University of Warsaw, Warsaw, Poland

e-mail: jacek.wojnarowicz@tlen.pl

Keywords: Co²⁺-Mn²⁺ co-doped ZnO NPs, Microwave Solvothermal Synthesis (MSS), characterization techniques of nanomaterials, magnetic properties of Co²⁺-Mn²⁺ co-doped ZnO NPs

The expertise of the Laboratory of Nanostructures, IHPP PAS, lies in the synthesis of and comprehensive research on nanomaterials. The process is based on the Microwave Solvothermal Synthesis (MSS). The MSS process permits preventing contamination of synthesis by sealing the reaction vessel, which is made of a chemically inert material, so that an ultra-pure product can be obtained. The precursors of the reaction (solutions, suspensions) are enclosed in a pressure vessel and as a result of heating with the microwave energy the temperature increases above the boiling point.

The authors obtain Zn_(1-x-y)Co_xMn_yO NPs characterized by a narrow size distribution in MSS which can be expressed as follows:



The synthesis of Zn_(1-x-y)Co_xMn_yO NPs took place in a solution of ethylene glycol over the period of 25 minutes in Ertec 02-02 microwave reactor. The content of Co²⁺ and Mn²⁺ in Zn_(1-x-y)Co_xMn_yO ranged from 1 to 15 mol%. The following Zn_(1-x-y)Co_xMn_yO NPs properties were investigated: skeleton density, specific surface area (SSA), phase purity (XRD), dopant content, average particle size, crystallite size distribution, morphology. The effect of the concentration of the doping ions on the magnetic properties of Zn_(1-x-y)Co_xMn_yO NPs is presented.

Research on the size control mechanism of ZnO nanoparticles obtained in microwave solvothermal synthesis

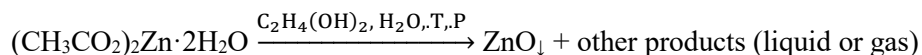
*Jacek Wojnarowicz¹, Tadeusz Chudoba¹, Witold Lojkowski¹

¹Laboratory of Nanostructures, Institute of High Pressure Physics, Polish Academy of Sciences, Warsaw, Poland

e-mail: jacek.wojnarowicz@tlen.pl

Keywords: nano zinc oxide (ZnO NPs), NPs size control, size control mechanism of ZnO NPs, Microwave Solvothermal Synthesis (MSS), physical properties of ZnO NPs

The Laboratory of Nanostructures, IHPP PAS, is an expert in the synthesis of nanoparticles (NPs) characterised by a small size distribution using the microwave solvothermal synthesis (MSS) technology. MSS technology permits precise control of NPs synthesis parameters such as reaction time, temperature and pressure. The authors obtain zinc oxide particles characterised by a narrow size distribution in a solvothermal synthesis which can be expressed as follows:



The synthesis of ZnO NPs took place in a solution of ethylene glycol over the period of 25 minutes in Ertec 02-02 microwave reactor. It was proved that by controlling the water concentration in the precursor it was possible to control the size of ZnO NPs in a programmed manner (*Wojnarowicz et al.; J. of Nanomat, 2016, doi: 10.1155/2016/2789871*). The lower the water content in the precursor, the smaller the size of ZnO NPs was obtained. The following parameters of the obtained ZnO NPs were determined: pycnometric density, specific surface area, phase purity, average particle size, particle size distribution. The authors synthesized pure, fully crystalline hexagonal ZnO NPs and the average particle size ranged from 22 nm to over 41 nm.

The size control mechanism of ZnO NPs was explained based on the results of the tests of:

- specific conductance and pH in precursors, post-reaction suspended matter;
- identification of the obtained intermediates and by-products.

Long Periods Fibers Grating made by filament heating

*Renata Wonko¹, Leszek R. Jaroszewicz¹

¹Institute of Applied Physic, Military University of Technology, 2 St. Kaliskiego, 01-476 Warsaw, Poland

e-mail: renata.wonko@wat.edu.pl

Keywords: *Long Periods Fiber Gratings, LPFG, filament heating, resonant peak, point-by-point method.*

The Long Period Fiber Grating (LPFG) is a periodic modulation of a refractive index of the fiber's core and cladding. The period should be in the range from 100 μm to 1000 μm . As a result, resonant peaks are created in the transmission spectrum at wavelengths where there is a coupling between the core and co-propagating cladding modes. Fundamentally, such structures are made by using UV irradiation, however it requires high photosensitivity of optical fibers. There is a good alternative to produce LPFG by periodically tapering optical fiber using point-by-point method.

We present the adiabatic tapered LPFG fabrication using "Omega- shape" filament, which is integrated part of optical splicer (VYTRAN GPX- 3000). Periodical tapers were manufactured by local heating and applying tensile to the fiber. Under this work, we have done the LPFGs on a commercial singlemode fiber SMF28 with the cladding's diameter of 125 μm and the singlemode fiber Nufern 1550B-HP-80 with the cladding's diameter up to 80 μm . The parameters which have been changed was: period, number of periods and technical parameters of filament. The analysis of attenuation bands was carried out by observing transmission spectrum in the range of 1200 nm to 1600 nm, whereas the fiber with LPFG was illuminated by a broadband light source.

We received satisfactory results for both types of optical fibers. We established the appropriate process parameters which allows to produce any structures. LPFGs are attractive devices for temperature, strain and changing refractive index detection.

Ultrasonic coating technology for improving bone implants

*Bartosz Woźniak¹, Julia Rogowska-Tylman¹, Agnieszka Chodara¹, Witold Łojkowski¹

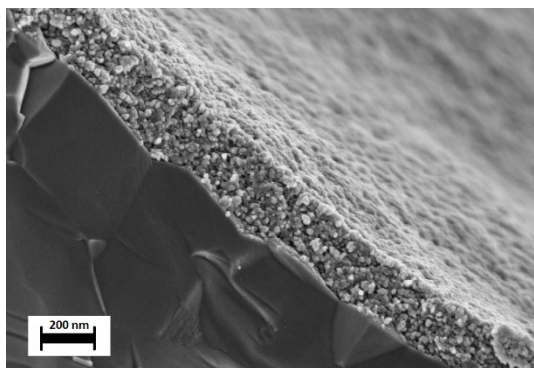
¹Institute of High Pressure Physics Polish Academy of Sciences, Warsaw, POLAND
e-mail: b.wozniak@labnano.pl

Keywords: *surface modification, ultrasonics, medical implants, nanotechnology*

The most commonly used techniques for surface modification of medical implants such as electrophoretic deposition, sputter, dip coating or plasma spraying are well developed to deposit hydroxyapatite, however, it is hard to produce coating in short time, low temperature process and good homogeneity at nanoscale. Additionally, it is a challenge to coat porous scaffolds with said parameters.

Proposed method relies on improving highly porous as well as solid like medical implants especially scaffolds by coating their surface with bioactive hydroxyapatite nanoparticles. Ultrasonic coating technology is based on cavitation phenomena where bubbles formation and implosion in liquid medium cause liquid jet formation with velocity up to 280 m/s. The jetting in the presence of solution with hydroxyapatite nanoparticles, enable to deposit thin layers on materials surface.

We have demonstrated that ultrasonic method is effective in view of process rate <10 minutes, low temperature 30°C and use small amount of hydroxyapatite powder. The main results have shown that is it possible to create uniform thin coating (up to 90%) on internal and external surfaces of porous objects. Coated surface has good influence on implant biocompatibility improvement.



Coated ceramic porous scaffold with hydroxyapatite nanoparticles.

Described method is sterile and environmental safe due to completely reduction of release hazardous compounds and mild process conditions. Proposed method has been the subject of patent application PCTIB/2016/052566 *Method for manufacturing bone implant and bone implant*.

Electrodeposition of the calcium-phosphate coatings on titanium for bone tissue engineering

Bartłomiej Wysocki^{1,2}, *Agata Supel^{1,2}, Agnieszka Brojanowska¹, Wojciech Świąszkowski¹

¹Faculty of Materials Science and Engineering, Warsaw University of Technology, Wołoska 141 Str., 02-507 Warsaw, POLAND

²Materialscare LLC, Zwirzyńska 10/1 Str., 15-300 Białystok, POLAND

e-mail: agata.supel@materialscare.eu

Keywords: *biomaterials, electrodeposition, calcium-phosphate coatings, tissue engineering, scaffolds*

Surface engineering of titanium implants can enhance their biocompatibility. It is very common to create thin calcium-phosphate (Ca-P) coating on them. This material provides adhesion and proliferation of bone cells, which supports regeneration of whole bone. Ca-P ceramics are being frequently manufactured by thermal spraying, but it is impossible to use it while covering porous structure in its whole volume.

The aim of this work is development of parameters to fabricate calcium-phosphate layers by electrodeposition on titanium implant manufactured by Selective Laser Melting (SLM). It concerns different post-process surface modification and approach to deposition of Ca-P layers using different parameters. Manufacturing layers in solution containing carbon nanotubes (CNTs) was used to enhance mechanical properties of implants.

Constructed electrodeposition unit allows to obtain repetitive results. Characterization of deposited layers confirms appropriately chosen deposition process parameters, including pH value oscillating around 4.7 and input voltage around -1.45 eV. SEM and STEM observations allowed identification of morphology characteristic for hydroxyapatite, natural Ca-P bone builder, and estimation of layer thickness. Cellular response for Ca-P coated implants gave the best results for heat treated layers and CNTs assisted process.

Acknowledgements

The authors would like to thank the NCBiR (National Center for Research and Development) for providing financial support to project LasIMP (Grant No. PBS3/A5/53/2015).

D-limonene-loaded Solid Lipid Nanoparticles (SLN) as innovative delivery system for pharmacy and cosmetic industries

*Aleksandra Zielińska^{1,2}, Irina Pereira^{2,3}, Agnieszka Feliczak-Guzik¹, Francisco J. Veiga^{2,4}, Amélia M. Silva², Ana C. Santos^{2,5}, Izabela Nowak,¹ Eliana B. Souto^{2,4}

¹ Faculty of Chemistry, Adam Mickiewicz University in Poznań, Poznań, POLAND,

² Faculty of Pharmacy, University of Coimbra, PORTUGAL, ³ Department of Biology and Environment, University of Trás-os-Montes and Alto Douro, PORTUGAL, ⁴ REQUIMTE/LAQV, Faculty of Pharmacy, University of Coimbra, PORTUGAL, ⁵ Institute for Innovation and Health Research, Institute for Molecular and Cell Biology, Porto, PORTUGAL

e-mail: ola.zielinska@amu.edu.pl

Keywords: *solid lipid nanoparticles, SLN, D-limonene, high pressure homogenization, chemical stability*

Solid lipid nanoparticles (SLN) are currently on the focus of pharmaceutical and cosmetic industry due to easily biodegradable lipids present in their structure. SLN are biocompatible and non-toxic nanoparticles, therefore they offer possibility to develop new therapeutics. In our study, we developed SLN loaded D-limonene (4-isopropenyl-1-methylcyclohexene) - relatively stable terpene - commonly used as a fragrance in perfumery and personal-care products, but also in food manufacturing and some medicines.

To produce D-limonene-loaded SLN dispersions, the high pressure homogenization method was combined with the rotor stator dispersion. In this case, formulation was composed of Imwitor 900K as solid lipid and Poloxamer 188 as surfactant. For the assessment of the physical and chemical stability, the freshly prepared SLN dispersions were stored at three different temperatures (4, 25 and 40°C) for a period of 1 month. The risk of creaming/sedimentation or flocculation phenomena of the different D-limonene-loaded SLN batches were examined using LUMiSizer (LUM GmbH). In turn, the mean particle sizes and zeta potential were analyzed by photon correlation spectroscopy (Malvern Zetasizer Nano ZS) for SLN dispersions were stored at 4, 25 and 40°C.

D-limonene-loaded SLN dispersions were successfully developed, depicting both physical and chemical stability. D-limonene was also found to be stable within the SLN matrices, which offer advances in functionality for a wide range of cosmetic preparations.

Synthesis of solid lipid nanoparticles and nanostructured lipid carriers for pharmaceutical and cosmetic purposes

*Aleksandra Zielińska, Izabela Nowak

Faculty of Chemistry, Adam Mickiewicz University in Poznań, Poznań, POLAND;

e-mail: ola.zielinska@amu.edu.pl

Keywords: *solid lipid nanoparticles, SLN, nanostructured lipid carriers, NLC high pressure homogenization, natural oils, meadowfoam seed oil*

Lipid nanoparticles, solid lipid nanoparticles (SLN) and nanostructured lipid carriers (NLC), are one of the most effective transport systems for potential applications in drug delivery. Their outstanding properties in drug delivery systems are a consequence of their small particle size (40-1000 nm). SLN and NLC are biocompatible and non-toxic nanoparticles, therefore they offer possibility to develop new therapeutics.

The aim of our study was to develop the methodology for the synthesis of SLN and NLC loaded systems, which are widely used in pharmacy or cosmetic industry. The substances that can be incorporated into lipid nanoparticles are mainly antioxidants such as retinol (vitamin A₁), coenzyme Q₁₀ (ubiquinone), and α -tocopherol (vitamin E), as well as lidocaine (anesthetic), carbamazepine (antiepileptic agent) and hesperidin (anticoagulant).

To produce different formulations of drug-loaded SLN and NLC nanoparticles, the hot high pressure homogenization (HPH) method was used. The SLN dispersions were composed of Compritol 888 ATO as a solid lipid and Tween 80 as a surfactant. In turn, for NLC the natural oil (meadowfoam seed oil, MSO) was additionally added as a natural liquid lipid matrix. To prepare all nanodispersions, the rotor stator dispersion (Ultra-Turrax T25) was combined with high pressure homogenization (Micron LAB 40, APV). For the investigation of the physical and chemical stabilities, all prepared dispersions were stored at 4, 25 and 40°C for 3 months. Chemical stability was assessed by using high performance liquid chromatography. The formulation stability was examined using Formulation Turbiscan LAB (multiple light scattering technique), the mean particle sizes and zeta potential by using photon correlation spectroscopy (Malvern Zetasizer Nano ZS), as well as the size distributions – by using laser diffractometry (Malvern Mastersizer 2000 E) for all nanodispersions.

Our study not only confirmed that HPH is currently one of the most effective methods for obtaining nanoparticles, but also proved a high stability of MSO, which can be applied in a wide range of pharmaceutical and cosmetic formulations.

Voltammetric profiling of tea infusions

*Justyna Zuziak, Małgorzata Jakubowska

AGH University of Science and Technology, Faculty of Materials Science and Ceramics, Department of Analytical Chemistry, al. Mickiewicza 30, 30-059 Cracow
e-mail: zuziak@agh.edu.pl

Keywords: *tea infusions, DP voltammetry, refreshable mercury film electrode, unsupervised multivariate analysis*

Nowadays food authenticity is a relevant quality criterion and an essential challenge that must be faced in many different quality control tasks. Quality control should be able to establish the actual origin of a product and detect deliberate or accidental adulteration of valuable food components. The combination of modern analytical techniques and chemometric pattern recognition is a powerful strategy which greatly contributes to promotion and quality assurance in the food industry.

Electrochemical experiments were carried out in a three electrode quartz cell with a multipurpose electrochemical analyzer 8KCA (mtm-anko, Poland). The working electrode was refreshable mercury film silver based electrode (Hg(Ag)FE). As reference Controlled Growth Mercury Dropping Electrode (CGMDE) was applied. As a subject of profiling three different tea species (black, red, green) were chosen, brewed, UV mineralized (or without sample preparation) and tested in complex electrolyte, which was optimized. Three separate repetitions were done. Recorded voltammograms were processed using especially prepared Matlab 2014a software, applying unsupervised algorithms such as: principal components analysis (PCA), cluster analysis and k-means method.

It was observed that voltammetric signal may be used to distinguish mentioned teas and effect of profiling is more satisfactory in the case of mineralized samples. In PCA first three principal components described always near 99% of variability. Using PC1/PC2 successive species form separate clusters, while using also PC3 infusions with and without citron were visible. Other multivariate methods confirmed previous conclusions.

Summarizing, it may be concluded that DP voltammetry with dropping and amalgam film electrodes in dedicated electrolyte is adequate, simple and inexpensive tool to profiling of tea infusions.

Voltammetric strategies of aluminium traces determination

*Justyna Zuziak, Małgorzata Jakubowska

AGH University of Science and Technology, Faculty of Materials Science and Ceramics, Department of Analytical Chemistry, al. Mickiewicza 30, 30-059 Cracow
e-mail: zuziak@agh.edu.pl

Keywords: *aluminium, stripping voltammetry, alizarin S, amalgam film electrode, water samples*

Direct voltammetric determination of aluminium is difficult, due to their high negative reduction potential of approximately -1.75 V, therefore peaks of aluminium complexes are often registered. As complexing agents palatine chrome black 6BN, chromazurol S and eriochrome black T, solochrome violet RS, arsenazo III, 1,2-dihydroxy-anthraquinone-3-sulphonic acid (DASA), cupferron, calmagite, morin and alizarin are applied. Voltammetric measurements are realized by the hanging-mercury drop electrode, mercury-film electrode prepared by electroplating a thin film of mercury on a solid support or bismuth-film electrode. Recent studies show that aluminium is involved in some important human pathologies, as for example, dialysis encephalopathy, osteomalacia, Parkinson's and Alzheimer's disease. So, the determination of aluminium is very important.

In this work Controlled Growth Mercury Dropping and Refreshable Amalgam Film Electrodes was applied with alizarin as complexing agent, in electrolyte consisted of 0.1 M ammonia buffer and 0.01 M KBrO₃. Ca-EDTA was used to eliminate Zn ions interferences.

In stripping voltammetry experiments on film electrode, with preconcentration potential -850 mV and time 4 seconds, it was observed that linear range in Al determination was 1-40 µg L⁻¹ with correlation 0.9955, and detection limit 0.13 µg L⁻¹. The operation of procedure was verified using CRM SPS-WW1 and SPS-WW2. As environmental samples water from Vistula River was measured, which was especially dotted by Al. Recovery was on the level 95-105%.

The proposed approach of aluminium determination is a simple, rapid and useful methodology of determination of this analyte in laboratory and environmental samples, on low level of concertation.

Fabrication of Al₂O₃-Ni composites via centrifugal gel casting

*Justyna Żygmuntowicz¹, Aleksandra Miazga¹, Katarzyna Konopka¹, Waldemar Kaszuwara¹

¹Faculty of Materials and Engineering, Warsaw University of Technology, Warsaw, POLAND

e-mail: justyna.zygmuntowicz@inmat.pw.edu.pl

Keywords: *centrifugal gel casting , functional graded material (FGM), Al₂O₃-Ni composites*

Ceramic–metal composites with gradient are important group of engineering materials, which have wide range of applications, e.g. as materials for energy technology or automobile or hollow for transport reactive medium and aerospace industry. There are still much more potential applications of ceramic metal composites with gradient concentration of metal particles. The most obvious advantage of functionally gradient materials is that they can favorably combine the dissimilar properties of ceramics and metals components in one material.

The goal of this study was to obtain Al₂O₃-Ni composites with gradient concentration of the metal particles by centrifugal gel casting. The method involves powders consolidation by the centrifugal force with simultaneous radical polymerization reaction of organic monomer within the composite slurry. This technique allows to obtain a composite with a variable gradient concentration of the metal in the cross section of the material.

The microstructure of samples was investigated using Scanning Electron Microscopy (SEM). The obtained samples were characterized by X-ray diffraction studies (XRD). The preliminary macroscopic observation as well as SEM reveal the changes of the Ni particles at the cross-section of the samples. The maximum of volume fraction of nickel particles was obtained at the outer zone of the composites. The XRD results confirmed only two phases: α -Al₂O₃ and Ni in composites. Application of the centrifugal gel casting method allows for the graded distribution of metal particles in the samples.

Acknowledgements

The results presented in this paper were obtained within the project from The Polish National Science Centre (NCN) No. 2013/11/B/ST8/0029.

Index

- Acznik Iłona, 259
Amrane Abdeltif, 274
Antkowiak Paweł, 236
- Bajda Tomasz, 237
Balogh György Tibor, 284
Baran Patryk, 236
Baraniak Marek, 253, 272, 275
Baś Bogusław, 266, 267, 333, 334, 335, 336
Bennis Noureddine, 307
Berezowski Tomasz, 320
Boroń Dominika, 328
Brojanowska Agnieszka, 345
Brylewska Kamila, 31, 237
Budnicka Monika, 40, 238
Burnat Barbara, 312, 313, 314
- Carvalho Jorge M.R., 211
Chodara Agnieszka, 239, 243, 344
Chormański Jarosław, 320
Chrunik Maciej, 254
Chrzanowska Justyna, 240
Chrzanowski Łukasz, 274
Chudoba Tadeusz, 239, 243, 292, 293, 341, 342
- Dąbrowska Marta, 241, 242
Dąbrowska Sylwia, 243, 292, 293
Denis Piotr, 240
Dębek Paulina, 244, 245
Didaskalou Christos, 251
Długoń Elżbieta, 255, 256
Dorosz D., 262, 263
Drozdek Emilia, 246
Drzewicz Anna, 52, 247, 248
Duda Aneta, 249, 282
- Farczak Łukasz, 269
Fedoryk Michał, 63, 236, 250
Feliczak-Guzik Agnieszka, 244, 245, 346
Fódi Tamás, 251, 284
Foszpańczyk Magdalena, 246
Fourcade Florence, 274
Frąk Magdalena, 320
- Gabryelczyk Agnieszka, 252, 253
Gadomska-Gajadhur Agnieszka, 40, 87, 176, 238, 281, 318
Gaładyk Katarzyna, 254
Garbiec Dariusz, 240
Gawęda Magdalena, 255, 256
Główka Aleksandra, 257, 258
Gmurek Marta, 246
Góra Tomasz, 158
Górski Łukasz, 324, 325
Grabarczyk Małgorzata, 333, 336
Grabowski Łukasz, 306
Grajek Henryk, 202, 332, 268, 269
Graś Małgorzata, 252, 259, 260, 273
Grobeln Jarosław, 307
Grzybowska Agnieszka, 289, 290, 291
- Harmata Piotr, 309
Havela Ladislav, 283
Hemedmin Ahmed E., 261
Herman Jakub, 309
Hoffman Jacek, 240
Huertas Salvador Perez, 164, 317
Huszthy Péter, 271, 278, 284
- Ibrahim Soran S., 261
Ignác Gergő, 284
Ismael M. Rosinda C., 211, 339
- Jadach Renata, 262, 263
Jakubowska Małgorzata, 324, 325, 348, 349
Jankowska Ewa, 253
Jarmolińska Sylwia, 264, 265
Jaroszewicz Leszek R., 135, 230, 285, 286, 294, 307, 308, 343
Jedlińska Katarzyna, 266, 267
Jeleń P., 262
Jonik Justyna, 202, 332, 268, 269
- Karpowicz Magdalena, 270, 294
Kaszuwara Waldemar, 350
Kisszékelyi Péter, 271, 278
Kmita Grzegorz, 296
Kochanowicz M., 262, 263

Kolanowski Łukasz, 260, 272, 273
 Konopka Katarzyna, 288, 350
 Konopka Małgorzata, 176, 318
 Kopczyński Kacper, 253, 274, 275
 Kornaus Kamil, 237
 Kos Marcin, 276
 Kotkowski Tomasz, 277
 Kowalski Jerzy K., 285
 Kozma Petra, 271, 278
 Krajewski Zbigniew, 285
 Kramek-Romanowska Katarzyna, 279
 Kraut Manfred, 63, 250
 Król Grzegorz, 79, 280
 Król Magdalena, 237, 316
 Kruk Aleksandra, 87, 281
 Krupska Magdalena, 249, 282, 283
 Krzosa Radosław, 236
 Kubiak Władysław W., 289, 290, 291
 Kula Przemysław, 149, 254, 307, 309, 310
 Kupai József, 271, 278, 284
 Kurpaska Łukasz, 240
 Kurzych Anna, 100, 108, 285
 Kuśnieruk Sylwia, 239, 315
 Kwiatkowska Marlena, 118, 286

Lechowska Joanna, 125, 287
 Lewak Michał, 277
 Locs Janis, 243
 Lojkowski Witold, 341, 342
 Lota Grzegorz, 252, 253, 259, 260, 272, 273, 274, 275
 Lota Katarzyna, 259

Łada Paula Maria, 288
 Ławrywianiec Martyna, 321, 322
 Łazińska Magdalena, 270
 Łojek Karolina, 87, 281
 Łojkowski Witold, 239, 243, 292, 293, 315, 344

Mackiewicz Agnieszka, 307
 Mackova Anna, 283
 Magda Łukasz, 289, 290, 291
 Majchrzycki Włodzimierz, 275
 Malinsky Petr, 283
 Małysa Maria, 292, 293
 Marć Paweł, 307, 308

Matras-Postołek Katarzyna, 297
 Mazurkiewicz-Pawlicka Marta, 298
 Miazga Aleksandra, 288, 350
 Miluski P., 262, 263
 Molga Eugeniusz, 277
 Molska Angelika, 308
 Moś Joanna, 135, 294
 Mościcki Tomasz, 240
 Mozgawa Włodzimierz, 237, 316
 Mukhovskiy Roman, 243, 292, 293

Nhu-Tarnawska Hoa Kim Ngan, 249, 282, 283
 Niebieszczańska Anna, 338
 Niemczak Michał, 274
 Nieroda Jolanta, 295, 296
 Niewiara Ewa, 338
 Nowak Elżbieta M., 297
 Nowak Izabela, 241, 242, 244, 245, 257, 258, 264, 265, 303, 346, 347
 Nowak Maksymilian, 298

Olcay Ali B., 261
 Omelchenko Myroslava, 341
 Omiotek Agnieszka, 292, 293
 Ostrowska Barbara, 315

Paczosa-Bator Beata, 304, 321, 322
 Pańcikiewicz Krzysztof, 158, 311, 330
 Partyka Janusz, 299, 300
 Pasiut Katarzyna, 299, 300
 Patyna Agnieszka, 301
 Pawlita-Posmyk Monika, 302
 Pereira Irina, 303, 346
 Pernak Juliusz, 253, 272, 275
 Pęziak-Kowalska Daria, 274
 Piecek Wiktor, 254
 Piech Robert, 304, 321, 322
 Pietrzykowska Elżbieta, 243, 292, 293
 Pięk Magdalena, 304, 305, 321, 322
 Pięta Paulina, 306
 Pilarek Maciej, 337
 Polański Marek, 270
 Polek Daria, 306
 Przybyło Henryk, 275
 Przybysz Natalia, 142, 307, 308
 Purchała Marcin, 268, 269, 332
 Pytlarczyk Marta, 149, 309, 310

Rakoczy Łukasz, 158, 311, 330
 Reis M. Teresa A., 211, 339
 Resztak Matylda, 257
 Robak Justyna, 312, 313, 314
 Rogowska-Tylman Julia, 315, 344
 Rożek Piotr, 316
 Ruśkowski Paweł, 40, 87, 176, 281, 318
 Ruśowski Paweł, 238
 Rybak Andrzej, 295, 296
 Rybusiński Jarosław, 341
 Rymuszka Diana, 164, 317
 Rzeszutek Waldemar, 253

Sanetra Jerzy, 297
 Santos Ana C., 303, 346
 Sebai Agnieszka, 176, 318
 Shareif Albasher, 319
 Sierczyńska Agnieszka, 259
 Silva Amélia M., 303, 346
 Sitarz M., 262, 263
 Sitarz Maciej, 255, 256, 262, 263, 295, 296, 331
 Skrzypek Sławomira, 312, 313, 314
 Słapińska Małgorzata, 320
 Smajdor Joanna, 304, 321, 322, 323
 Sobieszuk Paweł, 337
 Sordoń Wanda, 324, 325
 Sosnowski Tomasz R., 279
 Souto Eliana B., 303, 346
 Sovinska Svitlana, 297
 Sowa Sylwia, 249, 282, 283
 Stasiewicz Karol, 135, 294
 Stasiewicz Monika, 252
 Staszak Katarzyna, 221, 340
 Stobiński Leszek, 298
 Stodulska Urszula, 87, 281
 Supeł Agata, 345
 Synoradzki Ludwik, 87, 176, 281, 318
 Szaniawska Magdalena, 186, 194, 326, 329
 Szczytko Jacek, 341
 Székely György, 271, 278
 Szubert Karol, 260
 Szukiewicz Mirosław, 79, 280
 Szydłowska Adriana, 327
 Szyman Jakub, 328

Szymański Zygmunt, 240
 Szymczyk Katarzyna, 186, 326, 329
 Świąszkowski Wojciech, 315, 345

Tadeusz Chudoba, 239
 Taraba Anna, 186, 194, 326, 329
 Terpiłowski Konrad, 164, 317
 Tomaszewska Emilia, 307
 Tomczyńska-Mleko Marta, 164, 317
 Tuz Lechosław, 158, 311, 330
 Tykarska Marzena, 52, 247, 248

Veiga Francisco J., 303, 346

Wajda Aleksandra, 331
 Wawer Tomasz, 202, 268, 269, 332
 Wawrzyńczak Agata, 264, 265
 Węgiel Krystian, 266, 267, 333, 334, 335, 336
 Wierzchowski Kamil, 337
 Wieszczycka Karolina, 211, 221, 340
 Wilkosz Katarzyna, 338
 Witczak Stanisław, 301
 Wojciechowska Aleksandra, 211, 221, 339, 340
 Wojciechowska Irmina, 211, 221, 340
 Wojciechowski Jarosław, 260, 272
 Wojnarowicz Jacek, 239, 341, 342
 Wojtalik Michał, 236
 Wołosiewicz-Głąb Marta, 306
 Wonko Renata, 230, 343
 Woźniak Bartosz, 315, 344
 Wysocki Bartłomiej, 345
 Wzorek Małgorzata, 302

Yayla Sedat, 261

Zeller Bálint, 271
 Zielińska Aleksandra, 303, 346, 347
 Zielińska-Lipiec Anna, 158, 311
 Zmojda J., 262, 263
 Zuziak Justyna, 348, 349
 Zygmuntowicz Justyna, 350

Żaba Adam, 297
 Żurek Zbigniew, 330
 Żurowska Magdalena, 247, 248, 254